

Die approbierte Originalversion dieser Dissertation ist an der Hauptbibliothek der Technischen Universität Wien aufgestellt (<http://www.ub.tuwien.ac.at>).

The approved original version of this thesis is available at the main library of the Vienna University of Technology (<http://www.ub.tuwien.ac.at/englweb/>).



TECHNISCHE
UNIVERSITÄT
WIEN

Vienna University of Technology

Dissertation

Identification of vibration and elastic properties of aluminum foam using modal testing and analysis

Ausgeführt zum Zwecke der Erlangung des akademischen Grades eines Doktors der technischen Wissenschaften / der Naturwissenschaften unter der Leitung von

Ao.Univ.Prof. Dipl.-Ing. Dr.techn. Johann Wassermann

Institutsnummer: E325

Institut für Mechanik und Mechatronik

Eingereicht an der Technischen Universität Wien

Fakultät für Maschinenwesen und Betriebswissenschaften

von

MS. Engr. Saeed Badshah

Matrikelnummer: 0727889

Pakistan

Wien, Nov. 2011

Unterschrift

To my loving parents

For their moral support and encouragement.

ABSTRACT

Aluminum foams are being increasingly used as alternatives for conventional materials primarily because of their high strength, specific stiffness, light weight, and adjustable properties. However, before using this type of material with confidence in industrial applications a thorough characterization of the material properties is needed. Because of the number and the inherent variability of the constitutive properties of aluminum foam materials, the experimental characterization is quite cumbersome and requires a large number of specimens to be tested. An elegant way to circumvent this lack consists in using mixed numerical-experimental methods which constitute a powerful tool for estimating unknown constitutive coefficients. In this work, a mixed numerical-experimental identification technique based on the modal response of aluminum foam is presented. This technique is based on the minimization of the discrepancies between the eigenvalues and eigen mode shapes computed with a finite element model and the corresponding experimental quantities.

In order to maximize the quality of identification, optimal experimental conditions are selected for experimental determination of modal parameters. The specimens suspended by elastic soft bands are excited by a mini shaker, while the dynamic response is measured with a scanning laser vibrometer. The measured frequency response functions are then treated in modal analysis software package LMS Test.Lab to obtain modal data.

As accuracy of the identification technique directly depends on precision of the finite element model, a special procedure called density mapping method, has been applied to approximate the aluminum foam structure with continuum. The transformation of a discretely heterogeneous structure of aluminum foam to an approximated continuum was one of the major challenges. The microscopical density distribution of aluminum foam recorded by X-ray computed tomography has been averaged over a certain domain and is used as input to the finite element model of corresponding specimen. Gibson and Ashby model is implemented in FE model to present the elastic behavior. Numerical modal analysis is performed in ANSYS.

Levenberg-Marquardt nonlinear least squares minimization algorithm is used to solve the inverse problem of finding elastic constitutive parameters, which are best matching the experimental modal data. For comparing the computed and measured values, the implemented objective functions are based upon relative differences between the eigen frequencies, modal damping ratio, diagonal and off-diagonal terms of modal assurance criteria, and upon geometrical properties of the mode shapes such as nodal lines. The identification procedure is explained with the help of block diagrams. Some numerical investigations are presented to study the variable density distribution effect on modal behavior of aluminum foam.

Dynamic behavior of closed cell material ALPORAS is investigated experimentally and numerically. Modal test on four ALPORAS specimens shows that inhomogeneties in the mass distribution are a key factor in evaluating dynamic behavior of cellular materials. A comprehensive methodology for the identification of dynamic and elastic behavior of cellular materials has been proposed. In the context of materials engineering, the present approach can be very useful for designing cellular materials. Indeed, it enables the prediction of best way of combining the mechanical properties of solid material with feasible microstructures, in order to obtain expected mechanical properties.

KURZFASSUNG

Geschäumtes Aluminium wird zunehmend als Alternative für herkömmliche Materialien eingesetzt, vor allem wegen der hohen Festigkeit, spezifischen Steifigkeit, geringen Masse sowie der anpassbaren Eigenschaften. Bevor jedoch dieses vielversprechende Material in industriellen Anwendungen eingesetzt werden kann, ist eine vollständige Charakterisierung der Materialeigenschaften erforderlich. Aufgrund der Vielzahl und der damit einhergehenden Variabilität der Materialeigenschaften von Aluminium Schaumstoffen ist eine experimentelle Charakterisierung sehr aufwändig, da entsprechend viele Proben untersucht werden müssten. Dieser Problematik kann durch den gemeinsamen Einsatz von numerischen und experimentellen Methoden, die in Kombination ein sehr leistungsfähiges Werkzeug für die Abschätzung unbekannter Materialkoeffizienten darstellen, entgegengewirkt werden. In dieser Arbeit wird eine Methode zur numerisch-experimentellen Identifikation, basierend auf der modalen Strukturantwort von Aluminiumschaum, vorgestellt. Dieses Verfahren basiert auf der Minimierung der Abweichungen der Eigenwerte und Eigenschwingungsformen zwischen einem numerischen Finite-Elemente-Modell und den entsprechenden experimentell ermittelten modalen Größen.

Um eine möglichst hohe Qualität zur Identifikation der Materialparameter zu erreichen wird die experimentelle Bestimmung der modalen Parameter unter optimalen experimentellen Bedingungen durchgeführt. Die Proben, mit elastischen weichen Bändern aufgehängt, werden mit einem Shaker breitbandig angeregt, während die dynamische Strukturantwort mit einem Laser Scanning Vibrometer gemessen wird. Anschließend werden die erfassten Übertragungsfunktionen mit dem Modalanalyse Software-Paket LMS Test.Lab zu modalen Daten weiterverarbeitet.

Da die Genauigkeit der Identifikation unmittelbar von der Präzision des FE-Modells abhängt, wurde zur Annäherung der Aluminiumschaumstruktur an eine kontinuierliche Größe ein spezielles Verfahren, die sogenannte *Density Mapping Method*, eingesetzt. Die Transformation von Aluminiumschaum, eine diskret heterogene Struktur, in eine annähernd homogene Struktur war eine der großen Herausforderungen.

Die mikroskopische Dichteverteilung des Aluminiumschaums wurde mit Hilfe der Computer Tomographie erfasst, über bestimmte Bereiche gemittelt und als Eingangsgröße für das FE-Modell der entsprechenden Probe verwendet. Das elastische Verhalten wird durch das in das FE-Modell implementierte Gibson- und Ashby- Modell repräsentiert. Die numerische Modalanalyse erfolgt in ANSYS.

Die Lösung des inversen Problems zur Bestimmung der grundlegenden elastischen Parameter, die den experimentell ermittelten modalen Daten am besten entsprechen, wird nach dem nichtlinearen Levenberg-Marquardt Algorithmus zur Minimierung der kleinsten Fehlerquadrate ermittelt. Als Basis für den Vergleich zwischen den berechneten und den gemessenen Werten werden die relativen Unterschiede zwischen den Eigenfrequenzen, modale Dämpfung, Diagonal- und Nichtdiagonal-Termen hinsichtlich der modalen Qualitätssicherung sowie geometrische Eigenschaften der Schwingungsformen wie Knotenlinien verwendet. Der Ablauf der Identifizierung wird an Hand von Blockdiagrammen erläutert. Einige numerische Untersuchungen werden vorgestellt, um die variable Dichteverteilung hinsichtlich des modalen Verhaltens von Aluminium-Schaum zu prüfen.

Das dynamische Verhalten von ALPORAS, ein Material mit geschlossenen Zellen, wurde experimentell und numerisch untersucht. Modale Untersuchungen von vier ALPORAS Proben zeigen, dass Inhomogenitäten in der Massenverteilung ein entscheidender Faktor bei der Beurteilung des dynamischen Verhaltens zellulärer Werkstoffe sind. Eine umfassende Methode für die Identifizierung des dynamischen und elastischen Verhaltens zellulärer Werkstoffe wurde vorgeschlagen. Im Rahmen der Werkstofftechnik, kann der vorliegende Ansatz für die Gestaltung von zellulären Werkstoffen sehr nützlich sein. Er ermöglicht die Vorhersage der besten Kombination aus mechanischen Eigenschaften des festen Materials und realisierbaren Mikrostrukturen, um die gewünschten mechanischen Eigenschaften zu erhalten.

ACKNOWLEDGMENTS

This thesis is the fruit of nearly four years of research at the institute of mechanics and mechatronics, Vienna University of Technology (TU-Wien), where I was able to work and live in a unique atmosphere surrounded by motivated and sympathetic team. I wish to express my gratitude to my supervisor Prof. Dr. Johann Wassermann, hosting me in his institute and have thus provided me technical means necessary for the fulfillment of this research. As a Master and Commander, he gave me the guide and the freedom to experience the passion for the scientific research during these years. I also acknowledge his great patience and guidance during the writing up of this thesis.

I am also grateful to Prof. Dr. Heinz Pettermann, who was kind enough to give me valuable advises and technical comments.

I would also like to thank all my colleagues and friends at our institute especially to Ing. Manfred Neumann for his continuous support with many interesting discussion and technical support. I am thanking particularly to Dipl.-Ingr. Andreas Kottar from institute of material science and technology, TU-Wien, who provided me the aluminum foam specimens and their X-ray computer tomography data. Many thanks to Mr. Sajid Ghuffar from Institute of Photogrammetry and Remote Sensing, TU-Wien, who helped time to time in writing MATLAB routines.

I would like thanks to all friends in Vienna who made life easy for me by arranging and participating in extracurricular activities.

The PhD Scholarship provided by Higher Education Commission (HEC) of Pakistan is gratefully acknowledged.

Special thanks are due to my parents and all family members because without them I would not be here enjoying this life.

MS. Engr. Saeed Badshah

Nov. 2011

TABLE OF CONTENTS

CHAPTER 1.	Introduction.....	1.1
1.1	Motivation.....	1.1
1.2	Mixed Numerical-Experimental Technique (MNET)	1.2
1.2.1	Introduction.....	1.2
1.2.2	MNET approach for identification of material characteristics	1.6
1.2.2.1	<i>Identification based on static tests</i>	<i>1.8</i>
1.2.2.2	<i>Approaches based on dynamic tests.....</i>	<i>1.11</i>
1.2.3	Difference between MNETs and FE model updating.....	1.20
1.2.3.1	<i>Precision and accuracy of the numerical model.....</i>	<i>1.21</i>
1.2.3.2	<i>Selection of the variable parameters.....</i>	<i>1.22</i>
1.3	Focus of the thesis	1.22
1.4	Structure of the thesis	1.23
CHAPTER 2.	Experimental modal testing and analysis	2.1
2.1	Objective.....	2.1
2.2	Theoretical background	2.1
2.2.1	Establishment of temporal model	2.7
2.2.2	Transformation of the temporal model in frequency model	2.7
2.2.3	Estimation of modal parameters	2.8
2.3	Non-contact vibration measurements technology.....	2.9
2.3.1	Polytec Laser Doppler Vibrometer	2.10
2.4	Support of the structure.....	2.16
2.5	Excitation of the structure.....	2.18
2.6	Support of the excitation system.....	2.19
2.7	Attachment to the structure.....	2.20
2.8	Measurements by scanning laser vibrometer.....	2.22
2.9	Extraction of modal parameters (Modal analysis).....	2.26
2.9.1	Steps of applied technique for modal extraction	2.33
CHAPTER 3.	Material and modelling	3.1
3.1	Objective.....	3.1

3.2	Material specification	3.1
3.3	Viscoelastic constitutive modelling	3.2
3.4	Damping modelling and solution approaches.....	3.4
3.4.1	Viscous damping model.....	3.8
3.4.1.1	<i>Derivation of the equations of motion</i>	3.8
3.4.1.2	<i>Eigenvalue Equation</i>	3.14
3.4.1.3	<i>Special case: the proportional model</i>	3.16
3.4.1.4	<i>Frequency response function</i>	3.18
3.4.2	Hysteretic damping Model.....	3.22
3.4.2.1	<i>Derivation of the equations of motion</i>	3.22
3.4.2.2	<i>Eigenvalue equation</i>	3.24
3.4.2.3	<i>Hysteretic model in continues harmonic system</i>	3.26
3.4.2.4	<i>Frequency response function</i>	3.26
3.5	Complex matrix of elasticity.....	3.27
3.6	Cellular materials modelling.....	3.30
3.6.1	Finite element modelling	3.34
CHAPTER 4. Mixed numerical-experimental identification technique ...		4.1
4.1	Background and objectives.....	4.1
4.2	Modal error norms	4.3
4.3	Parametric study	4.8
4.3.1	Implementation of parametric study in MATLAB	4.9
4.3.2	Robustness of error functions	4.12
4.4	Algorithm for mixed numerical-experimental technique	4.16
4.4.1	Modal optimization problem	4.16
4.4.2	Minimization algorithms.....	4.17
4.4.3	Calculation error functional gradients	4.23
4.4.4	Implementation of identification technique in MATLAB	4.25
CHAPTER 5. Results and discussion		5.1
5.1	Summary of the proposed mixed identification method.....	5.1
5.1.1	Modal measurements of test specimens.....	5.1

5.1.2	Mixed numerical-experimental identification	5.1
5.2	Objectives and approach.....	5.1
5.3	Modal measurements	5.2
5.3.1	Measurement estimation and validation	5.2
5.4	Mixed numerical-experimental identification	5.14
5.4.1	ALPORAS_B2.....	5.14
5.4.2	ALPORAS_B3.....	5.19
5.4.3	ALPORAS_S3	5.23
5.4.4	ALPORAS_S2	5.27
CHAPTER 6.	Summary and conclusions.....	6.1
6.1	Future developments and perspectives	6.5
	References	I

LIST OF FIGURES

Figure 1.1 The general concept of MNET	1.3
Figure 1.2 The direct problem	1.4
Figure 1.3 The inverse problem.....	1.4
Figure 1.4 The general flow chart of MNET	1.5
Figure 2.1 Measurement grid points	2.2
Figure 2.2 Experimental mesh and transfer functions	2.5
Figure 2.3 Dynamic model interrelation.....	2.6
Figure 2.4 Experimental modal analysis stages.....	2.7
Figure 2.5 Identification of the third mode from the transfer function of the structure	2.8
Figure 2.6 Polytec LDV arrangement.....	2.11
Figure 2.7 Quarter wave plate working principle	2.12
Figure 2.8 Polytec system components, work station, controller OFV-3001-S, junction box PSV-Z-040	2.14
Figure 2.9 Polytec scanning head	2.15
Figure 2.10 Laser scanning head (OFV-056)	2.15
Figure 2.11 Free-Free support condition for testing structure	2.17
Figure 2.12 Shaker and structure attachment (Stinger assembly)	2.21
Figure 2.13 Experimental configuration.....	2.23
Figure 2.14 Grid of measurement points on testing structure.....	2.25
Figure 2.15 ODS @ 282Hz and 1524 Hz	2.26
Figure 2.16 Transfer mobility at point 37.....	2.26
Figure 2.17 Polytec PSV 200 for parameter extraction using SDOF	2.28
Figure 2.18 Stabilization diagram by applying PolyMAX estimation method.	2.32
Figure 3.1 Kelvin-Vogit Model	3.9
Figure 3.2 Representation of complex Young modulus in complex plane.....	3.23
Figure 3.3 Comparison of damping ratios of aluminum foam specimen	3.36
Figure 3.4 FE modelling of Alporas_B2	3.37
Figure 4.1 Flow diagram of mixed numerical-experimental technique.....	4.2
Figure 4.2 Eigen mode shape and grayscale image representing nodal lines (Alporas_B3, grid size 256×256, $\delta = 0.1$)	4.7
Figure 4.3 Block diagram of parametric study developed with MATLAB.....	4.10
Figure 4.4 Block diagram of post-processing of parametric studies with the developed MATLAB program.	4.11

Figure 4.5 Evolution of modal error norms (sum all modes) on a range of $\pm 30\%$ of each variable parameter (Alporas_B2)	4.13
Figure 4.6 MAC_nd based on non diagonal terms of MAC (Alporas_B2) matrix norm digital issue	4.14
Figure 4.7 New norm MAC_nd2 based on differences in non-diagonal matrix MAC (Alporas_B2).....	4.15
Figure 4.8 Block diagram of loading experimental modal model for mixed numerical experimental identification technique.....	4.26
Figure 4.9 Matlab routine summary of objective function (Algorithm 2).....	4.33
Figure 4.10 FE modelling of AF.....	4.33
Figure 4.11 Block diagram of the evaluation of modal error norms	4.34
Figure 4.12 General block diagram for solution of mixed numerical-experimental identification problem (Algorithm 1).....	4.35
Figure 5.1 Average measured frequency response function of testing specimens	5.3
Figure 5.2 Coherence function of testing specimens.....	5.5
Figure 5.3 Experimental Mode shapes of Alporas_S2	5.6
Figure 5.4 Experimental mode shapes of Alporas_B2	5.8
Figure 5.5 Experimental mode shapes of Alporas_B3	5.11
Figure 5.6 Experimental mode shapes of Alporas_S3.....	5.12
Figure 5.7 Measured Auto-MAC matrix of Alporas Specimens.....	5.13
Figure 5.8 MAC matrix of experimental and numerical modes of Alporas_B2 (paired and non-paired)	5.14
Figure 5.9 Graphs of convergence of identifying parameters (Alporas_B2)	5.15
Figure 5.10 Density distribution of Alporas_B2	5.17
Figure 5.11 MAC matrix of experimental and numerical modes of Alporas_B3 (paired and non-paired)	5.20
Figure 5.12 Graphs of convergence of identifying parameter (Alporas_B3).....	5.21
Figure 5.13 Density distribution of Alporas_B3	5.22
Figure 5.14 MAC matrix of experimental and numerical modes of Alporas_S3 (paired and non-paired)	5.24
Figure 5.15 Graphs of convergence of identifying parameters (Alporas_S3).....	5.25
Figure 5.16 Density distribution of Alporas_S3	5.25
Figure 5.17 Density distribution of Alporas_S3	5.26
Figure 5.18 MAC matrix of experimental and numerical modes of Alporas_S2 (paired and non-paired)	5.28
Figure 5.19 Graphs of convergence of identifying parameters (Alporas_S2).....	5.29
Figure 5.20 Density distribution of Alporas_S2.....	5.30

LIST OF TABLES

Table 3.1 Specification of aluminum foam specimen	3.2
Table 4.1 list of the modal error norms	4.8
Table 4.2 Algorithm for General optimization based on the principles of descent direction	4.20
Table 4.3 Minimization of Levenberg-Marquardt algorithm	4.22
Table 5.1 Experimental modal parameters of Alporas_S2	5.7
Table 5.2 Experimental modal parameters of Alporas_B2.....	5.9
Table 5.3 Experimental modal parameters of Alporas_B3.....	5.9
Table 5.4 Experimental modal parameters of Alporas_S3	5.11
Table 5.5 Convergence of identifying parameters (Alporas_B2).....	5.16
Table 5.6 Relative frequency error, Alporas_B2.....	5.16
Table 5.7 Frequencies (Hz) predicted from FE models based on densities distribution mapping (Alporas_B2).....	5.18
Table 5.8 Relative frequency error, Alporas_B3	5.19
Table 5.9 Convergence of identifying parameters (Alporas_B3).....	5.21
Table 5.10 Frequencies (Hz) predicted from FE model based on densities distribution mapping (Alporas_B3).....	5.23
Table 5.11 Relative frequency error Alporas_S3	5.24
Table 5.12 Convergence of identifying parameters (Alporas_S3)	5.25
Table 5.13 Frequencies (Hz) predicted from FE model based on densities distribution mapping (Alporas_S3).....	5.27
Table 5.14 Relative frequency error, Alporas_S2	5.28
Table 5.15 Convergence of identifying parameters (Alporas_S2)	5.29
Table 5.16 Frequencies (Hz) predicted from FE model based on densities distribution mapping (Alporas_S2).....	5.31
Table 5.17 Identified parameters of AF specimens.....	5.31

CHAPTER 1. INTRODUCTION

1.1 MOTIVATION

Metallic foam structures represent a fast developing area of new materials, which are still at the beginning of commercial production and industrial applications. A number of promising characteristics and applications may be realized in the future by metal foam and metal foam sandwich structures as, for example, light weight applications combined with high structural stiffness, high structural damping and high ultimate strength, high acoustic absorption capabilities, high crash worthiness for automotive applications, compatibility with common materials, and easy materials recycling properties. Aluminum foams are used increasingly as alternatives for conventional materials primarily because of favourable combination of good mechanical and physical properties, while maintaining very low weight. However, before using this material with confidence in industrial applications such as automotive or aerospace structural components, a thorough characterization of the material properties is required.

Numerical simulations have become an indispensable tool in the process that leads to the development of an engineering structure. Although these simulations have replaced a substantial amount of experimental tests, they have not rendered testing obsolete. A successful simulation requires an accurate knowledge of the material parameters that are used in the numerical model. These parameters can be only obtained with an actual experiment. To improve the performance, durability or efficiency of mechanical equipment, material scientists are continuously developing new materials. Unfortunately, the mechanical behavior of these novel materials is becoming increasingly more complex. Cellular materials are one class of new materials that are becoming increasingly important for the production of high performance components. During design calculations, their stiffness properties are crucial. Mechanical properties of metallic foam structure depend on the relative density of the structure. Various constitutive laws have been suggested for the characterization and modelling of this relationship. Knowledge of the relationship between the micro structure and the macroscopic mechanical properties of a material is a prerequisite for modern material

design. The experimental validation of a constitutive model is an important issue in computational mechanics. The combined use of sophisticated measurement techniques, computational simulations and a numerical identification tool for the model parameters is necessary for proper material characterization. The aim of this work is to develop and validate realistic models of the investigated foam specimens based both on the foam microstructure and on the behavior of the bulk material. The material primary used is an alloy supplied by Shinko wire, with the trade name ALPORAS [1]. The density mapping method is used to approximate the Aluminum Foam (AF) by a continuous, 3-D density distribution. A continuum model is implemented using the Finite Element (FE) method to simulate the effect of local mass distribution on the modal behavior of metallic foam sample. A mixed numerical-experimental identification technique is used to identify elastic behavior of AF.

In this research work, a new mixed numerical-experimental identification technique based on the modal response of aluminum foam is developed. This technique is founded on the minimization of the discrepancies between the eigen values and eigen modes, computed with an accurate parametric FE model and the corresponding experimental quantities. One of the objectives of this research is to explore the possibility of solving such mixed numerical-experimental identification problems accurately using two powerful software packages ANSYS and MATLAB, which are available at most universities. This is achieved by developing a suitable automation code in MATLAB that incorporates a FE analysis tool ANSYS and experimental results from modal analysis software package LMS Test.Lab, with a suitable optimization algorithm.

1.2 MIXED NUMERICAL-EXPERIMENTAL TECHNIQUE (MNET)

1.2.1 Introduction

Some physical properties are difficult or even impossible to measure in a direct way. Sometimes, the physical property can be measured with an indirect measurement procedure. Instead of measuring directly the property of interest, indirect procedures measure a number of related quantities and derive the unknown property from the

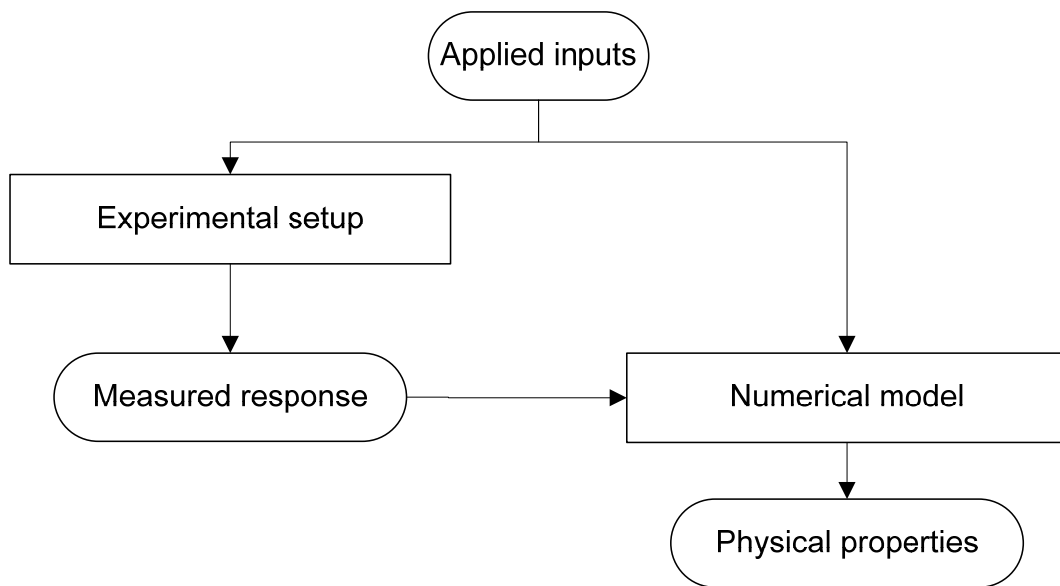


Figure 1.1 The general concept of MNET

experimental values of these measured quantities. Traditional indirect measurement techniques use analytical expressions to relate the physical property of interest to the measured quantities. This approach can only be used when there is a simple relation between the measured quantities and the physical property of interest. If this relation becomes too complex to be expressed analytically, the physical properties of interest have to be related to the measured quantities by means of a numerical model, and the properties of interest have to be identified by the MNET. Figure 1.1 illustrates the general concept of the mixed numerical-experimental approach.

Numerical models are usually formulated in such a way that they compute the response of a system using the applied inputs and system properties. The problem of determining the response from the input and system properties is called the direct problem and is illustrated in Figure 1.2.

However, the direct problem is not the problem that has to be solved by MNET (Figure 1.1). In an MNET, a number of model parameters have to be derived from the system's response to a particular input. This problem is called the inverse problem and is sketched in Figure 1.3. Most numerical models cannot be reformulated in the form that complies with the inverse problem. The inverse problem has to be solved in an iterative

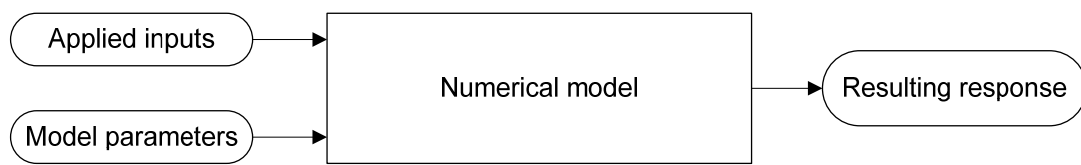


Figure 1.2 The direct problem

way by 'fine-tuning' the model parameters in such a way that the calculated response equals the measured response.

Incorporating the concept of inverse problems into the scheme of Figure 1.1 provides the general MNET flowchart as shown in 1.4. In the first phase, an experiment is performed and the applied inputs and resulting responses are recorded. In a second phase, a numerical model of this experiment is constructed. The responses are computed with this simulation model using a set of trial values of the unknown model parameters, i.e. the physical properties that have to be identified. The simulation responses are compared with the experimental responses and an improved set of model parameters is obtained by minimising the response differences. The improved model parameters are inserted into the numerical model and a new iteration cycle is performed. The iterative procedure is aborted once the solution has converged, and the model parameters can be extracted from the database of the numerical model. Note that vibration-based identification routines use resonant frequencies and mode shapes as response quantities.

The MNET approach might look like a quite complicated concept to measure physical parameters. However, if looked at from a modelling point of view, it is actually a very logical approach. For mechanical engineering applications, the identified material parameters will eventually be used in numerical simulations. An MNET routine will use this simulation code to identify the unknown values of the model parameters. It therefore creates a perfect synergy between the worlds of modelling and testing, since

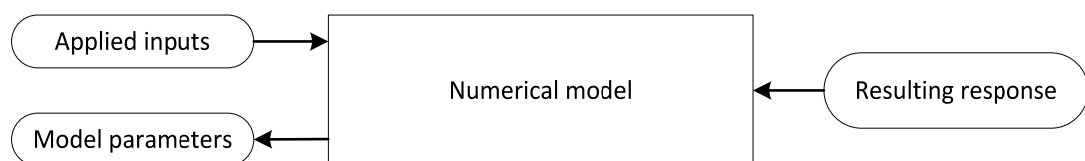


Figure 1.3 The inverse problem

the numerical simulation code is used to both determine the values of the model parameters and predict the behavior of a real structure. Note that the MNET approach is a generic concept allowing the identification of any parameter that is used in a numerical simulation code.

MNETs also have a number of other interesting advantages over traditional measurement techniques. For example, it is possible to extract more than one physical parameter from a single experiment or to extract a set of parameters from a combination of different experiments. Unlike conventional measurement approaches, MNETs can also handle more complex types of experimental data and this might become an important issue in the future. Due to recent technological advances, optical measurement devices like scanning laser vibrometers and CCD cameras are becoming more and more affordable. Although these systems provide a wealth of information, the information is only becoming useful when there are techniques to process the measured

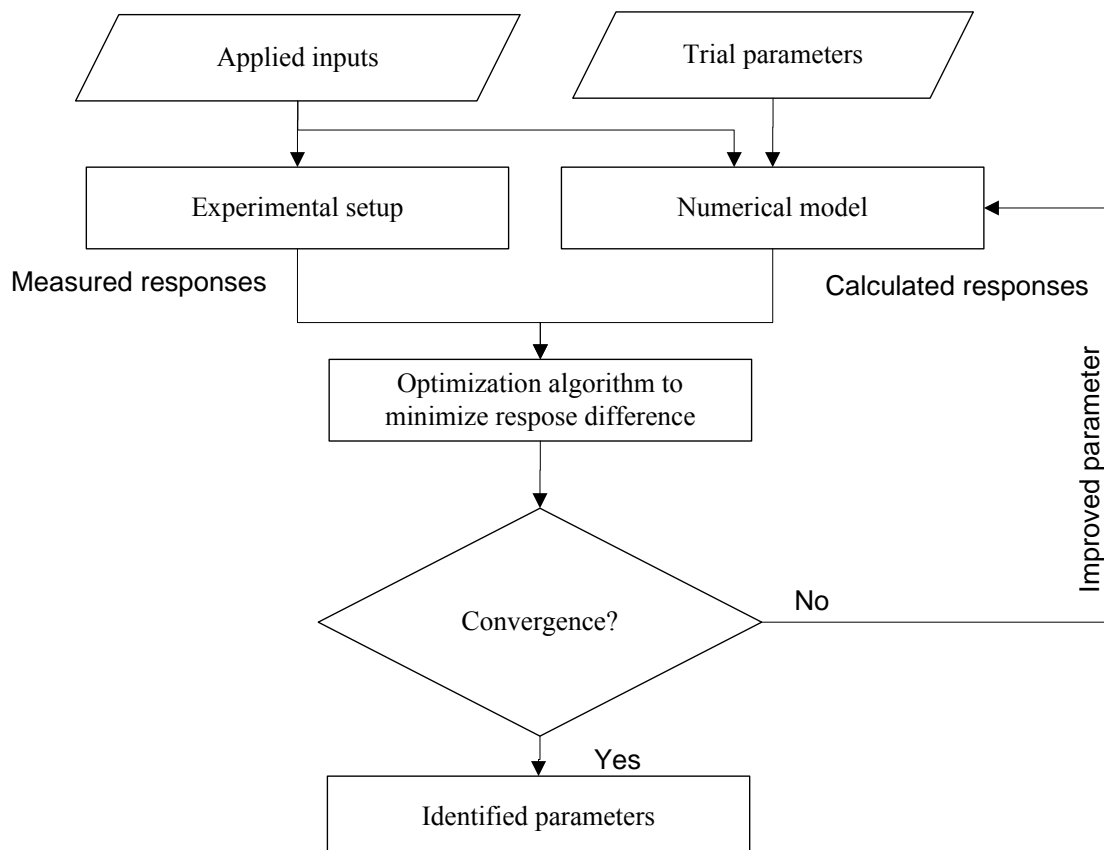


Figure 1.4 The general flow chart of MNET

data in an efficient way. MNETs could play an important role in this process.

1.2.2 MNET approach for identification of material characteristics

In MNETs, the response of a numerical model of a structure is correlated with experimental observations of the real structural behavior. A set of selected parameters in the numerical model is tuned in such a way that the numerically computed structural behavior matches the experimental observations as closely as possible. If the structure under consideration is a relatively simple test specimen, the method can be used for material identification. The unknown material properties are then the parameters in the numerical model of the test specimen. The identification of the elastic constants of a material is an inverse problem that can be formulated and resolved as an optimization problem.

The flow chart of a solution procedure is shown in Figure 1.4. Starting from a random initial trial set (initial solution), the set of elastic constants is updated iteratively (new solution) and this is given as input to an analytical or numerical model simulating the behavior of the structure until its output (calculated response) fits the experimental data (measured response). The last set of constants (the best solution) identifies the elastic properties of the material. In particular, the process attempts to minimize an error function based on the difference between the calculated and measured response of the structure under examination and stops when this becomes less than a specified tolerance. The optimizing technique to be used to generate new guess solutions must be selected on the basis of the number of unknown parameters and the shape of the error function.

The MNETs have proven to be very versatile and flexible tools for identification of material parameters. MNET-based identification routines have been introduced in a wide range of disciplines to estimate a broad variety of material parameters. Various MNETs have been developed till now. They are distinguished primarily by the techniques used for optimization of parameters, the definition of the functional error, the kind of experiments, by the type of experimental data used or the modelling and its numerical solution implementation. The accuracy and convergence properties of these methods depend mainly on the correlation between the experimental conditions and

their numerical simulations (consistency of the model and experiment), the sensitivity of numerical solutions of the model parameters to identify, the sensitivity of the error functional measuring the numerical-experimental correlation and the performance of the adopted optimization technique. Great effort has been devoted to emerging methodologies for the elastic characterization of materials. Such developing methodologies are usually classified into approaches based on static tests and approaches based on dynamic tests.

The static approaches are generally based on the stresses calculated from direct measurement of strains undergone by suitable specimens, during certain mechanical tests (tensile, compression, bending, torsion etc.). ASTM [2] and ISO [3] provide many standards for determining the elastic properties of isotropic as well as composite materials. These norms recommend the use of standard sized and shaped specimens. In the case of composite materials, they involve the analysis of a large number of specimens and consequently tedious and time-consuming procedures [4].

The above-mentioned methodologies usually require a significant range of stress-strain data to determine useful averaged values of the moduli. This necessarily involves destructive tests, as the deformation of the specimen must be measured until it fails, that is, until it deforms plastically or fractures. In either event, the sample is destroyed, and then is unavailable for further testing or other purposes.

In comparison with static approaches, dynamic approaches have the advantage of allowing the use of specimens with a greater variety of shapes and dimensions, and supplying, non-destructively, very precise measurements at a wide range of temperatures. Dynamic approaches can be classified into two groups: wave propagation based methods and modal vibration (or resonant) testing.

Much research has been dedicated to evaluating the possibility of measuring the material elastic properties by the methods belonging to the first group. Among these, the more commonly used is based on the measurement of the ultrasonic speed of wave propagation through the material or, in particular, the measurement of the transit time; i.e. the time that an ultrasonic impulse takes to cross a sample from the emitting transducer to the receiving transducer. Knowing the dimensions and the density of the

specimen and the transit time of the transversal and longitudinal waves it is possible to calculate the Young's modulus and the shear modulus of the material. Although these techniques are robust and quick to perform, they suffer the disadvantage of being sensitive to possible local inhomogeneities of the material between the transducers [5].

Ease of use and inexpensive equipment has recently increased the use of modal vibration testing in both research laboratories and industrial contexts. Such tests consist of making a specimen vibrate mechanically, at one or more vibration resonant modes. Knowledge of the resonant modal shapes and/or the values of the associated frequencies together with the sizes and mass of the sample allow the determination of the elastic constants of the material. ASTM had provided standardized procedures for testing isotropic materials [6, 7].

Independently of the approach followed (static or dynamic) an ideal methodology for determining the material elastic properties is a methodology, which allows the simultaneous measurement of all the unknown elastic parameters by testing a single specimen non-destructively. It would be even better if the methodology is also suitable for characterizing specimens of various shapes. This would be very useful when the production of proper bulk specimens is not feasible or when, the object to be analysed must not be damaged and reduced in a conventional testing geometry and, therefore, should be tested as it is. The review of developed identification methods based on static and dynamic tests are summarised below.

1.2.2.1 Identification based on static tests

The knowledge of the elastic properties of materials is very important for both structural design and engineering applications. Because of such importance, it is not surprising the great number of methodologies developed and presented in the scientific literature, hence, still today, the argument gives rise to a wide interest among the researchers, especially in the context of the development of new and more complex materials, for which the classical methods of characterization appear slow, expensive and not always suitable. When a body is loaded, each point undergoes a displacement whose amplitude depends on: the load, the coordinates of the point, the constraints and the geometry of the body and, obviously, the elastic properties of the material. If the

analytical solution of the adopted loading configuration is available, the elastic properties of the material could be determined by measuring the displacement fields, if the applied loads are previously measured or properly imposed. On the contrary, if a reliable theoretical solution does not exist, a numerical solution becomes necessary. Inverse procedures based on the updating of numerical models could be suitable for this purpose.

The idea of determining the elastic constants of a material from the surface displacement fields of specimens subjected to a static load has been exploited by many researchers [8-22]. Recently, inverse procedures based on FE model updating have been proposed for both point wise by F. Hild and S. Roux [22] and full-field measurements. In the last case, experimental data (usually strain or displacement fields) are measured on the surface of the testing specimen with an optical method, for example, an interferometric technique that measured the full-field surface displacement of an object with a very high resolution without any contact with the investigated surface [23]. Different tests and optical techniques have been used: in-plane loaded rectangular plate with speckle interferometry by K. Genovese, *et al.* [24], open-hole uniaxial tensile tests with Moire interferometry by J. Molimard, *et al* [25], and cruciform specimens under biaxial tests with digital image correlation technique by D. Lecompte, *et al.* [26].

In addition, a method that combines FE analysis and genetic algorithms in order to identify the elastic constants of materials from the full-field measurement of the surface displacements of plates under flexural loads was developed and presented by L. Pagnotta [27]. The method was tested on a thin square plate subjected to an out-of-plane loading condition but it is also suitable for characterizing either thin or moderately thick any-shaped anisotropic plates subjected to in-plane or out-of-plane loading and constraining configurations. In the paper, the feasibility of using the displacement component normal to the surface detected by speckle interferometry was investigated. Theoretical aspects of the methodology, numerical simulations for testing the accuracy and sensitivity of the method and an application to characterize metallic plates were presented.

It is worth pointing out that the amount of data provided by an optical whole-field technique is generally in excess of the data strictly necessary for identifying all the

unknown elastic properties. It follows that any material characterization using this approach becomes an over-posed inverse problem. Obviously, an accurate solution can only be obtained if the problem is well-posed. For this reason, great care needs to be taken in choosing the geometry and the way of loading and constraining the specimen in order to obtain displacement fields containing sufficient information for determining all the unknown parameters quickly and unambiguously. In addition, to reduce the effect of the measurement uncertainties on the solution, the displacement must also be sufficiently sensitive to the variation in each elastic parameter.

A numerical procedure for optimising the loading and constraining conditions of the specimen is proposed by L. Pagnotta in [27]. The procedure consists in determining the conditions, which minimize the "correlation index". This index represents the degree of statistical correlation between the variation in the displacement fields due to a variation in the elastic constants and its absolute value is, by definition, less than or equal to unity. In the case of isotropic plates, the correlation index is the same as the well-known correlation coefficient, while for orthotropic plates the correlation index is the mean of the absolute values of the correlation coefficients.

Such a procedure can be used to identify loading and constraining configurations that are practical and simple to replicate in the laboratory and also optimized with a view to obtaining faster and more stable solutions. Applications of the procedure are presented by L. Pagnotta and G. Stigliano [28] in which it was used to finding a suitable configuration for testing a square plate, and by L. Bruno, *et al* in [29] and [30] for testing any-shaped plates. In [30], an experimental set up and the feasibility of testing isotropic plates of generic form and orthotropic square plates was investigated and the results of the experimental assessment are reported and discussed. The components of the experimental apparatus for measuring the displacements are described with detail by L. Bruno, *et al* [30]. The apparatus was placed on an optical table supported by pneumatic vibration isolators. The laser beam is filtered and expanded and the resulting spherical wavefront is divided by a beam splitter into two equal intensity beams. The specimen and the reference surfaces are horizontal and are illuminated and observed by a 45° oriented mirror with respect to the propagation direction of the beams. The scattered speckle wavefronts interfere at the image plane of the CCD of the TV camera.

The camera is interfaced with a general purpose computer image processing system where the real time fringe patterns are generated by the subtraction of digitalized images. Essentially, the optical setup constitutes a speckle interferometer, based on the Michelson design, for measuring the out-of-plane component of displacements. The applicability and the robustness of the procedure were proved with success on aluminum and unidirectional Graphite laminate specimens. The results obtained for both the materials have shown a high repeatability and a good agreement with the reference values obtained with other measuring techniques [30].

1.2.2.2 Approaches based on dynamic tests

Unlike the static properties of structures, which are often dominated by local phenomena, dynamic properties such as natural frequencies and mode shapes are generally representative of the overall behavior of the materials used, making this information highly attractive for identification of elastic properties of a component. The measurement of natural frequencies of specimens vibrating in a single mode has been used for many years and is still used today for determining the elastic properties of materials. A typical methodology consists in subjecting the specimen to a vibration test to measure a single modal frequency (usually, the first or fundamental mode frequency) and then substituting the measured value into a "frequency equation". Such equations relate the fundamental resonant frequency to the sizes and the mass of the specimen and generally to only one elastic constant of the material. The latter can then be calculated in a direct way if the other quantities are known. Unfortunately, the frequency equations are known only for some simple specimen geometries and boundary conditions. Free-edge specimens such as bars or rods [31] and cantilever beam [32] are commonly used for the characterization of homogenous and isotropic materials. ASTM E1875-00e1 [33] establishes the application procedures for determining Young's modulus, shear modulus and Poisson's ratio of free bars or rods from the fundamental flexural and torsional resonant vibrations. The test consists in forcing the specimen to vibrate at a single but variable frequency by means of a suitable exciter system, while the dynamic response is detected by a proper receiving transducer and transformed into an electrical signal, which is analysed with a suitable system for extracting the fundamental resonant frequencies. Finally, the elastic constants are calculated with some recommended

numerical procedures based on the frequency equations. Even if the test procedures can be carried out automatically by computerized systems [34], they are typically slow and cumbersome. However, the advent of computers has made it possible to fast Fourier transform (FFT) a signal in real time and this has made impulsive excitation more attractive to use. This technique is fast and inexpensive and can be used on either small specimens or full-scale structural components. It is recommended in ASTM E1876-01 [35] for characterizing free-edge bars and rods following procedures similar to those indicated in ASTM E1875-00e1 [33].

It is worth noting that ASTM standards cover the determination of resonance frequencies and elastic properties of specific materials providing test methods that differ one from the other in several ways (for example; sample size, dimensional tolerances, sample preparation). Moreover, nowadays, systems for the elastic characterization of materials based on the standards mentioned above are available commercially (see, for example, [36, 37]). These test methods are particularly appropriate for materials that are elastic, homogeneous, and isotropic and specimens or structures must have specific geometries. Sometimes, the measurement of elastic properties is carried out directly during manufacturing on end products constituted of various materials with geometries different from those mentioned above and in conditions different from the environmental conditions. As a result, there have been a certain number of international patents [38-42].

All the direct methods mentioned above involve beam specimens and resonant frequency measurements. It is worth noting that some direct methods based on single modal testing involving both resonant frequencies measurements and mode shapes measurements have been developed for characterizing rectangular plates. In these methods, estimated analytical solutions providing explicit parameter dependencies are proposed (e.g., solutions obtained applying the Rayleigh method by J. L. Leveque, *et al* [40] or the concept of sinusoidal equivalent length by M. E. McIntyre and J. Woodhouse [43]). These methodologies have, unfortunately, the disadvantage of requiring sophisticated techniques to measure the mode shapes but, in compensation, they are also suitable for the elastic characterization of anisotropic plates.

As highlighted above, direct methods based on single modal testing are easy to apply to simple structures such as beams or rods, but generally, it is difficult to apply them to more complex structures such as plates and shells. More precisely, they are not applicable when the frequency equations are known but modal frequencies depend on more than one elastic constant or when the frequency equations are unknown in a closed form. In these cases, direct or indirect methods based on multiple mode testing must be used.

ASTM Standards [33, 35] provide procedures for isotropic circular thick plates with free edges by which Young's modulus and Poisson's ratio are obtained directly from the first two resonant frequencies of vibration excited by forced continuous wave and impulse, respectively. The shear modulus is then calculated exploiting the well-known relationship for isotropic materials relating it to Young's modulus and Poisson's ratio. Recently, Nieves et al. [44] reported a direct methodology for characterizing free short cylindrical isotropic specimens by using only two of the first resonant frequencies. More recently, Alfano and Pagnotta [45] have proposed a direct method for testing thin isotropic rectangular plate with free edges. Such method is based on suitable approximated frequency equations obtained by correcting the Warburton formulas [46] with proper factors obtained from FE analysis. The procedure requires the measurement of at least two of the first four natural frequencies in order to determine the Young's modulus and Poisson's ratio of the material sample. The experimental assessment of the method was carried out on square plates made with a variety of different materials by M. Alfano and L. Pagnotta [47, 48] and on aluminum rectangular plates by M. Alfano, *et al* [49]. In these papers, tables and formulas for practical use are reported.

It is worth noting that Grediac et al. [50, 51] treated the more general case of anisotropic plate specimens of any shape. In these cases, the frequency equations are not known but they proposed an original approach based on the Virtual Field Method. This method without requiring initial estimates of the stiffness or iterative computations allows the direct determination of the flexural stiffness from natural frequencies and mode shape measurements. When the frequency equations are not available, the inverse problem can also be solved indirectly using iterative optimization procedures. Ohno [52] first introduced a technique using such a kind of identifying procedure. This

technique, known now as RUS (acronym of Resonant Ultrasound Spectroscopy) [53-56], identified the elastic constants through a process minimizing the difference between the calculated and the measured frequency spectrum of parallelepiped-shaped samples. The values of the material elastic constants were updated iteratively in a numerical model able to calculate the resonance frequencies of the sample, until the calculated frequencies approximated as closely as possible to the measured frequencies. The resonance measuring system for very low dissipation materials consisted in a little rectangular parallelepiped specimen lightly held between two piezoelectric transducers. One transducer was used to generate an elastic wave of constant amplitude and varying frequency, whereas the other was used to detect the resonances. The identification of all the elastic constants took place simultaneously without damaging the specimen. Consecutively, Migliori invented a resonance spectrometer which can also be used with high dissipation materials [57] and developed software dedicated to derive the elastic constants from natural resonant response data using the subroutine implemented by Ohno. Today, the RUS technique allows small anisotropic cubic, spherical or cylindrical specimens to be characterized and appropriate instrumentation packages are commercially available.

Successively, numerous different dynamic approaches, the so-called MNETs, for characterizing square or rectangular plates of large dimensions have been introduced in the literature. These approaches require the measurement, in the sonic field, of a small number of natural frequencies of the free plate. W.P. De Wilde et al. [58, 59] and L.R. Deobald and R.F. Gibson [60] almost simultaneously proposed two similar approaches for determining the elastic constants of composite plates with free edges. L.R. Deobald and R.F. Gibson [60] investigated a thin plate with different boundary conditions and discovered that a plate with free-free boundary conditions can obtain better results than that with one or more fixed edges. Dynamic measurements were carried out using the impulse technique. Excitation was induced by impact hammer and a noncontact eddy current proximity probe was used for measurement the response of the plate, while the free-free boundary conditions are approximated by placing the specimen on a soft foam rubber and cotton pads. E. O. Ayorinde and R. F. Gibson [61] obtained the four independent elastic constants of a freely supported rectangular thin plate made from orthotropic materials with orthotropy ratio from one to thirteen, using the classical

lamination theory and an optimized three-mode Rayleigh formulation with a suitably formed least-squares objective function. T. C. Lai and T. C. Lau [62] extended the approach to deal with a generally orthotropic plate. The authors describes a method of finding the elastic constants of a generally orthotropic composite thin plate through modal analysis based on a Rayleigh-Ritz formulation. The natural frequencies and mode shapes for a plate with free-free boundary conditions are obtained with chirp excitation. Based on the eigenvalue equation and the constitutive equations of the plate, an iteration scheme is derived using the experimentally determined natural frequencies to arrive at a set of converged values for the elastic constants.

Gibson and Ayorinde [63], in particular, obtained a patent for a method and apparatus that allow the determination of the four independent elastic constants (longitudinal and transverse Young's moduli, in plane shear modulus and major Poisson's ratio) of a composite material from the modal resonance data of freely-supported rectangular thin plate. The impulse excitation technique together with dedicated software for calculating properties from the vibration data, still today, constitute one of the most popular vibration systems for determining composite elastic constants. Meanwhile, M. E. McIntyre and J. Woodhouse [43] identified both elastic and damping constants of thin orthotropic plates by measuring and analysing the low modes of vibration. The authors used time-honoured method of Chladni patterns for measuring mode. A loudspeaker is mounted beneath a sufficiently large flat surface, and the plate is supported over it on the softest and smallest feasible blocks of foam. These blocks are adjusted to lie accurately under nodal lines of the mode under observation. The loudspeaker is driven by a sine wave generator, and the frequency is adjusted until the plate resonates in the desired mode, as revealed by a suitable powder sprinkled on the surface. Having tuned to the peak response as carefully as possible, the frequency is determined from a standard counter. The main advantages of this method are; one can be sure which mode corresponds to which measured frequency (unlike a method based solely on response function peaks, where identification of which mode corresponds to which peak is harder); the free boundary conditions assumed by the theory are realized quite accurately since, provided the foam blocks are carefully adjusted, the plate vibration is essentially unconstrained by the method of support; and no transducer is attached to the plate, which might perturb the results by adding mass. H. Sol [64] is the

first to use the Bayesian estimation theory in MNET and applied the method to the vibration behavior of anisotropic plates. The MNET he presented identifies the four in-plane engineering constants of an orthotropic material, from the resonant frequencies of the fundamental flexural modes of two beam-shaped specimens, and the first three resonant frequencies of a plate shaped specimen. The analytical approaches based on the Rayleigh-Ritz [58-60, 62-65] or Rayleigh [66-69] methods and the numerical approaches based on the FE method [70-84] have been adopted for determining the elastic constants of materials.

A new method for identifying elastic and damping properties of composite materials has been developed by J. De Visscher, H. Sol, W. P. De Wilde and J. Vantomme [85]. This technique seeks to determine the complex moduli of elasticity by comparison between the measured modal parameters and the results of a numerical model. The damping properties are obtained by comparing experimental modal parameters and the corresponding results from a numerical model in combination with the modal strain energy method. A link between the complex elastic moduli and modal parameters is derived for the case of a thin plate. It is concluded that measurement of modal damping ratio of at least four eigen modes allows for the determination of the four independent loss tangents of the complex moduli. An exclusively non contacting measurement method of high quality based on an acoustic excitation and response measurement by laser Doppler interferometer, suspending the specimen by thin wires attached at the nodal lines of the considered eigen mode is used. The parameters of damping, however, were identified with an error of about 2-15%, which is still a good value. Guan-Liang Qian, Suong V. Hoa and Xinran Xiao [78] presents a method for identifying elastic and damping properties of composite laminates by using vibration test data. The analysis model is established based on a FE model, which considers the effect of transverse shear deformation and hysteretic damping. The reduced elastic constants and material loss factors are selected as the updated parameters. Since the damping mainly causes a change of the imaginary part in eigenvalues and eigenvectors, the complex modal parameters are measured. The selected parameters are identified by minimizing an error function containing the difference of eigenvalues and responses between experiment and analysis. The numerical study shows that satisfactory results including transverse shear moduli can be obtained by designing a suitable plate

specimen. This allows all elastic constants and damping factors to be determined simultaneously.

Thick rectangular plates were used to determine all five of the engineering elastic constants of transversely isotropic materials. In this case, the transverse properties, such as transverse shear modulus, are determined by including not only the effects of bending, but also transverse shear and rotary inertia effects in describing the vibration behavior of the plates [71, 79-81, 83, 86-88].

It has been shown that Poisson's ratio and the transverse shear modulus are not as sensitive, with regard to the eigen frequencies, as the other parameters. A way to avoid this low sensitivity and identify the material properties correctly consists in using a specific size of the plate [43, 65, 87] and/or processing either the natural frequencies or the mode shapes of the plate [61, 66, 67, 69]. The optimal design of the plate has to be determined in advance by preliminary tests. A method was presented in [89] whereby the Poisson's ratio and the other in-plane elastic properties were determined by matching the experimental modal testing results with theoretical modal analysis calculations for a set of plate bending modes and one in-plane compression mode. A great part of these techniques involves the measurement of natural frequencies of samples or structures while only a few of them also involve mode shape observation. whatever the method employed, the apparatus for testing a material must always be constituted by the same components: a device to induce the solid to vibrate, a device for detecting the vibration of the specimen and, a system for extracting the modal parameters from the vibration and calculating the elastic constants.

Continuous variable excitation (generally, forced sinusoidal or random stationary excitation) is commonly obtained by loudspeakers or piezoelectric actuators fed by a variable frequency oscillator, while impulse excitation is produced striking the object with a suitable impulser (e.g., a hammer). Vibrations are generally detected by means of a signal pickup transducer that can be in direct contact with the specimen or not. Contact transducers are commonly accelerometers using piezoelectric or strain gauges, while non-contact transducers are commonly acoustic microphones, but laser, magnetic, or capacitance methods are also used. Pickup transducers transform the mechanical vibration into an electric signal that is successively analysed in order to determine the

resonant frequencies by a system consisting in a conditioner/amplifier, signal analyser, and a frequency readout device. More inexpensively, the electrical signal can be addressed to an ordinary personal computer provided with a sound card and then analysed and processed by a suitable virtual instrument. This latter must operate as a spectrum analyser and then it must transform the sampled time function into a frequency spectrum by a fast Fourier transform algorithm and identify the values of the natural frequencies of vibration. The observation of the mode shapes is generally more difficult than frequency measurements and requires specific and more complex equipment [43, 50, 61, 66, 67, 69, 90].

It should be pointed out that many procedures for the elastic identification involve iterative optimization processes requiring a starting point. Sometimes the solution depends on the starting point (especially when the error function presents more than one minimum) in such cases particular attention must be paid to the choice of the initial guess point. A suitable way to overcome this disadvantage is to use Genetic Algorithms (GAs). Due to the way the GA explores the region of interest, it avoids getting trapped at a particular local minimum and is able to locate the global optimum [91]. GAs does not require initial estimates, but instead work within a suitable set of bounds, which can often be rather broad. For these reasons, during the past few years, GAs have been used, by many researchers, for determining the elastic constants with static approaches [27-30], wave propagation based methods [92-95] and resonant tests [71, 83]. Reference [71], in particular, describes a method combining FE analysis, genetic algorithms and vibration test data. The effectiveness of such a method was successfully verified on thin and thick laminate plates of materials such as carbon/epoxy, glass/epoxy and aluminum. One disadvantage of GAs is their high computational cost.

It has been shown in references [43, 65, 96, 97] that Poisson's ratio is well-determined when aspect ratio $a/b = (E_1/E_2)^{1/4}$. If the aspect ratio is not near to the value provided by this formula the accuracy of Poisson's ratio can be very poor, even making the estimated values completely inaccurate [63]. The considerations reported above hold qualitatively also for moderately thick plates, but in this case, due to the transverse shear effects, the aspect ratio a/b obtained from the formula applies only approximately [97]. Moreover, it must be observed that, when dealing with relatively thin plates, the

dynamic response of the material is rather insensitive to the transverse shear modulus. It is well known that the transverse shear modulus can only be safely predicted from experiments with thick plates [88, 98]. It is important that the specimen be thick enough that the effects of transverse shear become significant. In contrast, it is also essential that the specimen is not so thick as to produce in-plane modes (at least for the number of natural frequencies required for solving the inverse problem) that are much more difficult to detect experimentally than out-of-plane modes. It was found that in any case, plates with material axes parallel to the plate axes appear more advantageous compared to plates having other material directions.

Fällström et al. [66, 67] used a real-time TV-holography system to obtain the modes of vibration. In addition to the Rayleigh-Ritz technique for modelling the vibration of plates, the superposition method was applied by Moussu and Nivoit [99] and FE analysis was used by Fällström and Jonsson [67]. Although, the mixed numerical-experimental approaches have mainly been developed for the characterization of anisotropic materials, they can also be applied to the simplest isotropic materials. Applications of this kind are reported in most of the papers cited above in which they were always carried out with the aim of testing the methodologies proposed. The current greater availability of commercial FE codes for carrying out, quickly and accurately, the dynamic analysis of complex structures, and the low-cost accessibility to large calculation resources, has opened up the possibility of extending the application of the mixed numerical-experimental methods to specimens of various shapes.

An optimizing procedure generates trial solutions (couples of E and ν) and identifies from among them the solution with the lowest error function value. It is worth noting that in the case of isotropic material, each resonant frequency only depends on two elastic properties and, as a consequence, the error function is a function of two variables. The minimization process is obviously simpler than the case of composite materials and will be very fast and accurate if the minimum of the error function is unique and easy to find inside its existence domain. The error function assumed influences the choice of the optimization procedure and, so it is crucial in terms of solution times and accuracy. Different optimization methods and error functions were

compared in [75], in order to select the combination that provides the best compromise in terms of solution time, accuracy and stability of the results. The best performance was obtained combining the square root of the sum of the squares error function with the simplex method. In the same paper, the effectiveness of the procedure has been shown by means of numerical simulations executed on a series of typical and atypical shaped plate models. Moreover, the robustness of the procedure with respect to the effects of measurement noise was assessed. It was observed that the shape of the plate negligibly affects the sensitivity to the experimental errors of the Young's modulus, while the sensitivity of the Poisson's ratio is highly dependent on it. Thus, to avoid incorrect estimations of the Poisson's ratio of plates with particularly complex shapes, before starting the characterization process, a numerical check on the sensitivity of the error function to Poisson's ratio is always recommended. The experimental assessment of such a methodology was carried out with success on thin rectangular plate [70], thin and thick plates of various shapes [73, 76] and irregular drilled plates [74].

This thesis will only consider the resonant-based approach, since it is a very attractive option from both an experimental and a numerical point of view. Resonant based testing is standardised by an ASTM standard [100] which presents a number of analytical formulas to estimate the elastic material properties of homogeneous, isotropic materials. The use of analytical formulas to describe the vibratory behavior of test specimens is, however, the main obstacle for extending the vibration-based methods to more complex materials.

1.2.3 Difference between MNETs and FE model updating

The reader with a background in mechanical engineering might have the impression that MNET is just another name for FE model-updating. Both techniques are based on the same mathematical tools: numerical modelling, correlation analysis, sensitivity analysis and optimization theory. In spite of these important similarities, there is a significant difference. Both methods differentiate themselves from each other based on their main objective. To be more specific, model updating focuses on the mathematical model, while MNETs focus on the model parameters. All other differences between model updating and MNETs are the outcome of this fundamental difference.

The quality of a numerical model can be assessed by determining its conformance to the responses of the real structure. However, every mathematical model is based on a number of assumptions and has therefore a limited accuracy. In the case of FE models, the incorrectness of the model can be caused by approximating the geometry of the considered structure with a limited number of elements, the type of elements and element formulation, uncertainties on the material properties or any other simplification made during the construction of the numerical model. Because of these assumptions and simplifications, the results of the numerical model will not exactly match the experimental responses of the real structure. The objective of model updating is to improve the reliability of a mathematical model by fine-tuning a number of model parameters, in order to obtain an optimal correlation between the numerical results and a set of experimental data.

An MNET aims to identify the values of a set of physical parameters by minimising the differences between a data set measured during an experiment and the results of a numerical simulation of this experiment. Like model-updating routines, MNETs minimise the differences between experimental and numerical results by fine-tuning a set of model parameters. However, the goal of MNETs is not to compensate the shortcomings of the model, but to measure a set of physical properties. This leads to the following practical differences between model updating and MNETs:

1.2.3.1 Precision and accuracy of the numerical model

In model updating, the model parameters are fine-tuned to improve the reliability of the model. In some cases, the simulation model was even deliberately simplified, e.g. to obtain a shorter computation time. This is not a serious problem, since the optimised parameter values can compensate the inaccuracies of the model. However, the optimised parameter values will only compensate the inaccuracies of that particular model. The optimised parameters are thus model-dependent and meaningless, if they are not used in combination with the associated model. MNETs aim at identifying the values of physical parameters, which are by definition model-independent. The inaccuracy of the simulation model of a certain MNET will have a negative effect on the quality of the identified parameters. Therefore, the mathematical model of any

MNET should be as accurate as possible. This can only be achieved by combining a rather simple experiment with a detailed simulation model.

1.2.3.2 Selection of the variable parameters

The proper selection of the updating parameters is a key step for the successful updating of a FE model. If the selected model parameters are indeed the ones with incorrect values, the procedure should converge and yield an updated model that is reliable. On the contrary, if the model parameters with correct values are selected, the updating process might not converge or might yield a model that is not very reliable or contains parameters with unrealistic values. Usually, the selection of the proper updating parameters is a difficult process, however in the case of an MNET this process is very straightforward. The updating parameters are simply the ones that represent the physical quantities that have to be identified.

1.3 FOCUS OF THE THESIS

The main objective of this thesis was to develop a vibration-based identification procedure to determine the elastic properties of the foam materials. In order to achieve this objective, a lot of intermediate steps had to be taken, some of which provided better insight in vibration-based material identification or resulted in new identification procedures for foam materials. More specifically, the original contributions of this thesis are:

- To develop a FE model based on inhomogeneous mass distribution in aluminum foam using the density data measured by X-ray computer tomography.
- To extract the experimental modal characteristics of aluminum foam using a precise measurement setup.
- To develop a mixed numerical experimental identification technique based on modal characteristics, for extraction of elastic properties of the said material.
- To investigate the influence of inhomogeneous density distribution on the mechanical behavior of aluminum foam.

- To investigate the influence of mesoscopic inhomogeneous density distribution on the modal characteristics of aluminum foam.

1.4 STRUCTURE OF THE THESIS

Due to the multidisciplinary approach of the proposed development, the structure of this thesis is reported into six chapters, each chapter (from chapter 1-4) corresponds to the different research areas addressed. This chapter (Chapter 1) lists the State of current knowledge in the field of MNETs for identification and objectives of this research study. The experimental setup for modal testing and analysis is explained in Chapter 2. The material to be investigated and details of the developed FE model based on inhomogeneous density distribution will be explained in Chapter 3. Chapter 4 is dedicated to the developments of new mixed numerical experimental identification technique. This section constitutes the heart of the thesis. Finally in chapter 5 the obtained results are compared with each other and the applicability of the developed model will be discussed. A summary of each chapter is given here.

Chapter 2 describes the experimental modal testing and analysis setup. The developed process of the vibration measurement technique aims to measure the vibration response of the test specimen by maximum mastering the experimental boundary conditions. Indeed, any model error in mixed numerical-experimental identification process would be based on accurate measurements, so a high correlation between the experimental measurement conditions and FE modelling is necessary. This is done by selecting and carefully controlling the boundary conditions of the test specimen under investigation. The boundary conditions include the support of the specimen, the technique of dynamic excitation, effect of the vibration response measurement system and the effect of vibrations from surroundings (environmental conditions). The main purpose of experimental modal testing setup developed for this work is to measure a large number of modes (eigen frequencies and mode shapes) of aluminum foam specimens, as precisely as possible. The objective is to obtain a wide range of experimental values that serve as targets for the mixed numerical experimental identification method. Thus, a well controlled and reproducible measurement setup is developed for measurement of modal characteristics of aluminum foam specimens.

Chapters 3 summarize the FE modelling of aluminum foam. Literature on porous metals and metallic foams is increasing at a fast pace, supported by conferences, symposia, seminars, books and web sites. Most of the recent R&D activities on closed-cell metallic foams have focused on the development of aluminum based foams. Inhomogeneous mass distribution within the aluminum foam is obtained by X-ray Computer Tomography (CT). The distribution of local relative density is calculated using density mapping method based on CT data. Heterogeneous microstructure of aluminum foam is transformed to an approximated continuum. The obtained continuum body is then implemented in FE method. A 3D FE model is describe to simulate the effect of local mass distribution on modal properties of the aluminum foam specimen. The specifications of investigated specimen of aluminum foam and details of their density mapping are presented in this chapter.

Chapter 4 is completely devoted to the implementation of the proposed mixed numerical experimental identification technique. The different routines developed for parametric study are explained with the help of block diagrams. The modal error norms used for identification are explained in details. Parametric study of large-scale FE analysis on aluminum foam plate to identify the robustness and sensitivity of the proposed modal error norms is presented. Analysis, selection and implementation of optimization algorithm corresponding to needs are explained in detail. The Levenberg-Marquardt algorithm with assessment of gradients by finite difference method is used for optimization and is implemented in mixed-numerical experimental identification technique for minimization of modal error norms.

Chapter 5 is focused on the description of the results obtained from the modal testing and the developed identification technique. Four aluminum foam specimens are investigated, their modal properties are explained in detail. Identification of variable parameters of aluminum foam FE model is presented to illustrate the application of the developed identification technique.

Chapter 6 include summary of the research work. In addition, suggestions for the advancement of research in future developments are given.

CHAPTER 2. EXPERIMENTAL MODAL TESTING AND ANALYSIS

2.1 OBJECTIVE

For the prediction of the global properties in materials, dynamic tests have shown important advantages over static tests. Despite the superiority of dynamic tests, a high level of precision is required on the measured modal information. The accuracy of the constitutive properties estimated with mixed numerical-experimental identification technique depends directly on the quality of the experimental measurements and on modelling the actual test conditions. To characterize aluminum foam by MNET, use of measured modal information as a basis of comparison seems a wise choice in terms of accuracy and representativeness. The purpose of this section is to develop a technique to measure the eigen frequencies and modes shapes of aluminum foam specimens, accurately. Free boundary conditions have been chosen for the specimens tested, in order to improve the correlation between the experimental test setup and the numerical model.

2.2 THEORETICAL BACKGROUND

In linear vibration theory the deformations of a mechanical structure can be simulated either by discrete or continuous models or by a mixture of both. In general, for the reason of computational effort, the number of degrees of freedom (DOF) of a given structure is limited to a certain number of translational and angular displacements at given structural mesh points. The generalized displacement vector

$$\mathbf{q} = \{\mathbf{q}_1, \mathbf{q}_2, \mathbf{q}_3, \mathbf{q}_4 \dots \mathbf{q}_n\}^T \quad (2.1)$$

contains these n (number of DOFs) independent displacements, which are assumed quite small as compared to the dimensions of the structure. The experimental study of the dynamic behavior of a structure is traditionally based on discretization of the structure into a set of measuring points, thus forming an experimental mesh.

Subsequently, all necessary measurements and analysis are based only on these mesh points. An example of a discrete model of the structure is shown in Figure 2.1.

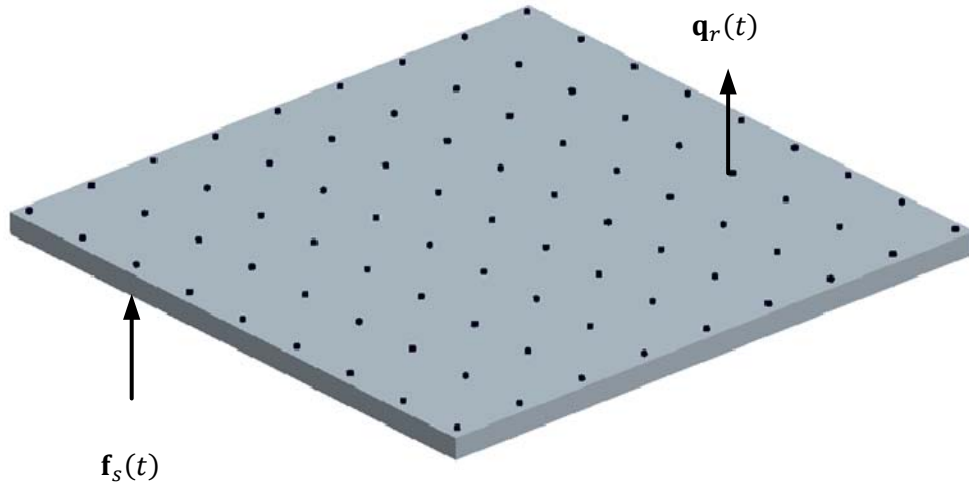


Figure 2.1 Measurement grid points

The experimental modal analysis of a structure usually assumes that the dynamic behavior described by the equations of motion of the system can be represented by a system of linear differential equations with constant coefficients as a function of time. The equations of motion for the displacement vector \mathbf{q} of a vibrating structure have the usual form

$$\mathbf{M}\ddot{\mathbf{q}}(t) + \mathbf{D}\dot{\mathbf{q}}(t) + \mathbf{K}\mathbf{q}(t) = \mathbf{f}(t) \quad (2.2)$$

With \mathbf{M} , \mathbf{D} , \mathbf{K} being constant $(n \times n)$ – dimensional mass-, damping-, and stiffness- matrices, respectively. The vectors $\mathbf{q}(t)$ and $\mathbf{f}(t)$ represents the field of displacements and external excitation forces acting on the degrees of freedom of the mesh points, respectively.

Considering first the damped harmonic system (2.2) in its homogeneous form (free vibration response, $\mathbf{f}(t) = 0$), from differential equation theory the solution can be assumed to be of the form

$$\mathbf{q}(t) = \boldsymbol{\varphi}_k e^{-\lambda_k t} \quad \text{where } \lambda_k = -\delta_k \pm j\omega_k \quad (2.3)$$

Where λ_k is the k -th complex eigenvalue (whose real and imaginary parts represent the modal damping coefficient δ_k and the angular frequency ω_k) and $\boldsymbol{\varphi}_k$ is the corresponding eigenvector.

As $e^{-\lambda_k t} \neq 0$ for any instant of time t , so taking appropriate derivatives and substituting the solution (2.3) in the homogeneous form of equation (2.2), the generalized eigenvalue problem from the equation of motion of the system is obtained.

$$(-\lambda_k^2 \mathbf{M} - \lambda_k \mathbf{D} + \mathbf{K}) \boldsymbol{\varphi}_k = 0 \quad (2.4)$$

The solution of equation (2.4) is composed of k -th eigenvalues λ_k^2 and corresponding eigenvectors $\boldsymbol{\varphi}_k$ ($k = 1, 2, 3, \dots, n$). The square roots of these eigenvalues are the natural frequencies of the system and the eigen vectors its mode shape. From linear algebra it is known that, if the natural frequencies are non-zero and distinct, then all the mode shapes are independent. Therefore, ' n ' eigenvectors $\boldsymbol{\varphi}_k$ ($k = 1, 2, 3, \dots, n$), due to their orthogonality properties, are linearly independent (no vector in the set can be obtained by a linear combination of the remaining ones) and therefore ' n ' mode shapes collectively form a basis in the ' n ' vector space. Thus, mode shapes are able to 'diagonalize' the matrix equation of motion (2.2) and decouple the ' n ' intertwined equations into ' n ' independent equations.

By transforming the system (2.2) in the modal coordinates, it is possible to decouple the differential equations of the system. The relation corresponding to this projection is written as,

$$\mathbf{q}(t) = \sum_{k=1}^n X_k(t) \boldsymbol{\varphi}_k = \boldsymbol{\Phi} \mathbf{X}(t) \quad (2.5)$$

Where X_k ($k = 1, 2, 3, \dots, n$) denotes the modal or principal coordinate of mode k . The vector \mathbf{X} assemble all the modal coordinates of the vector space \mathbf{q} , while the matrix $\boldsymbol{\Phi}$ is the modal matrix built up from all mode shape vectors $\boldsymbol{\varphi}_k$ ($k = 1, 2, 3, \dots, n$) of the system. Pre-multiplying the equation (2.4) by $\boldsymbol{\Phi}^T$, and using the principal of

orthogonality, this equation can transform into an uncoupled equation of motion. Thus through a simple coordinate transformation, the system has been transformed into ‘ n ’ uncoupled equations of motion. This equation (2.6) is the foundation of vibration analysis for multiple degree of freedom systems.

$$m_k \ddot{X}_k(t) + c_k \dot{X}_k(t) + k_k X_k(t) = \boldsymbol{\varphi}_k^T \mathbf{f}(t) = F_k(t) \quad (2.6)$$

for ($k = 1, 2, 3, \dots n$). Where m_k , c_k and k_k are called the modal mass, modal damping, and modal stiffness of the k -th mode respectively, but they do not have the same units as mass and stiffness. In equation (2.6);

$$m_k = \boldsymbol{\varphi}_k^T \mathbf{M} \boldsymbol{\varphi}_k, \quad c_k = \boldsymbol{\varphi}_k^T \mathbf{D} \boldsymbol{\varphi}_k \text{ and } k_k = \boldsymbol{\varphi}_k^T \mathbf{K} \boldsymbol{\varphi}_k \quad (2.7)$$

Note also that the force term $\mathbf{f}(t)$ is transformed by projection into the modal coordinate, the modal excitation force $F_k(t) = \boldsymbol{\varphi}_k^T \mathbf{f}(t)$.

By applying Fourier transformation to equation (2.6) and isolating certain terms, an expression for the contribution of k -th mode to the system response is obtained. This transformation has the advantage of converting a differential equation into algebraic equation. Thus, equation (2.6) can be written as:

$$X_k(j\omega) = \frac{F_k(j\omega)}{m_k(\omega_k^2 + 2j\zeta_k\omega_k\omega - \omega^2)} \quad (2.8)$$

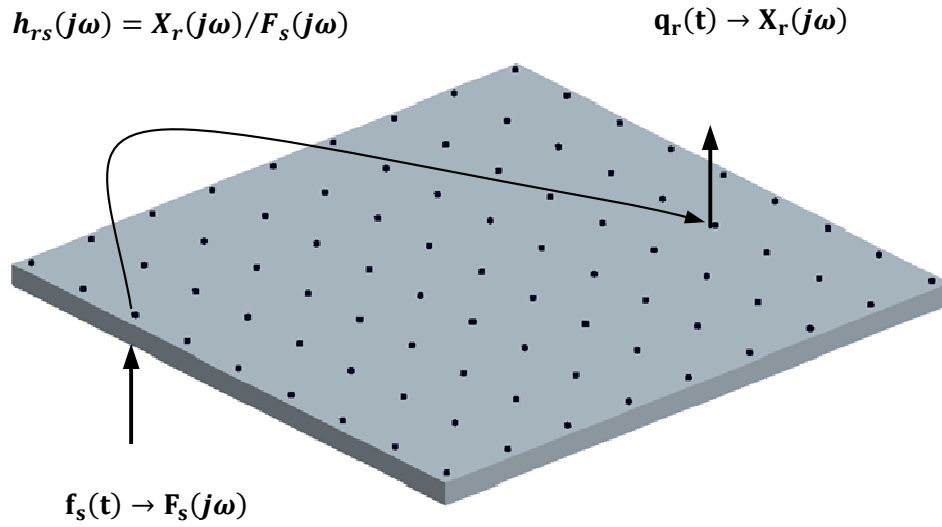


Figure 2.2 Experimental mesh and transfer functions

Where ζ_k is the modal damping (damping ratio) and ω is the angular frequency. The denominator of equation (2.8) is known as characteristic equation of the system. Summing the contributions of each mode, the expression for the transfer functions of discrete system can be written as;

$$h_{rs}(j\omega) = \frac{X_r(j\omega)}{F_s(j\omega)} = \sum_{k=1}^n \frac{\varphi_r^k \varphi_s^k}{m_k(\omega_k^2 + 2j\zeta_k \omega_k \omega - \omega^2)} \quad (2.9)$$

Where $h_{rs}(j\omega)$ is known as frequency response function of the system. The frequency response function relates the Fourier transform of the system input to the Fourier transform of the system response. The transfer function $h_{rs}(j\omega)$ represents, in the frequency domain, the response in degree of freedom r due to single harmonic excitation force of unit magnitude and frequency ω applied in degree of freedom s or, in other words, the Fourier transform of the impulse response. Thus, the system of differential equations of the spatial formulation of the problem (2.2) turns into a matrix of transfer functions $\mathbf{H}(j\omega)$ which completely describes the dynamics of the system. By reworking expression 2.9, it is possible to write transfer functions matrix $\mathbf{H}(j\omega)$ as follows;

$$\mathbf{H}(j\omega) = \sum_{k=1}^n \frac{1}{m_k(\omega_k^2 + 2j\zeta_k \omega_k \omega - \omega^2)} (\varphi_k \otimes \varphi_k) \quad (2.10)$$

In this equation, the transfer function matrix have sum of all modes k ($k = 1, 2, 3, \dots, n$) of frequency factors (the fraction $j\omega$) and spatial (dyadic product of eigen vectors). As this matrix is derived from the dyadic product of a vector with n components, it is enough to know n distinct components in order to determine the matrix $n \times n$.

It has been seen that the dynamic properties of a system with n DOF may be describe by three types of models: the spatial model, the modal model and the response model. Each spatial model of a structure is characterized by the matrices \mathbf{K} , \mathbf{C} , \mathbf{M} and the vectors $\mathbf{q}(\mathbf{t})$ and $\mathbf{f}(\mathbf{t})$, it correspond to a frequency response model defined by the matrix $\mathbf{H}(j\omega)$ and the spectra $\mathbf{X}(j\omega)$ and $\mathbf{F}(j\omega)$, and also to a modal model consisting of the modal vector φ_k and scalar ω_k , ζ_k , m_k , $X_k(t)$ and $F_k(t)$ for ($k = 1, 2, 3, \dots, n$). Modal analysis, as an experimental or numerical technique is designed to identify the parameters of modal model from spatial or frequency response model. In the experimental area, modal analysis approach is generally as follows:

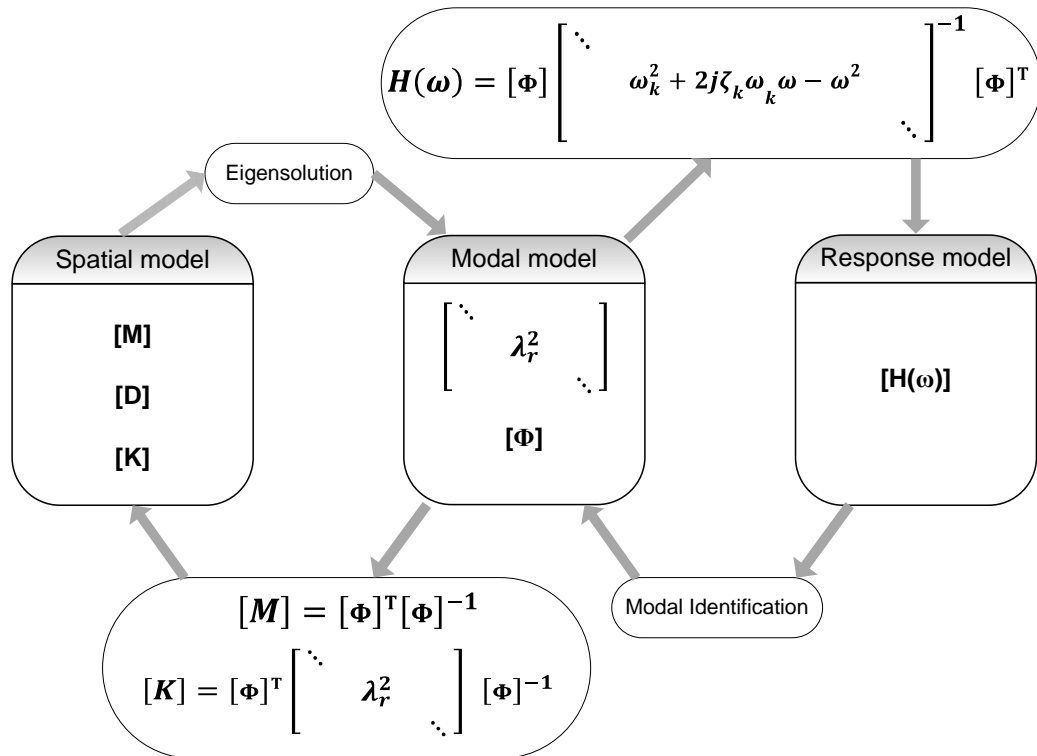


Figure 2.3 Dynamic model interrelation

2.2.1 Establishment of temporal model

The structure under study is positioned with the representative support conditions and is discretized into a set of measuring points. It is then excited at one point s with a force $\mathbf{f}_s(t)$. Simultaneously responses $\mathbf{q}_r(t)$ at each point r of the structure and the excitation force $\mathbf{f}_s(t)$ is recorded. The temporal model (time domain) of the structure is then completely determined by the functions $\mathbf{q}_r(t)$ and $\mathbf{f}_s(t)$ measured during the experiment.

2.2.2 Transformation of the temporal model in frequency model

The temporal model characterized by measured functions $q_r(t)$ and $f_s(t)$ is converted into a set of complex spectra $X_r(j\omega)$ and $F_s(j\omega)$ with a Fourier-transform (generally discrete Fourier transform and Fast Fourier Transform or FFT). Transfer

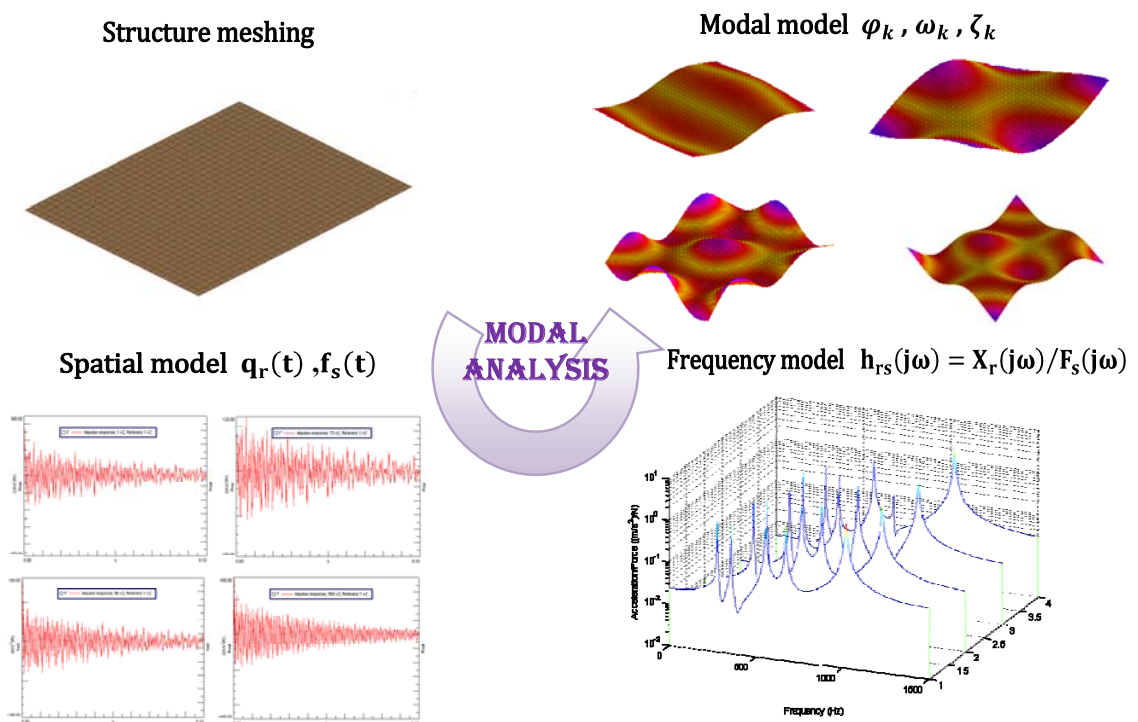


Figure 2.4 Experimental modal analysis stages

functions (also called frequency response functions) $h_{rs}(j\omega)$ are then calculated using the quotient $h_{rs}(j\omega) = X_r(j\omega)/F_s(j\omega)$ of frequency response spectra $X_r(j\omega)$ and excitation $F_s(j\omega)$. The frequency model is then completely defined when a row or column of the matrix $\mathbf{H}(j\omega)$ is determined.

2.2.3 Estimation of modal parameters

The modal model is created by identifying the set of modal parameters $\boldsymbol{\varphi}_k$, ω_k , ζ_k and m_k for all modes k ($k = 1, 2, 3 \dots n$) from the frequency model $\mathbf{H}(j\omega)$. Because of inertial effects, the dynamic response of the structure is, however, usually dominated by the influence of the modes of lowest eigen frequencies, so it is possible to address only a limited number of modes without losing information on the dynamics of whole structure under investigation. Each mode requires the determination of eigen vector $\boldsymbol{\varphi}_k$ with n components and at least two modal parameters (ω_k and ζ_k), the identification problem to be solved become rather complicated at given the large number of parameters to be extracted. However, thanks to the local characteristics of the resonance peaks, the identification of modal parameters can usually be done independently for each mode or each group of modes (Figure 2.5).

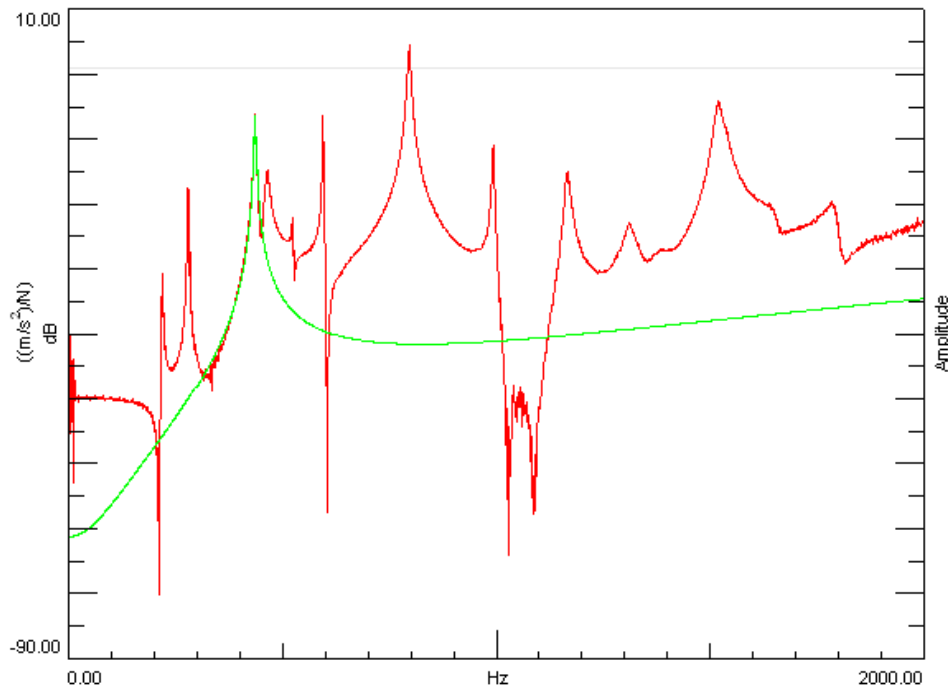


Figure 2.5 Identification of the third mode from the transfer function of the structure

2.3 NON-CONTACT VIBRATION MEASUREMENTS TECHNOLOGY

The main purpose of experimental modal setup developed for this work is to measure eigen frequencies and mode shapes of aluminum foam samples, as precisely as possible and noninvasive. The objective is to obtain a wide range of experimental values that serve as targets for the mixed numerical experimental identification technique. The experimental measurement conditions should ensure optimal correlation with the numerical simulating model. Thus, the experimental method must be well controlled and reproducible and should be very accurately simulated in a FE model.

A high correlation between the experimental conditions and FE modelling can be ensured by selecting and carefully controlling the boundary conditions of the test specimen under investigation. The boundary conditions include the support of the specimen, the dynamic excitation technique, effect of the vibration response measurement system and the effect of vibrations from surroundings (environmental conditions).

The development process of the vibration measurement technique aims to measure the vibration response of the test specimen by maximum mastering the experimental boundary conditions. In the field of modal analysis, this objective is the minimization of any effects of added mass to specimen, or additional external rigidities and external damping effects, which are more difficult to control. The optical measurement methods can minimize the effects of added mass and stiffness and external damping, in this category, the method of laser Doppler interferometry is the only one to provide an excellent frequency resolution and high dynamic in a frequency range sufficient to measure aluminum foam specimens. Thus, in order to minimize these undesirable effects, the commercial optical measurement system, Polytec Scanning Vibrometer is used for response measurements. Moreover, as this method can be automated by redirecting the laser beam to change the point of measurement, it is easy to perform measurements of mode shapes with a spatial resolution sufficient for identification purposes.

2.3.1 Polytec Laser Doppler Vibrometer

Commercial Laser Doppler Vibrometer (LDV) systems consist of two major components: the optical sensor and the data acquisition system. The optical sensor contains the actual laser, the optical elements, and electrical components needed to spatially position the laser beam. The controller processor, containing the electronic components needed to process the velocity information provided by the optical sensor, constitutes the interface between the interferometer and the data acquisition computer. The data acquisition system consists of the equipment and software needed to manipulate the scan mirrors and to acquire the velocity data.

Commercial system Polytec Scanning Vibrometer (PSV) a product of Polytec is available at institute (Institute of Mechanics and Mechatronics, TU Wien). The Polytec system is a modified Mach-Zehnder interferometer, which allows the laser beam to exit from the "inner" interferometer cell and to hit the external target. A linearly polarised He-Ne laser is employed as a light source, which has polarisation orientated at 45° to the horizontal plane.

Polytec uses as coherent light source a multi-mode (in the longitudinal direction) Helium-Neon laser, linearly polarised with an output power between 2.2 and 3.0 mW. This fact means that there are several modes of oscillation, with different wavelengths, in the laser length (longitudinal axis), while only a transverse mode is dominant in the distribution of light across the beam and this is the uniphase mode TEM_{00} (characterised by its Gaussian profile and circular symmetry). It is important that in the transverse direction only one mode occurs, since other transverse modes have frequencies slightly different from the TEM_{00} mode and their beating may be then confused with the Doppler signal. On the contrary the occurrence of multi-modes in the longitudinal direction is not so critical, because they can be distinguished by their distinct numbers of wavelengths within the laser length. In order to privilege one mode (say the one with wavelength λ) the optical path length travelled by the wave that is twice the cavity length (distance between the mirrors placed in the laser oscillator system) must equal a whole number of wavelengths:

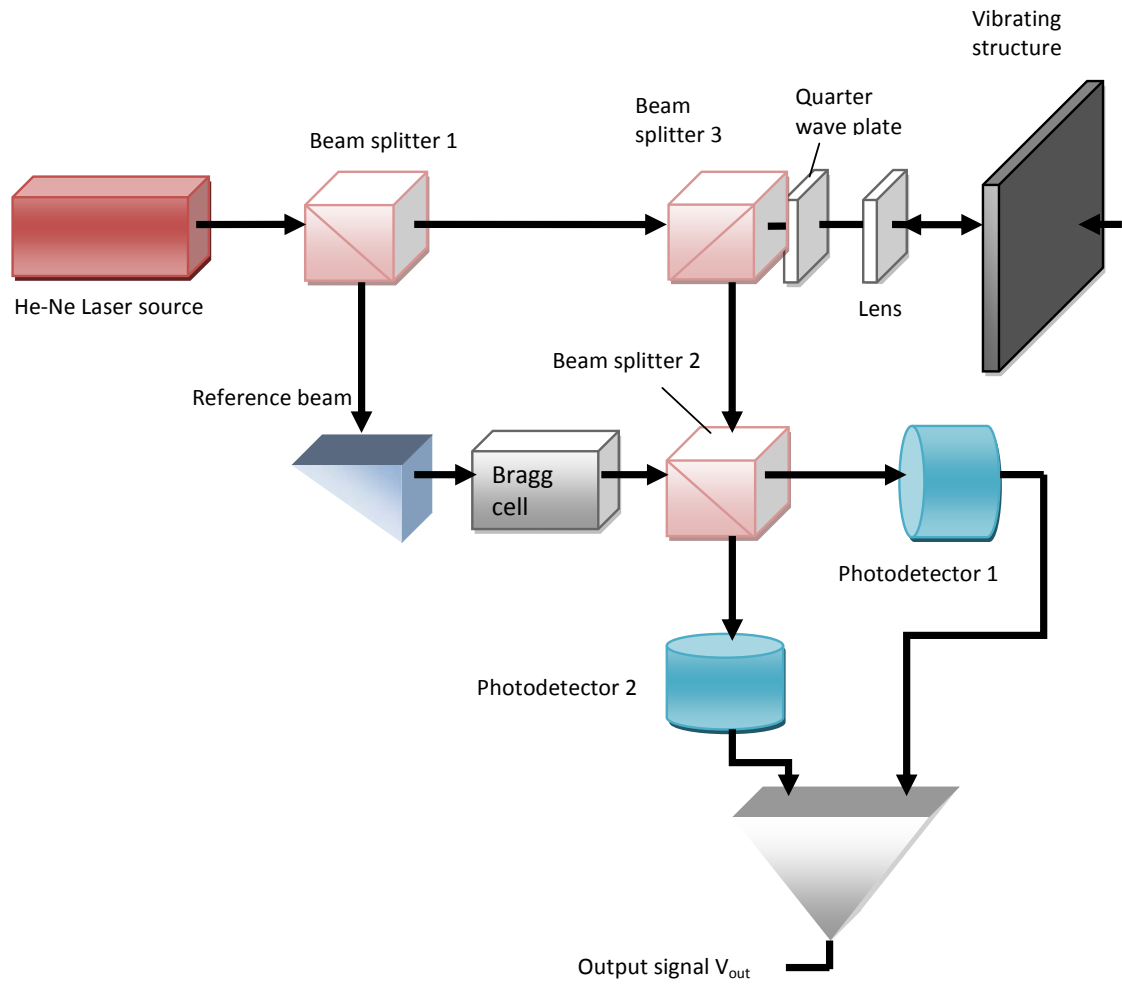


Figure 2.6 Polytec LDV arrangement

$$2L_c = \eta\lambda \quad (2.11)$$

Where L_c is the cavity length and $\eta = 1, 2, 3, \dots$. In this case the wave passing backwards and forwards between the mirrors reinforces itself each time around because each successive passage is in phase. The cavity length in the Polytec laser head is 205 mm [101]. In order to assure that the same longitudinal mode will be emphasized during the travel of the laser beam towards to and backwards from the object tested the path followed (L_p) must be an integer multiple of the cavity length:

$$2L_p = \eta L_c \quad (2.12)$$

Where now $\eta = 2, 3, \dots$. Since the minimum optical path of the beam must be at least twice the cavity length. L_p can be seen as a sort of 'coherence repeat distance' because it is the length where the Doppler interference is maximum and the signal output from the laser is also maximum. Therefore, if during the operation, a signal level minima is encountered, i.e. fluctuations of signal level occur mostly in the course of the laser warm-up, a change of the operating distance of half cavity length should resolve the problem.

The Polytec system is a modified Mach-Zehnder interferometer [102]. A third polarising beam splitter with a quarter wave plate is introduced at the place of the actual moving target (in Mach-Zehnder interferometer) in order to realise a directional coupling: the light coming from the laser is directed straight through the object, while the reflected beam is deflected downwards to the second beamsplitter. The quarter wave plate is used as optical insulator, in order to avoid that the light reflected by the target can return towards the laser source. This optical element, also called retardation plate, has the main characteristic to modify the polarisation of the wave incident. In the case of quarter wave plate the polarisation direction is deviated of $1/4$, i.e. 45° . The entry beam, coming from the polariser beam splitter, see Figure 2.7, owns a polarisation of 45° with respect to the plate axis, then it is transformed in a circularly polarised beam inside the plate. Being reflected back by the target surface the rotation is inverted and

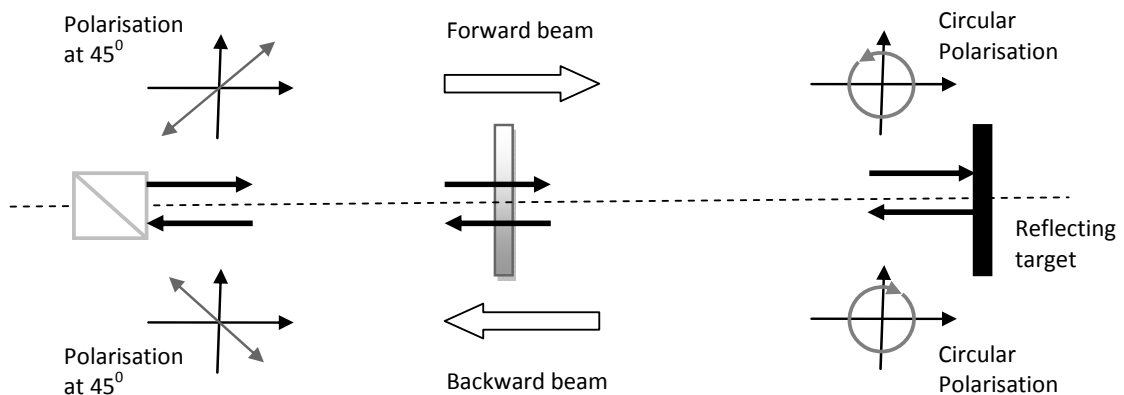


Figure 2.7 Quarter wave plate working principle

the travel across the plate will transmit to the beam a polarisation of 45° but on the opposite direction. Owing this polarisation the light cannot pass again inside the beam splitter and it is deviated downwards.

Therefore, a second difference with the Mach-Zehnder configuration is the insertion of a Bragg cell as a device to discriminate the target velocity direction. The frequency shift introduced is 40 MHz. The light intensities $I_1(t)$ and $I_2(t)$ seen by the photodetectors have the following relationships.

$$I_1 = \frac{1}{2} K_1 A^2 \left\{ 1 + \cos \left[2\pi \left(f_b \pm \frac{2v}{\lambda} \right) t \right] \right\} \quad (2.13)$$

$$I_2 = \frac{1}{2} K_2 A^2 \left\{ 1 - \cos \left[2\pi \left(f_b \pm \frac{2v}{\lambda} \right) t \right] \right\} \quad (2.14)$$

Where A is the amplitude of the optical signal of the laser, f_b denotes the frequency shift (controlled) of the Bragg cell and v represents the speed of the vibrating object, λ is the wavelength of the beam provided by the laser. Both output signals from the photodetectors, which actually are photodiodes, are converted to electrical signals. Combining them together using a differential pre-amplifier stage the resulting output voltage V_{out} is given:

$$V_{out} = K \cos \left[2\pi \left(f_b + \frac{2v}{\lambda} \right) t \right] \quad (2.15)$$

Where K indicated the conversion efficiency. The voltage V_{out} constitutes the output signal of the interferometer and it is transmitted to the processor controller where the Doppler signal is frequency demodulated to extract the velocity information. To improve the signal quality, affected by velocity drop-outs, the Polytec system has introduced in the controller an optional device, which is the tracking filter². The continuous nature of the Doppler signal from a solid surface measurement allows frequency tracking demodulation. To obtain real time demodulation of photodetector signal giving voltage proportional to instantaneous velocity component a tracking filter is activated instead of using a conventional spectrum analyzer. The tracking scheme is applying the principle of Phase Locked Loop (PLL), where a Voltage-Controlled Oscillator (VCO), controlled via the feedback loop, tracks the incoming Doppler signal

[103]. A mixer at the input stage produces an "error" signal between the Doppler and VCO frequencies which is band-pass filtered and weighted before being integrated and used to control the oscillator to drive the error to a minimum. The feedback loop has an associated "slew rate" which limits the frequency response of the processor. The overall effect of the tracker is to act as a low pass filter, which output the VCO voltage as a time, resolved voltage analogue of the changing frequency. The frequency range of interest for most vibration measurements is well within the range of this form of frequency demodulation. The tracker incorporates weighting networks, which tailor the control of the VCO according to the signal to noise ratios of the incoming signal. The network will hold the last value of Doppler frequency being tracked if the amplitude of the signal drops below a pre-set level. In this way the Doppler signal effectively drops out and careful consideration must be given to the statistics of what is essentially a sampled output, especially when high frequency information of the order of a dropout period is required. Fortunately for most practical applications this period, typically $0.2 \mu\text{s}$, is negligible. Another option provided within the Polytec LDV is the auxiliary filter, which is applied to the force-signal to compensate for filter gain and phase-shifts.



Figure 2.8 Polytec system components, work station, controller OFV-3001-S, junction box PSV-Z-040



Figure 2.9 Polytec scanning head

A measurement system Polytec PSV 300-F scanning laser Doppler vibrometer is available at institute (Institute of Mechanics and Mechatronics, TU Wien), keeping in view the advantages of this measurement technique, it is decided to use this measurement tool for modal characteristics of the structures. The Polytec Scanning Vibrometer measures the two-dimensional distribution of vibration velocities on the basis of laser interferometry. The system components are shown in Figure 2.8 and Figure 2.9.

The interferometer signal is decoded in the controller with the velocity decoder. An analog voltage signal is thus generated which is proportional to the vibration velocity. The junction box is the central connection point between the system components and provides the interfaces for peripheral devices. The scanning head (Figure 2.9) consists of the interferometer, the scanners to deflect the laser beam and a video camera to visualize the measurement object. The measurement data is digitally recorded in the workstation. The software controls the data acquisition and offers user-friendly functions to evaluate the measurement data.

The heart of the system is the optical sensor head (OFV-056) which consists of a single-point interferometer which focuses the laser beam towards the x-y scanner mirrors driven by the scanner driver electronics. Further, a compact video camera is installed in the case of the head for the visual observation of the test item and the scanning procedure. In fact, by means of a video control box settled on the PSV computer, the grid of measurement points to be followed over the structure surface is defined on top of the video image displayed on the computer monitor. In order to

perform a correct measurement, the laser beam must be aligned to the video image and this is done by a calibration routine included in the Polytec software (PSV-200, version 7.2). This routine automatically corrects parallax errors and distortions to allow accurate positioning of the beam. In conjunction with the optical head there is the electronic signal processor/controller unit (OFV-3001-S) which controls the measuring parameters and processes the output of the laser sensor in order to derive the velocity information.

This dynamic test system allows to measure vibration velocity ranging from a few $\mu\text{m/s}$ to several m/s over a frequencies range from 10 Hz to 250 kHz. The software controlling the acquisition system allows easy measurement of transfer function on grids of points up to more than 300×300 points and provides intuitive function of post-processing and visualization of Spectra, frequency response functions and measured modes.

2.4 SUPPORT OF THE STRUCTURE

In the measurements encountered in solid mechanics and structures, the support conditions of a test specimen generally represent an important source of side effects often not repeatable or easily quantifiable, making it very difficult analytical or numerical modelling of actual experiment. The boundary conditions of the plates in the static tests are usually common type clamping fixture or simply supported. Although this kind of support conditions seem easy to model using FE and appears to provide a good correlation between numerical model and measurement technique, it is not the case in practice. Indeed, it is almost impossible to achieve a perfect stiffness (fitting rigidity) and attempts to achieve a good approximation of these boundary conditions do not generally provide repeatable results close to few percent. For example, in the case of a simple clamping fixture, the torque of fixing clamping screw can strongly influence contact pressure used to hold the specimen and thereby introduce significant variation in local stiffness of the fixture. Similarly, the conditions for simple supports in the analytical models or FE are not feasible in practice due to the significant thickness of actual specimens and local effects of friction and detachment.

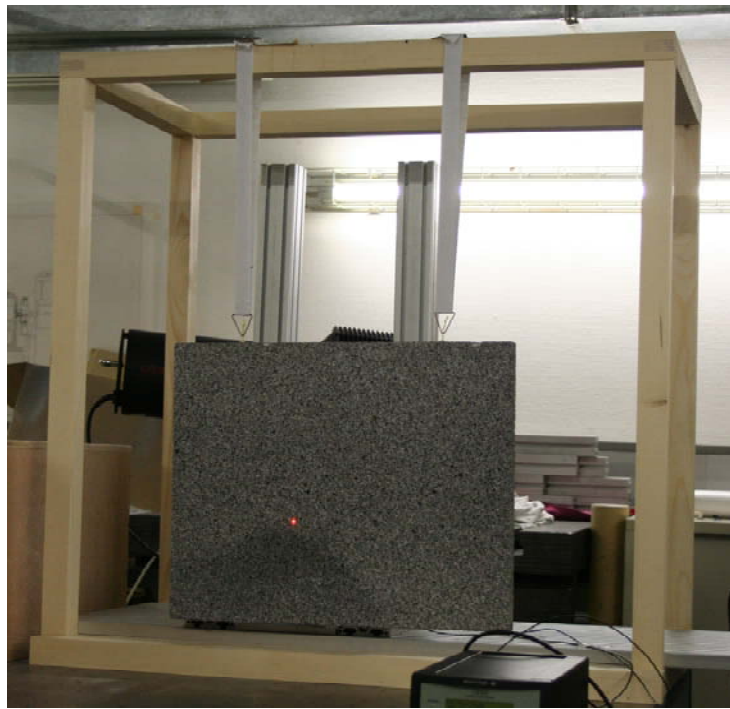


Figure 2.11 Free-Free support condition for testing structure

Consideration of the support of the structure under test is an important part of the test set-up. The support conditions should be well defined and experimentally repeatable if the results of the dynamic measurements are to reflect the properties of the structure without undue influence from the support. Unlike static measurement methods, experimental modal analysis can fortunately be achieved even in cases where the structure is not constrained and is completely free to carry out rigid body motions. Using this advantage, it is possible to consider natural homogeneous boundary conditions, known as generally free-free boundary conditions.

The first decision, which has to be taken, is whether the structure is to be tested in free-free boundary condition or grounded. It is almost impossible for either of these two conditions to be achieved in practice; a grounded structure will have movements at the grounding point (usually rotation) and there will be some small restraint of a, nominally, free structure. For a structure to be really free, it should be suspended in the air, free in space with no holding points whatever. Such a situation is commonly designated as ‘free-free’ or freely supported and is clearly impossible. However simulation of free-free condition is very easy to achieve. Although free-free experimental conditions are

unrealizable without weightlessness, they can be approached in practice with a high accuracy and repeatability while minimizing any effects of added mass as well as stiffness and damping of support. The technique used (and probably the most accurate too) is that suspend the structure to be measured using thin elastic bands of negligible mass and practically contributing almost no stiffness in the transverse direction. Thus the test plate is very weakly constrained in this direction, which is ideal for measuring the elastic modes of interest. However, adjusting the position of elastic wire on the test plate has an influence on the measured modal values, but in general these effects are mainly dissipative and essentially change the modal damping ratios. It has actually been observed that the position of elastic bands has no significant effect on the measured eigen frequencies and the mode shapes. The test plates are suspended with thin elastic bands from the top edge of the plate and on the nodal line of the first bending mode, as shown in Figure 2.11.

2.5 EXCITATION OF THE STRUCTURE

To develop a dynamic model of the structure, it is obviously necessary to excite it with a set of forces $f_s(t)$ depending on time. To satisfy the criteria for consistency and reliability of the numerical modelling of actual experiments, it is necessary to minimize any external effect in particular influence of rigidity and masses that can account for any system of dynamic excitation. Among all known dynamic excitation methods, only a small number requires no direct contact with the tested specimen, almost all conventional methods make additional mass and/or rigidity for excitation of structures. At first glance, only impact excitation can be considered the best one, but because of its impulse nature, this technique proved incompatible with a measure of dynamic response in completely free conditions. Indeed, the impact is not a symmetrical signal; it generates significant rigid body motions which completely drown the vibration response the test plate.

The excitation system can affect the dynamic behavior of a structure in just the same way as force or response transducer. The size of the excitation system is generally much larger than a force or response transducer and, hence, the influence will be greater. Various devices are available for exciting the structure and several of these are

in widespread use. Basically they can be divided into two types: contacting and non-contacting. The first of these involves the connection of an exciter of some form which remains attached to the structure throughout the test. Whether the excitation type is continuous (sinusoidal, random etc.) or transient (pulse, chirp). The second type includes devices which are either out of contact throughout the vibration (such as provided by a non-contacting electromagnet) or which are only in a contact for a short period, while the excitation is being applied (such as a hammer blow).

Perhaps the most common type of exciter is the electromagnetic shaker in which supplied input signal is converted to an alternating magnet field. A coil is placed inside the electromagnetic shaker which is attached the drive part of the device, and to the structure. In this case, the frequency and amplitude of excitation are controlled independently of each other, giving more operational flexibility – especially useful as it is generally found that it is better to vary the level of the excitation as resonance are passed through. However, it must be noted that the electrical impedance of these devices varies with the amplitude of motion of the moving coil and so it is not possible to deduce the excitation force by measuring the current passing through the shaker because this measures the force applied not to the structure itself, but to the assembly of structure and shaker drive. Although it may appear that the difference between this force (generated within the shaker) and that applied to the structure is likely to be small, it must be noted that just near resonance very little force is required to produce a large response and what usually happens is that without altering the settings on the power amplifier or signal generator, there is a marked reduction in the force level at frequencies adjacent to the structure's natural frequencies. As a result the true force applied to the structure becomes the (small) difference between the force generated in the exciter and the inertia force required to move the drive rod and shaker table and is, in fact, much smaller than either [104].

2.6 SUPPORT OF THE EXCITATION SYSTEM

The support of the excitation system is not quite so important as the support of the structure under test, but it should still be considered [105]. Rigid mounting of shaker on

the floor or stands is simple and straight forward, but care should be taken to avoid any ground transmission between the shaker.

The other common method of supporting a shaker is by suspension on some kind of hoist. Although this is a most convenient arrangement for positioning and aligning the shaker, it is important to remember that the shaker on the hoist is now a dynamic system in its own right. The shaker will move as a result of the internal force generated. The degree of movement will be related to the inertial mass of the shaker, the larger the mass, the smaller the movement. This movement of the shaker can cause problems at low frequencies when modes of the shaker suspension can be excited. This results in excessive motion and can lead to damage of the shaker, push-rod and force transducer.

A fixture is designed for positioning and aligning shaker, which allowed free movement of shaker along x, y, and z axis. When the shaker is positioned and aligns at right place for excitation, it is clamped tightly with the nut and bolts. The second problem of ground or external vibration transmission to the shaker is avoided by placing the whole arrangement of the excitation system on optical table (vibration isolation table).

2.7 ATTACHMENT TO THE STRUCTURE

The majority of structural excitation techniques in common usage require some physical contact with the structure. The objective is to transmit controlled excitation to the structure in a given direction and, simultaneously, to impose as little restraint on the structure as possible in all other directions. However, to achieve this purpose, the shaker must be rigidly attached to the structure and this connection is bound to introduce constraints that will affect the force transducer signal. In fact and except in particular cases of symmetry, the structure responds to the excitation by both translating and rotating, and therefore the shaker (and force transducer) will be affected by a torque that will distort the force signal and introduce errors in the measurements. To avoid this, a flexible push-rod, or stinger, or drive rod, usually forms some part of the link between a shaker and the structure under test. Ideally, the stinger should have high axial stiffness but low lateral or bending stiffness so as to excite the structure axially and to minimise excitations in all the other DOFs. However, forces and moments other than the axial



Figure 2.12 Shaker and structure attachment (Stinger assembly)

excitation force component may also be introduced and act on the test structure and influence the force and/or response measurements. This will cause a systematic error in the measurement.

Some cares must be taken while designing a stinger, like, if the stinger is made too long, or too flexible, then it begins to introduce the effects of its own resonances into the measurements and these can be very difficult to extricate from the genuine data. For most general structures, an exposed length of some 5-10 mm of 1 mm diameter wire is

found to be satisfactory [104]. Keeping these precautions in mind a stinger is designed so that it is relatively flexible to lateral and rotational motions between its ends, but very stiff axially. The designed stinger and other parts of assembly of the structure-shaker attachment fixture are shown in Figure 2.12. The locking screw bush fixtures at each end allow for simple adjustment of the stinger length, which simplifies the positioning of the shaker along the excitation direction of the free-free structure under investigation. The washer headed screw is bounded with the stiff glue, impedance head is installed on this washer headed screw and is attached to the shaker through the designed stinger assembly, as shown in Figure 2.12. Once set up, the push-rod linkage is then easily positioned, removed or replaced, thereby avoiding damage to the shaker or structure either overnight, or while transducers are being repositioned.

2.8 MEASUREMENTS BY SCANNING LASER VIBROMETER

Two-dimensional vibration Operating Deflection Shapes (ODSs) of structures can be derived by measuring FRFs on a grid of points selected over the test structure. The measurement philosophy is the same as that which uses accelerometers moved across the grid. The evident advantage is the use of a non-contact transducer, as in a laser sensor, and the automation of the measurement technique together with the time saving that can be achieved. The experiments were performed on four simple aluminum foam rectangular plates, in free-free condition and excited in a range of frequencies between 0 and 5 kHz, using a pseudo-random excitation via an electromagnetic shaker attached to the structure, as shown in Figure 2.13.

The laser was made to scan step by step over a grid of 1044 points (the big plate case) as shown in Figure 2.14. The velocity range set for the velocity decoder was 125 mm/s/V which represents the scale factor between the actual point velocity and the vibrometer output voltage. The acquisition was performed by activating the tracking filter and the 'Signal Enhancement' routine to improve the signal quality. Furthermore, a third option was selected via software: the so-called 'Remeasure' option whose purpose is to reject measurement points which do not have a valid status (i.e. during the acquisition there was an over-range or the signal level was low) and to remeasure again in the same location until the signal quality is acceptable.

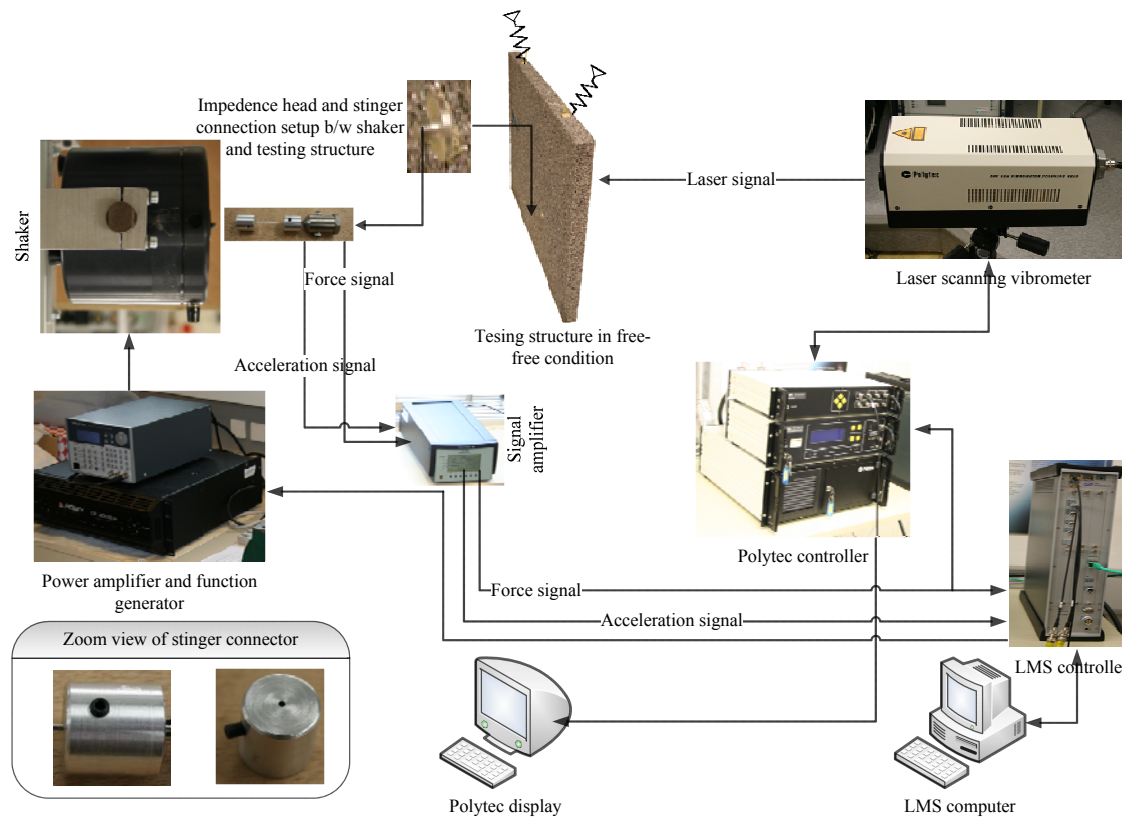


Figure 2.13 Experimental configuration

'Signal Enhancement' and 'Remeasure' routines have the sole disadvantage of increasing the acquisition time of the test but it is worth using them to achieve good output signals for most of the points on the grid. In order to minimise the noise level, averages were also performed; in the experiment included here thirty averaging were found to be sufficient to obtain the optimal measuring response. Vibrometer output signals and reference signals, acquired from a force transducer attached to the plate, were measured at each point with an antialiasing (low-pass) filter activated. The analogue signal had to be sampled for a certain amount of time with a suitable sampling frequency, namely 2.56 times bigger than the frequency bandwidth chosen for the measurement (5 kHz). The numbers of samples which the analogue signal will be cut into are defined, again, as 2.56 times the FFT lines set in the PSV data acquisition (6400 lines in the actual experiment). From these data the time required to measure the velocity at one point could be calculated as:

$$\begin{aligned}
 \text{time window} &= \frac{\text{number of samples}}{\text{sample frequency}} = \frac{6400 \times 2.56}{5000 \times 2.56} \\
 &= 1.28 \text{ s}
 \end{aligned} \tag{2.16}$$

For an area scan, the total measurement time can be derived as the following product:

$$\begin{aligned}
 \text{total time} &= \text{time window} \times \text{no of measurements point} \\
 &\quad \times \text{no of averaging} = 1.28 \times 1044 \times 30 \\
 &= 40889.6 \text{ s} = 11.136 \text{ hrs}
 \end{aligned} \tag{2.17}$$

In reality, together with this ideal quantity, additional times must be considered:

- time required for remeasuring measurement points which do not have a valid status;
- time necessary for waiting until the scanner mirror is at rest, which is set by default at 10 ms. The so-called settling time must be greatly emphasised as the mirrors should be in a stable position before the measurement starts, otherwise the laser spot on the structure will not be steady on the selected measurement point and the relative motion between laser beam and tested surface will produce speckle pattern motions with consequential dropouts.

The measurement time will increase further if additional facilities for signal quality improvement (i.e. signal enhancement) are selected. The total acquisition time for the actual test (1044 points) was in excess of 12 hours.

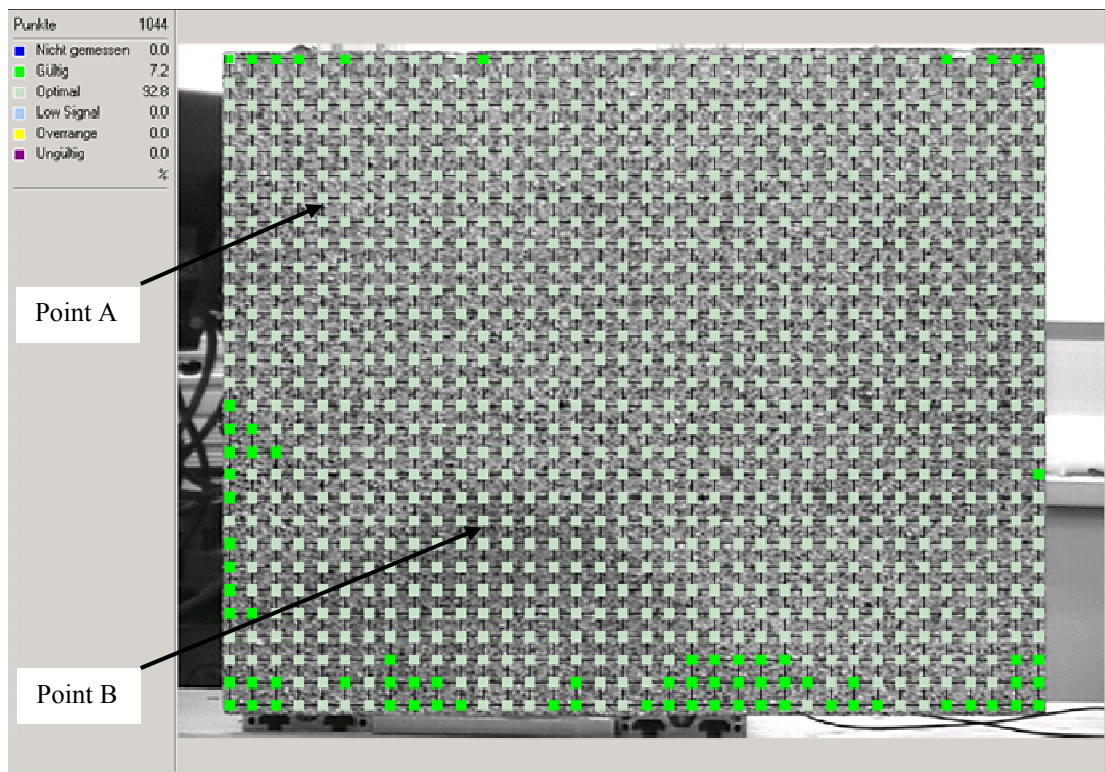


Figure 2.14 Grid of measurement points on testing structure.

During the acquisition, an on-line processing of the data could be carried out. In the PSV software FRFs were stored for each point on the grid. They were derived at each measurement point by dividing the Fourier spectrum of the vibrometer output, at the actual acquisition point, by the reference signal, taking into account the averages. Since the quantity measured by the laser is a velocity, the resulting FRF will be mobility, estimated with averaged measurement values (H1 estimator), i.e. output noise on vibrometer channel is suppressed. The transfer mobility between the measurement point **A** and the excitation point **B**, illustrated in Figure 2.14, is shown in Figure 2.16.

After the area scan had taken place, FRFs for all valid measurement points would be saved in order to be post-processed by using the standard PSV200 presentation module. Velocity maps for each resonance frequency chosen within the average spectrum of all grid points could be displayed. These patterns could be seen as ODSs at the selected frequency. Modal analysis was not performed on the data acquired, and therefore it is not appropriate to use the expression of "mode shapes".

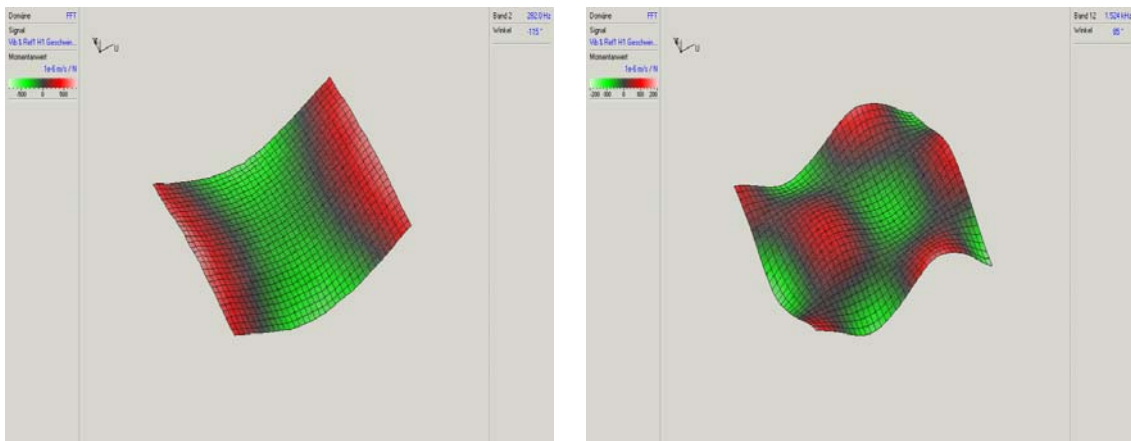


Figure 2.15 ODS @ 282Hz and 1524 Hz

Two frequencies were selected: 282 Hz (2nd resonance) and 1524 Hz (12th resonance). Values of velocity/force at each measurement point are shown in Figure 2.15, plotted against the x and y coordinates of the points in a 3-D reference system.

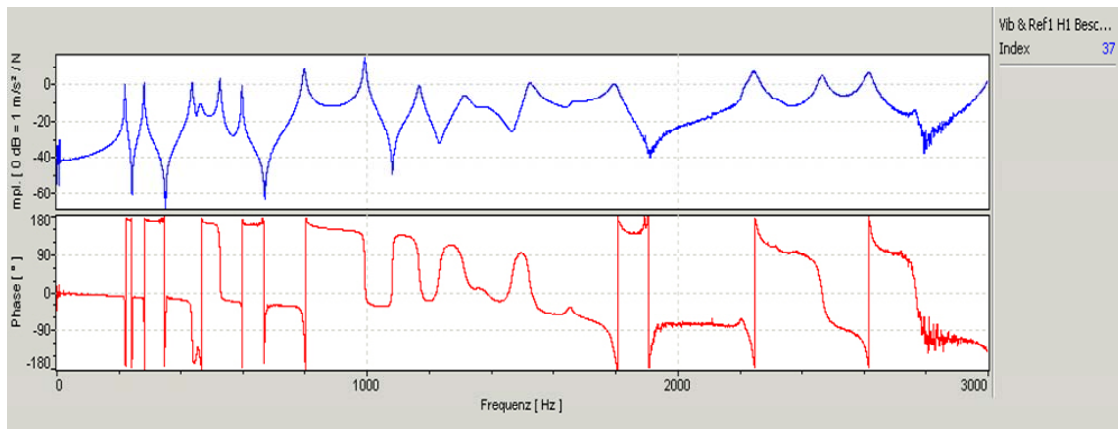


Figure 2.16 Transfer mobility at point 37

2.9 EXTRACTION OF MODAL PARAMETERS (MODAL ANALYSIS)

Once the experimental conditions are under control, dynamic measurement of the test specimen is carried out under ideal excitation and measurement conditions. The

transfer functions of the structure type velocity/force is calculated by the internal software system PSV200 and an average of several measurements is performed to further increase the quality of the experimental frequency model.

The frequency model is established, it is now necessary to extract the different modal parameters in the measured frequency range. Conventional techniques for extracting modal parameters are all based on the same principle that consists of identifying, from the frequency model $\mathbf{H}(j\omega)$ (or time in some cases), all the modal parameters $\boldsymbol{\varphi}_k$, ω_k , ζ_k and m_k for all modes k ($k = 1, 2, 3 \dots n$) in the measuring range. This identification is generally performed using an optimization method (e.g. least squares type) trying to minimize the overall difference between the measured transfer functions (considered as the actual transfer functions) and theoretical transfer functions synthesized from modal parameters identification.

$$h_{rs}(j\omega) = \frac{X_r(j\omega)}{F_s(j\omega)} \xleftrightarrow{\text{identification}} \bar{h}_{rs}(j\omega) = \sum_{k=1}^n \frac{\varphi_r^k \varphi_s^k}{m_k(\omega_k^2 + 2j\zeta_k\omega_k\omega - \omega^2)} \quad (2.18)$$

Among all modal extraction methods, the most common is based on the assumption that in the vicinity of the k -th resonance peak, the transfer function can be approximated by a frequency response function of a simple oscillator type single degree of freedom. Algebraically, this means that the magnitude of FRF is effectively controlled by one of the terms in the series that being the one relating to the mode whose resonance is being observed. This technique, commonly known as SDOF (Single-Degree-Of-Freedom) modal extraction method, allows to retrieve correctly and relatively simple modal parameters of modes whose resonance peaks are clearly separated and the modal damping is low. It is based on identification of measured transfer functions $h_{rs}(j\omega)$ using the following simplified approximation.

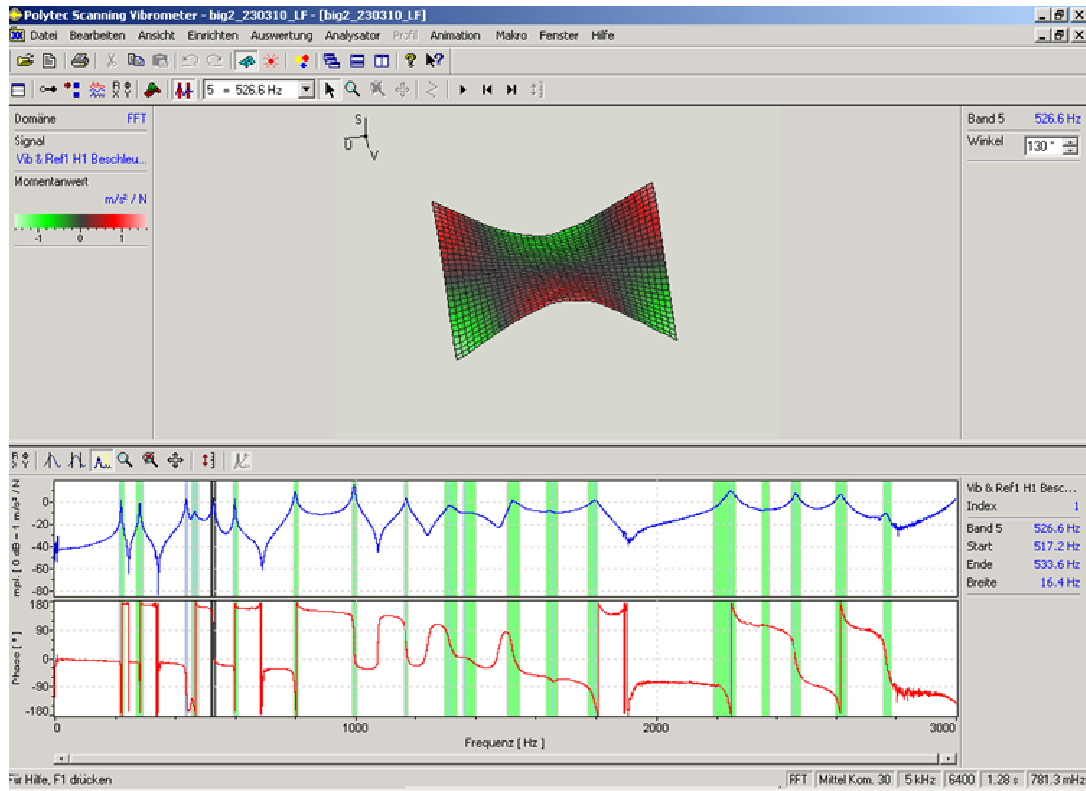


Figure 2.17 Polytec PSV 200 for parameter extraction using SDOF.

$$\begin{aligned}
 \bar{h}_{rs}(j\omega) &= \sum_{k=1}^n \frac{\varphi_r^k \varphi_s^k}{m_k(\omega_k^2 + 2j\zeta_k \omega_k \omega - \omega^2)} \cong R_{rs}^m \\
 &\quad + \frac{\varphi_r^k \varphi_s^k}{m_k(\omega_k^2 + 2j\zeta_k \omega_k \omega - \omega^2)} + R_{rs}^k \\
 &= R_{rs} + \frac{\varphi_r^k \varphi_s^k}{m_k(\omega_k^2 + 2j\zeta_k \omega_k \omega - \omega^2)}
 \end{aligned} \tag{2.19}$$

For ω in the vicinity of the natural frequency ω_k and where R_{rs}^m and R_{rs}^k represent the inertial and elastic residues respectively, whose sum R_{rs} is generally ignored in identification. This simple technique has the advantage of almost directly identify the eigen frequencies based on the resonant frequency amplitude and easily reconstruct the shape of the eigen modes by extracting the imaginary component of the transfer function displacement/force at the same frequency.

PSV200 system automates this task and requires the user select a frequency band in which the software will seek mode to extract. For this technique to work properly, however, requires that the residues of the neighboring modes of identified mode k are negligible, which is not always the case. The unexpected side effects that can occur with this extraction method are as follows:

- The eigen frequency can be distorted in a large proportion if close modes perturb the resonance peak of desired mode. This effect is also present to a lesser extent if desired mode, even though isolated from others, is highly damped.
- The extracted mode shapes are even more perturbed by the presence of modes near the eigen frequencies, so it is sometimes difficult to reconstruct precisely shape of an isolated eigen mode. The use of a SDOF method based on the adjustment of a circle in the Nyquist diagram (Circle Fitting) allows obtaining better results, but generally requires manual processing to be really effective. The source of the most commonly observed error comes from the fact that the desired mode k identified by SDOF method is often a complex superposition of the desired mode and one or more close modes. It should be noted however that contributions from neighboring modes have usually slightly different phase, so that it is sometimes possible to distinguish the approximate shape of each of the contributions in a temporal animation of identified mode.

The purpose of the modal measurement technique developed here is to measure precisely a large number of modal quantities, the density of modes in the measured frequency response functions is generally very high (approximately 10 to 20 modes in the measured frequency range). This high modal density introduces coupling effects such that it is not possible to extract the eigen frequencies and especially the eigen modes with a SDOF modal extraction method. Indeed, even under ideal measurement conditions, a significant number of modes are often too close, even with low structural damping, considered to be decoupled. It is then necessary to use a modal analysis method based on simultaneous identification of multiple modes k ($k = k_0, k_0 + 1, \dots, k_0 + m$) based on a minimization problem in the sense of least squared deviation between the measured transfer functions $h_{rs}(j\omega)$ and synthetic frequency response functions of the form $\bar{h}_{rs}(j\omega)$:

$$\bar{h}_{rs}(j\omega) = R_{rs}^m + \sum_{k=K_0}^{K_0+m} \frac{\varphi_r^k \varphi_s^k}{m_k(\omega_k^2 + 2j\zeta_k \omega_k \omega - \omega^2)} + R_{rs}^k \quad (2.20)$$

For $\omega \in [\omega_{K_0} - \Delta\omega, \omega_{K_0+m} + \Delta\omega]$ included in the vicinity of $\pm\Delta\omega$ of desired eigen frequency and where R_{rs}^m and R_{rs}^k again represent the inertial and elastic residues of identification.

By analogy with the SDOF method, this class of techniques is called MDOF (Multiple-Degree-Of-Freedom). MDOF curve fitting algorithms developed for fitting FRFs can be grouped into three classes:

Local MDOF curve fitting: These methods operate on one measurement at a time, but they can simultaneously estimate the parameters of multiple modes at a time. If a set of FRFs contains modes which are heavily coupled (resulting from the combined effect of heavy damping and small modal frequency separation), then an MDOF fitter is usually required to adequately identify the modal parameters. These fitters typically apply expression (2.18) to the data in a least squared error sense. That is, a set of parameters for two or more modes is found which minimizes the squared difference between the FRF data and the model, with modes > 1 .

Global curve fitting: Expression (2.18) makes it clear that all of the FRFs of a structure contain the same denominator, hence the same modal pole locations. Only the numerators, or residues, are different from measurement to measurement. Global curve fitting take advantage of this fact and use all, or a large number of, the FRFs to estimate the poles first, and then estimate the residues during a second pass through the data. This process yields one global estimate of frequency and damping for each mode, and usually provides better mode shape estimates, especially near nodal points where a mode's residues are small and not well defined.

PolyReference curve fitting: This class of curve fitting extends the idea of a global fitter to include multiple references, or multiple rows or columns, of the FRF matrix. PolyReference curve fitting method obtains additional estimates of the mode shape by curve fitting multiple rows or columns of data from the FRF matrix. These multiple

estimates are then combined in a manner which favors the references where each mode is more strongly represented, (i.e. its modal participation is greater), to yield a better estimate of each mode shape. Repeated roots, (i.e. two or more modes at approximately the same frequency but with different mode shapes), can also be found from multiple rows or columns of FRF data. A single row or column is not sufficient for this.

As these processes for modal analysis are relatively complex to properly implement from numerical point of view and they require a user-friendly interface to be effective, given the available time, to develop internally such methods are not tried. In the market of modal analysis software packages, there are indeed a large number of programs that implement various versions of these modal parameters extraction methods and generally allow direct import of the measurement data from PSV200 system into the universal (UNV) file format.

After a comparison of these programs, LMS Test.Lab software that combines benefits of fast computing, friendly user and import data of wide variety of file formats is selected. In addition, the curve fitting technique implanted in this software is based on an approach called "PolyMAX". This technique is regarded today as being more accurate and robust MDOF modal analysis method.

The new LMS PolyMAX is part of the LMS Test.Lab Structures solution for Modal testing and analysis and LMS PolyMAX provides a state-of-the-art modal parameter estimation [106]. LMS Test.Lab Structures is an integrated suite of applications covering the range of structural dynamic engineering completely. A dedicated modal analysis module automatically accesses the measurements taken by PSV 200, to compute the modal parameters: mode shape vector, resonant frequency, damping factor and modal mass. The new LMS PolyMAX method brings a revolutionary modal parameter estimation technique that is easy to use, quick to perform, substantially reduces operator-dependant judgment, and that delivers high quality modal parameter estimations, even on complex data.

The LMS PolyMAX method is a further evolution of the least-squares complex frequency-domain (LSCF) estimation method. That method was first introduced to find initial values for the iterative maximum likelihood method [107]. The method estimates

a so-called common-denominator transfer function model [108]. It was found that these “initial values” yielded already very accurate modal parameters with a very small computational effort [107, 109, 110]. The most important advantage of the LSCF estimator over the available and widely applied parameter estimation techniques [111] is the fact that very clear stabilization diagrams are obtained. A thorough analysis of different variants of the common-denominator LSCF method can be found in [110]. A complete background on frequency-domain system identification can be found in [112].

It was found that the identified common denominator model closely fitted the measured frequency response function (FRF) data. However, when converting this model to a modal model by reducing the residues to a rank-one matrix using the singular value decomposition (SVD), the quality of the fit decreased [109]. Another feature of the common denominator implementation is that the stabilization diagram can only be constructed using pole information (eigen frequencies and damping ratios). Neither participation factors nor mode shapes are available at first instance [113]. The theoretically associated drawback is that closely spaced poles will erroneously show up

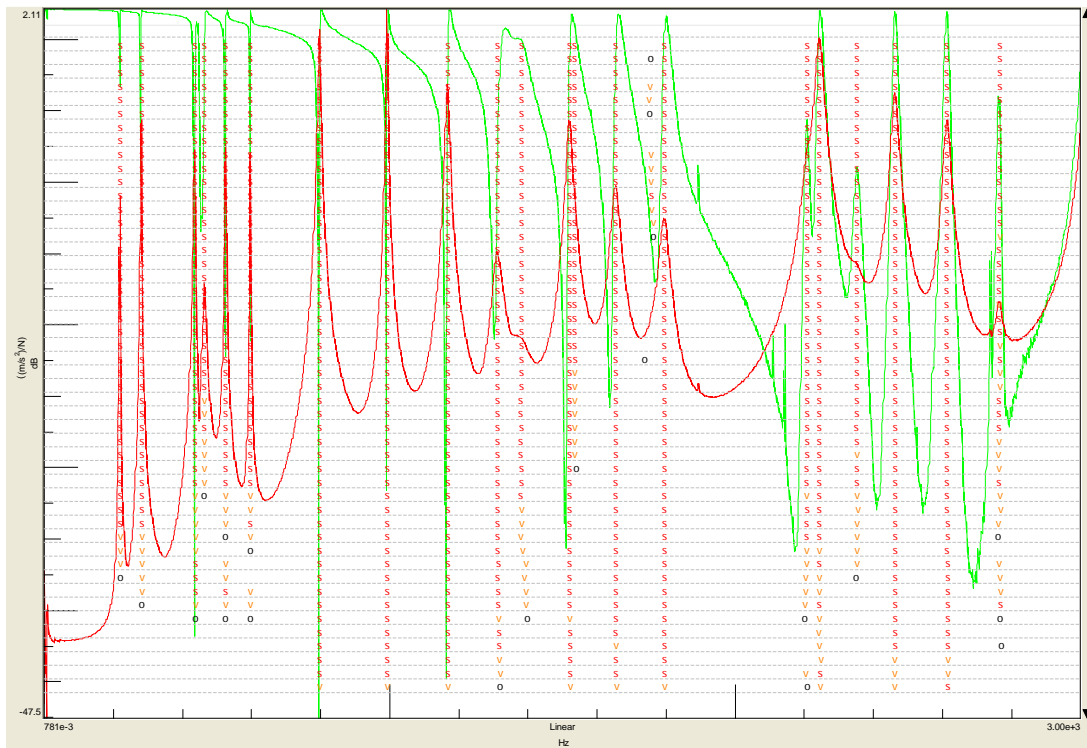


Figure 2.18 Stabilization diagram by applying PolyMAX estimation method.

as a single pole.

These two reasons provided the motivation for a polyreference version of the LSCF method, using a so-called right matrix-fraction model. In this approach, also the participation factors are available when constructing the stabilization diagram. The main benefits of the polyreference method are the facts that the SVD step to decompose the residues can be avoided and that closely spaced poles can be separated. The method was introduced in [106, 113].

2.9.1 Steps of applied technique for modal extraction

Finally, the steps of a typical modal extraction process are described. The various stages of this procedure are as follows:

1. Export of the transfer functions measured from the PSV200 into a UNV file format.
2. Import of the data into LMS Test.Lab and making some small modification to the data, to make it compatible with the LMS Test.Lab software for modal analysis.
3. Modal analysis of experimental data in LMS Test.Lab using LMS PolyMAX estimation method.
 - a. The first step is to establish the stabilization diagram to determine the true modal frequency, damping and participation factors. The values of rank (order), freq, damp and type (pole, vector or stable etc.) at the bottom of the stabilization diagram can be seen by placing the mouse cursor on the pole in stabilization diagram.
 - b. A modal indication function (MIF) measuring the probability of a mode as function of frequency is then calculated relying preferably on the amplitude of the measured transfer functions (Figure 2.17). This step generally helps to identify the number of modes present globally in the selected frequency range, but can sometimes provide an inaccurate estimate. The user must manually check the number of phase jumps and the peaks present.

- c. Visually inspecting the symbols in the stabilization diagrams, which are based on similarity in frequency, damping ratio and/or mode vector between poles belonging to subsequent model order: o-type represents unstable poles; f-type represents frequency within a given precision is stable, v-type represents frequency and modal participation factors is stable, s-type means the pole's frequency, damping and pole vector are stable within the tolerances, d-type means the pole's frequency and damping do not change within the tolerance. Search for a vertical column of poles, especially the column, which contain lot of s-type and d-type poles. It is not important that this column should exist at the lower model orders, nor that it is a straight column at the lower orders.
 - d. Checking the s-type and d-type poles in the selected column and search for the pole in the column that is most stable in frequency and which stabilizes in damping.
 - e. Based on the user-interpretation of the stabilization diagram, computation of the mode shapes and the lower and upper residuals in a least-squares sense is performed.
4. Evaluation of the quality of identified modes and selection of modes.
 - a. The auto Modal Assurance Criterion (MAC) is used to investigate the validity of the estimated modes within the same mode set. If mode shape vectors are estimates of the same physical mode shape, the modal assurance criterion should approach unity (100%). If mode shape vectors are estimates of the different physical mode shapes, the modal assurance criterion should be low. A high quality mode set must correspond to a MAC matrix close to identity matrix. In this case, the non-diagonal terms are also of interest, each of these terms symbolizes some sort of coupling of mode pair.
 - b. For proportionally damped systems, each modal coefficient for a specific mode of vibration should differ by 0° or 180° . The Modal Phase Colinearity (MPC) is an index expressing the consistency of the linear relationship between the real and imaginary parts of each modal coefficient. This

concept is essentially the same as the ordinary coherence function with respect to the linear relationship of the frequency response function for different averages or the modal assurance criterion (MAC) with respect to the modal scale factor between modal vectors. The MPC should be 1.0 (100 percent) for a mode that is essentially a normal mode. A low value of MPC indicates a mode that is complex (after normalization) and is an indication of a non-proportionally damped system or errors in the measured data and/or modal parameter estimation.

- c. Another indicator that defines whether a modal vector is essentially a normal mode is the Mean Phase Deviation (MPD). This index is the statistical variance of the phase angles for each mode shape coefficient for a specific modal vector from the mean value of the phase angle. The MPD is an indication of the phase scatter of a modal vector and should be near 0° for a real, normal mode.
 - d. The eigen modes that do not meet the MAC, MPC or MPD criteria are either removed from the table of modal vectors, or identified again by curve fitting by changing slightly the frequency range of extraction or the number of identified modes simultaneously.
5. For further procedure of mixed numerical experimental identification of constituent properties, the modal data (mesh, frequencies, damping and mode shapes) are exported into a UNV file format.

Finally, using the proposed modal testing and analysis technique, it is possible to extract a large number of eigen modes (average between 10 and 20) with an excellent quality of mode shapes, even when the modes are relatively close and the internal damping becomes important. In general, approximately 80% of found modes in the selected frequency range can be extracted with sufficient accuracy for further use in mixed numerical-experimental identification process.

CHAPTER 3. MATERIAL AND MODELLING

3.1 OBJECTIVE

An accurate and efficient numerical model is of prime importance for developing a powerful mixed numerical experimental identification technique. In the context of mixed numerical experimental identification technique, the role of the simulation model is to provide an assessment to the response of the tested specimen for variable identified parameters. During the iterative solution of the inverse problem of mixed identification, consistency and accuracy of numerical model directly influence the accuracy of identified parameters. In order to ensure their determination with a good degree of precision, numerical solution of the problem needs to be as sensitive as possible to all the identified parameters. The FE method is the most attractive method for dealing with such problems. It is possible to incorporate various FE models which improve the accuracy of the solution, simplify the formulation, introduce numerical stability and guarantee convergence, and cost-effectiveness of computation. In addition, because of the iterative nature of mixed identification procedures, computational efficiency of the software solving numerical directly determines inevitable productivity and performance of mixed identification technique.

3.2 MATERIAL SPECIFICATION

The specifications of test specimen are listed in Table 3.1 below. Specimens are named in the present work as follow.

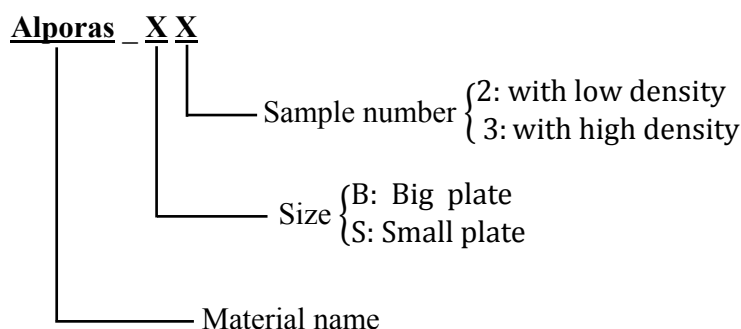


Table 3.1 Specification of aluminum foam specimen

Material	Size (cm³)	Average density (g/cm³)	Experimental response mesh	Density mesh measured by CT
Alporas_B2	49.6×40×3.02	0.247	36×29	55×40×5
Alporas_B3	49.7×40×3.09	0.466	36×29	55×40×5
Alporas_S2	40×31.2×3	0.246	32×26	40×35×5
Alporas_S3	40×31×3.02	0.443	32×26	40×35×5

Alporas foams were supplied as large plate, $2000 \times 400 \times 30 \text{ mm}^3$, without skin on the outer surface which cut into smaller panels with the dimensions mentioned in Table 3.1. The density of individual specimens was calculated by weighting the specimens on a balance and measuring their dimensions using a digital calliper. Dimensions, relative densities, experimental response mesh (measured by scanning laser vibrometer) and the density mapping mesh measured by CT are summarised in Table 3.1.

3.3 VISCOELASTIC CONSTITUTIVE MODELLING

In general, the constitutive behavior of viscoelastic materials might be said to depend upon the frequency, working temperature, amplitude and type of excitation [114-117]. A mathematical model considering all these effects simultaneously has not yet been developed, is very difficult to conceive and in practice has somewhat limited interest and applicability. Thus, for simplicity, since the amplitude and type of excitation effects have been reported to be of reduced importance, these parameters are often overlooked. However, the temperature and frequency dependent mechanical properties of the viscoelastic materials still introduce serious difficulties in the definition of an accurate mathematical model able to simulate properly the dynamic behavior of the damped structure. Therefore, for practical reasons, isothermal conditions are usually assumed in the simulation conditions and merely the frequency dependent constitutive behavior is directly taken into account upon the constitutive mathematical model. Following this assumption, the design of passive viscoelastic damping

treatments, for broad temperature range applications, is usually conducted at several constant temperature levels, selected within the temperature range, considering isothermal conditions.

The three primary mechanisms of damping which are important in the study of mechanical systems are: namely internal (or material) damping, structural damping (at joints and interfaces) and fluid damping (through fluid-structure interaction). In current work, interests are in modelling material damping. Material damping, referred to as internal damping, is the phenomenon within the material in which energy is dissipated [118]. Damping plays an important role in attenuating the response of system at resonance. Understanding material damping is an important step in the development of the analytical tool that is needed by design engineers. Since the first experimental observation of material (or internal) damping performed by Coulomb [119], where he not only hypothesized regarding the microstructural mechanisms of damping but also undertook experiments which proved that the damping of torsional oscillations is not caused by air friction but by internal losses in the material, over the following centuries different methods to characterize frequency dependent damping, in general, and the viscoelastic material's constitutive behavior (viscoelastic damping), in particular, were proposed [120].

The integration of the damping properties in a modal identification process needs to have a numerical modelling tool that can provide the modal properties of a damped structure. To incorporate the material damping character in mixed numerical-experimental identification technique for determination of materials elastic properties, it is necessary to adopt FE code which is capable to extract the damped modal properties. The desire to include damping effects in a simulation of the dynamic behavior of a structure using the FE method is to pose an eigenvalue problem arising from a model of dissipative physical behavior. In order to integrate these aspects in simulation model, the FE software should have the capabilities to solve the corresponding complex eigenvalue problem.

3.4 DAMPING MODELLING AND SOLUTION APPROACHES

In engineering practice, the quality of a vibration model of a mechanical system is essential for a wide range of applications such as, the prediction of system dynamic behavior, damage detection, system design and optimization. Most mechanical systems exhibit damped dynamic behaviors, which may prevent the systems from being accurately identified since understanding of damping mechanisms is still quite primitive. Therefore, the estimation or identification of damping models is always the central topic in experimental modal analysis. By far the most common damping model employed in practice is the so-called 'proportional damping' or 'Rayleigh damping' introduced by Rayleigh [121], which is linear and supposed to be determined only by the instantaneous generalized velocity. And the damping matrix is assumed to be a linear combination of system's mass and stiffness matrices and hence real normal modes as those of the undamped case can be preserved. Caughey [122] presented the general conditions on the form of proportional damping matrix, under which a damped system processes classic real normal modes. A series expression for damping matrix in terms of mass and stiffness matrices was proposed by Caughey and O'Kelly [123] so that a damped system can be decoupled by real normal modes. And it was also shown that the Rayleigh damping is just a special case of this general expression. Since the proportional damping matrix can be diagonalized simultaneously with the mass and stiffness matrices using real normal modes, a proportionally damped system can be decoupled into a set of principal single-degree-of-freedom (SDOF) systems. Based on the decoupled damped system, for majority modal analysis applications [104, 124], general expression of frequency response function (FRF) in the form of real normal modes can be derived. Then the damping parameters can be easily estimated using measured FRFs and the modal damping matrix (viscous or hysteretic) can be established by using the normal mode theory.

However, most practical structural systems under modal testing possess general non-proportional damping and hence exhibit complex mode behavior. For a non-proportionally damped system, the equations of motion cannot be decoupled in the modal coordinates due to the non-diagonal nature of the modal damping matrix. And consequently the system possesses complex modes instead of real normal modes. From

the viewpoint of mathematics, complex modes refer to the complex solution of the eigenproblem of a general damped system, which can be transformed into the vibrational characteristics of the system. For complex modes, each natural frequency and mode shape of the system is described in terms of complex quantities. In spite of lots of research efforts, understanding and identification of complex modes is not as well developed as those for real normal modes. To overcome the difficulties induced by the existence of complex modes in the identification of a mechanical system, real normal modes are usually required in experimental modal analysis. Ibrahim [125], Lin and Ibrahim [126] and Chen et al. [127] proposed methods to obtain the best real normal modes from identified complex modes. The extracted normal modes were then used to construct a proportional damping model together with modal damping matrix.

Proportional damping is well understood and commonly accepted in the description of damped dynamic behavior of a system. Based on a generalized proportional damping model, Adhikari [128] presented a method for identification of damping matrix using experimental modal analysis in the case where the system to be identified is effectively proportionally damped and the modes almost complex. In view of identification of damping in time domain, Gaylard [129] presented an improved weighted matrix integral of system response functions to identify proportional damping model by introducing a state-space approach. Angeles and Ostrovskaya [130] proposed a method to extract proportional damping component of an arbitrary damping matrix, which approximates optimally the original damping matrix in the least-square sense. However, even results drawn from the best proportional-damping approximation can be practically misleading in most cases.

In 1990s, a large number of literatures were devoted to the investigation of non-proportional damping of a mechanical system [131-134], which still remains an issue in modal parameter estimation. A few effective methods have been developed to identify non-proportional damping matrix from experimentally measured complex modes in case of lightly damped structures [135-137]. Woodhouse [135] discussed linear damping models: the familiar dissipation-matrix model and the general linear model and presented simple expressions for complex modal data and transfer functions. Following this idea, Adhikari and Woodhouse [136] presented a first order perturbation method to

obtain a full viscous (non-proportional) damping matrix from complex modal data in the case of sufficiently light damping. This method constructs the physical damping matrix using the inverse transformation of the modal damping matrix from the decoupling of the damped system. The two authors [137] further developed the first perturbation method to identify a non-viscous (non-proportional) damping model by using experimentally identified complex modal data together with the system mass matrix. Prells and Friswell [138] considered to determine symmetric non-proportional modal damping matrix using real normal modes and undamped natural frequencies based on a generalized modal model of a system. In this case the modal damping matrix is symmetric but non-diagonal due to non-proportional damping. Kasai and Link [139] presented a measure of non-proportional damping in terms of damping ratio based on the investigation of the difference between proportional and general viscous damping models.

To date, most proposed methods to identify or estimate damping whether it is proportional or non-proportional [128-139] are based on a viscous damping model, whose mechanism is well understood. In fact, for simplicity in engineering calculation and analysis, both viscous damping and hysteretic damping models are generally adopted to describe damping properties in linear vibratory mechanical systems [104, 124]. They are also the most often encountered damping types in practice. Although other damping models have been proposed from time to time, it has become common practice in modal analysis that either a hysteretic or viscous damping model can be readily used in the interpretation of measured vibration data. However, no verification has been made as to show whether or not this kind of arbitrary interpretation is physically reasonable. Due to the uncertainty of the type of damping model in practical complex structural systems, it is important to demonstrate theoretically whether this arbitrary choice of damping model will cause large errors in the estimation of modal parameters. Because these parameters are regarded as accurate ones once estimated and they are to be used with confidence to establish the system's mass and stiffness matrices or modify these matrices of the analytical model which are modeled using FE Method. A large number of studies [125-139] have ignored this topic, which may have an effect on the identified results of the modal analysis for a damped system. The primary research work on the issue was conducted by Balmes in Ref. [140], where an

identification procedure was proposed to extract the normal modes from the experimental complex modes. Meanwhile, the relation between normal modes (hysteretic damping case) and complex modes (viscous damping case) was investigated in details. It was found that the normal modes are clearly associated with the complex modes in terms of modal damping model and eigenvectors in the case of a proportionally damped system. In fact, for the general mechanical systems with same mass and stiffness matrices and different damping properties (such as viscous damping or hysteretic damping), there may exist a relationship between the modal models of these two systems since they have the similar FRF models, which may also represent systems' dynamic characteristics in nature. If this relationship can be shown, it may help to understand the difference between the same systems with various damping models and choose a suitable damping model for a mechanical system when modal analysis is performed.

The relationship between viscous and hysteretic damping models in proportional case and general non-proportional case are explained by R.M. Lin [141]. Based on the identified results of seven simulated numerical examples and an experimental test, the author shows that the error for the estimation of modal parameters due to the wrong interpretation of damping model (data from viscous damping model have been interpreted as hysteretic one or vice versa) is really very small. And in the case that the damping is distributed, for either types of damping, there exists a physically sensible (positive-definite or semi-positive definite) equivalent damping matrix on the basis that these two systems (in fact, only the damping matrix is different) have the same response model. On the other hand, however, if the damping is localized in the system, the correct interpretation of damping model becomes greatly important. Because if the mathematical model of damping is sought (damping matrix of the system), in this case there are no physically sensible equivalent damping matrices on that basis.

Several models with dissipative behavior are described in the literature, some are available in the commercial FE codes. Among the most common models in mechanical vibration include: viscous damping, proportional viscous damping or Rayleigh and hysteretic or structural damping.

3.4.1 Viscous damping model

The model with a viscous damping is assumed that the dissipative effects are proportional to the velocity. The mechanical analog that best fits this model is a dashpot. The simple constitutive relationship for a dashpot indicates that the force in the fluid depends on the rate the dashpot is displaced, or equivalently the velocity of the dashpot. The derivation of equation of motion, the eigenvalue problem and the frequency response functions for this type of model is presented here.

3.4.1.1 Derivation of the equations of motion

The general equation of equilibrium of elastodynamics is simply the equilibrium equation of elastostatics with an additional inertial term. It can be written as [104, 124, 142, 143],

$$\nabla^T \boldsymbol{\sigma}(\mathbf{x}, t) + \mathbf{f}(\mathbf{x}, t) - \rho(\mathbf{x}) \ddot{\mathbf{u}}(\mathbf{x}, t) = 0 \quad \forall \mathbf{x} \in \Omega \quad (3.1)$$

where $\boldsymbol{\sigma}$ denotes the vector associated with the stress tensor, \mathbf{f} is the body force per unit volume, \mathbf{u} is the displacement vector of a point in x -coordinate, ρ is the mass density, $(\)^T$ represents a transpose, ∇ represents the derivative operator and t is time.

Consider a model where the viscous dissipative effects are assumed to be proportional to the velocity and material strain rate. In this case, the damping has a component related to deformation that take place in the material constitutive law thus defining $\boldsymbol{\sigma}(\mathbf{x}, t)$ and a component related to displacement $\mathbf{u}(\mathbf{x}, t)$.

One of the elementary model is the ideal elastic element characterized by Hooke's law.

$$\boldsymbol{\sigma}(\mathbf{x}, t) = \mathbf{C}'(\mathbf{x}) \boldsymbol{\epsilon}(\mathbf{x}, t) \quad (3.2)$$

Where $\mathbf{C}'(\mathbf{x})$ is the matrix of elasticity. The hookean solid reflects only one property of a body, i.e. its elasticity. It does not reveal other rheological effects such as stress and strain relaxation.

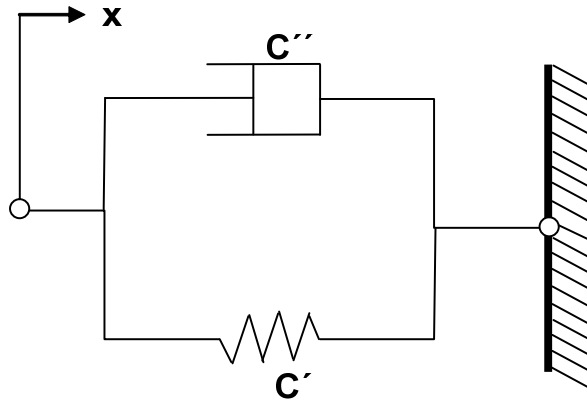


Figure 3.1 Kelvin-Voigt Model

Another elementary element is posed by a linear viscous damper filled with a Newtonian fluid. When the piston moves, the fluid flows through the gaps and thus generates a resistive force which results from the viscosity of the fluid. A constitutive formula has the form:

$$\sigma(\mathbf{x}, t) = \mathbf{C}''(\mathbf{x}) \dot{\boldsymbol{\epsilon}}(\mathbf{x}, t) \quad (3.3)$$

Where \mathbf{C}'' denotes the viscosity. The stress is directly proportional to the strain rate.

The connection of the spring and the damper in parallel creates the so called Kelvin-Voigt model (Figure 3.1). It is a very often used model for linear viscoelastic solid. The resistive force opposing external loading is posed by the sum of the spring and the damper resistive forces. With damping proportional to the strain rate, the constitutive law can be written as:

$$\sigma(\mathbf{x}, t) = \mathbf{C}'(\mathbf{x}) \boldsymbol{\epsilon}(\mathbf{x}, t) + \mathbf{C}''(\mathbf{x}) \dot{\boldsymbol{\epsilon}}(\mathbf{x}, t) \quad (3.4)$$

Where $\boldsymbol{\epsilon}$ is the strain tensor, \mathbf{C}' is the matrix of elasticity and \mathbf{C}'' is the damping matrix. The above equation illustrates an important characteristic of viscoelastic materials,

namely that the stress in the material depends not only on the strain, but also on the strain rate.

The part of damping associated with displacement, proportional to the velocity $\dot{\mathbf{u}}(\mathbf{x}, t)$ can be written in the form of vector of dissipative forces

$$\mathbf{f}_a(\mathbf{x}, t) = \mathbf{C}'''(\mathbf{x})\dot{\mathbf{u}}(\mathbf{x}, t) \quad (3.5)$$

With \mathbf{C}''' the matrix describing viscous behavior and is widely accepted as a basic measure of the damping.

The equilibrium equation (3.1) becomes,

$$\nabla^T \boldsymbol{\sigma}(\mathbf{x}, t) + \mathbf{f}(\mathbf{x}, t) = \rho(\mathbf{x})\ddot{\mathbf{u}}(\mathbf{x}, t) + \mathbf{C}'''(\mathbf{x})\dot{\mathbf{u}}(\mathbf{x}, t) \quad (3.6)$$

By inserting the equation (2.4) in the expression (2.6), while neglecting the volume forces, the following expression is obtained,

$$\nabla^T [\mathbf{C}'(\mathbf{x})\boldsymbol{\varepsilon}(\mathbf{x}, t) + \mathbf{C}''(\mathbf{x})\dot{\boldsymbol{\varepsilon}}(\mathbf{x}, t)] = \rho(\mathbf{x})\ddot{\mathbf{u}}(\mathbf{x}, t) + \mathbf{C}'''(\mathbf{x})\dot{\mathbf{u}}(\mathbf{x}, t) \quad (3.7)$$

Under the assumption of linearity in geometry, the strain and strain rate can be written as;

$$\boldsymbol{\varepsilon}(\mathbf{x}, t) = \nabla \mathbf{u}(\mathbf{x}, t) \quad (3.8)$$

$$\dot{\boldsymbol{\varepsilon}}(\mathbf{x}, t) = \nabla \dot{\mathbf{u}}(\mathbf{x}, t) \quad (3.9)$$

So the relationship (3.7) becomes

$$\nabla^T [\mathbf{C}'(\mathbf{x})\nabla \mathbf{u}(\mathbf{x}, t) + \mathbf{C}''(\mathbf{x})\nabla \dot{\mathbf{u}}(\mathbf{x}, t)] - \rho(\mathbf{x})\ddot{\mathbf{u}}(\mathbf{x}, t) - \mathbf{C}'''(\mathbf{x})\dot{\mathbf{u}}(\mathbf{x}, t) = 0 \quad (3.10)$$

To obtain the weak form of the dynamic equilibrium equations multiply both sides by an arbitrary test function $\delta \mathbf{u}^T$ and integrate over the entire space Ω by parts. This produces

$$\int_{\Omega} \delta \mathbf{u}^T \{ \nabla^T [\mathbf{C}' \nabla \mathbf{u} + \mathbf{C}'' \nabla \dot{\mathbf{u}}] - \rho \ddot{\mathbf{u}} - \mathbf{C}''' \dot{\mathbf{u}} \} d\Omega = 0 \quad \forall \delta \mathbf{u} \quad (3.11)$$

Where $\delta \mathbf{u}$ is the virtual displacement vector (to ease the writing, the coordinates \mathbf{x} and the time t will now be omitted if not necessary for understanding). Integrating by parts, the formulation (3.11) becomes in the weak form as

$$\begin{aligned} - \int_{\Omega} \nabla \delta \mathbf{u}^T [\mathbf{C}' \nabla + \mathbf{C}'' \nabla \dot{\mathbf{u}}] d\Omega + \int_{\partial\Omega} \delta \mathbf{u}^T \mathbf{N}^T [\mathbf{C}' \nabla \mathbf{u} + \mathbf{C}'' \nabla \dot{\mathbf{u}}] d\partial\Omega \\ - \int_{\Omega} \rho \delta \mathbf{u}^T \ddot{\mathbf{u}} d\Omega - \int_{\Omega} \delta \mathbf{u}^T \mathbf{C}''' \dot{\mathbf{u}} d\Omega = 0 \quad \forall \delta \mathbf{u} \end{aligned} \quad (3.12)$$

Where \mathbf{N} is the operator of the direction cosines of the outer normal to the surface $\partial\Omega$ of the body Ω . By inserting the matrix of shape functions \mathbf{H} to approach the real and virtual displacements

$$\mathbf{u} \cong \mathbf{u}^h(\mathbf{x}, t) = \mathbf{H}(\mathbf{x}) \mathbf{q}(t) \quad (3.13)$$

$$\delta \mathbf{u} \cong \delta \mathbf{u}^h(\mathbf{x}, t) = \mathbf{H}(\mathbf{x}) \delta \mathbf{q}(t)$$

Where \mathbf{q} and $\delta \mathbf{q}$ are the vectors of discrete real and virtual displacements and the index h represents the character approached, assuming the boundary $\partial\Omega$ free of constraints (free-free boundary condition type)

$$\mathbf{N}^T [\mathbf{C}' \nabla \mathbf{u} + \mathbf{C}'' \nabla \dot{\mathbf{u}}] = 0 \quad (3.14)$$

The following equation is obtained

$$\begin{aligned}
& \int_{\Omega} (\nabla \mathbf{H} \delta \mathbf{q})^T [\mathbf{C}' \nabla + \mathbf{C}'' \nabla \dot{\mathbf{u}}] d\Omega + \int_{\Omega} \rho (\mathbf{H} \delta \mathbf{q})^T \mathbf{H} \ddot{\mathbf{q}} d\Omega \\
& + \int_{\Omega} (\mathbf{H} \delta \mathbf{q})^T \mathbf{C}''' \mathbf{H} \dot{\mathbf{q}} d\Omega = 0 \quad \forall \delta \mathbf{q}
\end{aligned} \tag{3.15}$$

For the identification of virtual displacements, this equation becomes

$$\begin{aligned}
& \delta \mathbf{q}^T \left\{ \int_{\Omega} \nabla \mathbf{H}^T [\mathbf{C}' \nabla \mathbf{H} \mathbf{q} + \mathbf{C}'' \nabla \mathbf{H} \dot{\mathbf{q}}] d\Omega + \int_{\Omega} \rho \mathbf{H}^T \mathbf{H} \ddot{\mathbf{q}} d\Omega \right. \\
& \left. + \int_{\Omega} \mathbf{H}^T \mathbf{C}''' \mathbf{H} \dot{\mathbf{q}} d\Omega \right\} = 0 \quad \forall \delta \mathbf{q}
\end{aligned} \tag{3.16}$$

As this equality must be checked regardless of the discrete virtual displacements, the discrete weak form is written as;

$$\begin{aligned}
& \int_{\Omega} \nabla \mathbf{H}^T [\mathbf{C}' \nabla \mathbf{H} \mathbf{q} + \mathbf{C}'' \nabla \mathbf{H} \dot{\mathbf{q}}] d\Omega + \int_{\Omega} \rho \mathbf{H}^T \mathbf{H} \ddot{\mathbf{q}} d\Omega \\
& + \int_{\Omega} \mathbf{H}^T \mathbf{C}''' \mathbf{H} \dot{\mathbf{q}} d\Omega = 0 \quad \forall \delta \mathbf{q}
\end{aligned} \tag{3.17}$$

By identifying the global matrix of stiffness, damping and mass as

$$\mathbf{K} = \int_{\Omega} \nabla \mathbf{H}^T \mathbf{C}' \nabla \mathbf{H} d\Omega \tag{3.18}$$

$$\mathbf{D} = \int_{\Omega} \nabla \mathbf{H}^T \mathbf{C}'' \nabla \mathbf{H} d\Omega + \int_{\Omega} \mathbf{H}^T \mathbf{C}''' \mathbf{H} d\Omega \quad (3.19)$$

$$\mathbf{M} = \int_{\Omega} \rho \mathbf{H}^T \mathbf{H} d\Omega \quad (3.20)$$

Finally the semi-discrete matrix form relating the dynamic behavior in free condition to viscous damping of the structure is achieved.

$$\mathbf{M}\ddot{\mathbf{q}}(t) + \mathbf{D}\dot{\mathbf{q}}(t) + \mathbf{K}\mathbf{q}(t) = 0 \quad (3.21)$$

If it is assumed that damping is only due to the deformation of the structure, which has set aside \mathbf{C}''' , the structural damping matrix is written as,

$$\mathbf{D} = \int_{\Omega} \nabla \mathbf{H}^T \mathbf{C}'' \nabla \mathbf{H} d\Omega = \int_{\Omega} \mathbf{B}^T \mathbf{C}'' \mathbf{B} d\Omega \quad (3.22)$$

With \mathbf{B} the deformation matrix ($\mathbf{B} = \nabla \mathbf{H}$) .

viscous Model in continuous harmonic system

Assuming a deformation of the form

$$\tilde{\varepsilon}(t) = \varepsilon e^{j\omega t} \quad (3.23)$$

With $\tilde{\varepsilon}$ the complex strain of amplitude ε and of frequency ω , The constitutive law taking into account a viscous damping system for one-dimensional vibrations in a continuous harmonic system (considering the expression 3.4) can be written as,

$$\tilde{\sigma}(t) = C' \tilde{\varepsilon}(t) + j\omega C'' \tilde{\varepsilon}(t) \quad (3.24)$$

3.4.1.2 Eigenvalue Equation

In formulating the discrete displacements \mathbf{q} in the form

$$\mathbf{q}(t) = \mathbf{p}e^{\lambda t} \quad (3.25)$$

Where λ is a scalar and \mathbf{p} is a vector of constants, and introducing this expression in the relation (3.21), the following eigenvalue problem is obtained,

$$(\mathbf{K} + \lambda\mathbf{D} + \lambda^2\mathbf{M})\mathbf{p} = 0 \quad (3.26)$$

Where λ and \mathbf{p} are both the eigenvalue and eigenvector. To be able to easily solve this quadratic eigenvalue problem of dimension n , it is best to turn it into a classic linear form of size $2n$. Implementation of classical linearization, as featured in many vibration texts and papers, for example [144-149], requires the transformation of square matrices of size n to $2n$, by adding another set of equations in \mathbf{M} or \mathbf{K} to obtain,

$$\mathbf{A}\mathbf{u} = \lambda\mathbf{B}\mathbf{u} \quad (3.27)$$

Where, for \mathbf{K} augmentation,

$$\begin{aligned} \mathbf{A} &= \begin{bmatrix} \mathbf{0} & \mathbf{K} \\ -\mathbf{K} & -\mathbf{D} \end{bmatrix} \\ \mathbf{B} &= \begin{bmatrix} \mathbf{K} & \mathbf{0} \\ \mathbf{0} & \mathbf{M} \end{bmatrix} \\ \mathbf{u} &= \{\mathbf{q}, \dot{\mathbf{q}}\}^T \end{aligned} \quad (3.28)$$

or using \mathbf{M}

$$\mathbf{A} = \begin{bmatrix} \mathbf{0} & \mathbf{M} \\ -\mathbf{K} & -\mathbf{D} \end{bmatrix} \quad (3.29)$$

$$\mathbf{B} = \begin{bmatrix} \mathbf{M} & \mathbf{0} \\ \mathbf{0} & \mathbf{M} \end{bmatrix}$$

$$\mathbf{u} = \{\mathbf{q}, \dot{\mathbf{q}}\}^T$$

Where the matrices \mathbf{A} and \mathbf{B} of order $2n$ are symmetrical but not strictly positive definite and the magnitude \mathbf{u} is the state vector of the system. One advantage in using equation (3.29) is that the matrix \mathbf{B} remains symmetric and positive definite, if \mathbf{M} is already symmetric and positive definite. In equation (3.28), the symmetric form is preserved in \mathbf{B} , but in some \mathbf{K} may be not positive definite.

Inserting the general solution, based on (3.25),

$$\mathbf{u}(t) = \{\mathbf{p}e^{\lambda t}, \lambda \mathbf{p}e^{\lambda t}\}^T = e^{\lambda t} \{\mathbf{p}, \lambda \mathbf{p}\}^T \quad (3.30)$$

The linearized form of the generalized eigenvalue problem corresponding to the non-rotating dissipative structures can be written as,

$$(\mathbf{A} - \lambda \mathbf{B})\mathbf{u} = 0 \quad (3.31)$$

With

$$\mathbf{u} = \{\mathbf{p}, \lambda \mathbf{p}\}^T \quad (3.32)$$

Where λ and \mathbf{u} form the eigen pair the problem increased to size $2n$, the eigenvalue λ and the sub-vector \mathbf{p} of dimension n is identical to the grandeur of the quadratic eigen problem (3.26).

Since the matrices \mathbf{A} and \mathbf{B} are real symmetric but not strictly positive definite, it shows that for under-damped systems eigen solutions to the homogeneous matrix equation (3.31) consist of n pairs of complex conjugate eigenvalues

$$\lambda_i = -\alpha_i \pm j\omega_i \quad (i = 1, 2, \dots, n) \quad (3.33)$$

Where the positive quantities α_i and ω_i ($i = 1, 2, \dots, n$) are the modal damping coefficients and the eigen frequency of the structure, and n conjugate pairs of complex eigenvectors \mathbf{u}_i and $\bar{\mathbf{u}}_i$ ($i = 1, 2, \dots, n$) of dimension $2n$, whose first n components constitute the eigen form \mathbf{p}_i and $\bar{\mathbf{p}}_i$ ($i = 1, 2, \dots, n$) of the studied system,

$$\begin{aligned} (\mathbf{A} - \lambda_i \mathbf{B})\mathbf{u}_i &= [(\mathbf{A} - \alpha_i \mathbf{B}) - j\omega_i \mathbf{B}]\mathbf{u}_i = 0 \\ (\mathbf{A} - \bar{\lambda}_i \mathbf{B})\bar{\mathbf{u}}_i &= [(\mathbf{A} - \alpha_i \mathbf{B}) - j\omega_i \mathbf{B}]\bar{\mathbf{u}}_i = 0 \end{aligned} \quad (3.34)$$

Note that the characteristic ω_i and α_i ($i = 1, 2, \dots, n$) are conventionally related as;

$$\zeta_i = \frac{\alpha_i}{\sqrt{\alpha_i^2 + \omega_i^2}} \quad (i = 1, 2, \dots, n) \quad (3.35)$$

Where the ζ_i ($i = 1, 2, \dots, n$) are the modal damping factors or damping relation of the modal structure.

3.4.1.3 Special case: the proportional model

The model of proportional damping is a special case of the model where the viscous damping matrix is a linear combination of mass and stiffness matrices. To achieve this model, with the damping proportional to the velocity of the structure, simple forms for \mathbf{C}'' and \mathbf{C}''' are selected,

$$\mathbf{C}'' = \beta \mathbf{C}' \quad (3.36)$$

$$\mathbf{C}''' = \gamma \quad (3.37)$$

Where β and γ are the constants. In this case, the damping matrix is

$$\mathbf{D} = \beta \int_{\Omega} \nabla \mathbf{H}^T \mathbf{C}' \nabla \mathbf{H} \, d\Omega + \gamma \int_{\Omega} \mathbf{H}^T \mathbf{H} \, d\Omega = \beta \mathbf{K} + \alpha \mathbf{M} \quad (3.38)$$

With
$$\alpha = \frac{\gamma}{\rho} \quad (3.39)$$

This particular form of damping is also known as Rayleigh damping. With this model, the condition known as Caughey [8] is achieved.

$$\mathbf{KM}^{-1}\mathbf{D} = \mathbf{DM}^{-1}\mathbf{K} \quad (3.40)$$

Ensuring that the damped vibrational modes are real (classical normal modes), which allows to solve the problem without the need for a complex eigenvalue solver. This advantage explains why this type of damping is often included in codes of modal analysis by commercial FE packages, despite its low realism.

With these assumptions, it is easy to establish the relation between α and β , and the modal damping c_i of mode i

$$\begin{aligned} c_i &= \mathbf{p}_i^T \mathbf{D} \mathbf{p}_i = \mathbf{p}_i^T (\beta \mathbf{K} + \alpha \mathbf{M}) \mathbf{p}_i \\ &= \beta \mathbf{p}_i^T \mathbf{K} \mathbf{p}_i + \alpha \mathbf{p}_i^T \mathbf{M} \mathbf{p}_i = \beta k_i + \alpha m_i \end{aligned} \quad (3.41)$$

Where k_i and m_i are respectively the modal stiffness and mass of mode i and \mathbf{p}_i denotes the eigenvector of mode i .

Therefore, the modal damping factor ζ_k of mode k is a function of eigen frequency ω_k of mode k

$$\begin{aligned} \zeta_k &= \frac{C_k}{2m_k\omega_k} = \frac{\alpha m_k}{2m_k\omega_k} + \frac{\beta k_k}{2m_k\omega_k} \\ &= \frac{\alpha}{2\omega_k} + \frac{\beta\omega_k}{2} = \zeta_\alpha + \zeta_\beta \end{aligned} \quad (3.42)$$

With $\omega_k^2 = k_k/m_k$

Note that with Rayleigh damping, the changes in the frequency function of the modal damping factor is independent of mass and modal stiffness. This gives indeed a factor ζ_k composed of a proportional term ω_k and a term inversely proportional to ω_k . The modal damping factor is defined solely by α, β and the eigen frequency ω_k , e.g. geometry do not influence this factor.

It is possible to extend this approach to proportional damping said generalized, or damping matrix (D) takes the form [128]

$$\mathbf{D} = \alpha(\mathbf{M}^{-1}\mathbf{K})\mathbf{M} + \beta(\mathbf{K}^{-1}\mathbf{M})\mathbf{K} \quad (3.43)$$

With $\alpha(\mathbf{M}^{-1}\mathbf{K})$ and $\beta(\mathbf{K}^{-1}\mathbf{M})$ as the functions of frequency. Modal damping factors are then given by

$$\zeta_k = \frac{\alpha(\omega_k^2)}{2\omega_k} + \frac{\omega_k\beta(\omega_k^2)}{2} \quad (3.44)$$

Given the first equality in expression (3.42), taking $\beta = 0$,

$$\alpha(\omega_k^2) = 2\omega_k\zeta_k = \frac{c_k}{m_k} \quad (3.45)$$

This makes it possible to find functions α and β that allow to better correlate the modal damping factors of experimental and theoretical in the case strictly proportional.

3.4.1.4 Frequency response function

Resuming eigenvalue system presented in equation (3.31)

$$(\mathbf{A} - \lambda_i\mathbf{B})\mathbf{u}_i = 0 \quad (i = 1, 2, \dots, 2n) \quad (3.46)$$

The eigenvectors of this system have the characteristics of the following orthogonality

$$\begin{aligned}\mathbf{U}^T \mathbf{A} \mathbf{U} &= \text{diag}[\alpha_1, \dots, \alpha_i, \dots, \alpha_n, \bar{\alpha}_1, \bar{\alpha}_i, \dots, \bar{\alpha}_n] \\ \mathbf{U}^T \mathbf{B} \mathbf{U} &= \text{diag}[b_1, \dots, b_i, \dots, b_n, \bar{b}_1, \bar{b}_i, \dots, \bar{b}_n]\end{aligned}\quad (3.47)$$

With $\mathbf{U} = [\mathbf{u}_1, \dots, \mathbf{u}_i, \dots, \mathbf{u}_n, \bar{\mathbf{u}}_1, \bar{\mathbf{u}}_i, \dots, \bar{\mathbf{u}}_n]$ and where α_i and b_i are complex constants, while the eigen values can be written as;

$$\lambda_i = \frac{\alpha_i}{b_i} \quad (3.48)$$

The vector of forces is written as;

$$\mathbf{r} = \begin{Bmatrix} \mathbf{f} \\ 0 \end{Bmatrix} \quad (3.49)$$

Where \mathbf{f} is the vector of external excitation. Therefore, for a harmonic excitation of frequency ω , the expression become

$$(-\mathbf{A} + j\omega\mathbf{B})\mathbf{x}e^{j\omega t} = \mathbf{r}e^{j\omega t} \quad (3.50)$$

$$\text{and} \quad \mathbf{x} = (-\mathbf{A} + j\omega\mathbf{B})^{-1}\mathbf{r} = \mathbf{H}(\omega)\mathbf{r} \quad (3.51)$$

Where $\mathbf{H}(\omega)$ is the matrix of the transfer functions and \mathbf{x} the amplitude of the oscillations. Pre-and post-multiplying this matrix by \mathbf{U} and its transpose

$$\begin{aligned}\mathbf{U}^T \mathbf{H}(\omega) \mathbf{U} &= \mathbf{U}^T (-\mathbf{A} + j\omega\mathbf{B})^{-1} \mathbf{U} \\ &= \text{diag} \left[\frac{1}{-\alpha_1 + j\omega b_1}, \dots, \frac{1}{-\bar{\alpha}_n + j\omega \bar{b}_n} \right] \\ &= \text{diag} \left[\frac{1}{b_1(-\lambda_1 + j\omega)}, \dots, \frac{1}{\bar{b}_n(-\bar{\lambda}_n + j\omega)} \right]\end{aligned}\quad (3.52)$$

It follows

$$\begin{aligned}
\mathbf{H}(\omega) &= \mathbf{U} \text{diag} \left[\frac{1}{b_1(-\lambda_1 + j\omega)}, \dots, \frac{1}{\bar{b}_n(-\bar{\lambda}_n + j\omega)} \right] \mathbf{U}^T \\
&= \sum_{i=1}^n \left[\frac{\mathbf{u}_i \mathbf{u}_i^T}{b_i(-\lambda_i + j\omega)}, \dots, \frac{\bar{\mathbf{u}}_i \mathbf{u}_i^H}{\bar{b}_i(-\bar{\lambda}_i + j\omega)} \right]
\end{aligned} \tag{3.53}$$

The frequency response function between two points r and s of the structure can be written as;

$$\begin{aligned}
h_{rs}(\omega) &= \sum_{i=1}^n \left[\frac{\mathbf{u}_r^i \cdot \mathbf{u}_s^i}{b_i \left(\omega_i \zeta_i + j \left(\omega - \omega_i \sqrt{1 - \zeta_i^2} \right) \right)} \right. \\
&\quad \left. + \frac{\bar{\mathbf{u}}_r^i \cdot \bar{\mathbf{u}}_s^i}{\bar{b}_i \left(\omega_i \zeta_i + j \left(\omega + \omega_i \sqrt{1 - \zeta_i^2} \right) \right)} \right]
\end{aligned} \tag{3.54}$$

By using the fact $\lambda_i = \omega_i \left(-\zeta_i + j \sqrt{1 - \zeta_i^2} \right)$, this equation can be further reduced as

$$h_{rs}(\omega) = \sum_{i=1}^n \frac{\frac{\mathbf{u}_r^i \cdot \mathbf{u}_s^i}{b_i} R_i(\omega) + \frac{\bar{\mathbf{u}}_r^i \cdot \bar{\mathbf{u}}_s^i}{\bar{b}_i} S_i(\omega)}{\omega_i^2 - \omega^2 + 2j\zeta_i \omega \omega_i} \tag{3.55}$$

Where the coefficients $R_i(\omega)$ and $S_i(\omega)$ defined as

$$\begin{aligned}
R_i(\omega) &= \omega_i \zeta_i + j \left(\omega + \omega_i \sqrt{1 - \zeta_i^2} \right) \\
S_i(\omega) &= \omega_i \zeta_i + j \left(\omega - \omega_i \sqrt{1 - \zeta_i^2} \right)
\end{aligned} \tag{3.56}$$

Particular case of proportional damping

Consider a proportional damping, the equation of the transfer function reduces to a much more simple form. Indeed, in case of proportional damping

$$\mathbf{p}_i^T \mathbf{D} \mathbf{p}_i = \frac{c_i}{m_i} \quad (i = 1, 2, 3, \dots, n) \quad (3.57)$$

With m_i and c_i the mass and modal damping of mode i and \mathbf{p}_i is the i -th eigenvector of the system, normalized with respect to the mass matrix \mathbf{M} .

Starting from the equation (3.21) and performing the following transformation

$$\begin{aligned} \mathbf{q} &= \mathbf{x} e^{j\omega t} \\ \dot{\mathbf{q}} &= j\omega \mathbf{x} e^{j\omega t} \\ \ddot{\mathbf{q}} &= -\omega^2 \mathbf{x} e^{j\omega t} \end{aligned} \quad (3.58)$$

the equation becomes

$$[-\mathbf{M}\omega^2 + j\omega\mathbf{D} + \mathbf{K}]\mathbf{x} e^{j\omega t} = \mathbf{f} e^{j\omega t} \quad (3.59)$$

with \mathbf{f} representing the force excitation. Therefore, the transfer function $\mathbf{H}(\omega)$ can be obtained directly from the following relationship

$$\mathbf{x} = [-\mathbf{M}\omega^2 + j\omega\mathbf{D} + \mathbf{K}]^{-1} \mathbf{f} = \mathbf{H}(\omega) \mathbf{f} \quad (3.60)$$

Pre-and post-multiplying $\mathbf{H}(\omega)$ by the matrix of mode shape (normalized to mass) and its transpose

$$\begin{aligned} \mathbf{P}^T \mathbf{H}(\omega) \mathbf{P} &= \mathbf{P}^T [-\mathbf{M}\omega^2 + j\omega\mathbf{D} + \mathbf{K}]^{-1} \mathbf{P} \\ &= \text{diag} \left[\frac{1}{-\omega^2 + j\omega \frac{c_1}{m_1} + \frac{k_1}{m_1}}, \dots, \frac{1}{-\omega^2 + j\omega \frac{c_n}{m_n} + \frac{k_n}{m_n}} \right] \end{aligned} \quad (3.61)$$

With $\mathbf{P} = [\mathbf{p}_1, \dots, \mathbf{p}_n]$, it becomes

$$\begin{aligned} \mathbf{H}(\omega) &= \mathbf{P} \text{diag} \left[\frac{1}{-\omega^2 + j\omega \frac{c_1}{m_1} + \frac{k_1}{m_1}}, \dots, \frac{1}{-\omega^2 + j\omega \frac{c_n}{m_n} + \frac{k_n}{m_n}} \right] \mathbf{P}^T \\ &= \sum_{i=1}^n \frac{\mathbf{P}_i \mathbf{P}_i^T}{-\omega^2 + j\omega \frac{c_i}{m_i} + \frac{k_i}{m_i}} \end{aligned} \quad (3.62)$$

Element of the matrix $\mathbf{H}(\omega)$ has than expression

$$h_{rs}(\omega) = \sum_{i=1}^n \frac{p_r^i p_s^i}{\omega_i^2 - \omega^2 + 2j\zeta_i \omega \omega_i} \quad (3.63)$$

With recall,

$$\omega_i^2 = \frac{k_i}{m_i} \quad (3.64)$$

and

$$\zeta_i = \frac{c_i}{2\omega_i m_i} \quad (3.65)$$

3.4.2 Hysteretic damping Model

3.4.2.1 Derivation of the equations of motion

The hysteretic model - also known as structural [104] - provides a realistic description where the structure is subject to harmonic vibration-type. According to this model, the constitutive law is written

$$\boldsymbol{\sigma} = \tilde{\mathbf{C}}(\mathbf{x}) \boldsymbol{\varepsilon}(\mathbf{x}, t) = [\mathbf{C}'(\mathbf{x}) + j\mathbf{C}''(\mathbf{x})] \boldsymbol{\varepsilon}(\mathbf{x}, t) \quad (3.66)$$

with $\tilde{\mathbf{C}}$ the complex elasticity matrix defined as

$$\tilde{\mathbf{C}} = \mathbf{C}' + j\mathbf{C}'' \quad (3.67)$$

The matrix of elasticity \mathbf{C}' and the matrix of dissipation \mathbf{C}'' forming the real and imaginary parts of complex elasticity matrix. The matrix of dissipation of the hysteretic case is not identical to that of the viscous case; its elements also have not the same unit as in the case of viscous (viscosity units), whereas in hysteretic dissipating matrix elements are expressed in units of stress.

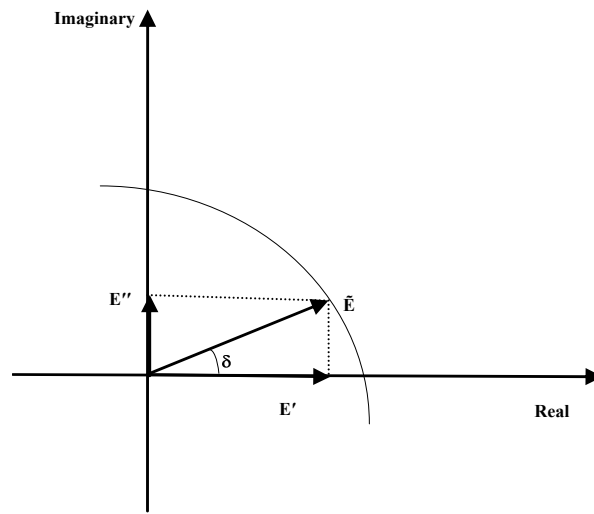


Figure 3.2 Representation of complex Young modulus in complex plane

Consider one-dimensional problem, the hysteretic model state that when imposing a harmonic stress σ , the strain ε has a frequency identical to the stress but will be out of phase by an angle δ . For one-dimensional case, the constitutive law is reduced then

$$\sigma = \tilde{E} \cdot \varepsilon = (E' + jE'')\varepsilon = E' \left(1 + j \tan \delta(\tilde{E}) \right) \varepsilon \quad (3.68)$$

with complex Young's modulus \tilde{E} , consisting of its real part or storage module E' and its imaginary part or loss modulus E'' . The loss tangent Young's modulus $\tan \delta(\tilde{E})$ defined as the following ratio.

$$\tan\delta(\tilde{E}) = \frac{E''}{E'} \quad (3.69)$$

is a measure of the damping of material, as shown in Figure 3.2 complex, Young's modulus is represented in the complex plane.

In a similar approach, that is developed in paragraph 3.4.1.1, the semi-discrete matrix form, governing the dynamic behavior in free system of the hysteretic damping structure is written as,

$$\mathbf{M}\ddot{\mathbf{q}}(t) + (\mathbf{K}' + j\mathbf{K}'')\mathbf{q}(t) = 0 \quad (3.70)$$

Where the mass matrix is identical to that of the relation (3.20), but where the stiffness matrices of storage \mathbf{K}' and loss \mathbf{K}'' is written as

$$\mathbf{K}' = \int_{\Omega} \nabla \mathbf{H}^T \mathbf{C}' \nabla \mathbf{H} d\Omega \quad (3.71)$$

$$\mathbf{K}'' = \int_{\Omega} \nabla \mathbf{H}^T \mathbf{C}'' \nabla \mathbf{H} d\Omega \quad (3.72)$$

3.4.2.2 Eigenvalue equation

The solution for the discrete displacement vector \mathbf{q} is of the form

$$\mathbf{q}(\mathbf{t}) = \mathbf{p}e^{j\lambda t} \quad (3.73)$$

The eigenvalue problem associated with free vibrations of the structure with internal damping is expressed as

$$(-\lambda^2 \mathbf{M} + \mathbf{K}' + j\mathbf{K}'')\mathbf{p} = (-\lambda^2 \mathbf{M} + \tilde{\mathbf{K}})\mathbf{p} = 0 \quad (3.74)$$

In this equation, the complex stiffness matrix $\tilde{\mathbf{K}}$ consists of real \mathbf{K}' and imaginary \mathbf{K}'' parts. According to the nature of depreciation, solutions are complex and consist of n pairs of complex conjugate eigenvalues $\lambda_i (i = 1, 2, \dots, n)$ and n pairs of complex conjugate eigenvectors $\mathbf{p}_i (i = 1, 2, \dots, n)$ of dimension n . Each eigenvalue takes the form

$$\lambda_i^2 = \omega_i^2 (1 + j\eta_i) \quad (i = 1, 2, \dots, n) \quad (3.75)$$

Where ω_i and η_i are eigen frequency and modal damping factor for the i -th mode. The comparison of eigenvalues expression for two damping types is presented here. For the hysteretic model, solution of the form (3.73) is assumed, which allows to explain the values of the form (3.75). It was seen that for a problem of viscous, it is common to choose the solutions of the form (3.25) to achieve the shape (3.33) of the eigenvalues. In both cases, the eigenvalue obtained is complex and, by comparing the shapes of the exponential part of (3.25) and (3.73) with the index i omitted, equality

$$j\lambda_c = \lambda_v \quad (3.76)$$

should be respected, the index v and c representing the viscous and hysteretic damping. This comparison is justified by the fact that it should be possible to seek solutions of the form (3.75) to the equation of the dynamic behavior with a viscous damping (3.21) or, conversely, the solutions of the form (3.25) to equation (3.70). It follows that

$$-\lambda_c^2 = \lambda_v^2 \quad (3.77)$$

However, according to the equalities (3.33) and (3.75), it becomes

$$\lambda_v^2 = (-\alpha + j\omega)^2 = \alpha^2 - \omega^2 - 2j\alpha\omega \quad (3.78)$$

$$\lambda_c^2 = \omega^2 (1 + j\eta) = \omega^2 + j\eta\omega^2 \quad (3.79)$$

Assuming α small against ω , the relation (3.35) becomes

$$\zeta = \frac{\alpha}{\sqrt{\alpha^2 + \omega^2}} \cong \frac{\alpha}{\omega} \quad (3.80)$$

so that the expression (3.78) takes the form

$$\lambda_v^2 \cong -\omega^2 - 2j\zeta\omega^2 \quad (3.81)$$

Therefore, comparing the forms of (3.79) and (3.81) to suggest that, for low damping, equality (3.76) is verified with

$$\eta = 2\zeta \quad (3.82)$$

3.4.2.3 Hysteretic model in continues harmonic system

Assuming deformation of the form

$$\tilde{\epsilon}(t) = \epsilon e^{j\omega t} \quad (3.83)$$

With $\tilde{\epsilon}$ the complex deformation of amplitude ϵ and of frequency ω , The constitutive law taking into account hysteric type damping for one-dimensional continues harmonic vibration system (considering relation 3.66) becomes

$$\tilde{\sigma}(t) = C'\tilde{\epsilon}(t) + jC''\tilde{\epsilon}(t) \quad (3.84)$$

3.4.2.4 Frequency response function

According to hysteresis model, starting from the equation (3.70) with second term and performing the following transformation

$$\begin{aligned} \mathbf{q} &= \mathbf{x}e^{j\omega t} \\ \ddot{\mathbf{q}} &= -\omega^2\mathbf{x}e^{j\omega t} \end{aligned} \quad (3.85)$$

the equation becomes

$$(-\omega^2 \mathbf{M} + \mathbf{K}' + j\mathbf{K}'')\mathbf{x}e^{j\omega t} = \mathbf{f}e^{j\omega t} \quad (3.86)$$

With \mathbf{f} representing the excitation force. The transfer function $\mathbf{H}(\omega)$ can be directly derived from the expression

$$\mathbf{x} = [-\mathbf{M}\omega^2 + \mathbf{K}' + j\mathbf{K}']^{-1}\mathbf{f} = \mathbf{H}(\omega)\mathbf{f} \quad (3.87)$$

Pre-and post-multiplying the transfer function matrix by the mode shape normalized to the mass and by its transpose

$$\mathbf{P}^T \mathbf{H}(\omega) \mathbf{P} = \mathbf{P}^T [-\mathbf{M}\omega^2 + \mathbf{K}' + j\mathbf{K}']^{-1} \mathbf{P} \quad (3.88)$$

$$\begin{aligned} \mathbf{H}(\omega) &= \mathbf{P} \text{diag} \left[\frac{1}{-\omega^2 + \lambda_1^2}, \dots, \frac{1}{-\omega^2 + \lambda_n^2} \right] \mathbf{P}^T \\ &= \sum_{i=1}^n \frac{\mathbf{P}_i \mathbf{P}_i^T}{-\omega^2 + \lambda_i^2} \end{aligned} \quad (3.89)$$

The transfer function between points r and s using equation (3.75) becomes;

$$h_{rs}(\omega) = \sum_{i=1}^n \frac{p_r^i p_s^i}{\omega_i^2 - \omega^2 + j\eta_i \omega_i^2} \quad (3.90)$$

3.5 COMPLEX MATRIX OF ELASTICITY

The global stiffness matrix \mathbf{K} and damping \mathbf{D} for the case viscous as well as the complex stiffness matrix $\tilde{\mathbf{K}}$ for the hysteresis cases are constructed from the complex matrix of elasticity expressed in the global coordinate system. It is necessary to formulate this complex matrix of elasticity from the constitutive properties of complex material. This complex matrix for isotropic constitutive law is based on the formulation

of the elasticity matrix for the conservative case, and can be used for an internal damping of hysteresis or viscous type.

Case hysteretic

In agreement with the viscoelastic correspondence principle, it is assume that the shape of the complex matrix of elasticity for a given type of FE is similar to the configuration of the matrix of elasticity of the corresponding conservative case, but with complex components. The complex elasticity matrix for a linear isotropic material is defined as

$$\tilde{\mathbf{C}} = \begin{bmatrix} \tilde{\mathbf{C}}_{11} & \tilde{\mathbf{C}}_{12} & \tilde{\mathbf{C}}_{12} \\ \tilde{\mathbf{C}}_{12} & \tilde{\mathbf{C}}_{11} & \tilde{\mathbf{C}}_{12} \\ \tilde{\mathbf{C}}_{12} & \tilde{\mathbf{C}}_{12} & \tilde{\mathbf{C}}_{11} - \frac{\tilde{\mathbf{C}}_{12}}{2} \\ & & \frac{\tilde{\mathbf{C}}_{11} - \tilde{\mathbf{C}}_{12}}{2} & \frac{\tilde{\mathbf{C}}_{11} - \tilde{\mathbf{C}}_{12}}{2} \\ & & & \frac{\tilde{\mathbf{C}}_{11} - \tilde{\mathbf{C}}_{12}}{2} \end{bmatrix} \quad (3.91)$$

With the components written according to the complex constitutive properties of the material

$$\tilde{\mathbf{C}}_{11} = \frac{\tilde{E}(1 - \tilde{\nu})}{(1 + \tilde{\nu})(1 - 2\tilde{\nu})} \quad (3.92)$$

$$\tilde{\mathbf{C}}_{12} = \frac{\tilde{\nu}\tilde{E}}{(1 + \tilde{\nu})(1 - 2\tilde{\nu})} \quad (3.93)$$

$$\frac{\tilde{\mathbf{C}}_{11} - \tilde{\mathbf{C}}_{12}}{2} = \frac{\tilde{E}}{2(1 + \tilde{\nu})} \quad (3.94)$$

The above equations provides the following relation between the three engineering constants of an isotropic material

$$\tilde{G} = \frac{\tilde{E}}{2(1 + \tilde{\nu})} \quad (3.95)$$

Note that for isotropic materials, every plane is a plane of symmetry. Therefore, the properties of isotropic materials cannot vary in function of the material orientation.

Where $\tilde{\mathbf{C}}_{ij}$ is the ij -th component of the complex elasticity matrix, and \tilde{E} , $\tilde{\nu}$ and \tilde{G} are respectively, Young's modulus, Poisson's ratio and shear modulus. The latter are defined as complex quantities

$$\tilde{E} = E[1 + j\tan\delta(E)] \quad (3.96)$$

$$\tilde{\nu} = \nu[1 + j\tan\delta(\nu)] \quad (3.97)$$

$$\tilde{G} = G[1 + j\tan\delta(G)] \quad (3.98)$$

Where $\tan\delta(\cdot)$ is the dimensionless factor loss associated with the complex quantity ($\tilde{\cdot}$) and phase δ .

Viscous case

In the viscous case, it is possible to keep the same architecture of the complex matrix of elasticity, but by constructing the elemental matrices of stiffness and damping from the real and imaginary parts of $\tilde{\mathbf{C}}_{ij}$

$${}^e\mathbf{K} = \int_{{}^e\Omega} {}^e\mathbf{B}^T \Re(\tilde{\mathbf{C}}) {}^e\mathbf{B} d\Omega \quad (3.99)$$

$${}^e\mathbf{D} = \int_{{}^e\Omega} {}^e\mathbf{B}^T \Im(\tilde{\mathbf{C}}) {}^e\mathbf{B} d\Omega \quad (3.100)$$

In addition, if engineering constants are keep similar to the case (3.96) to (3.98), it is important to note that in the case of a viscous damping, $\tan\delta$ is the size over a dimensionless loss factor, but it takes a time dimension (usually in seconds), so that the

elements of the damping matrix D have a unit of viscosity. It is therefore not possible to directly compare the values of loss tangent for the two models.

3.6 CELLULAR MATERIALS MODELLING

Porous metals, metallic foams and cellular materials are materials with pores deliberately integrated in their structure. Porous metals refer to the metals with a large volume fraction of porosity, whereas the term foamed metal or metallic foams applies to porous metals fabricated through the foaming process [150]. Metallic foams have become the new trend materials due to their low densities, good mechanical properties and some specialized functions like air and water permeability, high-energy absorption, novel physical, mechanical, thermal, electrical and acoustic properties.

Metallic foams possess a favourable combination of good mechanical and physical properties, while maintaining very low weight. They are excellent candidates for innovative future designs, in which high strength and low weight are design parameters. Special interest in this type of materials is currently devoted to investigating the potential use of metallic and non-metallic cellular materials to enhance vehicle crashworthiness. To characterize and model foam materials a large number of experimental and numerical investigations appeared in the literature.

Most of the mechanical properties of foam materials can be achieved with other materials, sometimes more effectively, but foams can offer a unique combination of several properties that cannot be obtained in one conventional material at the same time, like ultra-low density, high stiffness, the capability to absorb crash energy, low thermal conductivity, low magnetic permeability, and good vibration damping. Metal foams are thus promising in applications where several of these functions can be combined. These properties depend significantly on the porosity, so that a desired portfolio of properties can be tailored by changing the foam density [151]. This is one of the most attractive features of these remarkable materials.

Mechanical properties of metallic foam structure depend on the relative density of the structure. Relative density is the density of the foam material divide by that of the solid from which the cell walls are made. This influence, imperfectly understood at

present, is a topic of intense study. Various constitutive relations have been suggested for the characterization and modelling of this relationship. These laws, originally developed for polymeric foams, are usually based on the relative density of the foam, and therefore suppose uniform cellular structure, at least at a macroscopic level. However, metallic foams are dramatically different from polymeric foams: polymeric foams generally have a regular microstructure, whereas metallic foams may be highly disordered with a wide dispersion of cell size and shape. Moreover, many imperfections exist in a cell structure, such as cracks or holes in the cell walls, corrugated cells etc. These effects are inevitable due to manufacturing at significantly higher temperatures than in the case of polymers. If these features are not taken into account and the properties of the foam are characterized only in relation to average density, a higher scatter of properties is to be expected [151].

The design of mechanically efficient metallic foams is the paramount aspect of foam modelling and simulation, the aim being the development of "optimum" foam structures. Design engineers who use components made of metallic foams are interested in easy-to-use methods of describing the constitutive behavior of these materials, for example in the form of constitutive material laws for use with general-purpose FE codes. For such purposes, it is neither possible nor desirable to account for details of the foams micro geometry at each position in the component. Instead, the material behavior of the foam is described in terms of equivalent homogeneous material. Such constitutive models may be derived from micromechanical studies by homogenization, or they may take the form of phenomenological macroscopic descriptions that employ material parameters, which have to be obtained from experiments [152].

For some purposes full constitutive descriptions are not required and material characterization can provide the necessary information. This can take the form of experimentally based relations, for example in the form of stress-strain relations parameterized by the effective density of the foam. Alternatively, micromechanical reasoning may be used to derive generic mathematical relationships, which can then be fitted to experimental results and provide physically based regression formulae. Some approaches in modelling the inhomogeneties of foam exist in the literature: Daxenr et al. [153] and Gradingner and Rammerstorfer [154] have studied spring-mass models, while

Meguid et al. [155] modeled 3D foam with shell elements and let the thickness of the element vary with a Gaussian distribution. Several constitutive models for foam exist in literature, some of them are quite simple; others are more complicated with several material parameters. There are also few or no recommendations on how to include the uneven distribution of pores and fracture in the models [156].

Design calculations in mechanical engineering require some reliable constitutive description of the mechanical behavior of metallic foam. Such constitutive descriptions are usually extrapolated from bulk material including hydrostatic pressure influence and are implemented in FE software packages [157, 158], the material parameters are then obtained by means of calibration procedures in relation with experimental data normally compression test without any reference to the microstructure. However, the mechanical properties of metallic foams are mainly related to those of solid material and to the foam microstructure [159, 160]. In that sense, cellular materials can be themselves considered as structures at the micro scale. Then, the structure relationship issue includes two different aspects depending on the practical application point of view. In the mechanical context, the purpose is to quantitatively connect the macroscopic properties of the cellular material to those of the solid one and the microstructure. For this purpose, various mechanical models able to reproduce the deformation mechanisms observed in cellular materials can be used. Gibson and Ashby [161], Zhu [162] and Ko [163] proposed different approaches based on a regular cell. They assume scaling laws to link the elastic moduli, the elastic collapse stress and the plastic collapse stress of the cellular material to the elastic modulus and the yield stress of the solid material and to the relative density of the foam. The relative density is the only parameter available for the description of the microstructure [164]. Some approaches assume that the structure can be represented by a strut pattern that is either regular [165, 166] or irregular [166, 167]. The structures described in this way are more regular than the ones observed in reality. These models are also most of the time devoted to small density cellular materials. Another improvement in the mechanical description of the problem has been proposed by Roberts and Garboczi [168]. These authors use a voxel description of the solid volume as an input for the generation of a FE model of the material. This approach enables the complete description of the actual structure, numerically generated [168] or obtained by means of X-ray tomography images [169].

Several constitutive material laws describing the overall behavior of cellular metals have been proposed and applied in the simulation of components consisting of or containing metallic foams. Obviously, the selection of a particular material law is governed by the required material parameters and by the effort necessary for calibrating them by experiments or via micromechanical studies. Because they are based on the use of an equivalent homogeneous continuum, macroscopic material laws should only be used for studying components or samples that are considerably larger and thicker than the typical cell size of the foam.

The most basic aspect of the mechanical material characteristics of inhomogeneous material is their linear elastic behavior, which can be describe in term of overall elasticity tensor or appropriate effective moduli. Linear dependence of plateau stress, Young's modulus and energy absorption capacity with relative density is reported in [170-172]. Aluminum foam is one of the common metallic foam, many researcher have investigated the mechanical properties of various aluminum foams e.g. Alporas [159, 173] and Alulight [174]. All the results show that Young's modulus and yield stress are related to the relative density. The general equation for the plateau stress of regular hexagonal closed-cell foam is suggested by Gibson and Ashby [161] and is given by;

$$\frac{\sigma_{pl}^*}{\sigma_{ys}} = 0.3\phi^{3/2} \left(\frac{\rho^*}{\rho_s}\right)^{3/2} + (1 - \phi) \frac{\rho^*}{\rho_s} \quad (3.101)$$

The equation for the theoretical elastic modulus of a closed-cell foam is expressed as [161];

$$\frac{E^*}{E_s} = \phi^2 \left(\frac{\rho^*}{\rho_s}\right)^2 + (1 - \phi) \frac{\rho^*}{\rho_s} \quad (3.102)$$

Where ϕ (Phi) is the volume fraction of solid contained in the cell edges, the remaining fraction $(1 - \phi)$ is in the cell faces. E^* , σ_{pl}^* , ρ^* are the Young's modulus, yield stress and density of metallic foam and E_s , σ_{ys} , ρ_s of matrix material respectively.

3.6.1 Finite element modelling

A large number of available software packages like COMSOL, ABAQUS, and ANSYS etc. incorporate finite elements based analysis. In this research work an attempt has been made with ANSYS (version 13.0) software package to bring into focus the versatility and powerful analytical capabilities of finite elements technique by objectively modeling the complete response of test specimens. ANSYS parametric design language (APDL) is used to compute the vibratory behavior of AF specimens. The proposed FE model partitioned foam specimen in to an arrangement of regions. The foam material is represented by an array of relative densities assigned to each region. Each foam region is represented by a sub-domain, the Young's modulus relationship of which is defined as function of the apparent density by (3.102). The parameter \emptyset in (3.102) for Young's modulus, Poisson's ratio and damping are considered as variable parameters of the FE model. Density mapping measured with X-ray computer tomography is given as input to this model.

In FE method the continuous model is reduced to discrete model with finite number of degrees of freedom. This is done by dividing the volume of the specimen into a number of elements. The AF specimens are modeled by using three-dimensional brick elements, also referred as hexahedron element. From finite element theory point of view [175], the formulation of this element is simple, efficient and reliable. The element is defined by eight nodes having three degrees of freedom at each node: translations in the nodal x, y, and z directions. The element has plasticity, creep, swelling, stress stiffening, large deflection, and large strain capabilities. For this type of element a reduced integration option with hourglass control is also available in ANSYS. The analysis with uniformly reduce integration method is not as accurate as with the full integration method [176]. So, despite the advantage of less CPU time and disk-space consumed by uniformly reduce integration method, full integration method is selected.

In case of 3D elements, the unknowns are the values of the displacement field at the nodes of the elements. The displacements of the point between the nodes are obtained from nodal displacements by interpolation. In FE terminology, the interpolation functions are called shape functions. Shape function matrix of an element is obtained by grouping the shape functions of all the degrees of freedom of that

element. Shape function matrix is used for relating the continuous displacement, strain, and acceleration to the nodal displacement, strain, and acceleration respectively. For the discrete model, the integral of the system equations can be expressed as a sum of integrals over elements. Discrete model equations (2.2) can be obtained by grouping the nodal displacements of the whole model into one global displacement vector.

A special procedure called density mapping method is applied to approximate the cellular structure of aluminum foam with continuum. The microscopical density distributions of the AF, recorded by X-ray computed tomography are averaged over a certain domain. The local average density represented by a mean density forms a so called ‘sub-domain’. All finite elements in the sub-domain behave mechanically in the same way. Each sub-domain is assumed to be homogeneous and isotropic. Density distributions of AF measured by X-ray computer tomography are used as input to the corresponding FE model of investigated specimen. Its mechanical properties are modeled using Gibson and Ashby scaling law (3.102) for regular foams. In this scaling law, the microstructure of cellular materials is homogenized over a scale infinitely larger than the typical microstructure. In other words these relations predict the behavior of a material that is assumed to be a homogeneous continuum. The input mechanical properties of the bulk material used in scaling law (3.102) for AF specimens are Young’s modulus of 69 GPa and density of 2700 Kg/m³.

It is already noted that the major difference between the two models, viscous damping and hysteresis, lies in the evolution of modal damping factor with frequency. The choice of the type of solver to use in the identification of damping properties of materials will depend on the realism of the underlying model. Therefore, it is interesting to compare the two models viscous and hysteresis to reality. Modal damping factors measured at each mode of several plates, including: Alporas_B2, Alporas_B3, Alporas_S2 and Alporas_S3 are shown in Figure 3.3.

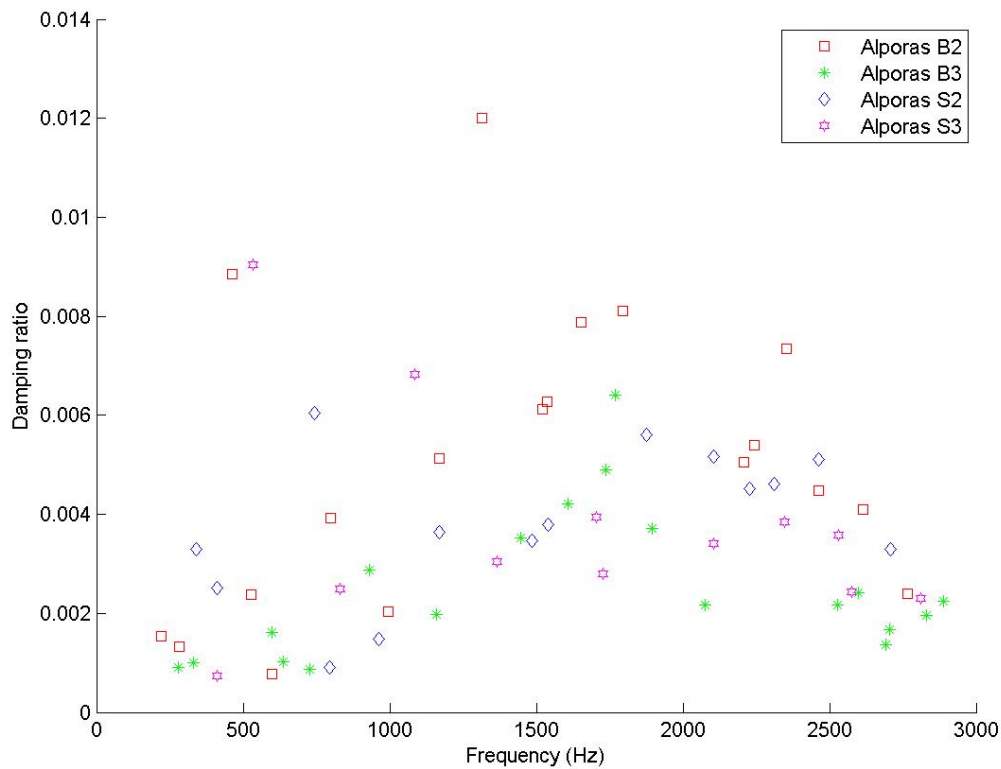


Figure 3.3 Comparison of damping ratios of aluminum foam specimen

Looking at the scatter plot of experimental modal damping ratios in Figure 3.3, it is difficult to see a clear dependence with frequency. None shows clearly taking damping effects in importance with the frequency. It is known that viscous damping model behavior of modal damping factors is clearly frequency dependent. Looking at the available models, material dependent damping is chosen in simulation although the hysteresis model type is preferred for use as part of the modal identification. Complex modal analysis is performed using QR Damped method. This method is faster and more stable than the existing damped solver. It combines the best features of the real eigensolution method (Block Lanczos) and the Complex Hessenberg method (QR Algorithm). Outputs are complex eigenvalues (frequency and stability) and damping ratio of each mode.

All numerical investigations are carried out by means of the FE package ANSYS that defines the preprocessor (parametric model of the AF specimen), solution and postprocessor phase of the finite element analysis. In the preprocessor phase, the geometry and the boundary conditions of the model are defined using a set of APDL commands. QR damped method is used in solution phase to solve the model, build in preprocessor phase. In the postprocessor phase the results from the analysis was gathered and saved in a suitable format (file) for further use. ANSYS FE model of Alporas_B2 is shown in Figure 3.4.

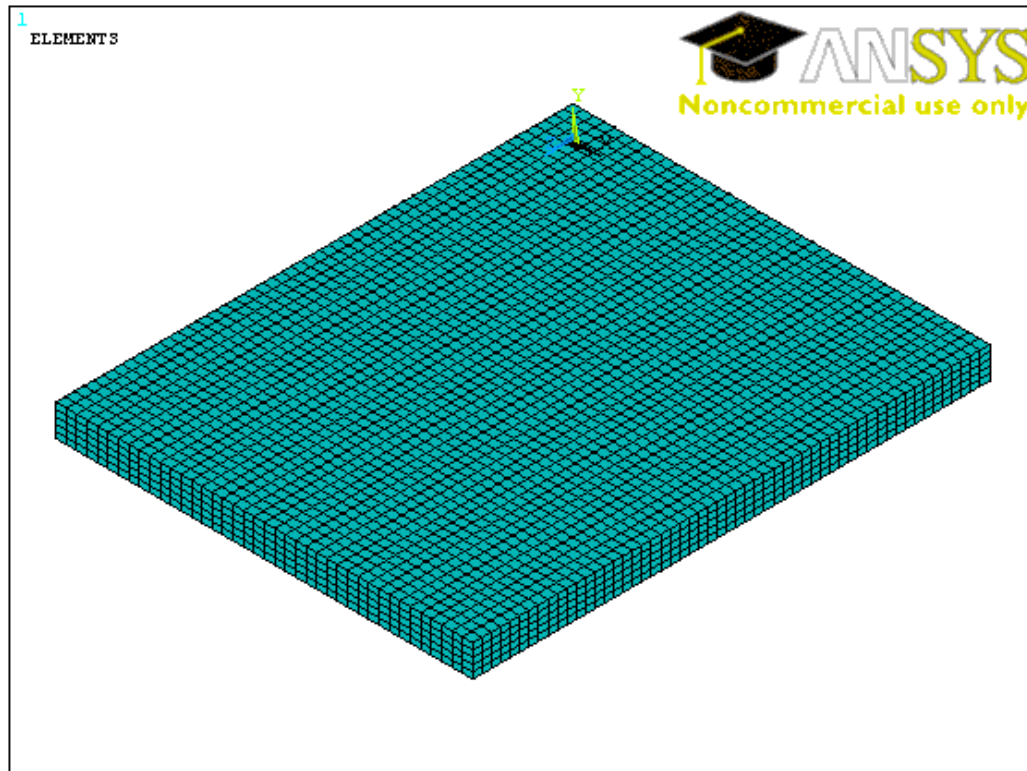


Figure 3.4 FE modelling of Alporas_B2

CHAPTER 4. MIXED NUMERICAL-EXPERIMENTAL IDENTIFICATION TECHNIQUE

4.1 BACKGROUND AND OBJECTIVES

The identification procedure can be considered as the key point of the process of mixed numerical-experimental identification technique. From a reference experimental modal model, this method evolved a parameterized numerical model (Figure 4.1) by changing a set of input parameters to identify at each iteration until a solution as close as the desired experimental modal model. The convergence of the numerical model to the experimental model is obtained by minimizing an error function which is representative of the difference between the two models, this difference is quantified from the various modal data. Thus, the identification routine is complete when standard error of this function - also called objective function - falls below a specified threshold value. During the last iteration, the input parameters of numerical model are the identified parameters.

In mixed numerical-experimental identification procedure, it is necessary to use an optimization method in order to identify the parameters of a numerical model, not invertible, to the target values that represent the experimental data. Thus, the optimization method is of prime importance in the parameter identification. However, the properties of error norms (or objective functions) to minimize also play an important role in the accuracy and robustness of the mixed numerical-experimental identification method, since these functions represent the extent of difference between numerical model of the current iteration and the experimental target values that the algorithm seeks to minimize. If these error norms are not sufficiently effective and does not capture all the physical effects of desired parameters, it is likely that a number of these parameters would ultimately find very poorly identified.

Thus in order to minimize the residual error in identification, while ensuring robustness and high rate of convergence, it is essential to develop a set of objective

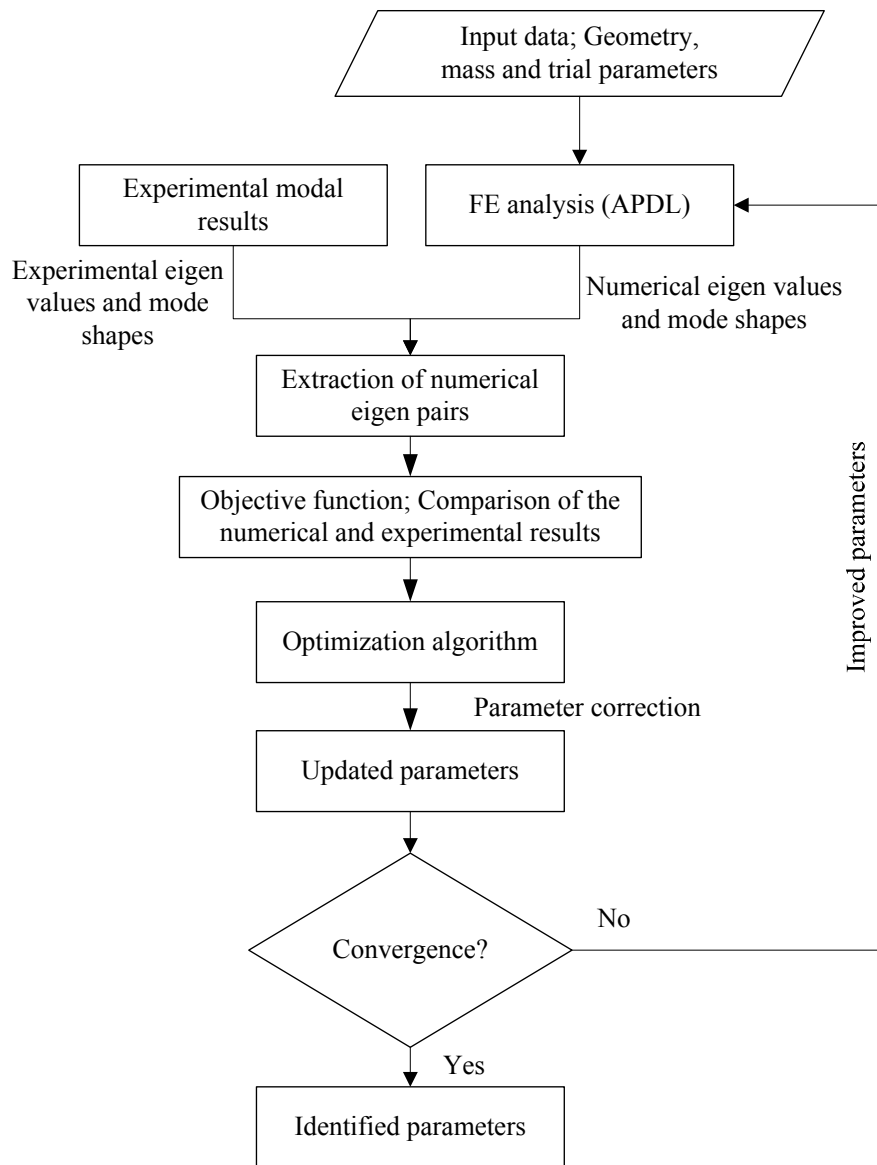


Figure 4.1 Flow diagram of mixed numerical-experimental technique.

functions suitable for available experimental and numerical data that meet the following conditions.

- **Sensitivity to parameters:** the objective functions must be sufficiently sensitive to identify all the parameters to ensure an excellent accuracy of identification. In addition, a high sensitivity but balanced error norms reduces the effects on the identified parameters of measurement uncertainties and possible experimental errors.

- **Robustness:** the error norms used must be convex and having only a single local minimum over a wide range of parameters to ensure the smooth running of the optimization procedure regardless of the initial estimate of parameters to identify .
- **Precision:** the objective functions must converge towards zero near the actual parameters and the residual error in identification must not come from effects of numeric truncation or approximation in the calculation of these functions.

The approach to develop the error functions and to develop the optimization algorithm is characterized by the following points:

1. Defining a set of functions possible based on the error norms commonly used in modal analysis and on original ideas.
2. Parametric study of large-scale FE on various types of aluminum foam plates to identify the robustness and sensitivity of the proposed error norms. The definition of the error norms function as a combination of selected elementary error functions.
3. Analysis, selection and implementation of a type of optimization algorithm corresponding to the needs.

4.2 MODAL ERROR NORMS

As the role of error norms is to measure the difference between all measured experimental and numerical modal data, thus error functions should not be based only on the measured and numerical eigen frequencies ω_k ($k = 1, 2, \dots, m$), but also on the experimental and numerical mode shapes ϕ_k ($k = 1, 2, \dots, m$). Finally, by analogy, the error norms required are the same as those used for years in the field of experimental modal analysis and identification of structures (i.e. [76, 104, 105, 124, 177, 178]). Thus, based on modal error norms proven in these areas, it is assured of obtaining high quality error functions.

The modal data that will be available for optimization algorithm for each mode k ($k = 1, 2, \dots, m$) at iteration i ($i = 1, 2, \dots, q$) are as follows:

- The measured eigen frequencies (target) ω_k ($k = 1, 2, \dots, m$) and the numerical at iteration i $\tilde{\omega}_k^i = \tilde{\omega}_k^i(x^i)$ ($k=1, 2, \dots, m$), where x^i represents the identification parameters vector at iteration i .
- The measured eigen modes (target) ϕ_k ($k = 1, 2, \dots, m$) and numerical at iteration i $\tilde{\phi}_k^i = \tilde{\phi}_k^i(x^i)$ ($k = 1, 2, \dots, m$), where x^i represents the identification parameters vector at iteration i .

However, the numerical and experimental meshes are not necessarily identical, these two modal vectors are not defined on the same mesh grids. In addition, it should be noted that only normal components of the displacement of the specimen are measured whereas numeric modal vector contains all the components. For the sake of simplicity and clarity, it is consider in this chapter that the measured and numerical eigen modes are already processed on a same reference mesh and only the degrees of freedom corresponding to the transverse displacements are retained.

The most conventional modal error norm is obviously based on the difference of measured eigen frequencies ω_k and numerical $\tilde{\omega}_k^i$ for each mode k ($k = 1, 2, \dots, m$) as the basis for identification. However, it is important to identify that the experimental mode shapes and the numerical modes must absolutely match before making any comparison of frequencies. Also, a method to precisely define pairs of numerical mode and corresponding experimental is applied before calculations of any error norms. It is assumed here that the numerical and experimental modes index k actually forms a pair of corresponding modes. Thus, the conventional error norm based on relative difference in eigen frequencies can be written:

$$F_k^{frq}(x^i) = \frac{\tilde{\omega}_k^i - \omega_k}{\omega_k} \quad (4.1)$$

Where x^i is the vector of estimates of parameters stored to identify constitutive properties at iteration i and k denotes the total number of mode considered. It is important to note here that the numerical predictions $\tilde{\omega}_k^i$ ($k = 1, 2, \dots, m$) are functions of the parameter vector x^i and are updated at each iteration of the optimization process.

Similarly, another objective function that quantifies the difference between the dissipative behavior of models is based on experimental and numerical modal damping factors. Measured modal damping factors ζ are obtained from the measured transfer functions and can be compared to numerical modal damping factors in the same way that the experimental and numerical eigen frequencies. This error norm can be written as

$$D_k^{mdr}(x^i) = \frac{\tilde{\zeta}_k^i - \zeta_k}{\zeta_k} \quad (4.2)$$

where x^i is again the vector of estimates of parameters stored to identify constitutive properties at iteration i and k denotes the total number of modes considered.

In modal analysis, the most commonly used method to evaluate the quality of measured eigen modes or the correlation between two sets of eigen modes is called MAC (Modal Assurance Criterion) method. The MAC method is based on the principle of theoretical orthogonality of specific ways to calculate projections of a set of eigen modes on the base formed by a second set of eigen modes. The MAC method thus provides a matrix $M_{jl} = MAC(\boldsymbol{\varphi}_j^a, \boldsymbol{\varphi}_l^b)$, scalar product between two sets of modes $\boldsymbol{\varphi}_j^a (j = 1, 2, \dots, m^a)$ and $\boldsymbol{\varphi}_l^b (l = 1, 2, \dots, m^b)$, which can be define as follow

$$M_{jl} = MAC(\boldsymbol{\varphi}_j^a, \boldsymbol{\varphi}_l^b) = \frac{(\boldsymbol{\varphi}_j^a \cdot \boldsymbol{\varphi}_l^b)^2}{(\boldsymbol{\varphi}_j^a \cdot \boldsymbol{\varphi}_j^a)(\boldsymbol{\varphi}_l^b \cdot \boldsymbol{\varphi}_l^b)} \quad (4.3)$$

Thus, if both set of modes $\boldsymbol{\varphi}_j^a$ and $\boldsymbol{\varphi}_l^b$ are identical, the MAC matrix M_{jl} is equal to an identity matrix, which corresponds to the case of a perfect correlation. In the field of modal analysis, it is generally considered that two modes $\boldsymbol{\varphi}_j^a$ and $\boldsymbol{\varphi}_l^b$ are similar or close if $M_{jl} > 0.7$ or 0.8 depending on the tolerance used for the intended application. Using the properties of the MAC matrix thus defined, first modal error norm can be written in the following form;

$$F_k^{mac-d}(x^i) = 1 - MAC(\tilde{\boldsymbol{\varphi}}_k^i, \boldsymbol{\varphi}_k) \quad (4.4)$$

for each mode pair, $k = 1, 2, \dots, m$.

However, under the orthogonality property of modes, a perfect correlation between two sets of eigen modes also implies that all non-diagonal terms in corresponding MAC matrix are zero. By exploiting this property, a second error function based on the modal matrix MAC can be defined by

$$F_k^{mac-nd}(x^i) = \sum_{j=1, j \neq k}^m MAC(\tilde{\boldsymbol{\varphi}}_j^i, \boldsymbol{\varphi}_k) \quad (4.5)$$

for each mode pair $k = 1, 2, \dots, m$.

Alongside the principle of modal projection used by the MAC method, it is also possible to measure the difference between the two sets of mode shapes simply by calculating a sum of absolute differences between components of the modal vectors. However, it is absolutely necessary in this case that the sets of modes are normalized and assigned in the same manner, for example by setting the maximum component to unity. An error function based on the components of modal vectors can be defined as:

$$F_k^{msv}(x^i) = \sum_{j=1}^r \left(\frac{(\tilde{\boldsymbol{\varphi}}_k^i)_j}{\max_l((\boldsymbol{\varphi}_k)_l)} - \frac{(\boldsymbol{\varphi}_k)_j}{\max_l((\boldsymbol{\varphi}_k)_l)} \right) \quad (4.6)$$

for each mode pair $k = 1, 2, \dots, m$

Where $(\tilde{\boldsymbol{\varphi}}_k^i)_j$ and $(\boldsymbol{\varphi}_k)_j$ represent the j -th components of the vectors $\tilde{\boldsymbol{\varphi}}_k^i$ and $\boldsymbol{\varphi}_k$ while r symbolizes the number of components of the modal vectors.

Finally, a last correlation method commonly used in modal analysis, certainly more visual and quantitative, is based on comparing the shape and nodal lines position of each mode pair. The advantage of this method of comparison is mainly to be potentially less sensitive to noise and measurement errors than other error norm based on mode shapes, due to the intrinsic nature of the nodal lines. To automate and

rigorously quantify this measurement error, principle of image correlation is used. The process of modes pairing $\boldsymbol{\varphi}_k$ and $\tilde{\boldsymbol{\varphi}}_k^i$ begins first by a bicubic interpolation of mode shapes on a grid of relatively fine dimension approximately 256×256 points. The two tables of amplitudes ${}^k A_{rs}^i$ and ${}^k \tilde{A}_{rs}^i$ thus obtained are normalized absolute value so that each item is included in the interval $[0,1]$, allowing then to assimilate these tables to bitmap images of grayscale ${}^k I_{rs}^i$ and ${}^k \tilde{I}_{rs}^i$. These images are then filtered to show the nodal lines in grayscale on a black background, producing the images ${}^k J_{rs} = g({}^k I_{rs})$ and ${}^k \tilde{J}_{rs} = g({}^k \tilde{I}_{rs})$. The filter function $g({}^k I_{rs})$ linear interpolation of grayscale used during this treatment is defined as:

$$g({}^k I_{rs}) = \begin{cases} 0 & \text{if } {}^k I_{rs} > \delta \\ 1 - \frac{{}^k I_{rs}}{\delta} & \text{if } {}^k I_{rs} \leq \delta \end{cases}$$

Where δ symbolizes the tolerance relative amplitude defining the nodal lines (typical value of 10% for example).

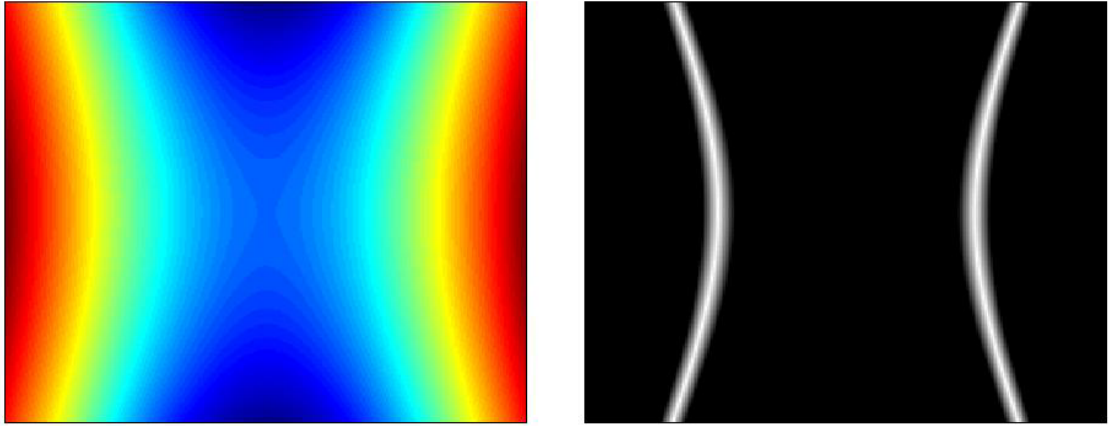


Figure 4.2 Eigen mode shape and grayscale image representing nodal lines (Alporas_B3, grid size 256×256 , $\delta = 0.1$)

Finally, the error norm between the nodal lines of the two modes $\boldsymbol{\varphi}_k$ and $\tilde{\boldsymbol{\varphi}}_k^i$ is calculated by the sum of the squares of the differences between the two images:

$$F_k^{nod}(x^i) = \frac{1}{a^2} \sum_{r=1}^a \sum_{s=1}^a ({}^k \tilde{J}_{rs}^i - {}^k J_{rs})^2 \quad (4.7)$$

For each mode pair of index $k = 1, 2, \dots, m$. Table 4.1 summarizes the error norm and nomenclature used in this work.

Table 4.1 list of the modal error norms

Analytical error norms	Nomenclature
$F_k^{freq}(x^i) = \frac{\tilde{\omega}_k^i - \omega_k}{\omega_k}$	RFreqD
$D_k^{mdr}(x^i) = \frac{\tilde{\zeta}_k^i - \zeta_k}{\zeta_k}$	MDRD
$F_k^{mac_d}(x^i) = 1 - MAC(\tilde{\boldsymbol{\varphi}}_k^i, \boldsymbol{\varphi}_k)$	MAC_d
$F_k^{mac_nd}(x^i) = \sum_{j=1, j \neq k}^m MAC(\tilde{\boldsymbol{\varphi}}_j^i, \boldsymbol{\varphi}_k)$	MAC_nd
$F_k^{msv}(x^i) = \sum_{j=1}^r \left(\frac{(\tilde{\boldsymbol{\varphi}}_k^i)_j}{\max_l((\boldsymbol{\varphi}_k)_l)} - \frac{(\boldsymbol{\varphi}_k)_j}{\max_l((\boldsymbol{\varphi}_k)_l)} \right)$	SumMSD
$F_k^{nod}(x^i) = \frac{1}{a^2} \sum_{r=1}^a \sum_{s=1}^a ({}^k \tilde{J}_{rs}^i - {}^k J_{rs})^2$	NLD

4.3 PARAMETRIC STUDY

To investigate the robustness and sensitivity of error norms, as well as to study the influence of variable parameters on the modal quantities, a parametric FE model study of AF specimens is conducted. The parameter Phi in (3.102) for Young's modulus,

Poisson's ratio and damping are considered as variable parameters in FE analysis. For each parameter thirty values "disturbed" at most $\pm 30\%$ around of the nominal value are defined. These parameters are distributed as follow; $\pm 0.09\%$, $\pm 0.18\%$, $\pm 0.36\%$, $\pm 0.8\%$, $\pm 1.6\%$, $\pm 3\%$, $\pm 6\%$, $\pm 9\%$, $\pm 12\%$, $\pm 15\%$, $\pm 18\%$, $\pm 21\%$, $\pm 24\%$, $\pm 27\%$ and $\pm 30\%$. In this study, only one parameter varies from the nominal values, the complete parametric study in the parameter space representing a cross, centered on the reference values. Thus, for each plate considered in the study, 3 combinations of parameters are evaluated, which make the entire study in 12 simulated cases. For each case, a FE model is generated for free boundary conditions and first 15 eigenvalues (excluding rigid body modes) are extracted by the developed MATLAB code which execute ANSYS for modal analysis. Finally, the results of each case of FE analysis are stored and modal error norms are calculated between the reference case (nominal parameters) and each perturbed case.

4.3.1 Implementation of parametric study in MATLAB

To complete this parametric study, a program is developed in the MATLAB environment. This program is based on two data sources: on one hand, the FE model and the problem to be solved are described in the traditional format of an APDL file of ANSYS, on the other hand, the parametric study itself is described in an executable MATLAB file, defining a data structure containing the specifications for all the parameters needed to study. The program developed for the parametric study consists of MATLAB functions that can be classified into three main categories:

1. Functions for performing calculations on all the case studies, including the functions of defining the parameter space, routines to merge the parametric FE model with a vector of parameters to generate a FE model (APDL) for ANSYS classic, procedures to execute and control the FE solver ANSYS and functions for reading the output files.
2. Functions performing the post-processing of FE data, including routines that ensure the conducting error norm calculations and synthesis of information from the parametric study, or which allow to load studies, search specific cases in the parameter space and load the corresponding modal data.

3. The functions for calculating modal error norm that implements the error functions presented in section 4.2. These functions are standardized and all use the same arguments, namely a pair of data structure storing the modal data to compare as well as sorted a list of numbers of modes to treat each case (defining pairs of modes).

The overall workflow execution of parametric study program is divided into two main stages: first, compute all FE models that are used in the study and store the modal data in a hierarchical file structure, then in a second step, run a large number of calculations based on post processing of the data created. The workflow of these two phases of processing is detailed below (Figure 4.3 and Figure 4.4).

The error norms, presented in Section 4.2, were implemented in the MATLAB program that calculates error vectors by comparing two data structures containing all modal information of a numerical "perturbed" case and the reference case. As in this study the mesh size of numerical models to be compared are always the same, as derived from the same parametric FE model, the development of modal error functions is very simple, because it is not necessary to project meshes on each other to calculate

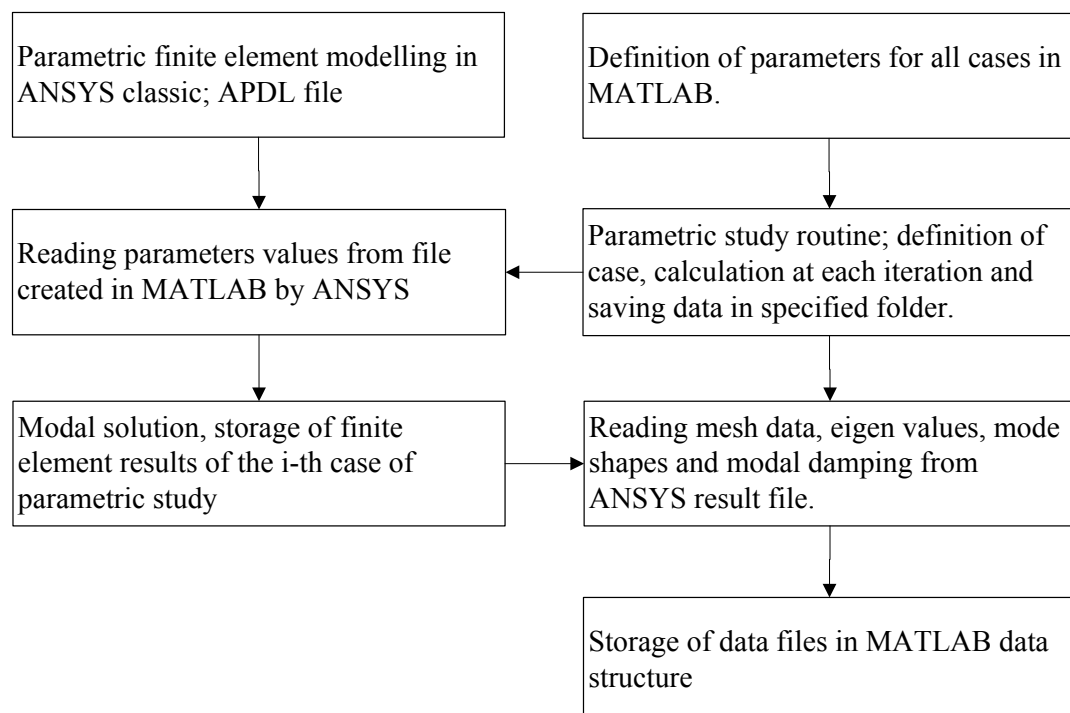


Figure 4.3 Block diagram of parametric study developed with MATLAB

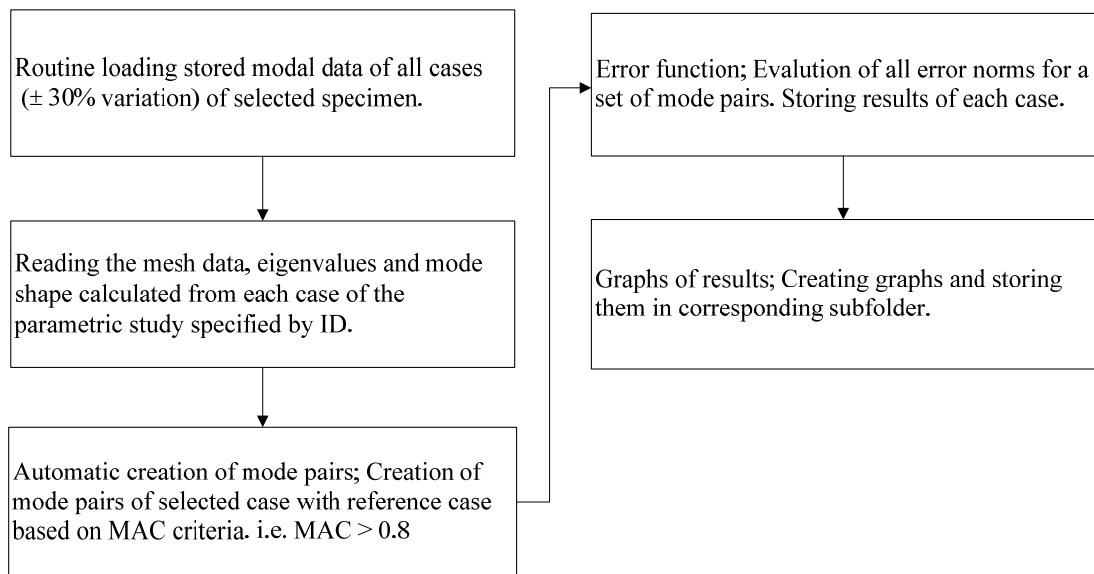


Figure 4.4 Block diagram of post-processing of parametric studies with the developed MATLAB program.

the error norm. However, the order of the modes can change significantly depending on the variable parameters, it is absolutely necessary to define (automatically) pairs of corresponding modes before performing the comparison of two models. The method of sorting and creation of pairs of modes used here is based again on the MAC matrix of two sets of modes (in full), in which each column and each row correspond respectively to a mode of reference model and a perturbed model. For each mode of the reference model specified in the list of modes to be studied (user input), the maximum component of the corresponding column of the matrix MAC is desired, thereby determining how that (perturbed) is best correlated with the reference mode. If this component exceeds a maximum limit (classical tolerance 0.7), the mode pair is then validated.

The study of the evolution of error functions over a range of parameters is investigated. A variable parameter is selected and a range of values of this parameter is specified by the user. A search is then performed on the entire database to select corresponding cases and calculate their error norms. The results are finally presented as 2D graphs. This study is achieved by using a macro-procedure automating this task.

4.3.2 Robustness of error functions

To ensure efficient identification, modal error norms must not only be sensitive to all parameters to be identified, but having only a single minimum over a wide range of parameters, thus ensuring the robustness of the method. In fact, during the first iteration of the identification method, a set of variable parameter estimated roughly is used to initialize the algorithm, resulting in generally significant deviations from the actual parameters. The robustness of the identification procedure is therefore conditioned partly by the evolution of different modal error norms over a wide range of variable parameters. These error functions are eventually intended to be incorporated into a modal error norms of hybrid weighted least squares type. Convexity of the functions or the sign of these have no impact on the convexity of the final hybrid error norm; only the presence of multiple extreme and possible inflection points in the error functions are really important for the robustness of identification method.

Using the database of parametric studies conducted in this work, each error norm on a large number of parameter vectors (4 cases over 10 modes and 6 error norms) can be analyzed. A post-processing procedure has been created specifically for this purpose and to generate graphs evolving error norms in the range of a parameter. As this analysis generates a large number of figures only results of Alporas_B2 for example are shown in the following figures.

Figure 4.5 illustrates the evolution of modal error norms on a range of $\pm 30\%$ of variable parameters for Alporas_B2 plate. It shows expected behavior of quasi-linear nature of each parameter in the error norm frequency (EcRelFreq). Norms based on the MAC (MAC_d and MAC_nd) matrix were a quadratic character directly resulting from the definition of this modal correlation matrix. Nodal lines difference (NLD) also has this quadratic character and its evolution proved to be very close to those of norms based on the MAC matrix.

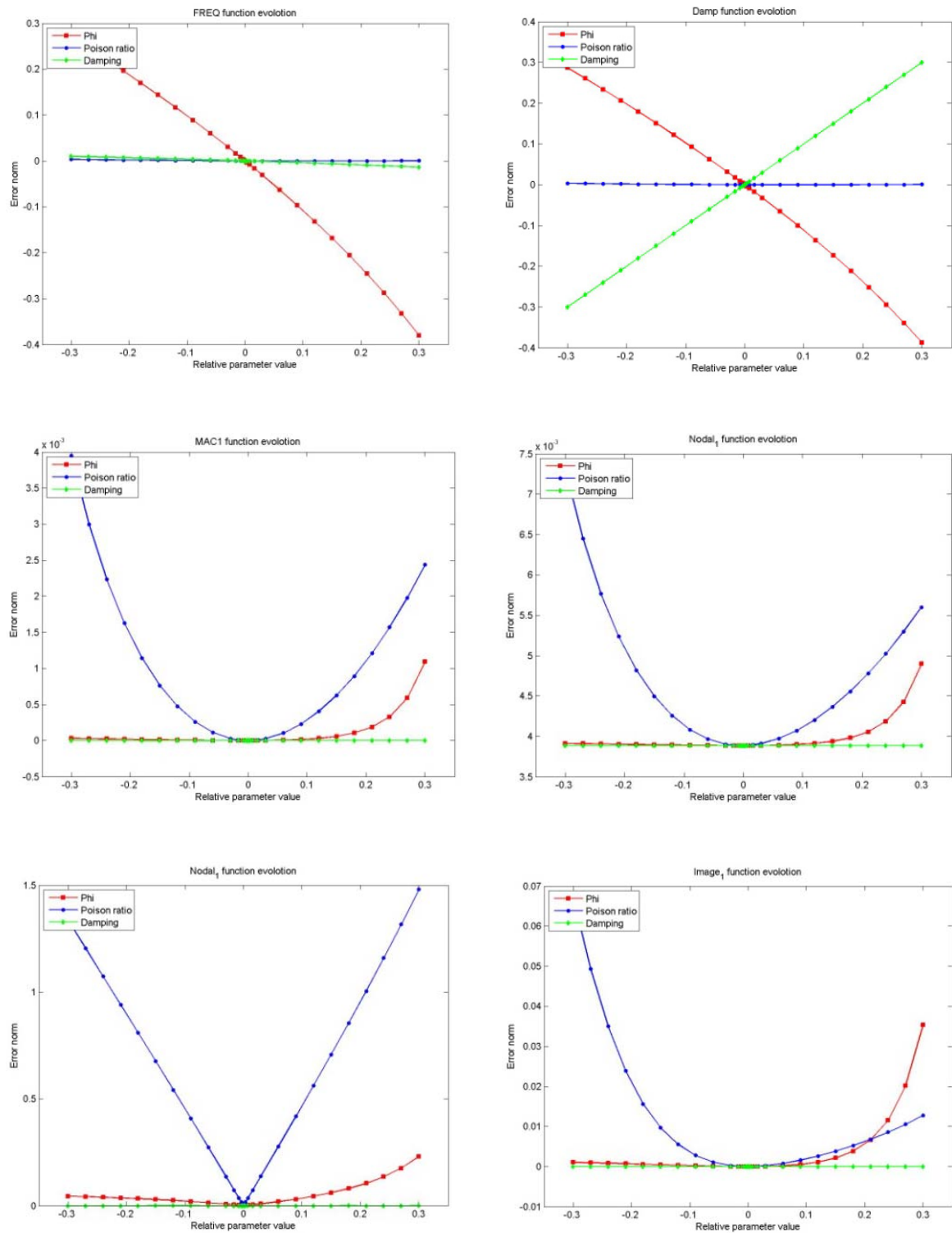
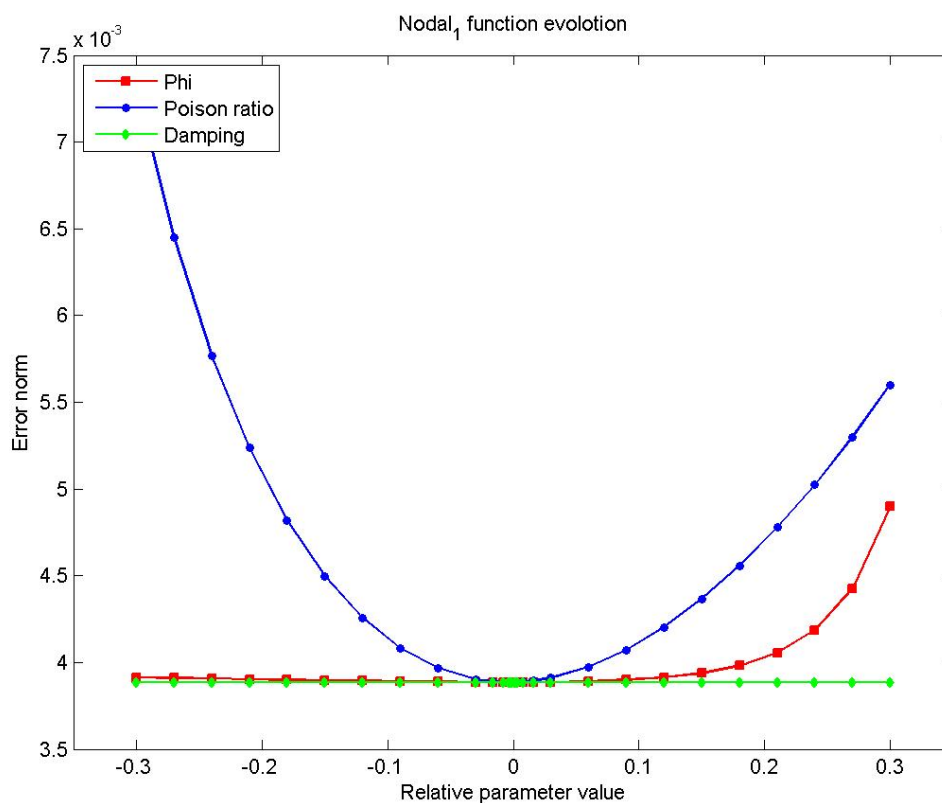


Figure 4.5 Evolution of modal error norms (sum all modes) on a range of $\pm 30\%$ of each variable parameter (Alporas_B2)

Finally, the norm of the sum of the absolute modal components (SumMSD) differentials reveals very clearly a character "absolute" highlighted by very sharp at the minimum point slope discontinuity measurement which may cause difficulties at the level of identification algorithm if the error norm is used alone or too heavily weighted. Graphs of evolving error norm based on the parameters slopes can regain the sensibilities of error functions and of course lead to the same conclusions as presented sensitivity study previously.

The evolution of MAC norm off-diagonal (Figure 4.6) is not only zero at reference case, but more often tends to decline in absolute values when it moves away from the reference case. This curious behavior comes presumably that eigen modes calculated by FE are read from a file created by the ANSYS, introducing some rounding errors from text to binary mode conversion performed by the transfer of data between ANSYS and



**Figure 4.6 MAC_{nd} based on non diagonal terms of MAC (Alporas_B2) matrix norm
digital issue**

MATLAB. These slight truncation errors then make numerical modes imported into MATLAB slightly non-orthogonal between them, which leads to off diagonal terms non-zero in the base case MAC matrix. This edge effect can unfortunately severely disrupt method for minimizing subsequently used in mixed identification procedure due to incorrect error gradients from occasionally opposite to the direction of minimization. Thus, to correct this effect, the MAC norm off-diagonal MAC_nd is modified by MAC_nd2 (Figure 4.7) as follows;

$$F_k^{mac_nd2}(x^i) = \sum_{i=1}^m \sum_{j \neq k} |MAC(\tilde{\varphi}_j^i, \varphi_k) - MAC(\varphi_j, \varphi_k)| \quad (4.8)$$

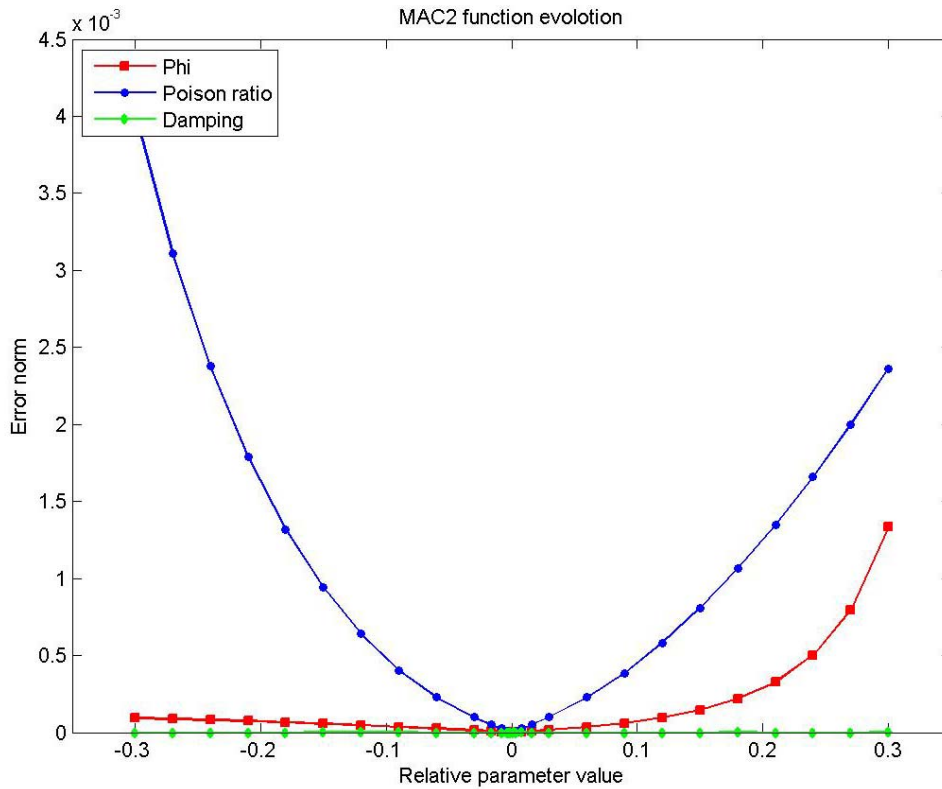


Figure 4.7 New norm MAC_nd2 based on differences in non-diagonal matrix MAC (Alporas_B2)

4.4 ALGORITHM FOR MIXED NUMERICAL-EXPERIMENTAL TECHNIQUE

4.4.1 Modal optimization problem

In an approach of mixed numerical-experimental technique, progressive convergence of numerical modal data of FE model, whose parameters are unknown to the target values that represent the experimental data is usually performed iteratively with the aid of a minimization algorithm seeking to minimize the overall difference between these two data sets. The identification method is then reduced to a problem of minimizing a global error functional $f(x^i)$ with respect to the vector of unknown parameters x^i . This problem can arise in the following manner:

Search $x^i \in \mathbb{R}^n$ such that x^i minimizes the norm of error $f(x^i)$

where x^i is the vector of identification parameters at iteration i . In this case, the unknown variable parameters x^i must satisfy inequality constraints to ensure that the law identified is physically qualified. From a practical point of view, it is also possible to search the variable parameters in a range of reasonable values, so that variation limits are imposed on parameters

$$(x^{min})_j < (x^i)_j < (x^{max})_j \quad (4.9)$$

However, as by definition experimental data are physically admissible (with errors of measurement), minimizing the difference between the numerical model and measurement tends automatically to enforce physical constraints imposed on parameter x^i . Thus, it is possible to consider this minimization problem with strong explicit constraints or without constraints, they are implicit in the experimental values "targets".

In a sense the least squares minimization, the overall error functional $f(x^i)$ can be written as a function of the vector error norms previously developed as follows;

$$f(x^i) = \frac{1}{2} \|F^{tot}(x^i)\|^2 = \frac{1}{2} \sum_{k=1}^q [F_k^{tot}(x^i)]^2 \quad (4.10)$$

with,

$$\mathbf{F}^{\text{tot}} = \begin{bmatrix} \alpha^{frq} \mathbf{F}^{frq}, \alpha^{damp} \mathbf{F}^{damp}, \alpha^{mac1} \mathbf{F}^{mac1}, \alpha^{mac2} \mathbf{F}^{mac2}, \dots \\ \dots \alpha^{nod} \mathbf{F}^{nod}, \alpha^{ecm} \mathbf{F}^{ecm}, \alpha^{stab} (\mathbf{x}^i - \mathbf{x}^0) \end{bmatrix}^T \quad (4.11)$$

Where α^{stab} represents the weight optional terms of stabilization.

A direct benefit of a global least squares error function is to guarantee the convexity and the sign of the functional error, irrespective of the properties of components of the vector error $\mathbf{F}^{\text{tot}}(\mathbf{x}^i)$, thus making identification method particularly stable when the number of components q of the error vector is much greater than the number n of parameters to identify. In current cases, the number of measured modes are in the order of 10, to ensure both the over determination of the problem of least-squares minimization while ensuring a variety of methods to obtain sufficient balanced sensitivity to all parameters \mathbf{x}^i .

In order to avoid direct numerical packaging problems associated with highly variable magnitude of the parameters to identify (10^{10} difference between v and E for example), the vector of parameters \mathbf{x}^i is defined relative to the initial values. In summary, the problem of minimization with or without constraint can be defined as;

$$\begin{aligned} \underset{\mathbf{x}^i \in \mathbb{R}^n}{\text{minimiser}} f(\mathbf{x}^i) \text{ with } f(\mathbf{x}^i) &= \frac{1}{2} \|\mathbf{F}^{\text{tot}}(\mathbf{x}^i)\|^2 \\ &= \frac{1}{2} \sum_{k=1}^q [\mathbf{F}_k^{\text{tot}}(\mathbf{x}^i)]^2 \end{aligned} \quad (4.12)$$

With optional constraints

$$(\mathbf{x}^{\min})_j < (\mathbf{x}^i)_j < (\mathbf{x}^{\max})_j \quad (4.13)$$

Where the error function can be written as;

$$\mathbf{F}^{\text{tot}} = \begin{bmatrix} \alpha^{frq} \mathbf{F}^{frq}, \alpha^{damp} \mathbf{F}^{damp}, \alpha^{mac1} \mathbf{F}^{mac1}, \alpha^{mac2} \mathbf{F}^{mac2}, \dots \\ \dots \alpha^{nod} \mathbf{F}^{nod}, \alpha^{ecm} \mathbf{F}^{ecm}, \alpha^{stab} (\mathbf{x}^i - \mathbf{x}^0) \end{bmatrix}^T \quad (4.14)$$

4.4.2 Minimization algorithms

By adopting a pragmatic development approach with regard to the identification algorithm, it is decided to base this work on an existing library of optimization routines

that have already been proven in many applications. An important set of MATLAB routines for solving problems with parametric FE software ANSYS has already been developed (section 4.3.2). As a part of minimization problem, the number n of parameters to identify ($n = 3$) and the number of components of error q ($q = 6 \times m$, where $m \approx 10$ is the number of measured modes) can be considered relatively low, thus classifying this problem in the category of small and medium-scale optimizations (low number of parameters, the small number of error norm not decoupled).

The main algorithms used in this field are either nonlinear least squares (Gauss-Newton, the maximum gradient or Levenberg-Marquardt methods) for unconstrained problems [179, 180] or type sequential quadratic programming (SQP, Sequential Quadratic Programming) for constrained problems. Optimization by Nonlinear least squares method is used in the procedure for mixed numerical-experimental developed in this work.

Let's start by defining the matrices gradients (slopes) and Hessian (curvature) of the overall error norm $f(x^i)$. Thanks to the particular shape of the functional error total least squares type, these matrices can be connected to the Jacobian matrices $J(x^i)$ and Hessian of the error vector $F^{\text{tot}}(x^i)$. The Jacobian matrix $J(x^i)$ of the error vector $F^{\text{tot}}(x^i)$ and the gradient vector $G(x^i)$ of the global error functional $f(x^i)$ can then be formed into,

$$J(x^i) = \frac{\partial F^{\text{tot}}(x^i)}{\partial x^i} \quad (4.15)$$

and

$$G(x^i) = \nabla f(x^i) = J(x^i)^T F^{\text{tot}}(x^i) \quad (4.16)$$

Hessian matrix $H^j(x^i)$ of the second derivatives of the j -th component of the error vector $F^{\text{tot}}(x^i)$ and the Hessian matrix $H(x^i)$ of the global error functional $f(x^i)$ are linked by relationships;

$$H^j(x^i) = \frac{\partial^2 F_j^{\text{tot}}(x^i)}{(\partial x^i)^2} \quad (4.17)$$

and

$$\begin{aligned} H(x^i) &= J(x^i)^T J(x^i) + Q(x^i), \text{ with} \\ Q(x^i) &= \sum_{j=1}^q F_j^{\text{tot}}(x^i) \cdot H^j(x^i) \end{aligned} \quad (4.18)$$

From these definitions, consider now the overall functional $f(x^i)$. If it is sufficiently regular in the vicinity of x^i , this functional can be approximated by the following Taylor expansion

$$f(x^i + h) = f(x^i) + h^T G(x^i) + \frac{1}{2} h^T H(x^i) h + O(\|h\|^3) \quad (4.19)$$

where the vector h denotes a local perturbation parameters around x^i .

The necessary and sufficient conditions to ensure that x^* is a local minimum, the error functional $f(x)$ can be defined by

$$\begin{aligned} x^* \text{ is a local minimum of } f(x) \text{ if } G(x^*) = 0 \text{ and } H(x^*) \text{ is} \\ \text{positive definite.} \end{aligned} \quad (4.20)$$

Most methods for nonlinear least square type minimization are based on an iterative method for "descent", designed to look at each iteration i a direction of descent h (vector space parameters) such as h is a descent direction for the overall error norm $f(x)$ around x^i if:

$$f(x^i + \alpha h) < f(x^i) \text{ (for small values of } \alpha) \Leftrightarrow h^T G(x^i) < 0 \quad (4.21)$$

The most well known technique for determining a descent direction based on the gradient of the total error functional to calculate the descent direction of h_{SD} "maximum slope"

$$h_{SD}(x^i) = -f'(x^i) = G(x^i) \quad (4.22)$$

In summary, Table 4.2 presents the overall flow of an optimization algorithm for nonlinear least squares.

Table 4.2 Algorithm for General optimization based on the principles of descent direction

Definition of a vector of initial parameter x_0 .

Iteration until the convergence is reached or the maximum number of iterations are exceeded;

1. Calculate descent direction $h(x^i)$ such that $f(x^i + \alpha h) < f(x^i)$.
2. Search along the descent direction $h(x^i)$ the factor α minimizing the function α :
 $f(x^i + \alpha h)$
3. Update the parameters vector: $x^{i+1} = x^i + \alpha h(x^i)$.

In the case of non-linear least squares method, the Hessian matrix $H(x)$ of the total error functional $f(x)$ has a particular property. Indeed, as the matrix $Q(x^i)$ tends to zero as soon as the residual error $\|F^{\text{tot}}(x^i)\|$ itself tends to zero, the Hessian matrix takes the following specific form when the residue error $\|F^{\text{tot}}(x^i)\|$ is zero or very low (x^i close to the minimum):

$$H(x^i) \cong J(x^i)^T J(x^i) \quad (4.23)$$

This implies that for x^i close to the minimum x^* , the second order approximation of the total error functional $f(x)$ is written as

$$\begin{aligned} f(x^i + h) &= f(x^i) + h^T J(x^i) F^{\text{tot}}(x^i) + \frac{1}{2} h^T J(x^i)^T J(x^i) h \\ &\quad + O(\|h\|^3) \end{aligned} \quad (4.24)$$

This development limited the total error function corresponds perfectly to the approximate form of $f(x)$ that would be obtained by a linear approximation of each component of the error vector $F^{\text{tot}}(x^i)$ around x^i

$$F^{\text{tot}}(x^i + h) \cong F^{\text{tot}}(x^i) + J(x^i)h + O(\|h\|^2) \quad (4.25)$$

Which leads to

$$\begin{aligned}
f(x^i + h) &= \frac{1}{2} \left(F^{tot}(x^i + h) \right)^T F^{tot}(x^i + h) \cong \\
&\frac{1}{2} \left(F^{tot}(x^i) \right)^T F^{tot}(x^i) + \frac{1}{2} \left(J(x^i)h \right)^T F^{tot}(x^i) + \\
&\frac{1}{2} \left(F^{tot}(x^i) \right)^T J(x^i)h + \frac{1}{2} h^T J(x^i)^T J(x^i)h = \\
&f(x^i) + h^T J(x^i)^T F^{tot}(x^i) + \frac{1}{2} h^T J(x^i)^T J(x^i)h
\end{aligned} \tag{4.26}$$

This observation is the basis of the Gauss-Newton optimization method, based on a linear approximation of the components of the error vector $F^{tot}(x^i)$ at each iteration, thus forming a quadratic approximation of the total functional error $f(x^i)$. This method has quadratic convergence properties when the final residual error is small or zero, or otherwise linear. The descent direction h_{GN} calculated by Gauss – Newton method at each iteration is the solution of the following system:

$$\left(J(x^i)^T J(x^i) \right) h_{GN} = -J(x^i)^T F^{tot}(x^i) \tag{4.27}$$

The primary advantage of the Gauss-Newton is of course its quadratic convergence in the final iterations if the minimum residual error is small. However, during the early iterations, the Hessian matrix $H(x)$ of $f(x)$ can be indefinite or even negative definite, completely disrupting the procedure, so that h_{GN} may not be a descent direction for $f(x)$. Therefore, during the early iterations, the use of a descent direction of maximum slope h_{SD} may be more appropriate. The idea of a hybrid between the maximum descent and Gauss-Newton method has motivated a series of algorithms, the best known (and perhaps most effecient) is the Levenberg-Marquardt [179, 180]. The difficulty of any hybrid algorithm is mainly to choose when and under what conditions switch from the method of maximum descent to Gauss-Newton and vice versa. To do this, the method of Levenberg-Marquardt introduced a parameter λ_i varying in the interval $[0, \infty]$. The descent direction h_{LM} is then calculated by solving

$$\left(J(x^i)^T J(x^i) + \lambda_i I \right) h_{LM}(x^i) = -J(x^i)^T F^{tot}(x^i) \tag{4.28}$$

If λ_i is close to zero, the descent direction h_{LM} tends toward the descent direction h_{GN} of Gauss-Newton type, whereas when λ_i becomes relatively large descent direction

h_{LM} approaches to $-1/\lambda_i h_{SD}$ representing a small "step" in the direction of maximum descent. It should be noted that λ_i influence both the direction of lowering the amplitude of the step performed at iteration i , allowing to pass from a line search method. However, any performance of this method lies in fact how to evolve λ_i during the iterations. The idea used here is to reduce λ_i when the linear approximation of the components of the error vector provides good results (insignificant quadratic terms) to approximate the descent direction of Gauss-Newton (super linear convergence if the residue is low), and λ_i increase when the terms of the second order component of the error vector F^{tot} are important, so that the algorithm tends towards a maximum descent method.

Table 4.3 Minimization of Levenberg-Marquardt algorithm

Definition of a vector of initial parameter x_0 .

Iteration until the convergence is not reached (tolerance) or the maximum number of iterations is not exceeded;

1. Calculate the vector error $F^{tot}(x^i)$ and its derivatives $J(x^i)$
2. Evaluate the depreciation factor λ_i of the current iteration
 - a. linear extrapolation of the error function: $f_L(x^i + h^i)$
 - b. cubic interpolation $f_c(x)$ of $f(x^{i-1})$ and $f(x^i)$ and search for the minimum of interpolation leading to $f_c(x^*)$ and α^*
 - c. calculation of λ_i
 - i. if $f_L(x^i + h^i) < f_c(x^*)$ then $\lambda_{i+1} = \frac{\lambda_i}{1+\alpha^*}$
 - ii. if $f_L(x^i + h^i) > f_c(x^*)$ then $\lambda_{i+1} = \lambda_i + \frac{f_c(x^*) - f_L(x^i + h^i)}{\alpha^*}$
3. Search for a descent direction $h^i = h(x^i)$ by solving

$$(J(x^i)^T J(x^i) + \lambda_i I) h^i(x^i) = -J(x^i)^T F^{tot}(x^i)$$
4. Find along the descent direction $h^i(x^i)$ the factor α minimizing $f(x^i + \alpha h^i)$ using a quadratic interpolation procedure/cubic \Rightarrow calculation error vectors intermediate $F^{tot}(x^i + \alpha_k h^i)$ (for $k \in [1,3]$) .
5. Update the parameter vector $x^{i+1} = x^i + \alpha h^i$.

Although a search line is not applied directly in the Levenberg-Marquardt method, implementation carried out in the MATLAB Optimization Toolbox library [180] determines still line search by a factor α^* used for measuring the nonlinearity of the components of the vector error. The step length α^* is evaluated by searching a minimum x^* on a cubic interpolation $f_c(x)$ of the error function (based on the values of errors and gradients computed in iterations i and $i-1$). The effectiveness of the local linear approximation $f_L(x^i + h^i)$ of Gauss-Newton is then compared with the cubic approximation $f_c(x^*)$, in order to decide whether to increase or decrease λ_{i+1} . The updated value of λ_{i+1} of the current step is based ultimately on the step length of the cubic interpolation α^* . Table 4.3 summarizes the final minimization algorithm Levenberg-Marquardt.

In conclusion, the method of optimization by least squares Levenberg-Marquardt is recognized as being very robust and generally perform well in a wide variety of cases. Although theoretically converges slower than the Gauss-Newton in some very specific cases, this algorithm is most efficient on the majority of cases encountered. Moreover, the very rapid convergence of the algorithm, combined with the fact that it does not require systematic evaluation of gradients of error functions during the line search, this procedure is one of the least demanding in computing error norm and gradient.

4.4.3 Calculation error functional gradients

As it is observed in the explanation of minimization algorithm that it is necessary to compute at each iteration of the main process not only the vector of modal error functions between the numerical and experimental models, but also the gradient of this vector with respect to the identification parameters. Gradients (or Jacobians) modal error norms obviously depend on modal solutions of numerical model, but also the gradient of these solutions with respect to variable parameters. Thus, it is necessary to build on each major iteration of the identification method, both modal solutions of parametric FE model but also their derivatives with respect to each identification parameter. The derivatives of the eigen frequencies are relatively simple to calculate, it does not hold true for the derivatives of the modes, which require much more computational effort to be evaluated. For the sake of clarity and concision, abandon here

the index i representing the iterations. Recall that the problem of modal extraction can be stated as follows,

$$(\mathbf{K}(\mathbf{x}) - \lambda_j \mathbf{M}) \boldsymbol{\varphi}_j = 0 \Rightarrow \lambda_j(\mathbf{x}), \boldsymbol{\varphi}_j(\mathbf{x}) \text{ for } j = 1, 2, \dots, m \quad (4.29)$$

where \mathbf{K} and \mathbf{M} are global stiffness and mass matrices, and where λ_j and $\boldsymbol{\varphi}_j$ represent respectively the j -th eigenvalue (the square of the j -th angular eigen frequency ω_j) and j -th eigen vector of the system, m is indicating the number of considered modes pairs. In current case of identification, the mass matrix \mathbf{M} does not depend on the parameter vector \mathbf{x} because the density and geometric dimensions are not part of the parameters vector and therefore remain constant.

Directly deriving the equation (4.23) with respect to parameter x_k and using the normalization property of modes in the metric of the mass matrix, one can easily make the calculation of the derivatives of eigenvalues [178, 181-184].

$$\frac{\partial \lambda_j}{\partial x_k} = \boldsymbol{\varphi}_j^T \frac{\partial \mathbf{K}(\mathbf{x})}{\partial x_k} \boldsymbol{\varphi}_j \text{ for } j = 1, 2, \dots, m \quad (4.30)$$

The derivatives of the eigen modes are the solutions of the following system:

$$(\mathbf{K}(\mathbf{x}) - \lambda_j \mathbf{M}) \frac{\partial \boldsymbol{\varphi}_j}{\partial x_k} = \frac{\partial \lambda_j}{\partial x_k} \mathbf{M} \boldsymbol{\varphi}_j - \frac{\partial \mathbf{K}(\mathbf{x})}{\partial x_k} \boldsymbol{\varphi}_j \text{ for } j = 1, 2, \dots, m \quad (4.31)$$

The classical technique of finite differences can be implemented very easily in this case, either for the calculation of derivative of frequencies and eigen modes, or for the calculation of the derivative of modal error norms directly.

Modal derivatives calculated by finite differences require calculation of a "reference" case of parametric FE model as well as the calculation of n "perturbed" cases.

Let λ_j^0 and $\boldsymbol{\varphi}_j^0$ is the modal solutions of the reference case (the parameters vector $\mathbf{x} = \mathbf{x}^0$) and λ_j^k and $\boldsymbol{\varphi}_j^k$ is the modal solutions according to the perturbed k -th parameter x_k with a step Δx_k than modal derivative can be approximated by

$$\frac{\partial \lambda_j}{\partial x_k} \cong \frac{1}{\Delta x_k} (\lambda_j^k - \lambda_j^0) \text{ and } \frac{\partial \varphi_j}{\partial x_k} \cong \frac{1}{\Delta x_k} (\varphi_j^k - \varphi_j^0) \quad \text{for } j=1, 2, \dots, m \quad (4.32)$$

Obviously, resolution of $n+1$ large scale eigenvalue problems is not very economical in terms of computing time, but simplicity and accuracy of this method provide very good evaluation of the Jacobiens error $\mathbf{J}(\mathbf{x})$.

Thus, the identification method developed here will use derivation by finite differences method. As in the resolution by nonlinear least squares algorithm for MATLAB, an option enables the automatic calculation of error gradients by finite difference.

4.4.4 Implementation of identification technique in MATLAB

The identification method developed here is based on Levenberg-Marquardt algorithm with assessment of gradients by finite difference. The majority of the development of the method focused on modal error functional calculation and therefore on the comparison of numerical and experimental modal values.

Before the calculation of modal norms, experimental modal data, previously processed in the LMS software, must be imported into the MATLAB environment and the experimental mesh must be converted into the same coordinate system of the numerical model used subsequently for identification. A routine treatment to load the experimental modal model from a UNV file and interactively define the geometry data necessary to correct coordinates on the basis of an experimental image of the mesh exported from the LMS Software. The experimental modal model is stored in a data structure of MATLAB in the same way as numerical modal models.

A set of routines for parametric definition and execution of ANSYS FE models are already presented in the operating procedure of the parametric study in section 4.3.

However, as the mesh used for the measurement and the numerical model are dissimilar in principle, a strategy of projecting modal data on a reference mesh was necessary to calculate the error norms based on the shape of the eigen modes. Therefore, each routine based on error norm calculation of modes (MAC_d, MAC_nd, NLD, and

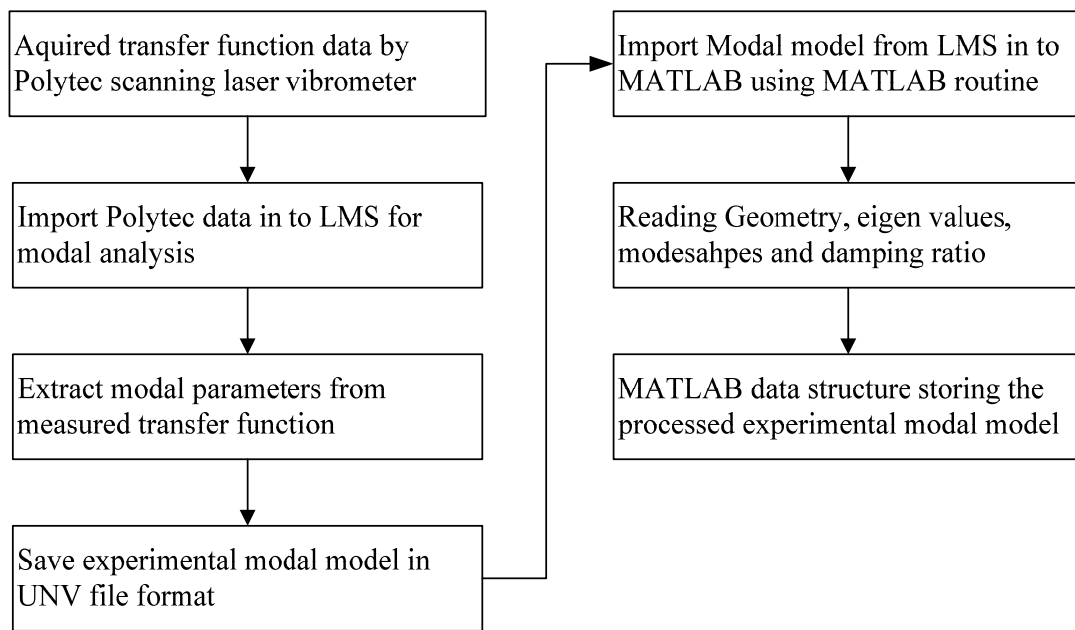


Figure 4.8 Block diagram of loading experimental modal model for mixed numerical experimental identification technique

SumMSD) uses a version of "interpolated" procedures for determining MAC matrices or sums modal components differences.

Thus a reference mesh of variable size is generated and the cubic interpolation of normal components of deformed mode shapes are calculated. Since the eigen modes numerically extracted are generally more numerous than the measured modes and it is not necessary that they may appear in the same order as the previous, so numbering of the modes must be corrected before the calculation of error norm. A strategy for the automatic creation of pairs of numerical and experimental methods, based on the maximum terms of the correlation matrix MAC is used to ensure mode shapes compatibility. In addition, the rigid body modes are also filtered not to disturb the identification procedure. Modal vectors interpolated are defined on the same mesh and numbered in the same way, modal norms can be estimated easily as in their theoretical definition. The Algorithm 1 and Algorithm 2 will explain implementation of proposed mixed numerical-experimental technique and objective function respectively in detail.

Synopsis of Algorithm 1:

This algorithm load experimental modal data, extract the required data and executes optimize algorithm to solve the mixed numerical-experimental problem. It calls several MATLAB routines, which include;

readuff.m, this routine read the experimental modal data from universal file format.

LMFnlsq.m, Solve a set of nonlinear equations in least squares sense. A solution is obtained by a Fletcher's version of the Levenberg-Maquardt algorithm for minimization of a sum of squares of equation residuals.

Objective_function.m, output of this routine is optimized by Levenberg-Maquardt algorithm.

Algorithm 1: Computing FE model parametric variable by optimizing the objective function.

Input:

Objective function, Experimental modal data (UNV. file format), Initial parametric variables, Options for optimization algorithm. i.e. Max no of iteration, tolerance, etc.

Output:

Optimized parametric variable, experimental modal data in MATLAB format (mode shape matrix, eigen frequency vector and modal damping ratios vector).

Body script:

1. Read experimental modal data which is saved in UNV. file format (see Fig 4.8) by MATLAB.
2. Extract the required data;

for $i = 1: \text{max};$

Experimental mode shapes (i)

end

Output = contains mode shapes data matrix, with rows consisting of degrees of freedom and each column representing a mode.

for $i = 1: \text{max};$

Experimental eigen frequency (i)

end

Output = contains frequency vector, listing the eigenvalues (resonant frequencies in Hz). The size of the frequency vector is (modes) x (1).

for $i = 1: \text{max};$

Experimental modal damping ratios (i)

end

Output = contains damping ratio vector. The size of the vector is (modes) x (1).

3. Optimizing the objective function using Fletcher's version of the Levenberg-Marquardt algorithm for minimization of a sum of squares of equation residuals.
-

Synopsis of Algorithm 2:

This algorithm computes the objective function for optimization. It reads the output variable parameters from Algorithm 1, invokes ANSYS to solve the FE problem using these parameters, read the FE solution results, load the experimental results, compare them and make mode pairs. It also computes the six objective functions of modal error norms. Assembling and weighting of these error norms in term of stabilization is also performed in this algorithm. It calls the following subroutines.

FE_mode_specimenl.mac is ANSYS input file (in APDL format) that builds the FE model of AF, calculates eigenvalues and eigenvectors, outputs the frequency listing,

damping ratios and eigenvectors, plots the mode shapes. This script consists of several sub macros for reading and writing of MATLAB data format.

Readansysarray_mode.m read ANSYS eigenvector results and converts them to MATLAB format.

Readansysarray_Freq.m read ANSYS eigenvalues results and converts them to MATLAB format.

Readansysarray_Damp.m converts ANSYS file of damping ratios into MATLAB format.

Algorithm 2: Compute the objective function (modal error norm vector).

Input:

Optimized parametric variable and experimental modal data in MATLAB format (Output of Algorithm 1), ANSYS FE model of specimen (APDL).

Output:

Error (r) for MATLAB optimization, MAC matrix plot (paired and non paired).

Body script:

4. Read optimized parametric variables (output of Algorithm 1).
5. Execute ANSYS to solve FE model of specified specimen (see section 3.6.1, Figure 3.4, and Figure 4.10 for details).
6. Read required mode shapes values from ANSYS result files using **Readansysarray_Mode.m**.
7. Read required eigen frequency values from ANSYS result files using **Readansysarray_Freq.m**.
8. Read required modal damping ratios from ANSYS result files using **Readansysarray_Damp.m**.
9. Read experimental modal data (output of Algorithm 1).

10. Interpolate experimental and numerical data on same mesh for first fifteen mode shapes.

for $i = 1: 15$;

Interpolate numerical mode shapes (i)

end

Output: contains mode shapes data matrix, with rows consisting of degrees of freedom and each column representing a mode.

11. Calculate MAC matrix for mode pairing.

for $j, l = 1$: number of modes;

$$M_{jl} = MAC(\boldsymbol{\varphi}_j^a, \boldsymbol{\varphi}_l^b) = \frac{(\boldsymbol{\varphi}_j^a \cdot \boldsymbol{\varphi}_l^b)^2}{(\boldsymbol{\varphi}_j^a \cdot \boldsymbol{\varphi}_j^a)(\boldsymbol{\varphi}_l^b \cdot \boldsymbol{\varphi}_l^b)}$$

end

- Plot non-paired MAC matrix (see for example in Figure 5.8, 5.11, 5.14, 5.18).
- Select first mode pairs whose $MAC > 0.7$ (these mode pairs will be used in further calculations).
- Plot paired MAC matrix (see for example in Figure 5.8, 5.11, 5.14, 5.18).
- Rearrange numerical and experimental data according to selected mode pairs.

12. Calculate modal error norms.

Note: Read section 4.2 for details of modal error norms equation used in this algorithm.

- Relative difference of the eigen frequencies.

for $k = 1$: number of modes;

$$F_k^{frq}(x^i) = \frac{\tilde{\omega}_k^i - \omega_k}{\omega_k}$$

end

Output = Error1

- Relative difference of modal damping ratio.

for $k = 1$: number of modes;

$$D_k^{mdr}(x^i) = \frac{\tilde{\zeta}_k^i - \zeta_k}{\zeta_k}$$

end

Output = Error2

- Error norm based on non-diagonal terms of MAC matrix.

for $j, k = 1$: number of modes;

$$F_k^{mac.nd}(x^i) = \sum_{j=1, j \neq k}^m MAC(\tilde{\boldsymbol{\varphi}}_j^i, \boldsymbol{\varphi}_k)$$

end

Output = Error3

- Error norm based on diagonal terms of MAC matrix.

for $k = 1$: number of modes;

$$F_k^{mac.d}(x^i) = 1 - MAC(\tilde{\boldsymbol{\varphi}}_k^i, \boldsymbol{\varphi}_k)$$

end

Output = Error4

- Error norm based on components of interpolated mode shape difference.

for $j = 1 : r$ (component of mode shape)

for $k = 1$: number of modes;

$$F_k^{msv}(x^i) = \sum_{j=1}^r \left(\frac{(\tilde{\boldsymbol{\varphi}}_k^i)_j}{\max_l((\boldsymbol{\varphi}_k)_l)} - \frac{(\boldsymbol{\varphi}_k)_j}{\max_l((\boldsymbol{\varphi}_k)_l)} \right)$$

end

end

Output = Error5

- Error norm based on nodal line difference.

for $k = 1$: number of modes;

$$F_k^{nod}(x^i) = \frac{1}{a^2} \sum_{r=1}^a \sum_{s=1}^a ({}^k \tilde{J}_{rs}^i - {}^k J_{rs})^2$$

end

Output = Error6

13. Assembling and weighting modal error norm.

The mixed numerical-experimental identification procedure takes place according to the following steps:

1. Loading the experimental data (Figure 4.8).
2. Solving objective function by invoking ANSYS to work out FE model of AF (Figure 4.9).
3. FE modelling of aluminum foam specimens in APDL (Figure 4.10).
4. Calculating error norms (Figure 4.11).
5. Solving the problem of mixed numerical-experimental identification using Levenberg-Marquardt algorithm (Figure 4.12).

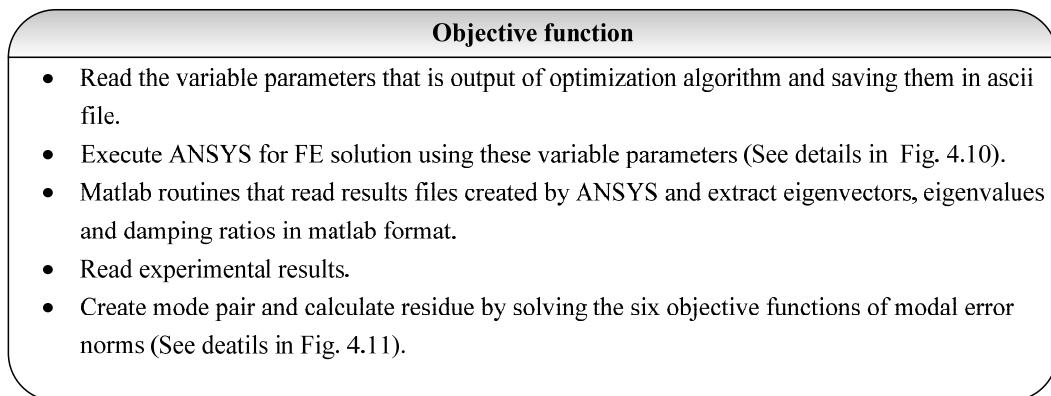


Figure 4.9 Matlab routine summary of objective function (Algorithm 2)

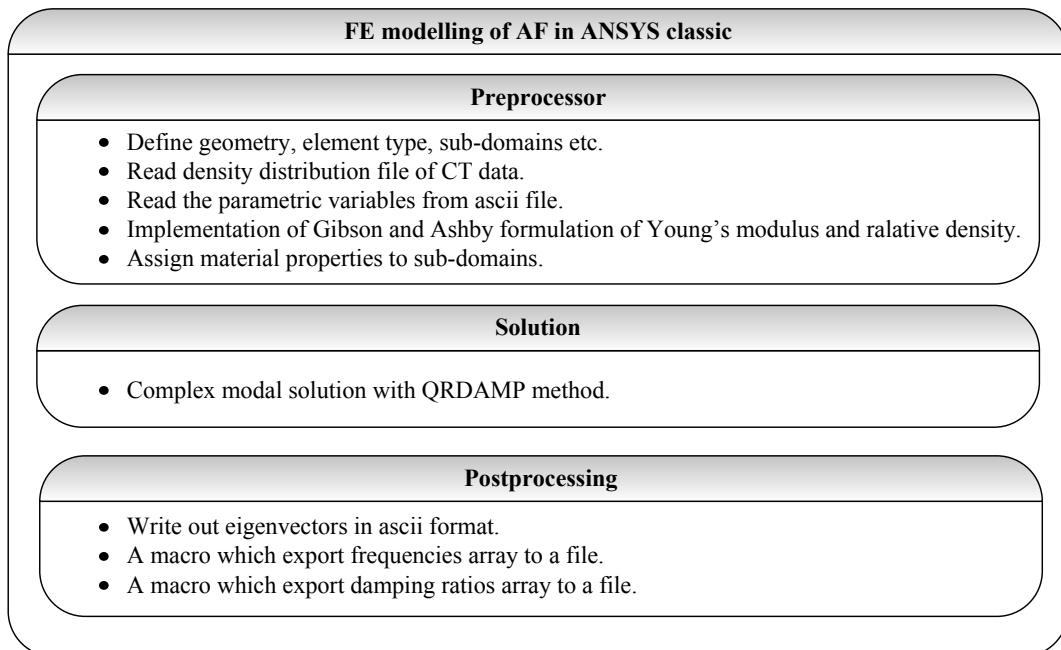


Figure 4.10 FE modelling of AF.

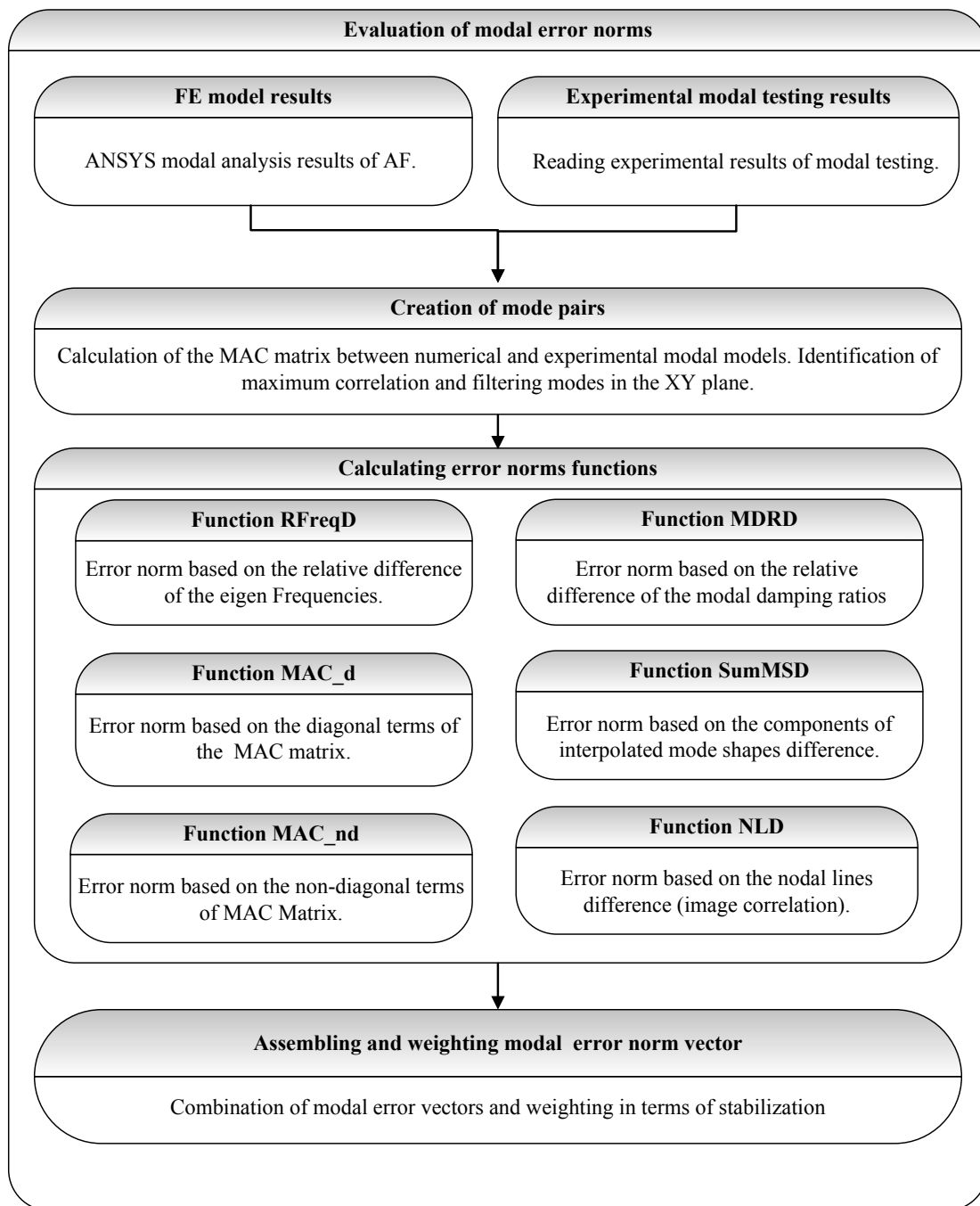


Figure 4.11 Block diagram of the evaluation of modal error norms

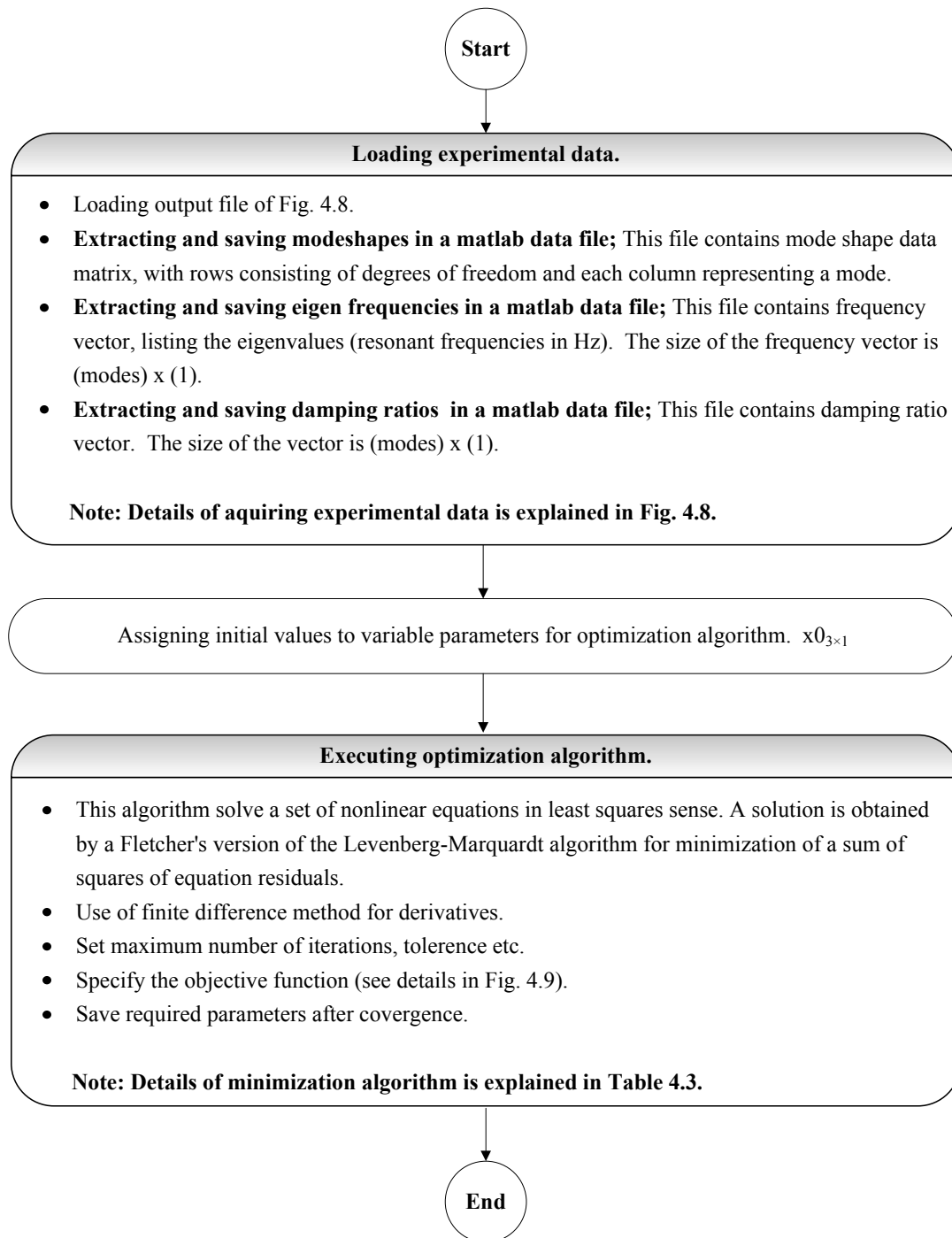


Figure 4.12 General block diagram for solution of mixed numerical-experimental identification problem (Algorithm 1)

CHAPTER 5. RESULTS AND DISCUSSION

In this last chapter, experimental modal analysis results of four aluminum foam specimens are presented. The developed MNET is implemented to identify the variable parameters in the FE model of these specimens.

5.1 SUMMARY OF THE PROPOSED MIXED IDENTIFICATION METHOD

Before the description of results, first summon up the actual approach of the proposed mixed numerical-experimental identification process:

5.1.1 Modal measurements of test specimens

- a. Selection of the specimen
- b. preparation of the experimental test setup
- c. dynamic measurements on test specimens
- d. modal parameters extraction

5.1.2 Mixed numerical-experimental identification

- e. import of the experimental modal model in MATLAB
- f. initial estimation of the variable parameters
- g. parametric FE model of test specimens
- h. definition of the identification problem
- i. execution of the optimization algorithm

5.2 OBJECTIVES AND APPROACH

At this stage of development, the mixed numerical-experimental identification method based on natural frequencies and mode shapes of AF specimens, is fully developed in terms of theory and implementation. However, before implementation of the proposed technique it is necessary to check the accuracy of dynamic measurements and validation of the estimated modal parameters. Section 5.3 is devoted to this task.

After validation of experimental modal analysis results the proposed MNET is implemented on these specimens and results of each specimen is discussed.

5.3 MODAL MEASUREMENTS

Modal analysis of four aluminum specimens are conducted on a range of frequency from 10 Hz to 3 kHz on experimental mesh of 36×29 and 32×26 measuring points for specimen of size B and S respectively. The spectral lines measured are set to 3200 lines and an average of 30 measurements per point is made to increase the signal-noise ratio.

5.3.1 Measurement estimation and validation

There are a couple of estimators used to calculate the FRF. For noise at the output, a useful estimator is H_1 . The function H_1 is derived by using least squares method, and is the cross spectrum divided by the autospectrum of the force F see equation 5.1. If averaging the FRFs measured with H_1 , the random noise will suppress and H_1 will converge towards the true H [185].

$$H_1(\omega) = \frac{G_{FX}(\omega)}{G_{FF}(\omega)} \quad (5.1)$$

For noise at the input H_2 is a useful estimator for the FRF. It is derived from the same principle as the H_1 estimator, and is defined as the autospectrum of the response divided by the cross spectrum. The noise at the input is removed more and more from the cross spectrum with increased averages.

$$H_2(\omega) = \frac{G_{XX}(\omega)}{G_{XF}(\omega)} \quad (5.2)$$

H_1 estimator for the FRF's calculations is used in this work. The average spectrum of measured transfer functions is shown in Figure 5.1. Measured transfer function quality is excellent with a large number of close peaks, thus providing the effectiveness of the laser scanning (non contact) measurement method. Very strong mutual influence of some resonance peaks is evident here and the LMS PolyMAX extraction procedure is essential to accurately determine the close eigen frequencies and mode shapes. On average, between 12-15 modes are identified for small plates while between 18-20 modes are identified for big plates in a frequency range of 10 Hz to 3 kHz. The eigen

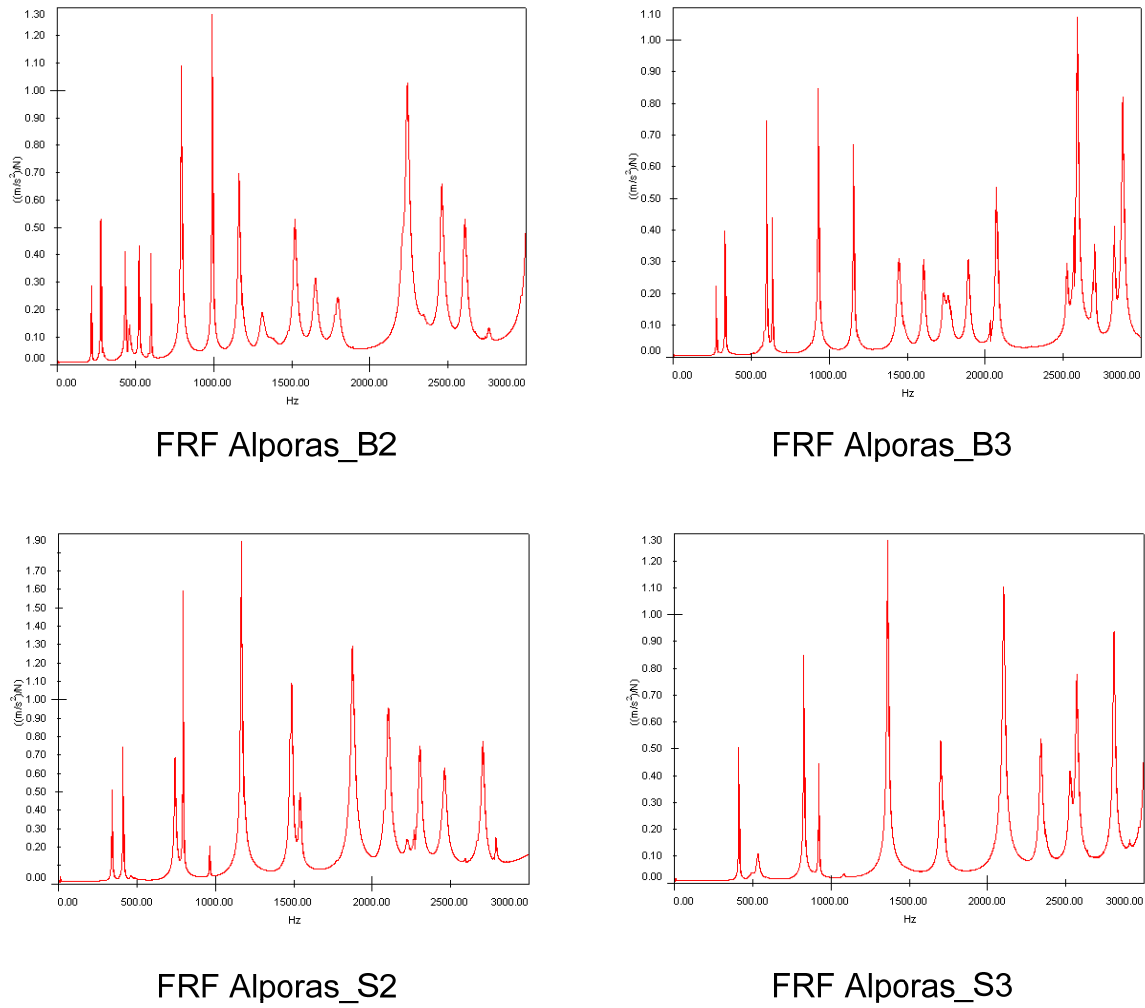


Figure 5.1 Average measured frequency response function of testing specimens

modes which have been identified with sufficient quality are shown in Figure 5.3, 5.4, 5.5 and 5.6 for Alporas_S2, Alporas_B2, Alporas_B3, and Alporas_S3 specimen respectively.

A way to validate the measurements is to observe the coherence function, shown in equation 5.4. It is derived from the cross spectrum inequality (equation 5.3) which states that if the autospectrum contains non-coherent noise, the magnitude of the squared cross spectrum is smaller than the product of the autospectrum.

The coherence functions have the boundaries described in equation 5.5. For the value 1, the measurement contains no noise, and for the value 0, there is pure noise in the measurement. The coherence function also indicates the linearity between the input and

output signal. When the coherence is 1, estimator H_1 and H_2 will yield the same result, therefore the estimators are overcompensated, and the true FRF will be somewhere in between.

$$|Q_{XF}(\omega)|^2 \leq G_{XX}(\omega) \cdot G_{FF}(\omega) \quad (5.3)$$

$$\gamma(\omega)^2 \equiv \frac{|Q_{FX}(\omega)|^2}{G_{XX}(\omega) \cdot G_{FF}(\omega)} \quad (5.4)$$

$$0 \leq \gamma(\omega)^2 \leq 1 \quad (5.5)$$

To calculate the autospectrum, the spectrum is multiplied with its complex conjugate. The complex conjugate is the same spectrum but with opposite sign for the imaginary part. The autospectrum is always real.

The cross spectrum is calculated by multiplying a spectrum with the complex conjugate of a different spectrum. For instance the spectrum of the force and the response. Cross spectrum is a complex entity which describes the phase shift between the different spectrums. The magnitude of the cross spectrum describes the coherent product of power in the spectrums [185]. Coherence function of all four AF specimens is shown in Figure 5.2.

After verifying the quality of measurements, FRF's are saved in UNV file format and are imported in LMS Test.Lab. The LMS PolyMAX method is used to estimate the modal parameters precisely. Experimental modal results of all four testing specimen are shown below in Table 5.1, 5.2, 5.3, and 5.4 for Alporas_S2, Alporas_B2, Alporas_B3, and Alporas_S3 specimen respectively. Since some measured eigen modes are highly complex and identification procedure requires real reference modes, these complex modes are normalised by keeping the amplitude with its sign, corresponding to the average phase of the measured complex mode.

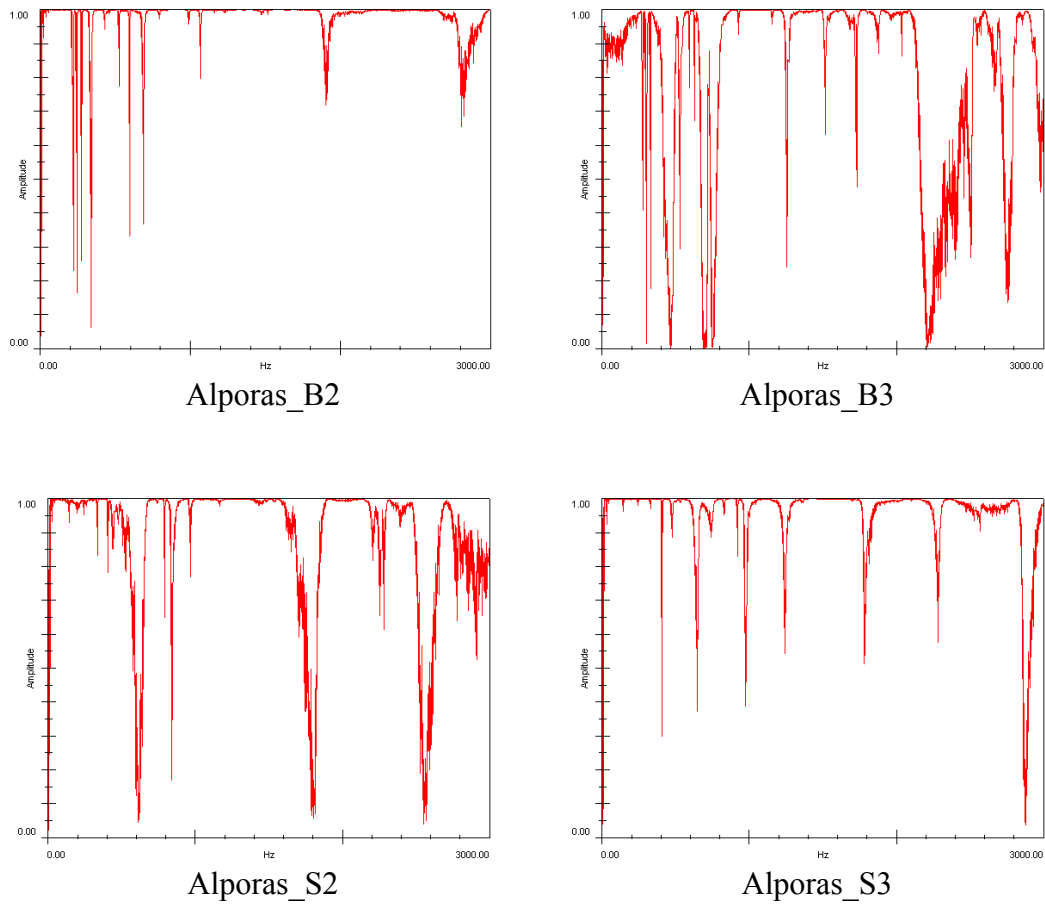


Figure 5.2 Coherence function of testing specimens

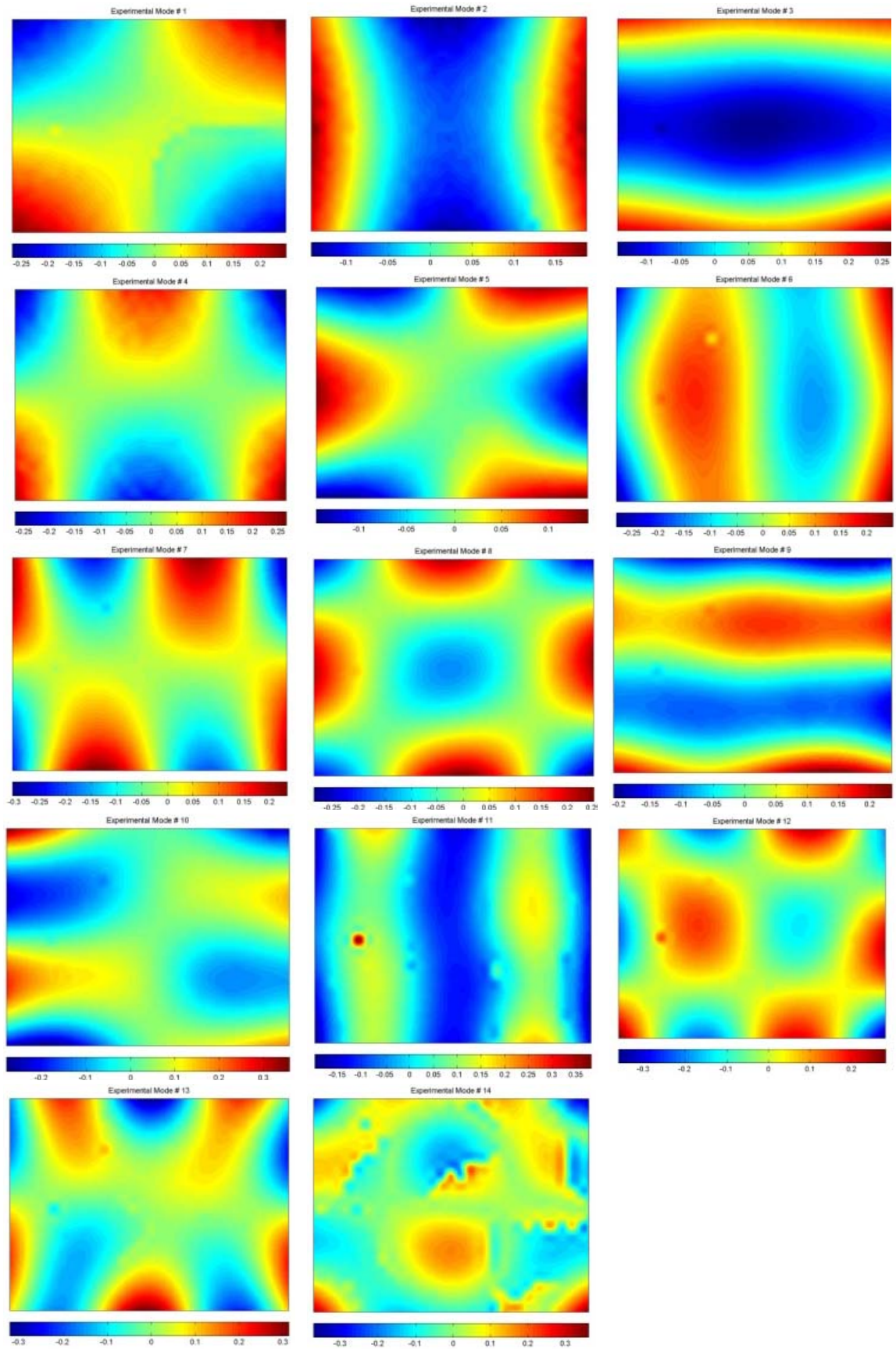
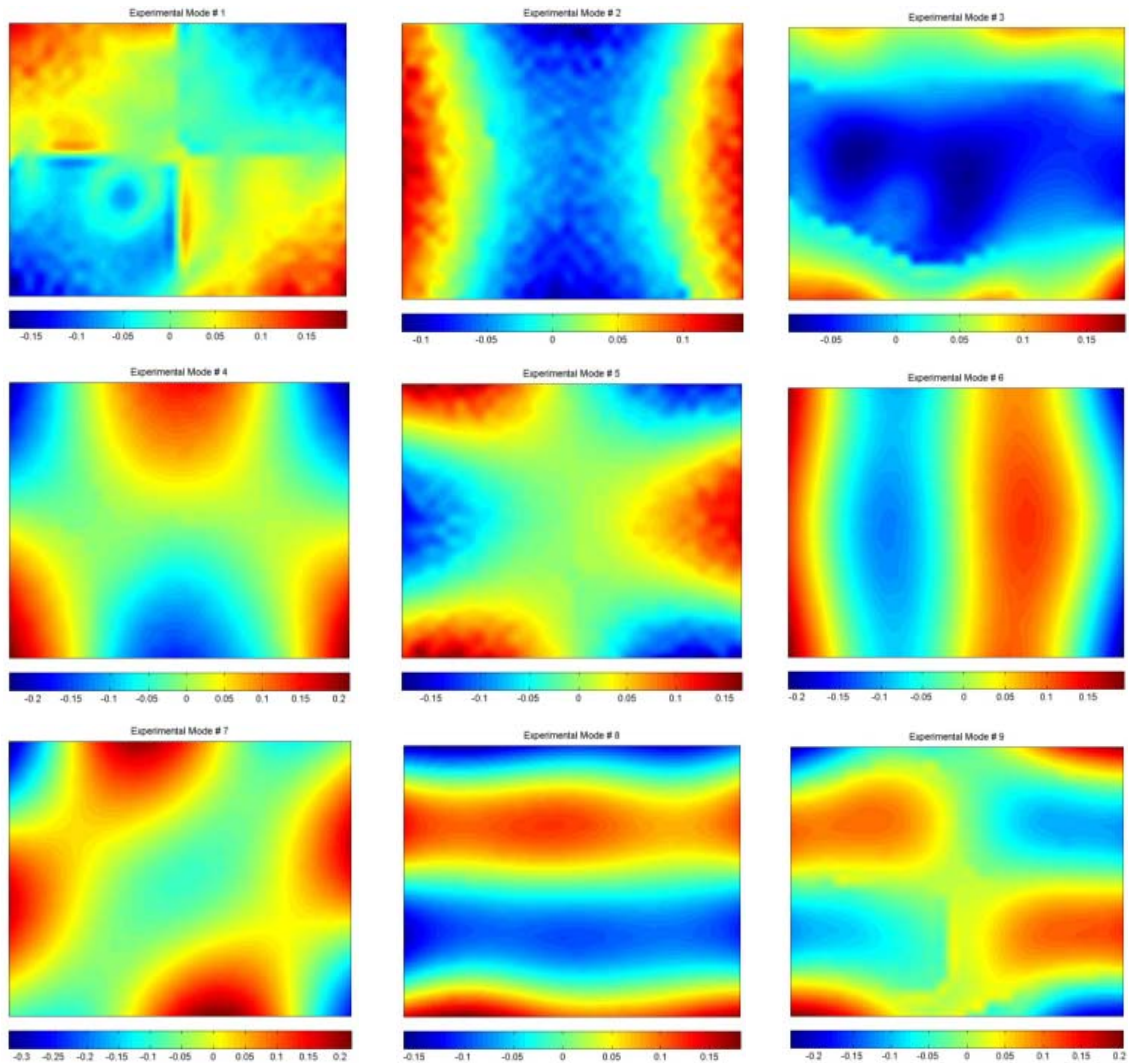


Figure 5.3 Experimental Mode shapes of Alporas_S2

Table 5.1 Experimental modal parameters of Alporas_S2

Mode No.	1	2	3	4	5	6	7	8
Frequency(HZ)	339.536	411.748	744.493	796.497	963.683	1170.93	1486.4	1541.01
Damping (%)	0.33	0.25	0.603	0.090	0.148	0.364	0.346	0.379

Mode No.	9	10	11	12	13	14
Frequency(HZ)	1877.11	2104.23	2226.53	2310.23	2464.3	2708.14
Damping (%)	0.56	0.516	0.452	0.461	0.512	0.329



To be continued on next page.

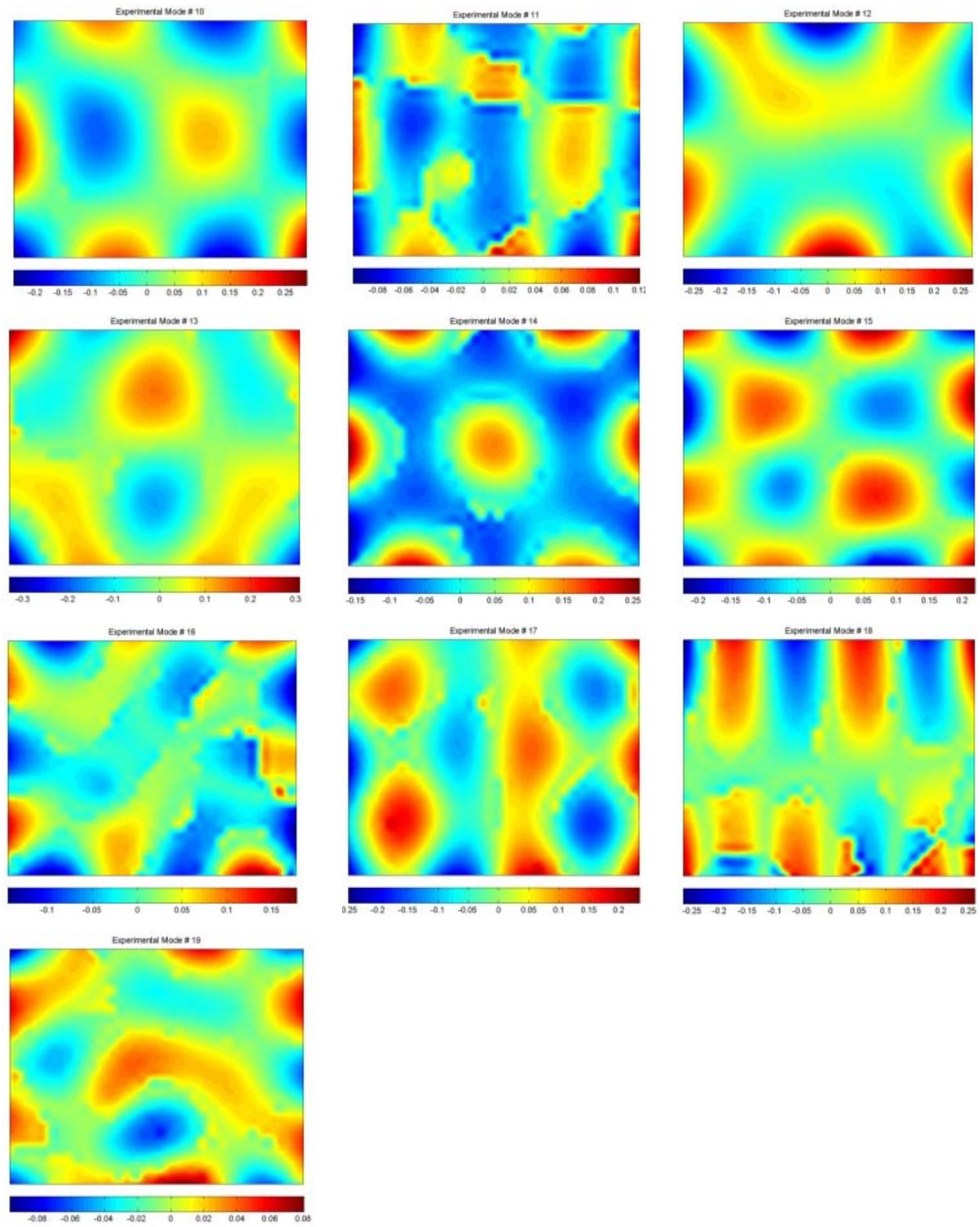


Figure 5.4 Experimental mode shapes of Alporas_B2

Table 5.2 Experimental modal parameters of Alporas_B2

Mode No.	1	2	3	4	5	6	7	8
Frequency(HZ)	219.84	281.33	462.616	525.82	597.41	797.26	993.59	1168.32
Damping (%)	0.153	0.00132	0.885	0.237	0.0778	0.393	0.203	0.513

Mode No.	9	10	11	12	13	14	15	16
Frequency(HZ)	1313.01	1521.79	1537.19	1654.81	1796.64	2208.56	2244.39	2352.23
Damping (%)	1.20	0.611	0.628	0.787	0.8101	0.505	0.54	0.735

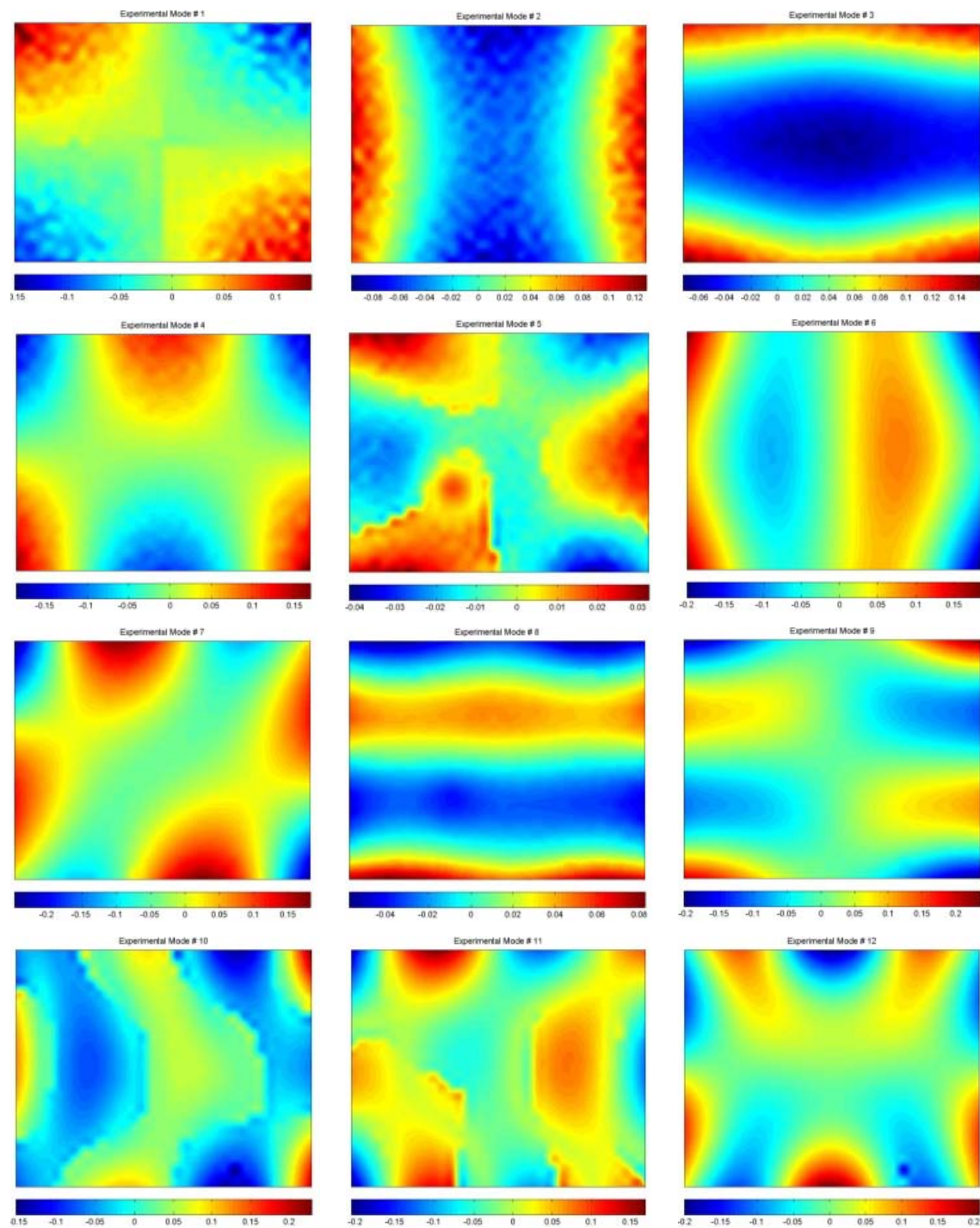
Mode No.	17	18	19
Frequency(HZ)	2463.35	2614.45	2765.79
Damping (%)	0.447	0.44	0.240

Table 5.3 Experimental modal parameters of Alporas_B3

Mode No.	1	2	3	4	5	6	7	8
Frequency(HZ)	280.4	331.65	597.36	635.61	727.4	929.99	1160.89	1445.59
Damping (%)	0.092	0.101	0.161	0.102	0.087	0.288	0.197	0.352

Mode No.	9	10	11	12	13	14	15	16
Frequency(HZ)	1608.12	1738.66	1770.32	1894.64	2077.2	2528.06	2597.04	2690.680
Damping (%)	0.422	0.491	0.64	0.372	0.217	0.216	0.243	0.137

Mode No.	17	18	19
Frequency(HZ)	2704.39	2832.08	2888.6
Damping (%)	0.166	0.196	0.225



To be continued on next page.

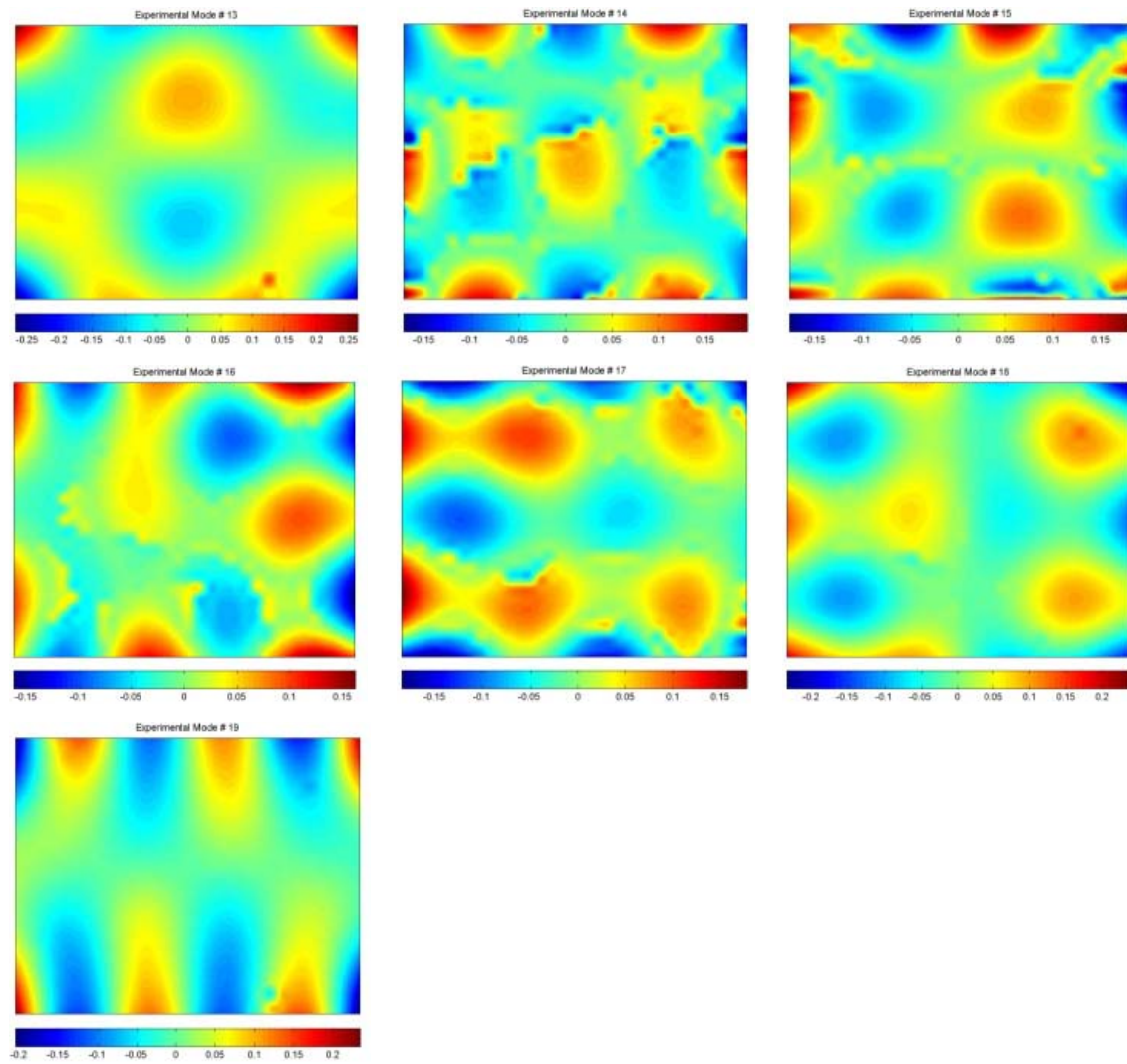


Figure 5.5 Experimental mode shapes of Alporas_B3

Table 5.4 Experimental modal parameters of Alporas_S3

Mode No.	1	2	3	4	5	6	7	8
Frequency(HZ)	412.059	535.27	829.99	1084.5	1365.14	1705.07	1728.16	2104.12
Damping (%)	0.073	0.905	0.248	0.683	0.305	0.395	0.280	0.341

Mode No.	9	10	11	12
Frequency(HZ)	2346.69	2531.96	2575.94	2811.96
Damping (%)	0.386	0.358	0.243	0.23

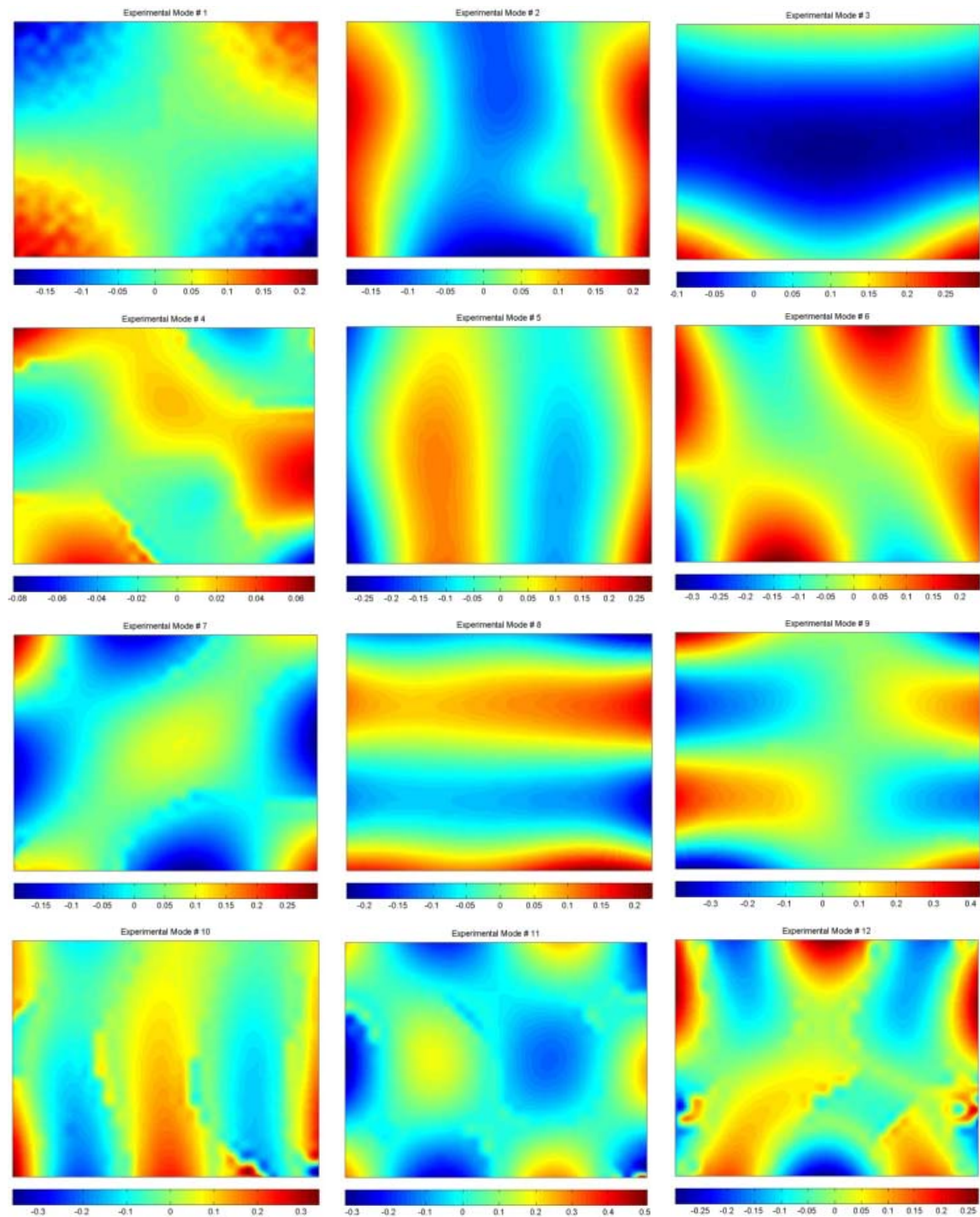


Figure 5.6 Experimental mode shapes of Alporas_S3

Mode shapes extracted using LMS PloyMax estimation technique are also verified using the modal assurance criteria (MAC) to evaluate the orthogonality of experimental

modes. The Modal Assurance Criterion (MAC) matrix is a mathematical tool to compare two vectors to each other. It is used to investigate the validity of estimated modes (see details in section 4.2).

The MAC matrix of all four testing specimen is shown in Figure 5.7. The MAC matrix non diagonal terms in Alporas_B2 and Alporas_B3 indicates some coupling (or non-orthogonality) while in Alporas_S2 and Alporas_S3 they are really negligible, which demonstrates the excellent orthogonality of measured modes. These mode shapes can be used with confident in the identification process.

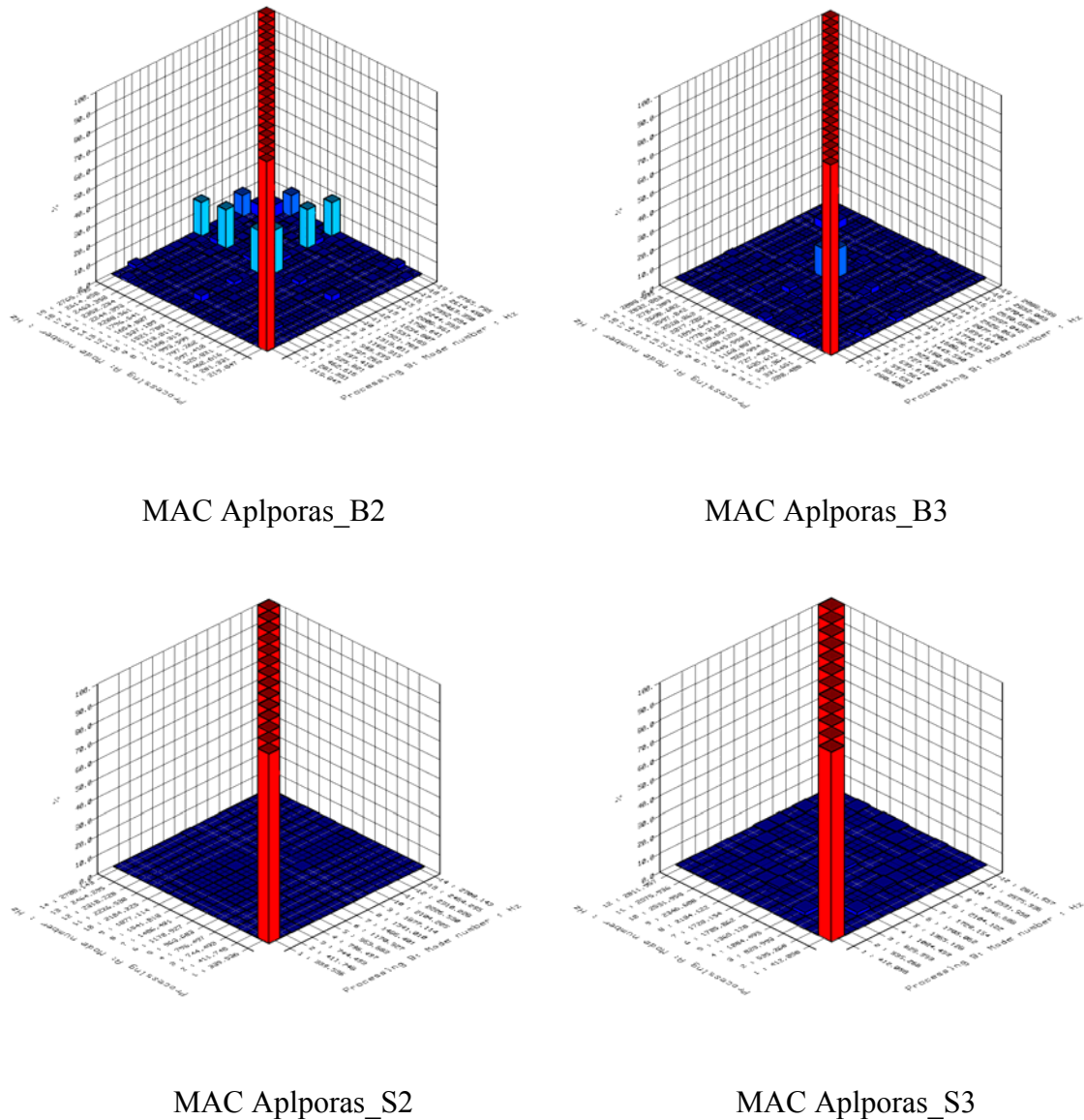


Figure 5.7 Measured Auto-MAC matrix of Alporas Specimens.

5.4 MIXED NUMERICAL-EXPERIMENTAL IDENTIFICATION

5.4.1 ALPORAS_B2

Identification of variable parameters in parametric FE model is performed by choosing following initial values: $\emptyset = 0.6$, $\nu = 0.20$ and damping = $5.0E-05$. The formulation for calculation of Young's modulus (3.102) and density pattern of the material is specified in the parametric FE model. The measured density array of 11000 components is given as input to the FE model of Alporas_B2, based on this density array 11000 materials are defined in this FE model. This measured density distributed model (MDDM) is used further for identification process. Automatic creation of numerical and experimental mode pairs based on the maximum terms of MAC, correlation matrix is used to ensure the compatibility of the eigen modes. Numerical mode shapes are interpolated on the same mesh size as that of experimental mesh (36×29). The mixed identification process is executed and after every optimization step each time a correlation is performed to choose the eigenvectors from the numerical eigen solution to be matched with the experimental ones, writing the Mode Pair Table (MPT). Due to change of the variable parameters, at each optimization step in the identification process, the numerical eigen modes related to the experimental ones might be shifted and interchanged in the sequence, which brings to a new evaluation of the MPT. An automatic routine has been developed to provide at each optimization step the

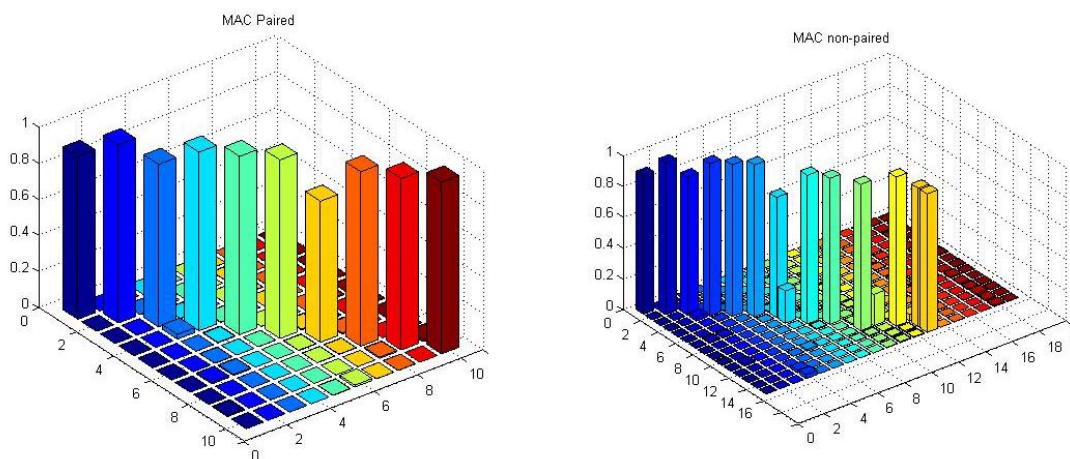


Figure 5.8 MAC matrix of experimental and numerical modes of Alporas_B2 (paired and non-paired)

updated MPT before executing the norm error function in the identification process. This step consists of computing the MAC values between the numerical mode shapes and the experimental mode shapes stored in the reference database. The combinations that result in the highest MAC-values are the mode shape pairs. The non-paired MAC matrix (modal correlation between all measured mode shapes and first 15 numerical mode shapes) and paired MAC matrix (modal correlation between first 10 experimental and corresponding numerical modes whose MAC values exceed 0.7) of Alporas_B2 is shown in Figure 5.8. The first ten mode shape pairs having MAC values greater than 0.7 are further used in identification process.

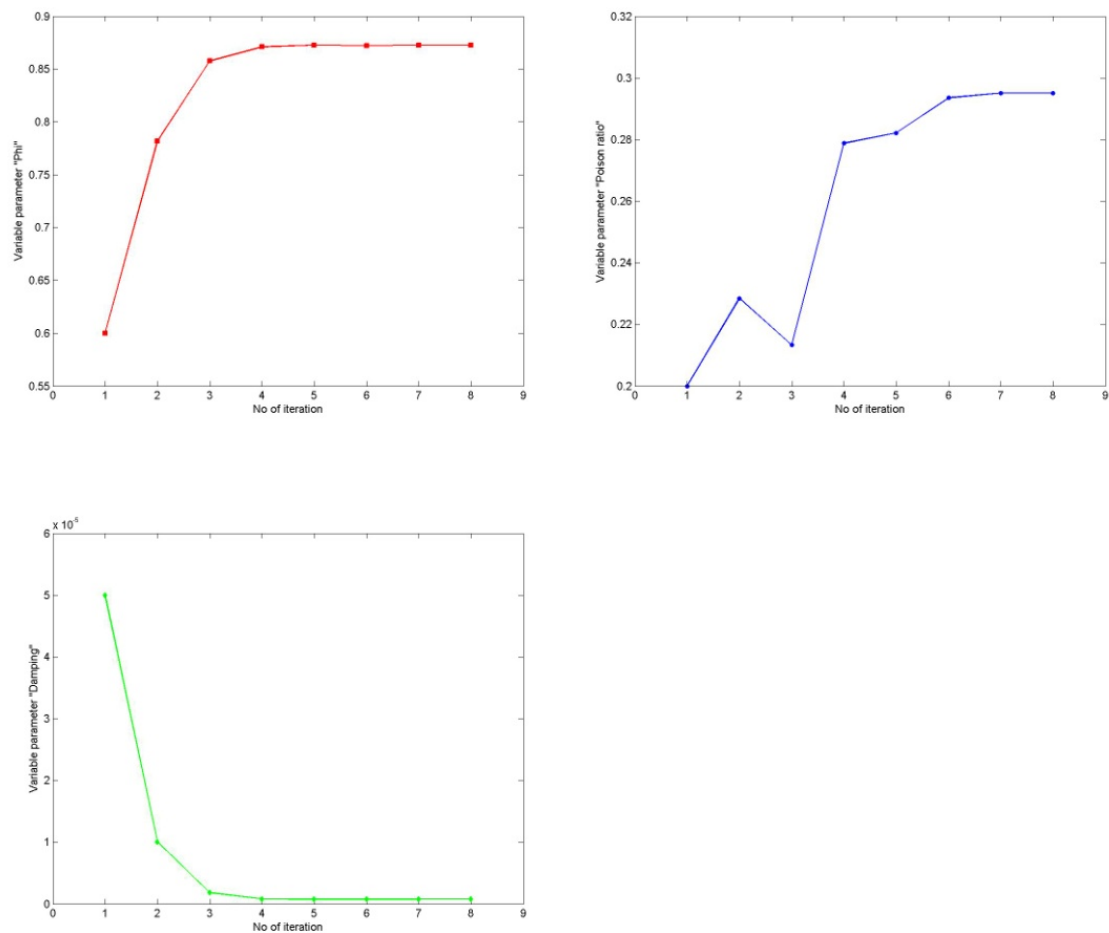


Figure 5.9 Graphs of convergence of identifying parameters (Alporas_B2)

Table 5.5 Convergence of identifying parameters (Alporas_B2)

Parameter	Iter.1	Iter.2	Iter.3	Iter.4	Iter.5	Iter. 6	Iter. 7	Iter. 8
Phi	0.6	0.782	0.858	0.871	0.873	0.872	0.873	0.873
Poisson's ratio	0.2	0.228	0.213	0.279	0.282	0.294	0.295	0.295
Damping	5.0E-5	1.0E-05	1.8E-06	7.9E-07	7.6E-07	7.6E-07	7.6E-07	7.6E-07

The progress of the algorithm and evolution of variable parameters during the identification procedure are presented in Table 5.5. The convergence of the parameters is also presented graphically in Figure 5.9 and identified numerical eigen frequencies along with corresponding experimental eigen frequencies are illustrated in Table 5.6. The convergence of the Phi parameter and damping is fast while Poisson's ratio converges slightly slower and is less stable than others.

The measured eigen frequencies and identified eigen frequencies for Alporas_B2 at the end of optimization process are shown in Table 5.6. Quality of the identified mode shapes are excellent because the maximum error of the measured eigen frequencies and identified is ± 1.5 %. Diagonal terms of paired MAC matrix shows the correlation

Table 5.6 Relative frequency error, Alporas_B2

Mode No.	1	2	3	4	5
Experimental Frequency (Hz)	219.85	281.33	462.62	525.82	597.41
Numerical Frequency (Hz)	220.75	279.21	463.95	523.31	601.07
Error (%)	0.41	-0.75	0.29	-0.48	0.61

Mode No.	6	7	8	9	10
Experimental Frequency (Hz)	797.26	993.60	1168.32	1313.01	1521.79
Numerical Frequency (Hz)	794.04	983.29	1185.00	1331.10	1502.30
Error (%)	-0.40	-1.04	1.43	1.38	-1.28

between the first ten experimental and numerical modes, which is quite good as minimum component remains greater than 0.7, with an average of 0.9. The off diagonal terms of paired MAC matrix are very negligible which shows a good correlation between experimental and numerical mode shapes.

The measured density distribution of Alporas_B2 is shown in Figure 5.10. This density mapping is measured by computer tomography and the values are saved in an array of size $55 \times 40 \times 5$ in x, y and z direction respectively. The density distribution shown in Figure 5.10 is the average distribution in z direction. Some numerical investigations are performed to analyse the behavior of aluminum foam due to variable density distribution. In first case a coarse sub-domain density model (CSDM) is used in collaboration with the identified parameters of MDDM. Array of size $11 \times 8 \times 1$ in x, y and z respectively, in which each component is average of 5 components in each direction (average of total 125 components as MDDM is of size $55 \times 40 \times 5$) is assigned to CSDM. In second case a uniform average density model (UADM) is used in which density assigned is a single uniform value.

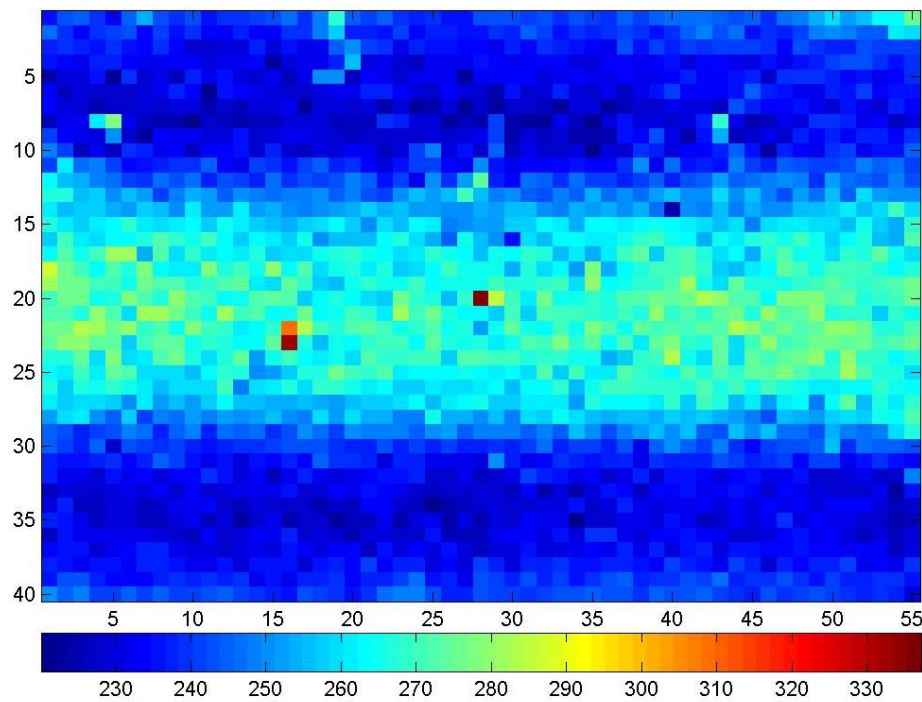


Figure 5.10 Density distribution of Alporas_B2

Table 5.7 Frequencies (Hz) predicted from FE models based on densities distribution mapping (Alporas_B2)

Mode No	MDDM	CSDM	UADM	RDDM_1	RDDM_2	RDDM_3
1	220.75	220.30	214.33	214.12	213.96	213.71
2	279.21	285.14	277.97	277.58	277.39	277.38
3	463.95	459.37	447.32	446.90	446.86	446.19
4	523.31	533.63	510.29	509.62	509.80	509.15
5	601.07	617.23	595.53	594.88	594.37	594.48
6	794.04	838.97	786.78	785.26	785.14	785.55
7	983.29	1032.00	975.91	974.08	974.44	973.72
8	990.44	1051.30	986.25	985.01	984.84	985.26
9	1185.00	1277.40	1177.20	1176.00	1174.80	1175.90
10	1331.10	1443.00	1324.20	1322.40	1322.40	1323.30
11	1492.90	1613.50	1482.60	1480.70	1480.20	1480.00
12	1502.30	1644.40	1508.70	1506.60	1506.30	1507.20
13	1637.80	1794.50	1626.90	1623.90	1624.90	1623.10
14	1747.90	1803.10	1742.70	1739.90	1740.50	1740.70
15	1749.90	1930.40	1765.10	1763.40	1761.60	1763.60

In 3rd, 4th and 5th cases random distributed density model (RDDM) is used. In these cases different random distributions of measured density are assigned to the FE models. Numerical modal analysis is performed for all cases with the identified variable parameters of MDDM. The results of all cases are shown in Table 5.7. It is observed that the difference between the corresponding eigen frequencies of UADM and RDDM's for Alporas_B2 is very small. It is also observed that corresponding eigen frequencies of all these models (UADM and RDDM's) are less than the MDDM. The

difference in corresponding eigen frequencies of RDDM's is negligible among themselves while lower than the MDDM. Similarly in case of UADM the corresponding eigen frequencies are lower than the MDDM while slightly higher than the RDDM's. In case of CSDM the first torsion (mode # 1) and bending (mode # 3) modes have lower while all other have higher frequencies than MDDM.

5.4.2 ALPORAS_B3

Identification of variable parameters of FE model Alporas_B3 is performed by choosing the following initial values of the parameters: $\phi = 0.7$, $\nu = 0.20$ and damping = 0.00006. The paired and non-paired MAC matrix of Alporas_B3 is shown in Figure 5.11. The measured eigen frequencies and identified eigen frequencies for Alporas_B3 at the end of optimization process are shown in Table 5.8.

The progress of the algorithm and the evolution of variable parameters during the identification procedure are presented in table 5.9. The convergence of the parameters is

Table 5.8 Relative frequency error, Alporas_B3

Mode No.	1	2	3	4	5
Experimental Frequency (Hz)	280.41	331.65	597.36	635.61	727.4
Numerical Frequency (Hz)	275.02	328.2	595.94	637.17	732.28
Error (%)	-1.92	-1.04	-0.24	0.25	0.67

Mode No.	6	7	8	9	10
Experimental Frequency (Hz)	929.99	1160.89	1445.59	1608.12	1770.32
Numerical Frequency (Hz)	942.32	1173.9	1444.7	1612.6	1760.9
Error (%)	1.33	1.12	-0.06	0.28	-0.53

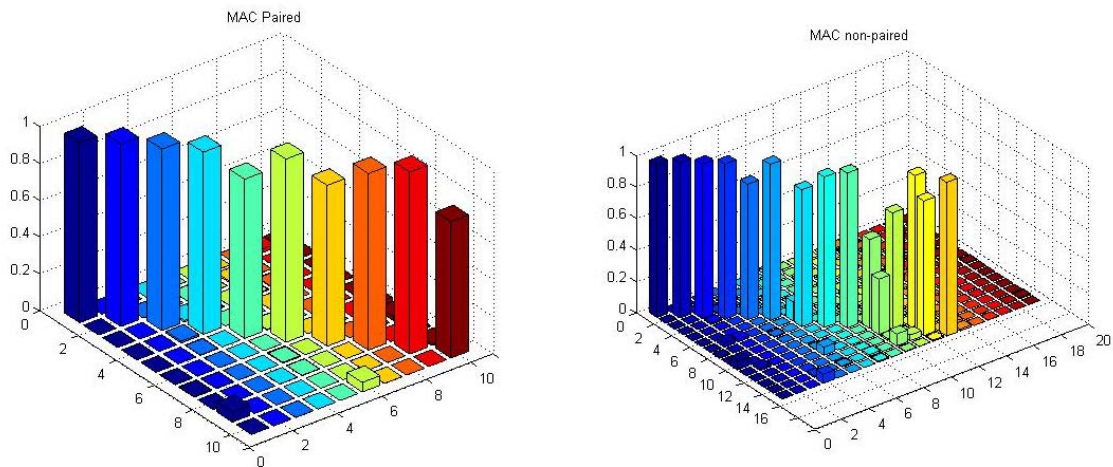


Figure 5.11 MAC matrix of experimental and numerical modes of Alporas_B3 (paired and non-paired)

also presented graphically in Figure 5.12 and identified numerical eigen frequencies along with corresponding experimental eigen frequencies are illustrated in Table 5.8. The convergence of the Phi and damping parameters needed only five iterations to determine these parameters, while Poisson's ratio converge slightly slower

The measured density distribution of Alporas_B3 is shown in Figure 5.13. This density mapping is measured by computer tomography and the calculated values of sub-domains are saved in an array of size $55 \times 40 \times 5$ in x, y and z direction respectively. The density distribution shown in Figure 5.13 is the average distribution in z direction. It can be observed that Alporas_B3 specimen is roughly divided in to five areas based on the average density values. Looking at Figure 5.13 and starting from the top edge, the first uniform density area (UDA) is with blue color than second thin UDA with aqua and third UDA comparatively wide, with android green having some sub-domains with yellow color, fourth UDA again with aqua color and fifth UDA with blue color having yellow and red color sub-domains. The color bar is also shown along Figure 5.13.

Table 5.9 Convergence of identifying parameters (Alporas_B3)

Parameter	Iter.1	Iter.2	Iter.3	Iter.4	Iter.5	Iter. 6	Iter. 7	Iter. 8
Phi	0.7	0.79	0.84	0.85	0.85	0.85	0.85	0.85
Poisson's ratio	0.2	0.21	0.25	0.31	0.3	0.31	0.31	0.31
Damping	6E-5	6.23E-6	9.47E-7	6.16E-7	6.22E-7	6.22E-7	6.22E-7	6.22E-7

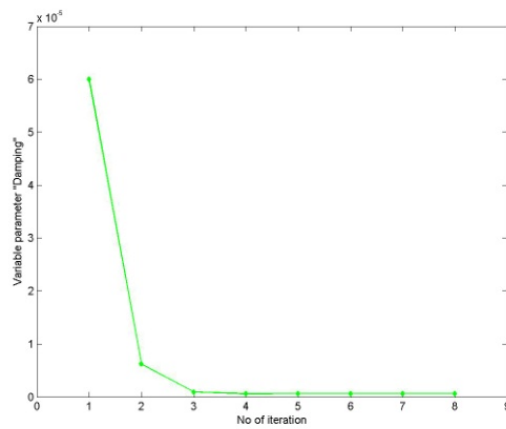
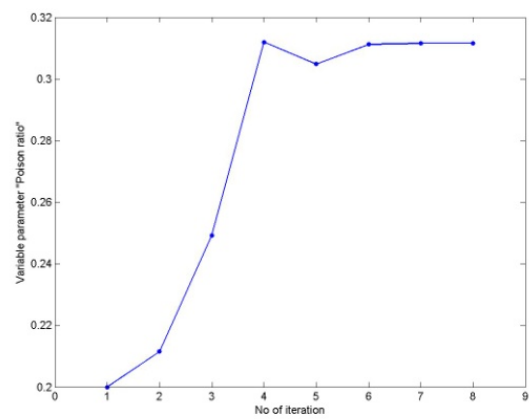
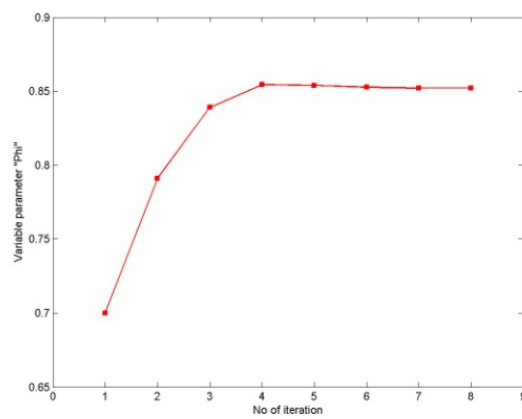


Figure 5.12 Graphs of convergence of identifying parameter (Alporas_B3)

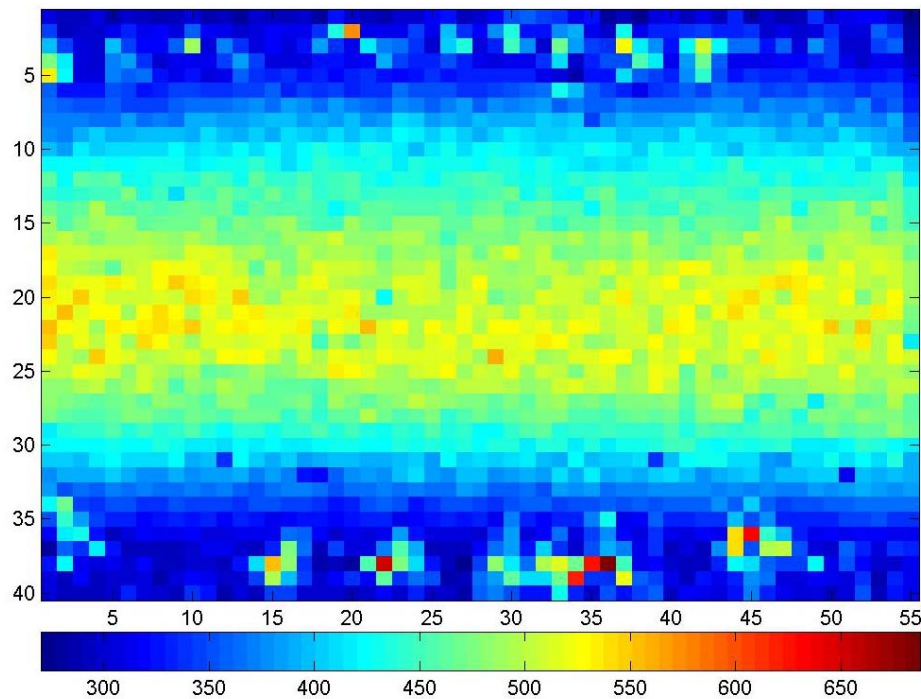


Figure 5.13 Density distribution of Alporas_B3

Some numerical investigations are performed in the same way as in case of Alporas_B2. The eigen frequencies as a results of modal analysis solution for all cases are shown in Table 5.10. The eigen frequency of corresponding mode shapes of Alporas_B3 are higher than Alporas_B2 obviously due to high density of the specimen. The experimental mode shapes of Alporas_B2 and Alporas_B3 are shown in Figure 5.4 and Figure 5.5 respectively. In case of Alporas_B3 the corresponding eigen frequencies difference among the RDDM's is very minor but UADM has slightly higher corresponding values than RDDM's. Similarly like Alporas_B2, the corresponding eigen frequencies of UADM and RDDM's are less than MDDM. In case of CSDM, the corresponding eigen frequencies are higher than the MDDM for Alporas_B2 except the first torsional (mode #1) and bending mode (mode # 3).

Table 5.10 Frequencies (Hz) predicted from FE model based on densities distribution mapping (Alporas_B3)

Mode No	MDDM	CSDM	UADM	RDDM_1	RDDM_2	RDDM_3
1	275.02	259.87	250.03	248.31	248.46	247.69
2	328.20	339.44	325.45	323.87	323.38	323.94
3	595.94	541.59	528.55	524.51	526.81	526.16
4	637.17	637.78	596.10	591.88	592.77	591.11
5	732.28	724.90	696.82	691.53	694.42	693.20
6	942.32	1012.60	925.03	919.84	919.81	919.58
7	1163.50	1205.50	1140.40	1133.30	1135.20	1133.60
8	1173.90	1264.40	1153.10	1142.10	1146.80	1148.50
9	1444.70	1501.00	1386.30	1374.30	1380.30	1381.10
10	1612.60	1696.00	1556.10	1545.40	1549.20	1547.80
11	1744.00	1874.50	1738.40	1727.20	1730.60	1727.60
12	1760.90	1946.50	1762.80	1748.30	1751.80	1753.60
13	1904.10	2083.70	1901.00	1887.30	1891.60	1890.00
14	1970.80	2124.10	2022.30	2021.80	2012.70	2008.10
15	2067.00	2221.10	2043.60	2026.40	2030.00	2030.50

5.4.3 ALPORAS_S3

Identification of variable parameters of FE model Alporas_S3 is performed by choosing the following initial values of the parameters; $\emptyset = 0.7$, $\nu = 0.25$ and damping = 0.00005. Measured density array of 7000 component is given as input to the FE of Alporas_S3.

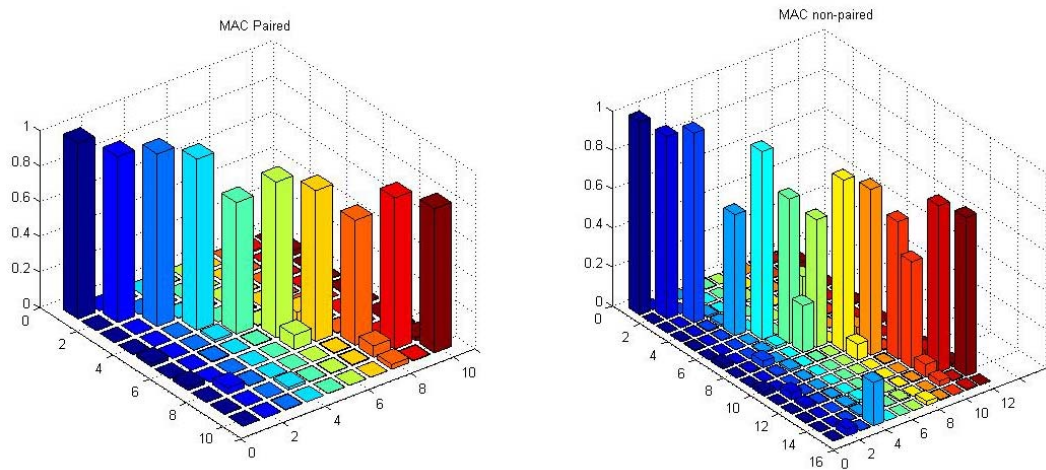


Figure 5.14 MAC matrix of experimental and numerical modes of Alporas_S3 (paired and non-paired)

Automatic creation of numerical and experimental modes pairs based on the maximum terms of MAC, correlation matrix is used to ensure the compatibility of the eigen modes. The paired and non-paired MAC matrix of Alporas_S3 is shown in Figure 5.14.

Table 5.11 Relative frequency error Alporas_S3

Mode No.	1	2	3	4	5
Experimental Frequency (Hz)	412.06	535.27	829.99	1365.13	1705.06
Numerical Frequency (Hz)	415.87	531.84	845.11	1381.80	1671.70
Error (%)	0.93	-0.64	1.82	1.22	-1.96

Mode No.	6	7	8
Experimental Frequency (Hz)	2104.12	2346.69	2531.96
Numerical Frequency (Hz)	2136.70	2325.90	2494.00
Error (%)	1.55	-0.89	-1.50

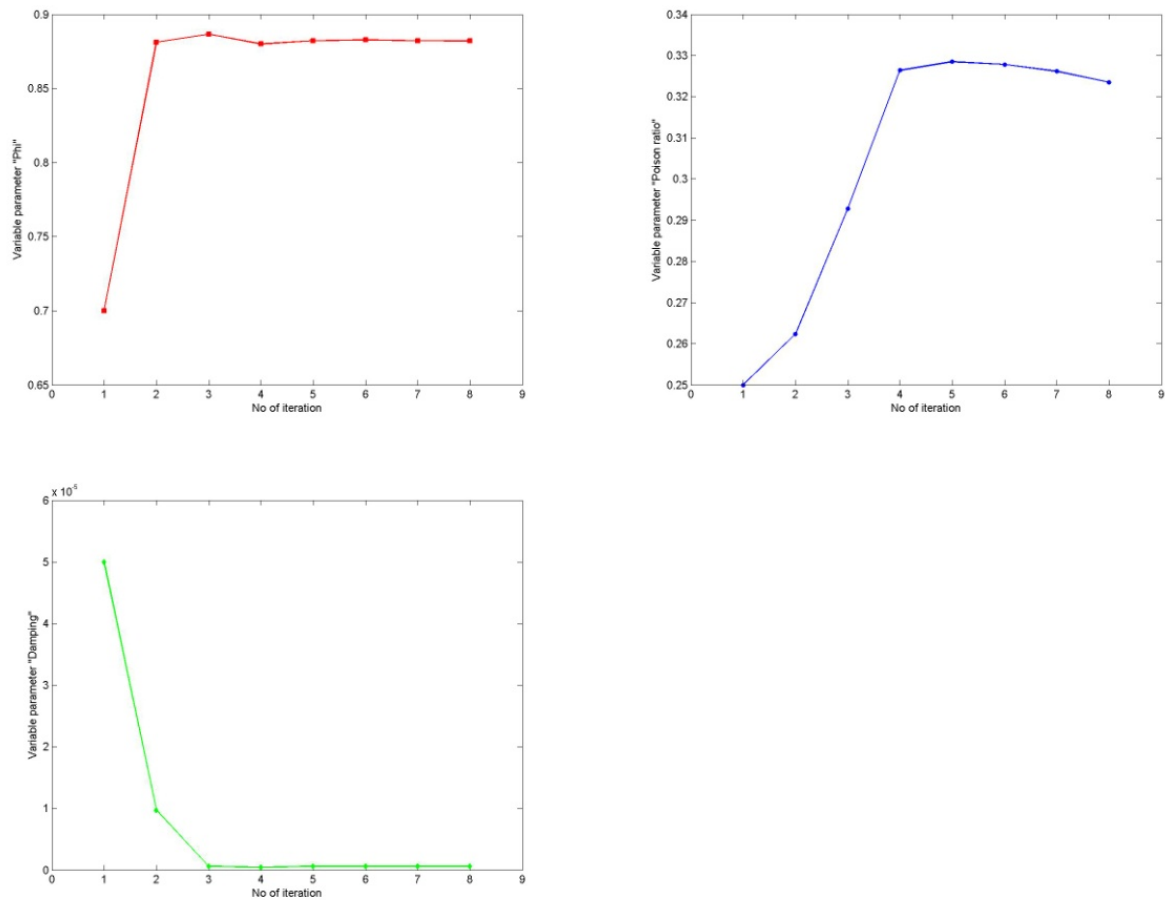


Figure 5.15 Graphs of convergence of identifying parameters (Alporas_S3)

The progress of the algorithm and the evolution of variable parameters during the identification procedure are presented in table 5.12. The convergence of the parameters is also presented graphically in Figure 5.15. The Poisson's ratio converge slightly slower and is less stable than other parameters. Identified numerical eigen frequencies along with corresponding experimental eigen frequencies are illustrated in Table 5.11.

Table 5.12 Convergence of identifying parameters (Alporas_S3)

Parameter	Iter.1	Iter.2	Iter.3	Iter.4	Iter.5	Iter. 6	Iter. 7	Iter. 8
Phi	0.7	0.88	0.89	0.88	0.88	0.88	0.88	0.88
Poisson's ratio	0.25	0.26	0.29	0.33	0.33	0.33	0.33	0.32
Damping	5E-5	9.7E-6	5.8E-7	4.9E-7	5.8E-7	5.8E-7	5.8E-7	5.8E-7

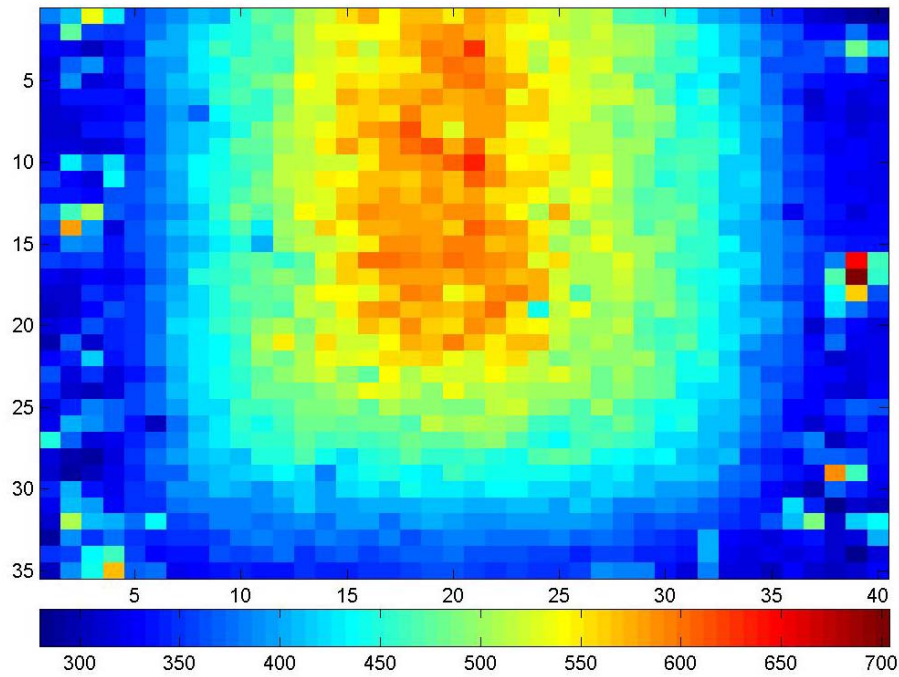


Figure 5.17 Density distribution of Alporas_S3

The density distribution shown in Figure 5.16 is the average distribution in z direction. The results of numerical modal solution of all cases (as explained in section 5.4.1) are shown in Table 5.13. In case of Alporas_S2 and Alporas_S3 the CSDM used array of size $8 \times 7 \times 1$ in x , y and z respectively. In this array each component is average of 125 components (5 components in each direction), as in MDDM the input density array is of size $40 \times 35 \times 5$.

The difference in corresponding eigen frequencies of RDDM's is negligible among themselves while lower than the MDDM. Similarly in case of UADM the corresponding eigen frequencies are lower than the MDDM while slightly higher than the RDDM's. In case of CSDM the first torsion (mode # 1) and bending (mode # 2) modes have lower while all other have higher frequencies than MDDM.

Table 5.13 Frequencies (Hz) predicted from FE model based on densities distribution mapping (Alporas_S3)

Mode No	MDDM	CSDM	UADM	RDDM_1	RDDM_2	RDDM_3
1	415.87	391.91	373.35	369.81	370.25	370.29
2	531.84	490.87	473.68	469.68	470.57	471.98
3	845.11	856.23	822.92	819.50	816.45	815.64
4	912.54	931.87	877.54	871.95	869.87	871.78
5	1085.60	1113.90	1050.00	1043.40	1039.60	1044.20
6	1381.80	1473.70	1339.80	1331.20	1328.20	1331.50
7	1671.70	1815.40	1651.30	1639.50	1638.50	1640.90
8	1701.50	1841.50	1704.40	1693.20	1689.20	1689.70
9	2136.70	2382.90	2120.80	2109.10	2102.30	2109.40
10	2325.90	2439.20	2349.30	2339.40	2327.20	2336.20
11	2494.00	2647.80	2403.10	2385.30	2388.70	2404.10
12	2525.90	2764.10	2476.40	2461.20	2457.40	2459.20
13	2537.30	2846.50	2559.60	2538.30	2536.20	2542.10
14	2746.70	2958.80	2734.30	2718.00	2716.40	2710.30
15	2985.70	3031.20	2745.60	2729.10	2732.20	2728.80

5.4.4 ALPORAS_S2

The following initial values of variable parameters; $\emptyset = 0.6$, $\nu = 0.20$ and damping = 0.00005 are assigned to FE model Alporas_S2. The paired and non-paired MAC matrix of Alporas_S2 is shown in Figure 5.17.

Table 5.14 Relative frequency error, Alporas_S2

Mode No.	1	2	3	4	5
Experimental Frequency (Hz)	339.53	411.75	744.49	796.49	963.68
Numerical Frequency (Hz)	340.7	435.9	736.22	780.79	936.98
Error (%)	0.34	5.86	-1.11	-1.97	-2.77

Mode No.	6	7	8	9	10
Experimental Frequency (Hz)	1170.93	1486.4	1541.01	1877.11	2104.23
Numerical Frequency (Hz)	1210.8	1468.2	1504.2	1877.5	2082.1
Error (%)	3.40	-1.22	-2.38	0.02	-1.05

The progress of the algorithm and the evolution of variable parameters during the identification procedure are presented in table 5.15. The convergence of the parameters is also presented graphically in Figure 5.18 and identified numerical eigen frequencies along with corresponding experimental eigen frequencies are illustrated in Table 5.14.

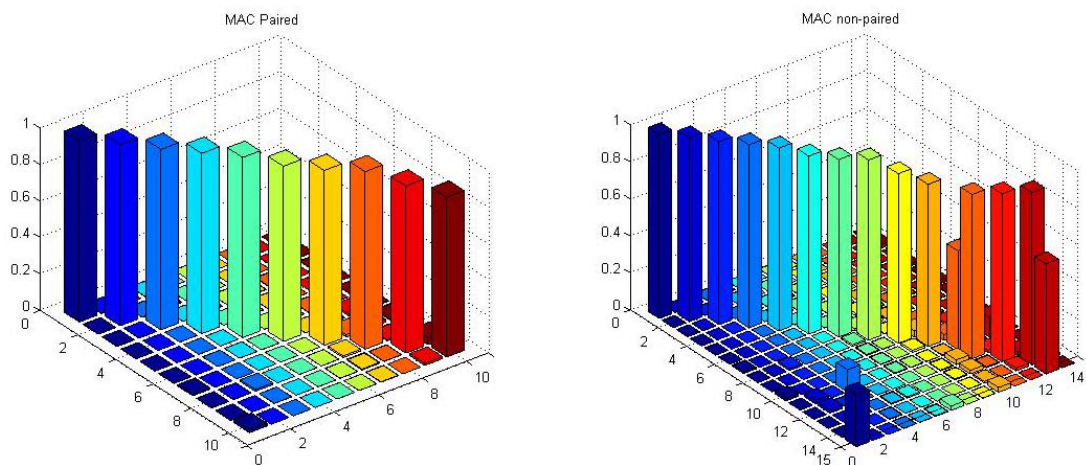


Figure 5.18 MAC matrix of experimental and numerical modes of Alporas_S2 (paired and non-paired)

Table 5.15 Convergence of identifying parameters (Alporas_S2)

Parameter	Iter.0	Iter.1	Iter.2	Iter.3	Iter.4	Iter. 5	Iter. 6	Iter. 7
Phi	0.6	0.81	0.87	0.87	0.87	0.87	0.87	0.87
Poisson's ratio	0.2	0.24	0.36	0.34	0.34	0.34	0.34	0.34
Damping	5E-5	1.2E-5	1.9E-6	6.4E-7	6.3E-7	6.3E-7	6.3E-7	6.3E-7

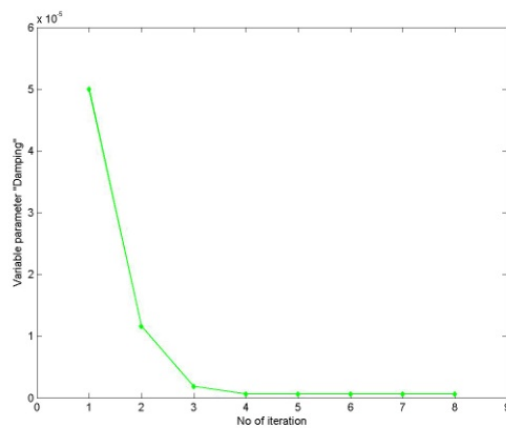
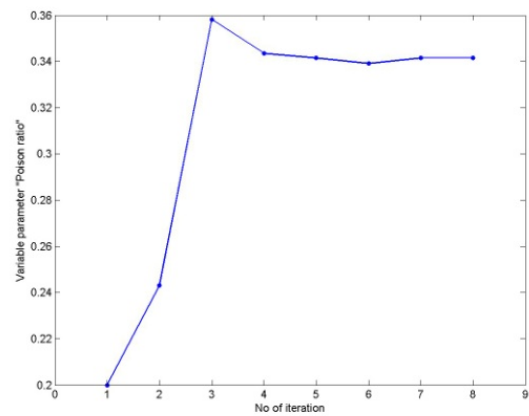
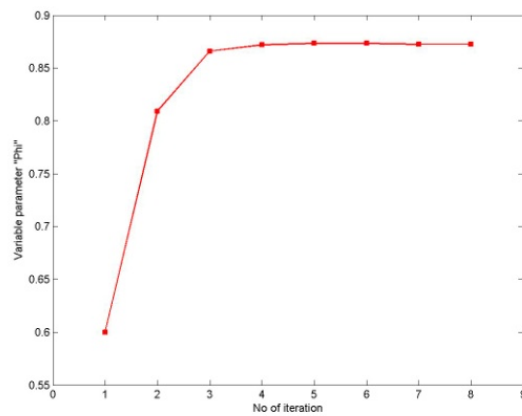


Figure 5.19 Graphs of convergence of identifying parameters (Alporas_S2)

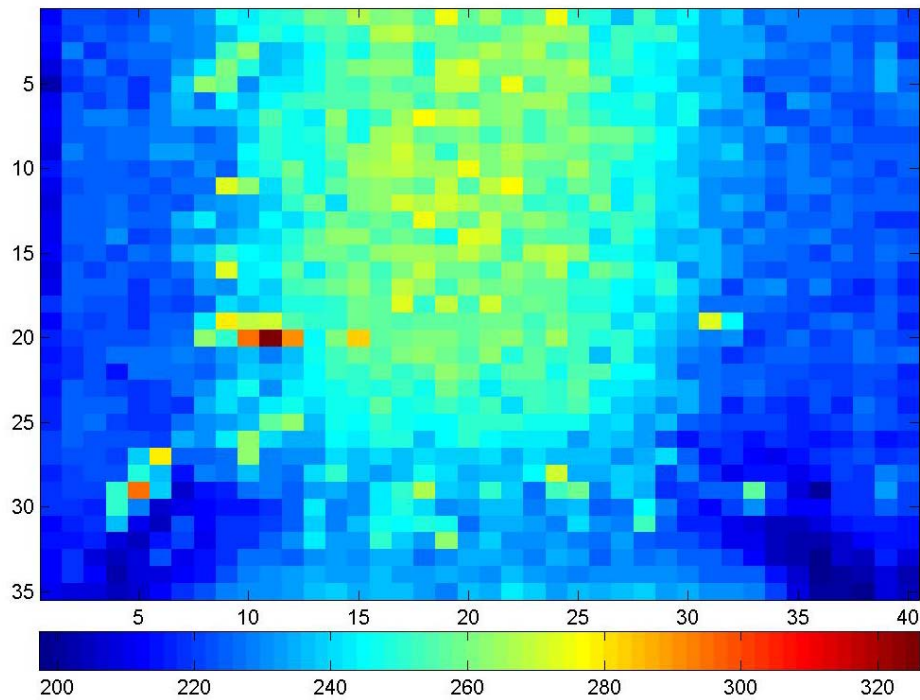


Figure 5.20 Density distribution of Alporas_S2

The measured average density distribution (in z direction) of Alporas_S2 is shown in Figure 5.19. The results of numerical investigations of Alporas_S2 are shown in Table 5.16. The eigen frequency of corresponding mode shapes of Alporas_S2 are lower than Alporas_S3 apparently due to lower relative density of the specimen. The experimental mode shapes of Alporas_S2 and Alporas_S3 are shown in Figure 5.3 and Figure 5.6 respectively. It is observed that the difference between the corresponding eigen frequencies of UADM and RDDM's for Alporas_S2 is very minute. It is also observed that corresponding eigen frequencies in all these cases (UADM and RDDM's) are less than the MDDM. Similarly in CSDM, the first torsion (mode # 1) and bending (mode # 2) modes have lower while all other modes have higher corresponding eigen frequencies than MDDM.

Table 5.16 Frequencies (Hz) predicted from FE model based on densities distribution mapping (Alporas_S2)

Mode No	MDDM	CSDM	UADM	RDDM_1	RDDM_2	RDDM_3
1	340.70	336.97	326.68	326.52	326.37	325.83
2	435.90	428.96	419.08	419.39	418.68	418.49
3	736.22	755.25	724.52	724.33	722.80	723.28
4	780.79	811.40	771.31	770.19	769.40	769.52
5	936.98	964.69	919.50	919.03	917.92	916.94
6	1210.80	1302.10	1192.50	1192.30	1190.50	1190.20
7	1468.20	1594.40	1456.90	1456.30	1453.20	1453.40
8	1504.20	1610.10	1497.40	1497.70	1492.70	1494.10
9	1877.50	2081.40	1864.30	1863.20	1859.80	1859.30
10	2082.10	2176.20	2065.80	2065.30	2061.10	2060.40
11	2197.20	2317.20	2143.20	2141.60	2144.70	2140.30
12	2218.00	2484.40	2202.90	2201.40	2196.70	2197.50
13	2262.10	2507.00	2255.00	2252.90	2247.80	2249.90
14	2425.30	2615.80	2416.20	2415.50	2411.40	2410.70
15	2527.50	2658.00	2423.90	2421.10	2422.60	2421.70

The identified parameters of four AF specimens are specified in the Table 5.17.

Table 5.17 Identified parameters of AF specimens.

AF specimen	Damping constant	Poisson's ratio	Phi (ϕ)	Young's modulus (GPa)
Alporas_S2	6.3E-7	0.34	0.87	1.25
Alporas_B2	7.6E-07	0.295	0.873	1.24
Alporas_S3	5.8E-7	0.32	0.88	2.80
Alporas_B3	6.22E-7	0.31	0.85	3.27

CHAPTER 6. SUMMARY AND CONCLUSIONS

The first task of the research work described in this thesis was to develop an experimental setup to evaluate modal parameters, precisely. To achieve precision, an experimental setup of non contact vibration measurement using scanning laser vibrometer has been developed to serve as a base for mixed numerical-experimental identification technique. A laser Doppler vibrometer was used to perform a continuous point-by-point scan over a particular test piece, the AF structure. The front surface of the AF specimen was scanned by the LDV and the excitation was applied from behind. The experiments were performed on four simple aluminum foam rectangular plates. These specimens were hung down with soft elastic cords to make them in free-free condition and excited using a pseudo-random excitation via an electromagnetic shaker attached to the structure, as shown in Figure 2.13. In the experimental set-up the LDV could be directed at any point on the test specimen almost perpendicularly to measure its z-axis vibration. The whole setup was placed on vibration isolated table to prevent the surrounding vibrations. Response measurements were obtained with the LDV scanning over the testing specimen at specified mesh grid points, see for example Figure 2.14. The transfer functions of the test specimen, velocity/force type was calculated by the internal software system PSV200 and an average of several measurements was performed to further increase the quality of the experimental frequency model. The FRFs from PSV200 were imported in LMS Test.Lab. The state of the art LMS PolyMAX parameter estimation technique was used to determine the eigen frequencies and corresponding mode shapes in range of 10 Hz to 3 KHz. The MAC, MPC and MPD criteria were used to investigate the validity of the estimated modes.

The second specific task of this research was to develop an FE model of AF material based both on the cellular microstructure and behavior of the bulk material. Computational modelling and simulation of materials with a cellular microstructure is a broad field of research that has drawn considerable interest for engineers. Simulations give the possibility of investigating several aspects of the relations between the parameters of the microstructure and the overall mechanical properties of cellular materials. Computed tomography as a non-destructive testing method has the potential

to study the internal configuration of the structure, in which density changes over a sufficient volume. Aluminum foams are composite consisting of metal and air can fulfill this condition very well. These metals can be analyzed in two ways; (i) reconstruction of the microstructure to analyze the 3D distribution of solid (ii) transformation of heterogeneous microstructure to an approximated continuum. To reconstruct the microstructure high resolution CT-data is required. Only micro-CT can provide this high resolution data, required for this purpose. Then a FE model of this reconstructed microstructure can be generated as described in [151, 186]. Such a model would have a high number of elements which makes the model too complex to easily handle in FE packages and computing time would be high as well. One of the most important feature of a cellular solid is its relative density; ρ^*/ρ_s where ρ^* is the density of the cellular material and ρ_s is the density of the solid from which the cell walls are made.

A special procedure called density mapping method, has been applied to approximate the cellular structure of aluminum foam with continuum. The transformation of a discretely heterogeneous structure of aluminum foam to an approximated continuum was one of the major challenges in this work. The microscopical density distribution of the aluminum foam recorded by X-ray computed tomography has been averaged over a certain domain. The obtained continuum body was implemented in FE package ANSYS. The finite elements were used for discretization of density fields. The local average density represented by a mean density forms a so called ‘sub-domain’. All finite elements in the sub-domain behave mechanically in the same way. Each sub-domain was assumed to be homogeneous and isotropic. Its mechanical properties were modeled using Gibson and Ashby scaling laws for regular foams scaled by experimental results. In this scaling laws, the microstructure of cellular materials was homogenized over a scale infinitely larger than the typical microstructure. In other words these relations predict the behavior of a material that was assumed to be a homogeneous continuum. Density distribution of aluminum foam measured by X-ray computer tomography was used as input to the corresponding FE model of investigated specimen. All numerical investigations were carried out by means of the FE package ANSYS. The ANSYS APDL file was developed such that it could handle multiple sets of input variables at a time during each call by MATLAB. Furthermore ANSYS APDL files of all AF specimens were generated that defines the

preprocessor (parametric model of the AF specimen), solution and postprocessor phase of the finite element analysis. In the preprocessor phase, the geometry and the boundary conditions of the model were defined using a set of APDL commands. The model, that has been defined in the preprocessor phase was then solved in the solution phase using a suitable modal solution process such as QR damped method. In the postprocessor phase the results from the analysis was gathered and saved in a suitable format (file). This file was then read by MATLAB for further optimization process. This APDL file thus created was used by ANSYS running in batch mode, during each system call command from MATLAB.

Another task in this work was to develop a mixed numerical-experimental identification technique which is based on experimental modal model, measured CT density distribution data and FE model of specimen under investigation. To achieve this task an automation code in MATLAB was developed that incorporates ANSYS the finite element solver, experimental modal analysis results from LMS Test.Lab and a suitable optimization tool. A system call command in MATLAB was employed to call ANSYS for each simulation run that involved calculation of the modal responses to the input variable parameters. Modal results file of each FE simulation was saved for further process. Several MATLAB routines were developed to read these FE results files and extract the required data in matrix form. The experimental modal data was exported from LMS Test.Lab in a universal file format. This universal file was read by a MATLAB routine which extracts the required data in matrix form. A set of error functions based on measured and numerical eigen frequencies and corresponding mode shapes was developed in MATLAB. These error functions have been combined to form a total functional error for optimization of the FE model input variable parameters. Levenberg-Marquardt algorithm with assessment of gradients by finite difference method was used for optimization. Proposed optimization method has proved very effective, since on average, all variable parameters converged at 5th iteration. All these routines were incorporated together to develop the proposed mixed numerical-experimental identification technique.

After identifying the variable parameters numerical investigations were performed to observe the behavior of aluminum foam due to the variable density distribution. In

first case a coarse sub-domain (which is 5 times greater in each direction than the previously modeled) was used in the FE model. The density assigned to elements in each sub-domain was the average density of that sub-domain. In second case a uniform average density was assigned to the whole FE model instead of measured one. In 3rd, 4th and 5th cases different random distribution of measured density was assigned to the FE model. MATLAB routines were developed to do these tasks of different density distributions. Numerical modal analysis was performed for all cases with the identified variable parameters from MDDM. It was observed that the corresponding eigen frequencies of the models with uniform and random density distribution are lower than the MDDM. Similarly in case of coarse sub-domain model the first torsional and bending (Alporas_B2 and Alporas_B3 in y-axis while in case of Alporas_S2 and Alporas_S3 in x-axis) mode have lower while other modes have higher corresponding eigen frequencies than MDDM. These observations show that density distribution should not be ignored in FE modelling of these cellular materials. It was therefore concluded from these investigations that FE modelling of specimen and non contact measurements method for modal analysis extend the scope of mixed numerical experimental technique.

Dynamic behavior of closed cell material ALPORAS was investigated experimentally and numerically. Modal test on four ALPORAS specimens shows that inhomogeneties in the mass distribution are a key factor in evaluating dynamic behavior of cellular materials. A comprehensive methodology for identification of dynamic and elastic behavior of cellular materials has been proposed. The actual mass distribution of ALPORAS foam has been obtained by processing of X-ray tomographic data. In the context of materials engineering, the present approach can be very useful for designing cellular materials. Indeed, it enables the prediction of the best way of combining the mechanical properties of the solid material with feasible microstructures, in order to obtain expected mechanical properties.

The effect of inhomogeneous distribution on the modal behavior of ALPORAS was investigated. Experimental results of modal testing show high scatter in the modal properties of investigated specimens. This phenomenon can be well described by the effect of inhomogeneous mass distribution. FE simulations of continuum model

confirmed the inhomogeneous mass distribution effect on modal properties of AF specimens. Gibson and Ashby model was implemented in FE model to provide the elastic behavior. Furthermore the model used in the present work was an isotropic model. It means that the model was unable to account for the anisotropy. The proposed approach distinguished from traditional finite element approaches of cellular metals [161-166], in respect that it is not based only on the cellular microstructure of the AF but also incorporate dynamic behavior of the bulk material.

One important aspect of the model was the bulk material properties. The computed behavior of the foam was very sensitive to these input parameters. The model can be adjusted by introducing a correction on the mechanical properties parameters of the bulky material. Modification can also concern the constitutive relation itself. The aim of this work was to develop and validate a realistic mechanical model of cellular materials based both on the cellular microstructure and on the behavior of the bulk material. The effect of more sophisticated material behavior and the influence of the input parameters will be exposed in future works.

6.1 FUTURE DEVELOPMENTS AND PERSPECTIVES

The performance of the developed method can be improved and extended for further future development using the following steps:

- In current study ALPORAS foam specimens with two different average densities are investigated. Thus, the issue of further studies will be to investigate other densities and types of foam.
- The dynamic behavior of specimens with specific density distribution (i.e. higher density distribution at corners, higher density distribution at center etc.) will be appealing to explore.
- Specimens with predefined limits of controlled density distribution (i.e. from 250-300 kg/m³, 300-400 kg/m³, 200-500 kg/m³ etc.) can be used to evaluate the consequence on variable parameters and dynamic behavior of the specimen.
- In this work Gibson and Ashby model was used in FE formulation. Other well known foam models can be implemented in this technique for their comparative study.

- Dimensional optimization of the test specimen and excitation technique can be performed to ensure ideal dynamic measurement quality (clearly decoupled modes) and high number of modes in the measured frequency range.
- Four AF specimens of two different sizes of rectangular shape were considered in this research study. It was observed that the geometry of the specimen has influence on the sensitivities of the error function. More investigations are needed to determine the ideal size of specimen for such identification technique. It will also be interesting to explore the behavior of such material for different geometrical shapes (like circular, square, rectangular etc.).

REFERENCES

- [1] S. Akiyama, *et al.*, "Foamed metal and method of producing same," ed: Google Patents, 1987.
- [2] *American Society for Testing and Materials, ASTM International Standards Worldwide, 100 Barr Harbor Drive, West Conshohocken, Pennsylvania, USA.* Available: <http://www.astm.org/>.
- [3] *International Organization for Standardization, ISO, 1, ch. de la Voie- Creuse, DCase postale 56DCH-1211 Geneva 20, Switzerland.* Available: <http://www.iso.org/>
- [4] L. Pipes, *et al.*, "Experimental Characterization of Advanced Composite Materials," ed: Technomic Publishing Co. Inc, 1997.
- [5] L. Pagnotta, "Recent progress in identification methods for the elastic characterization of materials," *International Journal of Mechanics*, vol. 2, pp. 129-140, 2008.
- [6] "ASTM Standard E1876-07, Standard test method for dynamic Young's modulus, shear modulus, and Poisson's ratio by impulse excitation of vibration," in *Book of Standards, Volume 03.01*, ed.
- [7] "ASTM Standard E1875-08, Standard test method for dynamic Young's modulus, shear modulus, and Poisson's ratio by sonic resonance " in *Book of Standards, Volume 03.01*, ed.
- [8] S. P. Timoshenko and J. N. Goodier, "Theory of elasticity. 1970," *McGraw, New York*.
- [9] R. Jones and D. Bijl, "A holographic interferometric study of the end effects associated with the four-point bending technique for measuring Poisson's ratio," *Journal of Physics E: Scientific Instruments*, vol. 7, p. 357, 1974.
- [10] E. Archbold, *et al.*, "The deformation of steel bars in a four-point bending machine, measured by holographic interferometry," 1977.
- [11] A. R. Ganesan, "Measurement of poisson's ratio using real-time digital speckle pattern interferometry," *Optics and Lasers in Engineering*, vol. 11, pp. 265-269, 1989.
- [12] F. Gascon and F. Salazar, "A procedure for calculating through laser speckle interferometry the elastic constants of isotropic materials," *Optics Communications*, vol. 123, pp. 734-742, 1996.

- [13] F. M. Furgiele, *et al.*, "A full-field procedure for evaluating the elastic properties of advanced ceramics," *Experimental Mechanics*, vol. 37, pp. 285-291, 1997.
- [14] I. N. Odintsev, *et al.*, "Implementation of compensation speckle interferometry for high-precision determination of material mechanical properties," 1999, p. 169.
- [15] L. Bruno, *et al.*, "Determination of elastic constants of anisotropic plates by phase stepping speckle interferometry," *Key Engineering Materials*, vol. 221, pp. 363-374, 2001.
- [16] L. Bruno, *et al.*, "A full-field approach for the elastic characterization of anisotropic materials," *Optics and Lasers in Engineering*, vol. 37, pp. 417-431, 2002.
- [17] L. Bruno and A. Poggialini, "Elastic characterization of anisotropic materials by speckle interferometry," *Experimental Mechanics*, vol. 45, pp. 205-212, 2005.
- [18] L. Bruno, *et al.*, "Elastic characterization of CVD diamond by static and dynamic measurements," *Journal of the European Ceramic Society*, vol. 26, pp. 2419-2425, 2006.
- [19] M. Grédiac, *et al.*, "The Virtual Fields Method for Extracting Constitutive Parameters From Full Field Measurements: a Review," *Strain*, vol. 42, pp. 233-253, 2006.
- [20] Z. Wang, *et al.*, "Inverse method to determine elastic constants using a circular disk and moiré interferometry," *Experimental Mechanics*, vol. 45, pp. 27-34, 2005.
- [21] J. F. Cárdenas-García, *et al.*, "Non-linear least-squares solution to the moiré hole method problem in orthotropic materials. Part II: Material elastic constants," *Experimental Mechanics*, vol. 45, pp. 314-324, 2005.
- [22] F. Hild and S. Roux, "Digital image correlation: from displacement measurement to identification of elastic properties—a review," *Strain*, vol. 42, pp. 69-80, 2006.
- [23] G. L. Cloud, *Optical methods of engineering analysis*: Cambridge Univ Pr, 1998.
- [24] K. Genovese, *et al.*, "A new hybrid technique for in-plane characterization of orthotropic materials," *Experimental Mechanics*, vol. 44, pp. 584-592, 2004.
- [25] J. Molimard, *et al.*, "Identification of the four orthotropic plate stiffnesses using a single open-hole tensile test," *Experimental Mechanics*, vol. 45, pp. 404-411, 2005.

- [26] D. Lecompte, *et al.*, "Mixed numerical-experimental technique for orthotropic parameter identification using biaxial tensile tests on cruciform specimens," *International Journal of Solids and Structures*, vol. 44, pp. 1643-1656, 2007.
- [27] L. Pagnotta, "Determining elastic constants of materials with interferometric techniques," *Inverse Problems in Science and Engineering*, vol. 14, pp. 801-818, 2006.
- [28] L. Pagnotta and G. Stigliano, "A numerical-experimental approach for identification of material constants of composite laminates by displacement field measurement," *WSEAS Transactions on Applied and Theoretical Mechanics*, vol. 1, p. 39, 2006.
- [29] L. Bruno, *et al.*, "A mixed numerical-experimental methodology for determining the elastic constants of orthotropic materials," 2006, p. 63410J.
- [30] L. Bruno, *et al.*, "Elastic characterization of orthotropic plates of any shape via static testing," *International Journal of Solids and Structures*, vol. 45, pp. 908-920, 2008.
- [31] S. Spinner and W. E. Tefft, "A method for determining mechanical resonance frequencies and for calculating elastic moduli from these frequencies," 1961, pp. 1221-1238.
- [32] R. F. Gibson, *Principles of composite material mechanics*: McGraw-Hill New York, 1994.
- [33] "ASTM Standard E1875-00e1, Standard Test Method for Dynamic Young's Modulus, Shear Modulus, and Poisson's Ratio by Sonic Resonance," in *Book of Standards Volume 03.01*, ed: ASTM International, West Conshohocken, PA.
- [34] F. M. Furgiuele and L. Pagnotta, "Misura delle costanti elastiche: un sistema computerizzato," *Automazione e Strumentazione*, vol. 46, pp. 147-152, 1998.
- [35] "ASTM Standard E1876-01, Standard test method for dynamic Young's modulus, shear modulus, and Poisson's ratio by impulse excitation of vibration," in *Book of Standards Volume 03.01*, ed: ASTM International, West Conshohocken, PA.
- [36] *Gridosonic*, . Available: <http://www.grindosonic.com/en/>
- [37] *BuzzMac* Available: <http://www.buzzmac.com>
- [38] D. Larsson, *et al.*, "Method and arrangement for non-destructive determination of the properties of an object," ed: Google Patents, 2002.
- [39] R. F. Gibson, *et al.*, "Apparatus and process for measuring mechanical properties of fibers," ed: Google Patents, 1993.

- [40] J. L. Leveque, *et al.*, "Method of and apparatus for the measurement of at least one mechanical property of an elastic material," ed: Google Patents, 1981.
- [41] M. A. Biot and W. L. Medlin, "Harmonic oscillator for measuring dynamic elastic constants of rock materials," ed: Google Patents, 1983.
- [42] R. J. Dill, *et al.*, "Methods and apparatus for measuring elastic modulus of non-solid ceramic materials by resonance," ed: Google Patents, 2007.
- [43] M. E. McIntyre and J. Woodhouse, "On measuring the elastic and damping constants of orthotropic sheet materials," *Acta Metallurgica*, vol. 36, pp. 1397-1416, 1988.
- [44] F. J. Nieves, *et al.*, "Measurement of the dynamic elastic constants of short isotropic cylinders," *Journal of Sound and Vibration*, vol. 265, pp. 917-933, 2003.
- [45] M. Alfano and L. Pagnotta, "Determining the elastic constants of isotropic materials by modal vibration testing of rectangular thin plates," *Journal of Sound and Vibration*, vol. 293, pp. 426-439, 2006.
- [46] G. B. Warburton, "The vibration of rectangular plates," *ARCHIVE: Proceedings of the Institution of Mechanical Engineers 1847-1982 (vols 1-196)*, vol. 168, pp. 371-384, 1954.
- [47] M. Alfano and L. Pagnotta, "Measurement of the dynamic elastic properties of a thin coating," *Review of Scientific Instruments*, vol. 77, p. 056107, 2009.
- [48] M. Alfano and L. Pagnotta, "An inverse procedure for determining the material constants of isotropic square plates by impulse excitation of vibration," *Applied Mechanics and Materials*, vol. 3, pp. 287-292, 2005.
- [49] M. Alfano, *et al.*, "Experimental assessment of a non-destructive method for measuring the elastic properties of thin isotropic plates," pp. 2033-2040.
- [50] M. Grédiac, *et al.*, "Direct identification of elastic constants of anisotropic plates by modal analysis: experimental results," *Journal of Sound and Vibration*, vol. 210, pp. 643-659, 1998.
- [51] M. Grediac and P. A. Paris, "Direct identification of elastic constants of anisotropic plates by modal analysis: theoretical and numerical aspects," *Journal of Sound and Vibration*, vol. 195, pp. 401-415, 1996.
- [52] I. Ohno, "Free vibration of a rectangular parallelepiped crystal and its application to determination of elastic constants of orthorhombic crystals," *J. Phys. Earth*, vol. 24, pp. 355-379, 1976.
- [53] R. G. Leisure and F. A. Willis, "Resonant ultrasound spectroscopy," *Journal of Physics: Condensed Matter*, vol. 9, p. 6001, 1997.

- [54] A. Migliori, "Resonant ultrasound spectroscopy," ed: Google Patents, 1991.
- [55] A. Migliori and T. W. Darling, "Resonant ultrasound spectroscopy for materials studies and non-destructive testing," *Ultrasonics*, vol. 34, pp. 473-476, 1996.
- [56] A. Yaoita, *et al.*, "Determination of elastic moduli for a spherical specimen by resonant ultrasound spectroscopy," *NDT & E International*, vol. 38, pp. 554-560, 2005.
- [57] A. Migliori, *et al.*, "Resonant ultrasound spectrometer," ed: Google Patents, 1990.
- [58] W. P. De Wilde, *et al.*, "Determination of the material constants of an anisotropic lamina by free vibration analysis," 1984, pp. 44-49.
- [59] W. P. De Wilde, *et al.*, "Coupling of Lagrange interpolation, modal analysis and sensitivity analysis in the determination of anisotropic plate rigidities," 1986, pp. 1058-1063.
- [60] L. R. Deobald and R. F. Gibson, "Determination of elastic constants of orthotropic plates by a modal analysis/Rayleigh-Ritz technique," *Journal of Sound and Vibration*, vol. 124, pp. 269-283, 1988.
- [61] E. O. Ayorinde and R. F. Gibson, "Elastic constants of orthotropic composite materials using plate resonance frequencies, classical lamination theory and an optimized three-mode rayleigh formulation," *Composites Engineering*, vol. 3, pp. 395-407, 1993.
- [62] T. C. Lai and T. C. Lau, "Determination of elastic constants of a generally orthotropic plate by modal analysis," *International Journal of Analytical and Experimental Modal Analysis*, vol. 8, pp. 15-33, 1993.
- [63] R. F. Gibson and E. O. Ayorinde, "Method and apparatus for non-destructive measurement of elastic properties of structural materials," ed: Google Patents, 1996.
- [64] H. Sol, "Identification of anisotropic plate rigidities using free vibration data," *Doctoral Thesis, Vrije Universiteit, Brussels, Belgium*, 1986.
- [65] P. Pedersen and P. S. Frederiksen, "Identification of orthotropic material moduli by a combined experimental/numerical method," *Measurement*, vol. 10, pp. 113-118, 1992.
- [66] K. E. Fällström, "Determining material properties in anisotropic plates using Rayleigh's method," *Polymer Composites*, vol. 12, pp. 306-314, 1991.
- [67] K. E. Fällström and M. Jonsson, "A nondestructive method to determine material properties in anisotropic plates," *Polymer Composites*, vol. 12, pp. 293-305, 1991.

- [68] K. E. Fallstrom and N. E. Molin, "A nondestructive method to determine material properties in orthotropic plates," *Polymer Composites*, vol. 8, pp. 103–108, 1987.
- [69] K. E. Fällström, *et al.*, "Dynamic material parameters in an anisotropic plate estimated by phase-stepped holographic interferometry," *Optics and Lasers in Engineering*, vol. 24, pp. 429-454, 1996.
- [70] M. Alfano, *et al.*, "Identifying elastic properties of isotropic materials by finite element analyses and vibration data," *Key Engineering Materials*, vol. 345, pp. 1327-1330, 2007.
- [71] C. Maletta and L. Pagnotta, "On the determination of mechanical properties of composite laminates using genetic algorithms," *International Journal of Mechanics and Materials in Design*, vol. 1, pp. 199-211, 2004.
- [72] L. Pagnotta and G. Stigliano, "Determining the dynamic elastic properties of isotropic plates of any shape."
- [73] M. Alfano, *et al.*, "Elastic properties of cold rolled aluminium plates with irregular shape by dynamic testing," pp. 1-5.
- [74] L. Pagnotta and G. Stigliano, "Assessment of elastic properties of isotropic plates by dynamic tests," *Experimental techniques*, vol. 34, pp. 19-24.
- [75] L. Pagnotta and G. Stigliano, "Elastic characterization of isotropic plates of any shape via dynamic tests: Theoretical aspects and numerical simulations," *Mechanics Research Communications*, vol. 35, pp. 351-360, 2008.
- [76] L. Pagnotta and G. Stigliano, "Elastic characterization of isotropic plates of any shape via dynamic tests: Practical aspects and experimental applications," *Mechanics Research Communications*, vol. 36, pp. 154-161, 2009.
- [77] C. M. Soares, *et al.*, "Identification of material properties of composite plate specimens," *Composite Structures*, vol. 25, pp. 277-285, 1993.
- [78] G. L. Qian, *et al.*, "A vibration method for measuring mechanical properties of composite, theory and experiment," *Composite Structures*, vol. 39, pp. 31-38, 1997.
- [79] S.-F. Hwang and C.-S. Chang, "Determination of elastic constants of materials by vibration testing," *Composite Structures*, vol. 49, pp. 183-190, 2000.
- [80] R. Rikards, *et al.*, "Method for identification of elastic properties of laminates based on experiment design," *Composites Part B: Engineering*, vol. 30, pp. 279-289, 1999.
- [81] A. Wereszczak, *et al.*, "Flexural and torsional resonances of ceramic tiles via impulse excitation of vibration," 2003, pp. 207-216.

- [82] T. Lauwagie, *et al.*, "Mixed numerical-experimental identification of elastic properties of orthotropic metal plates," *NDT & E International*, vol. 36, pp. 487-495, 2003.
- [83] M. F. T. Silva, *et al.*, "A genetic algorithm applied to composite elastic parameters identification," *Inverse Problems in Science and Engineering*, vol. 12, pp. 17-28, 2004.
- [84] T. Lauwagie, *et al.*, "Resonant-based identification of the elastic properties of layered materials: Application to air-plasma sprayed thermal barrier coatings," *NDT & E International*, vol. 41, pp. 88-97, 2008.
- [85] J. De Visscher, *et al.*, "Identification of the damping properties of orthotropic composite materials using a mixed numerical experimental method," *Applied Composite Materials*, vol. 4, pp. 13-33, 1997.
- [86] E. O. Ayorinde, "Elastic constants of thick orthotropic composite plates," *Journal of Composite Materials*, vol. 29, p. 1025, 1995.
- [87] S. Gagneja, *et al.*, "Design of test specimens for the determination of elastic through-thickness shear properties of thick composites from measured modal vibration frequencies," *Composites Science and Technology*, vol. 61, pp. 679-687, 2001.
- [88] H. Hua, "Identification of plate rigidities of anisotropic plate rectangular plates, sandwich panels and circular orthotropic discs using vibration data," PhD dissertation, Free University of Brussels, 1993.
- [89] D. Larsson, "Using modal analysis for estimation of anisotropic material constants," *Journal of engineering mechanics*, vol. 123, p. 222, 1997.
- [90] M. Alfano, *et al.*, "Determinazione delle costanti elastiche di piastre quadrate isotrope dalle frequenze naturali di vibrazione," *XXXII AIAS*.
- [91] M. Friswell, *et al.*, "A combined genetic and eigensensitivity algorithm for the location of damage in structures," *Computers & Structures*, vol. 69, pp. 547-556, 1998.
- [92] J. Cunha, *et al.*, "Application of genetic algorithms for the identification of elastic constants of composite materials from dynamic tests," *International Journal for Numerical Methods in Engineering*, vol. 45, pp. 891-900, 1999.
- [93] G. R. Liu, *et al.*, "A combined genetic algorithm and nonlinear least squares method for material characterization using elastic waves," *Computer Methods in Applied Mechanics and Engineering*, vol. 191, pp. 1909-1921, 2002.
- [94] G. R. Liu, *et al.*, "An inverse procedure for determination of material constants of composite laminates using elastic waves," *Computer Methods in Applied Mechanics and Engineering*, vol. 191, pp. 3543-3554, 2002.

- [95] K. Balasubramaniam and N. S. Rao, "Inversion of composite material elastic constants from ultrasonic bulk wave phase velocity data using genetic algorithms," *Composites Part B: Engineering*, vol. 29, pp. 171-180, 1998.
- [96] G. W. Caldersmith, "Vibrations of orthotropic rectangular plates," *Acustica*, vol. 56, p. 144, 1984.
- [97] P. S. Frederiksen, "Parameter uncertainty and design of optimal experiments for the estimation of elastic constants," *International Journal of Solids and Structures*, vol. 35, pp. 1241-1260, 1998.
- [98] P. S. Frederiksen, "Experimental procedure and results for the identification of elastic constants of thick orthotropic plates," *Journal of Composite Materials*, vol. 31, p. 360, 1997.
- [99] F. Moussu and M. Nivoit, "Determination of Elastic Constants of Orthotropic Plates By A Modal Analysis/Method of Superposition," *Journal of Sound and Vibration*, vol. 165, pp. 149-163, 1993.
- [100] A. E.-. 10, "Standard Practice for Measuring Ultrasonic Velocity in Materials," in *Annual book of ASTM Standards, Vol. 3.03.*, ed: ASTM International, West Conshohocken, PA.
- [101] P. S. Vibrometer, "Hardware Manual," ed: Auburn, MA: Polytec Pi, Inc, 2001.
- [102] M. Martarelli, "Exploiting the laser scanning facility for vibration measurements," *Imperial College of Science, Technology & Medicine*.
- [103] P. S. Vibrometer, "Theory Manual," ed: Version.
- [104] D. J. Ewins, *Modal testing: theory and practice*: Research Studies, 1984.
- [105] J. He and Z. F. Fu, *Modal analysis*: Butterworth-Heinemann, 2001.
- [106] B. Peeters, *et al.*, "A new procedure for modal parameter estimation," *Sound and Vibration*, vol. 38, pp. 24-29, 2004.
- [107] P. Guillaume, *et al.*, "Frequency-domain maximum likelihood identification of modal parameters with confidence intervals," 1998, pp. 359-366.
- [108] P. Guillaume, *et al.*, "Parametric identification of multivariable systems in the frequency domain- A survey," *ISMA 21*, pp. 1069-1082, 1996.
- [109] H. Van Der Auweraer, *et al.*, "Application of a fast-stabilizing frequency domain parameter estimation method," *Journal of Dynamic Systems, Measurement, and Control*, vol. 123, p. 651, 2001.
- [110] P. VERBOVEN, "Frequency-domain system identification for modal analysis," 2002.

- [111] W. Heylen, *Modal analysis theory and testing*, 1997.
- [112] R. Pintelon and J. Schoukens, *System identification: a frequency domain approach*: Wiley-IEEE Press, 2001.
- [113] P. Guillaume, *et al.*, "A poly-reference implementation of the least-squares complex frequency-domain estimator," 2003.
- [114] J. D. Ferry, *Viscoelastic properties of polymers*: John Wiley & Sons Inc, 1980.
- [115] A. D. Nashif, *et al.*, *Vibration damping*: Wiley-interscience, 1985.
- [116] E. Riande, *Polymer viscoelasticity: stress and strain in practice* vol. 55: CRC, 2000.
- [117] D. I. G. Jones, *Handbook of viscoelastic vibration damping*: Wiley, 2001.
- [118] C. W. Bert, "Material damping: An introductory review of mathematic measures and experimental technique," *Journal of Sound and Vibration*, vol. 29, pp. 129-153, 1973.
- [119] C. Coulomb, "Recherches th'eoriques et exp'erimentales: Sur la force de torsion et sur l'elasticit'e des fils de m'etal," *M'emoires de l'Acad'emie Royale des Sciences*, pp. 229-269, 1784.
- [120] C. Vasques, *et al.*, "Viscoelastic Damping Technologies–Part I: Modeling and Finite Element Implementation," *Mechanical Engineering*, vol. 1, pp. 96-110, 2010.
- [121] L. Rayleigh, "The theory of sound, vol. 2," *Mc. Millan & Co London and New York*, 1896.
- [122] T.K.Caughey, "Classical normal modes in damped linear dynamic systems," *Journal of Applied Mechanics* vol. 27, pp. 269–271, 1960.
- [123] T. Caughey and M. O'Kelly, "Classical normal modes in damped linear dynamic systems(Classical normal modes in discrete and continuous viscously damped linear dynamic systems)," *ASME, TRANSACTIONS, SERIES E-JOURNAL OF APPLIED MECHANICS*, vol. 32, pp. 583-588, 1965.
- [124] N. M. M. Maia and J. M. M. Silva, Eds., *Theoretical and experimental modal analysis*. Research Studies Press, Wiley, p.^pp. Pages.
- [125] S. Ibrahim, "Computation of normal modes from identified complex modes," *AIAA Journal*, vol. 21, pp. 446-451, 1983.
- [126] C.Lin and S. R. Ibrahim, "The use of complex versus normal modes in structural model improvement," presented at the Proceedings of the Second IMAC, 1984.

- [127] M. R. Wall and D. Neuhauser, "Extraction, through filter diagonalization, of general quantum eigenvalues or classical normal mode frequencies from a small number of residues or a short time segment of a signal. I. Theory and application to a quantum dynamics model," *The Journal of chemical physics*, vol. 102, p. 8011, 1995.
- [128] S. Adhikari, "Damping modelling using generalized proportional damping," *Journal of Sound and Vibration*, vol. 293, pp. 156-170, 2006.
- [129] M. Gaylard, "Identification of proportional and other sorts of damping matrices using a weighted response-integral method," *Mechanical systems and signal processing*, vol. 15, pp. 245-256, 2001.
- [130] J. Angeles and S. Ostrovskaya, "The proportional-damping matrix of arbitrarily damped linear mechanical systems," *Journal of applied mechanics*, vol. 69, p. 649, 2002.
- [131] C. Minas and D. Inman, "Identification of a nonproportional damping matrix from incomplete modal information," *Journal of Vibration and Acoustics*, vol. 113, p. 219, 1991.
- [132] M. Tong, *et al.*, "On the non-proportionality of generally damped systems," 1992, pp. 1301-1301.
- [133] K. Liu, *et al.*, "Evaluation of damping non-proportionality using identified modal information," *Mechanical systems and signal processing*, vol. 15, pp. 227-242, 2001.
- [134] W. Gawronski and J. Sawicki, "Response errors of non-proportionally lightly damped structures," *Journal of Sound and Vibration*, vol. 200, pp. 543-550, 1997.
- [135] J. Woodhouse, "Linear damping models for structural vibration," *Journal of Sound and Vibration*, vol. 215, pp. 547-569, 1998.
- [136] S. Adhikari and J. Woodhouse, "Identification of damping: part 1, viscous damping," *Journal of Sound and Vibration*, vol. 243, pp. 43-61, 2001.
- [137] S. Adhikari and J. Woodhouse, "Identification of damping: part 2, non-viscous damping," *Journal of Sound and Vibration*, vol. 243, pp. 63-88, 2001.
- [138] U. Prells and M. I. Friswell, "A measure of non-proportional damping," *Mechanical systems and signal processing*, vol. 14, pp. 125-137, 2000.
- [139] T. Kasai and M. Link, "Identification of non-proportional modal damping matrix and real normal modes," *Mechanical systems and signal processing*, vol. 16, pp. 921-934, 2002.

- [140] E. Balmes, "New results on the identification of normal modes from experimental complex modes," *Mechanical systems and signal processing*, vol. 11, pp. 229-243, 1997.
- [141] R. M. Lin and J. Zhu, "On the relationship between viscous and hysteretic damping models and the importance of correct interpretation for system identification," *Journal of Sound and Vibration*, vol. 325, pp. 14-33, 2009.
- [142] T. Gmür, *Dynamique des structures: Analyse modale numérique*: PPUR presses polytechniques, 1997.
- [143] Z. Osi ski, *Damping of vibrations*: Taylor & Francis, 1998.
- [144] L. Meirovitch, *Computational methods in structural dynamics* vol. 5: Springer, 1980.
- [145] P. Lancaster, *Lambda-matrices and vibrating systems*: Dover Pubns, 2002.
- [146] K. Gupta, "Eigenproblem solution of damped structural systems," *International Journal for Numerical Methods in Engineering*, vol. 8, pp. 877-911, 1974.
- [147] S. Utku and J. L. M. Clemente, "Computation of eigenpairs of $Ax=[\gamma] Bx$ for vibrations of spinning deformable bodies* 1," *Computers & Structures*, vol. 19, pp. 843-847, 1984.
- [148] F. Tisseur and K. Meerbergen, "The quadratic eigenvalue problem," *Siam Review*, pp. 235-286, 2001.
- [149] D. Afolabi, "Linearization of the quadratic eigenvalue problem," *Computers & Structures*, vol. 26, pp. 1039-1040, 1987.
- [150] L. P. Lefebvre, *et al.*, "Porous metals and metallic foams: Current status and recent developments," *Advanced Engineering Materials*, vol. 10, pp. 775-787, 2008.
- [151] H. P. Degischer and B. Kriszt, *Handbook of cellular metals: production, processing, applications*: Vch Verlagsgesellschaft Mbh, 2002.
- [152] T. Daxner, *Multi-Scale modeling and simulation of metallic foams*: VDI-Verl., 2003.
- [153] T. Daxner, *et al.*, "Mesoscopic simulation of inhomogeneous metallic foams with respect to energy absorption," *Computational materials science*, vol. 16, pp. 61-69, 1999.
- [154] R. Gradinger and F. G. Rammerstorfer, "On the influence of meso-inhomogeneities on the crush worthiness of metal foams," *Acta Materialia*, vol. 47, pp. 143-148, 1998.

- [155] S. Meguid, *et al.*, "FE modelling of deformation localization in metallic foams," *Finite elements in analysis and design*, vol. 38, pp. 631-643, 2002.
- [156] A. Reyes, *et al.*, "Constitutive modeling of aluminum foam including fracture and statistical variation of density," *European Journal of Mechanics-A/Solids*, vol. 22, pp. 815-835, 2003.
- [157] U. M. Ansys, "Theory Manual," *ANSYS revision*, vol. 8, 2003.
- [158] D. Systemes, "ABAQUS Theory Manual," *Dessault Systèmes, Providence, RI*, 2007.
- [159] H. Bart-Smith, *et al.*, "Compressive deformation and yielding mechanisms in cellular Al alloys determined using X-ray tomography and surface strain mapping," *Acta Materialia*, vol. 46, pp. 3583-3592, 1998.
- [160] J. Banhart, "Manufacture, characterisation and application of cellular metals and metal foams," *Progress in Materials Science*, vol. 46, pp. 559-632, 2001.
- [161] L. J. Gibson and M. F. Ashby, *Cellular solids: structure and properties*: Cambridge Univ Pr, 1999.
- [162] H. X. Zhu, *et al.*, "Analysis of the elastic properties of open-cell foams with tetrakaidecahedral cells," *Journal of the Mechanics and Physics of Solids*, vol. 45, pp. 319-325, 1997.
- [163] W. L. Ko, "Deformations of foamed elastomers," *Journal of Cellular Plastics*, vol. 1, p. 45, 1965.
- [164] S. Youssef, *et al.*, "Finite element modelling of the actual structure of cellular materials determined by X-ray tomography," *Acta Materialia*, vol. 53, pp. 719-730, 2005.
- [165] W. E. Warren and A. M. Kraynik, "Linear elastic behavior of a low-density Kelvin foam with open cells," *Journal of Applied Mechanics*, vol. 64, p. 787, 1997.
- [166] V. Shulmeister, *et al.*, "A numerical study of large deformations of low-density elastomeric open-cell foams," *Mechanics of Materials*, vol. 30, pp. 125-140, 1998.
- [167] H. X. Zhu, *et al.*, "Effects of cell irregularity on the elastic properties of open-cell foams," *Acta Materialia*, vol. 48, pp. 4893-4900, 2000.
- [168] A. P. Roberts and E. J. Garboczi, "Elastic moduli of model random three-dimensional closed-cell cellular solids," *Acta Materialia*, vol. 49, pp. 189-197, 2001.

- [169] E. Maire, *et al.*, "X-ray tomography applied to the characterization of cellular materials. Related finite element modeling problems," *Composites science and technology*, vol. 63, pp. 2431-2443, 2003.
- [170] J. Pawlicki, *et al.*, "MECHANICAL PROPERTIES OF CLOSED CELL AL FOAMS BASED ON TETRAKAIDECAHEDRONAL MODEL OF STRUCTURE."
- [171] O. B. Olurin, *et al.*, "Deformation and fracture of aluminium foams," *Materials Science and Engineering A*, vol. 291, pp. 136-146, 2000.
- [172] J. Banhart and J. Baumeister, "Deformation characteristics of metal foams," *Journal of Materials Science*, vol. 33, pp. 1431-1440, 1998.
- [173] Y. Sugimura, *et al.*, "On the mechanical performance of closed cell Al alloy foams," *Acta Materialia*, vol. 45, pp. 5245-5259, 1997.
- [174] K. Y. G. McCullough, *et al.*, "Uniaxial stress-strain behaviour of aluminium alloy foams," *Acta Materialia*, vol. 47, pp. 2323-2330, 1999.
- [175] D. Maurer, "8-Node Hexahedron Elements applied to Explicit Finite Element Methods," 2003.
- [176] A. CFX, "11.0 User Manual," *ANSYS Inc., Canonsburg, USA*, 2006.
- [177] J. Cugnoni, *et al.*, "Inverse method based on modal analysis for characterizing the constitutive properties of thick composite plates," *Computers & Structures*, vol. 85, pp. 1310-1320, 2007.
- [178] M. I. Friswell and J. E. Mottershead, *Finite element model updating in structural dynamics* vol. 38: Springer, 1995.
- [179] K. Madsen, *et al.*, "Methods for non-linear least squares problems," 1999.
- [180] J. More, "The Levenberg-Marquardt algorithm: implementation and theory," *Numerical analysis*, pp. 105-116, 1978.
- [181] J. Mottershead and M. Friswell, "Model updating in structural dynamics: a survey," *Journal of Sound and Vibration*, vol. 167, pp. 347-375, 1993.
- [182] R. B. Nelson, "Simplified calculation of eigenvector derivatives," *AIAA Journal*, vol. 14, pp. 1201-1205, 1976.
- [183] D. V. Murthy and R. T. Haftka, "Derivatives of eigenvalues and eigenvectors of a general complex matrix," *International Journal for Numerical Methods in Engineering*, vol. 26, pp. 293-311, 1988.
- [184] R. T. Haftka and H. M. Adelman, "Recent developments in structural sensitivity analysis," *Structural and Multidisciplinary Optimization*, vol. 1, pp. 137-151, 1989.

- [185] O. Døssing, *et al.*, *Structural Testing: Modal Analysis and Simulation*: Brüel & Kjær, 1988.
- [186] E. Maire, *et al.*, "Deformation of a Metallic Foam Studied by X-Ray Computed Tomography and Finite Element Calculations," in *Microstructural Investigation and Analysis*, ed: Wiley-VCH Verlag GmbH & Co. KGaA, 2006, pp. 68-73.

ENGR. SAEED BADSHAH

☎ : +43 (1) 58801 - 325423

✉ : saeed.badshah@tuwien.ac.at , saeedbadshah@hotmail.com

📍 : Linke Nordbahngasse 15/3/130, 1210 Wien, Austria.



Personal details

Date of birth 1st June 1980, Married, Pakistan Nationality

Education

- | | |
|---------------|---|
| 2007- Present | PhD (In progress) Institute of Mechanics and Mechatronics, Vienna University of Technology, Austria |
| 2004-2006 | Masters in Mechanical Engineering
N.W.F.P University of Engineering and Technology Peshawar, Pakistan. |
| 1999-2003 | Graduate in Mechanical Engineering
University of Engineering and Technology Taxila, Pakistan. |

Professional experience

- | | |
|---------------------|--|
| Nov. 2007- Present | Researcher, Institute of Mechanics and Mechatronics, Vienna University of Technology, Austria. |
| Feb. - Nov. 2007 | Lecturer, Air University, Mechanical and Mechatronics Engineering Department, Islamabad, Pakistan. |
| June 2004- Feb 2007 | Assistant Manager, National Engineering and Scientific commission, Islamabad, Pakistan. |

Research interest

- Experimental Modal testing and analysis.
- Finite element modeling.
- Cellular metals.
- Structural dynamics.
- Structural optimization.

Computer Skills

- Pro Engineer (Wild Fire)
- ANSYS
- IDEAS
- LMS Test.Lab
- Istra (software from Dantec dynamics for Q-300 and Q-500 systems)
- Scanning laser vibrometer (Polytec)
- MATLAB
- Auto CAD and AMD.

Conferences Proceedings

- Saeed Badshah, Johann Wassermann, *Mixed numerical experimental identification technique for closed cell aluminum foam based on modal analysis*, IBCAST, 10-13 Jan 2011, Islamabad, Pakistan.
- Saeed Badshah, Johann Wassermann, *Modal analysis of aluminum structure filled with aluminum foam using scanning laser vibrometer*, PIP International conference, 23-26 Feb 2009, Lahore, Pakistan.
- A. Schirrer, M. Kozek, A. Plank, M. Neumann, S. Badshah, J. Wassermann, *Vibration analysis of an actively controlled flexible structure using laser speckle interferometry*, ICSV15, 6-10 July 2008, Daejeon, Korea. Pages 1412-1419.
- Saeed Badshah, M. Neumann, Johann Wassermann, *Modal analysis of a damped aluminum structure*, ICSV15, 6-10 July 2008, Daejeon, Korea. Pages 1375-1381.

References

1. Prof. Dipl.-Ing. Dr.techn. Johann Wassermann
E325- Institut für Mechanik und Mechatronik
Vienna University of Technology, Austria.
Phone : +43 (1) 58801 - 325 431
E-Mail: johann.wassermann@tuwien.ac.at
2. Prof. Dipl.-Ing. Dr.techn. Heinz Pettermann
E317 - Institut für Leichtbau und Struktur-Biomechanik
Vienna University of Technology, Austria.
Phone : +43 (1) 58801 - 317 19
E-Mail: heinz.pettermann@tuwien.ac.at